



HAL
open science

Metasurfaces for electromagnetic energy harvesting and wireless power transfer in the railway environment

Mohammed Kalaagi

► **To cite this version:**

Mohammed Kalaagi. Metasurfaces for electromagnetic energy harvesting and wireless power transfer in the railway environment. Electromagnetism. Université de Lille, 2021. English. NNT : 2021LILUI049 . tel-04801889

HAL Id: tel-04801889

<https://theses.hal.science/tel-04801889v1>

Submitted on 25 Nov 2024

HAL is a multi-disciplinary open access archive for the deposit and dissemination of scientific research documents, whether they are published or not. The documents may come from teaching and research institutions in France or abroad, or from public or private research centers.

L'archive ouverte pluridisciplinaire **HAL**, est destinée au dépôt et à la diffusion de documents scientifiques de niveau recherche, publiés ou non, émanant des établissements d'enseignement et de recherche français ou étrangers, des laboratoires publics ou privés.



**MÉTASURFACES POUR LA RÉCUPÉRATION D'ÉNERGIE
ÉLECTROMAGNÉTIQUE ET LE TRANSFERT D'ÉNERGIE SANS FIL DANS
L'ENVIRONNEMENT FERROVIAIRE**

Thèse de doctorat

Université de Lille
Ecole doctorale “ Sciences pour ingénieurs ”
Unité de recherche “ COSYS-LEOST ”

Par

MOHAMMED KALAAGI

Soutenue le 13 juillet 2021

COMITÉ DE THÈSE

Omar M. Ramahi	Professeur à l'Université de Waterloo	-Rapporteur
Shah Nawaz Burokur	Prof. at Université Paris Nanterre	-Rapporteur
Hakim Takhedmit	Maître de conférences à Université Gustave Eiffel	-Examinateur
Christophe Loyez	Directeur de recherche CNRS	-Examinateur
Fouzia Boukour	Chargée de recherche à Université Gustave Eiffel	- Directrice de thèse
Divitha SEETHARAMDOO	Chargée de recherche à Université Gustave Eiffel	-Encadrante
Smail Ziani	Coordinateur Technique et Scientifique à RAILENIUM	-Invité
Matthieu Appenzeler	Ingénieur Signalisation Ferroviaire chez SNCF	-Invité



**METASURFACES FOR ELECTROMAGNETIC ENERGY HARVESTING AND
WIRELESS POWER TRANSFER IN THE RAILWAY ENVIRONMENT**

Doctoral Thesis

Presented in partial fulfilment of the requirements
for the degree of Doctor of Philosophy

**University of Lille
Doctoral school “ Sciences for engineers ”
Research unit “ COSYS-LEOST ”**

By

MOHAMMED KALAAGI

Defended on 13th of July 2021

THESIS COMMITTEE

Omar M. Ramahi	Prof. at University of Waterloo	-Reviewer
Shah Nawaz Burokur	Prof. at Université Paris Nanterre	-Reviewer
Hakim Takhedmit	Maitre de conférences à Université Gustave Eiffel	-Examiner
Christophe Loyez	Directeur de recherche CNRS	-Examiner
Fouzia Boukour	Researcher at Université Gustave Eiffel	- Thesis Director
Divitha SEETHARAMDOO	Researcher at Université Gustave Eiffel	-Supervisor
Smail Ziani	Coordinateur Technique et Scientifique at RAILENIUM	-Invited
Matthieu Appenzeler	Railway Signaling Engineer at SNCF	-Invited

Abstract

The interest for electric energy power supply to different components in the railway infrastructure, has become an interesting research topic with the gain of popularity for railway systems. To develop a smart, reliable, safe and autonomous railway system, specially with the rise of different technologies such as Internet of things (IoT) devices and wireless sensor nodes (WSN), electric power supply is needed for such that devices are implemented in a reliable and autonomous manner. Energy harvesting and wireless power transfer (WPT) technologies can be a key element for power supply to such devices, to build a sufficient and convenient system. A high level of EM energy has been shown to exist up to the microwave region and which can have a high potential for EM energy harvesting.

The aim of this work is to develop novel concepts based on metasurfaces, to enhance the potential and performance of EM energy harvesting and WPT technologies which can be compatible for the application in the railway environment. The main challenge is to design an efficient and compact device specially at low MHz frequencies where conventional rectenna systems can be insufficient. We first propose a novel concept to enhance the efficiency of EM conventional or off-the-shelf commercialized rectenna systems. It is based on the focusing of the ambient EM waves in an area where it can be harvested by a rectenna system. The design of focusing metasurface based on the hyperboloidal profile of the generalized phase law is proposed: the incident ambient EM energy in the far-field, is concentrated at a point known as the focal point at a given distance from the metasurface design. The metasurface designed is simulated and experimental validations in both near field and far field are proposed. Measurements have been carried in the anechoic chamber to validate the concept using a commercialized rectenna system and the focusing metasurface design at 900 MHz. The results have shown that, when implementing the rectenna system along side the focusing metasurface, the received power is enhanced by a factor of 5. Field tests were then conducted: the system was then implemented in the railway environment in the presence of a GSM-R base station, where the results have shown that, when implementing the metasurface along side the rectenna device, -20 dBm of received power was achieved which can be sufficient to wake up low-input-power devices such as wireless sensors, whereas the rectenna device (commercial energy harvester) alone showed poor results of received power around -40 dBm.

An alternative solution for wireless electric power supply in the railway system is WPT. However, one of the main challenges for such technologies in this case can be line of sight with mobility issues: better tracking and wider detection angle of the fed device is required. In this case, the design of multi-angle retrodirective metasurfaces based on different concepts such as cascading of various metamaterial super-cell designs, and surface impedance modulation are proposed. These designs can be implemented along side the fed device (IoT or WSN), in order to enhance the localization and tracking of the fed device beyond the common line-of-sight limitations reaching extreme oblique incident angles. Other solutions for efficiency enhancement and miniaturization for EM energy harvesting systems based on absorbing metasurfaces are proposed at low microwave frequencies.

Key words: Metasurfaces, metamaterials, EM energy harvesting, Wireless power transfer, railway environment, absorption, retro-reflection, focusing, generalized phase law, rectenna systems, performance enhancement.

Résumé

L'intérêt pour l'alimentation en énergie électrique des différents composants de l'infrastructure ferroviaire est devenu un sujet de recherche intéressant avec le gain de popularité des systèmes ferroviaires. Pour développer un système ferroviaire intelligent, fiable, et autonome, notamment avec l'essor de différentes technologies telles que les dispositifs de l'Internet des objets et les nœuds de capteurs sans fil, l'alimentation électrique est nécessaire pour que les dispositifs soient mis en œuvre de manière fiable et autonome. Les technologies de collecte d'énergie et de transfert d'énergie sans fil peuvent être un élément clé pour l'alimentation de ces dispositifs, afin de construire un système suffisant et pratique. Il a été démontré qu'un niveau élevé d'énergie électromagnétique existe jusqu'à la région des micro-ondes à fort potentiel

L'objectif de ce travail est de développer de nouveaux concepts basés sur les métasurfaces, afin d'améliorer le potentiel et la performance de la récolte d'énergie EM et des technologies WPT qui peuvent être compatibles avec l'application dans l'environnement ferroviaire. Le principal défi consiste à concevoir un dispositif efficace et compact, en particulier pour les basses fréquences MHz, où les systèmes rectenna être insuffisants. Nous proposons tout d'abord un nouveau concept pour améliorer l'efficacité des systèmes conventionnels EM ou des systèmes de rectenna commercialisés sur étagère. Ce concept est basé sur la focalisation des ondes EM ambiantes dans une zone où elles peuvent être captées par un système de rectenna. La conception d'une métasurface de focalisation basée sur le profil hyperboloïde de la loi de phase généralisée est proposée : l'énergie électromagnétique ambiante incidente dans le champ lointain est concentrée en un point appelé point focal à une distance donnée de la conception de la métasurface. La métasurface est simulée et des validations expérimentales en champ proche et en champ lointain sont proposées. Des mesures ont été effectuées dans la chambre anéchoïque pour valider le concept en utilisant un système de rectenna commercialisé et la conception de la métasurface de focalisation à 900 MHz. Les résultats ont montré que, lors de la mise en œuvre du système rectenna à côté de la métasurface de focalisation, la puissance reçue est améliorée d'un facteur 5. Des essais sur le terrain ont ensuite été réalisés : le système a été mis en œuvre dans l'environnement ferroviaire en présence d'une station de base GSM-R. Les résultats ont montré que, lorsque la métasurface est mise en œuvre à côté du dispositif à antenne rectangulaire, une puissance reçue de -20 dBm est obtenue, ce qui peut être suffisant pour réveiller des dispositifs à faible puissance d'entrée tels que des capteurs sans fil, que le dispositif à antenne rectangulaire seul a donné de mauvais résultats avec une puissance reçue d'environ -40 dBm.

Une solution alternative pour l'alimentation électrique sans fil dans le système ferroviaire est le WPT. l'un des principaux défis pour ces technologies dans ce cas peut être la ligne de vue avec des problèmes de mobilité : un meilleur suivi et un angle de détection plus large du dispositif

alimenté sont nécessaires. Dans ce cas, la conception de métasurfaces rétrodirectives multi-angles basée sur différents concepts tels que la mise en cascade de diverses conceptions de super-cellules métamatérielles et la modulation d'impédance de surface est proposée. Ces conceptions peuvent être mises en œuvre à côté du dispositif alimenté, afin d'améliorer la localisation et le suivi du dispositif alimenté au-delà des limites communes de la ligne de signal atteignant des angles d'incidence obliques extrêmes. D'autres solutions pour l'amélioration de l'efficacité et la miniaturisation des systèmes de récolte d'énergie EM basés sur des métasurfaces absorbantes sont proposées aux basses fréquences micro-ondes.

Traduit avec www.DeepL.com/Translator (version gratuite)

Mots clés: Métasurfaces, métamatériaux, collecte d'énergie électromagnétique, transfert d'énergie sans fil, environnement ferroviaire, absorption, rétro-réflexion, focalisation, loi de phase généralisée, systèmes de rectenna, amélioration des performances.

Related publications

Patent

- **Mohammed Kalaagi and Divitha Seetharamdoo.** “ Device for enhancing the power level harvested by Electromagnetic energy harvesting system .” Patent in process of filing.

Journal papers

- **Mohammed Kalaagi and Divitha Seetharamdoo.** “Retrodirective metasurfaces from non-reciprocal to reciprocal using impedance modulation for high-super-cell-periodicity designs.” *Applied Physics A* 126 (4), 1-7, 2020.
- **Mohammed Kalaagi and Divitha Seetharamdoo.** “Multiangle retrodirective cascaded metasurface”. *Journal of Applied Physics* 126 (10), 104901, 2019

International Communications

- **Mohammed Kalaagi and Divitha Seetharamdoo** “Multi-Band Metamaterial Absorbers to Efficient Energy Harvesters for Railway Applications”. 2020 International Workshop on Antenna Technology (iWAT), 1-3
- **Mohammed Kalaagi and Divitha Seetharamdoo** “Fano Resonance Based Multiple Angle Retrodirective Metasurface”. 2020 14th European Conference on Antennas and Propagation (EuCAP), 1-4
- **Mohammed Kalaagi and Divitha Seetharamdoo** “Electromagnetic energy harvesting systems in the railway environment: State of the art and proposal of a novel metamaterial energy harvester”. 2019 13th European Conference on Antennas and Propagation (EuCAP), 1-5
- **Mohammed Kalaagi and Divitha Seetharamdoo** “Eleven Channel Retrodirective Metasurface Based on the Combination of the Generalized Phase Law and Impedance Modulation”. 2019 13th European Conference on Antennas and Propagation (EuCAP), 1-3
- **Mohammed Kalaagi and Divitha Seetharamdoo** “Design of Dual Polarized Retrodirective Metasurfaces”. 2018 IEEE Radio and Antenna Days of the Indian Ocean (RADIO), 1-2
- **Mohammed Kalaagi and Divitha Seetharamdoo** “Reciprocal Optimized Surface Impedance Multiple Angle Retro-Reflective Metasurfaces”. 2018 IEEE Radio and Antenna Days of the Indian Ocean (RADIO), 1-2
- **Mohammed Kalaagi and Divitha Seetharamdoo** “Retrodirective metasurface operating simultaneously at multiple incident angles”. 2018 12th European Conference on Antennas and Propagation (EuCAP), 1-5M

Table of Contents

Abstract	i
Table of Contents	v
List of Figures	viii
Abbreviations	xvi
General Introduction to Thesis Work	1
I State of the art on energy harvesting in Railway environment	7
1 Energy Harvesting and Wireless Power Transfer Systems in The Railway Environment	9
1.1 Introduction	9
1.2 Application: Power-autonomous Wireless power sensor nodes	11
1.3 IOT for Railways	13
1.4 Wireless Power Transfer in the Railway Environment	14
1.5 Energy Harvesting in the Railway Environment	15
1.5.1 Vibration	15
1.5.2 Solar Power	18
1.5.3 Acoustic Energy	19
1.6 Electromagnetic Energy Sources in the Railway Environment	22
1.6.1 Measurements	24
1.7 Conclusion	25
2 Electromagnetic Energy Harvesting and Wireless Power Transfer	27
2.1 Introduction	27
2.2 State of the Art on Wireless Power Transfer	29
2.3 Ambient Electromagnetic Energy	30
2.4 State of the technology: RF harvesters - commercial products	32
2.4.1 Radiators	32
2.4.2 Rectifying circuits	34
2.5 State of the research on electromagnetic energy harvesters: Radiators	34
2.5.1 Antennas at 2.4 GHz	34
2.5.2 Antenna arrays	36
2.6 Use Cases for EM energy harvesters in the Railway Environment	37
2.6.1 Train or on Board EM Environments	38
2.6.2 Line and Track Electromagnetic Environment	38
2.6.3 EM sources from Telecommunication Base Stations	39
2.6.4 Tunnel Environments	40

2.6.5	IOT use cases for Railways	40
2.7	Conclusion	41
II Metasurface solutions for EM energy harvesting and WPT performance enhancement in Railway environment		44
3	An Overview on Metasurfaces; Focusing, Anomalous reflection and Absorption: Applications and Physics	46
3.1	Introduction	46
3.2	Metasurfaces Anomalous Wave Control	47
3.2.1	Generalized Snell's Law of Reflection and Refraction	47
3.2.2	Demonstration of the Generalized Phase Law	48
3.2.3	Retro-Reflection	50
3.3	Metamaterials and Metasurfaces Based on Absorption	52
3.4	Metasurface Energy Harvesters	55
3.5	Metasurface Lenses: Wavefront Shaping and Focusing	56
3.6	Conclusion and Future Work	58
4	Novel Concept for EM Energy Harvesting Based on Focusing Metasurfaces	60
4.1	Introduction	60
4.2	Rectenna Systems	61
4.2.1	Antenna efficiency improvement and metamaterial RF harvesters	61
4.2.2	Technologies Commercialized	62
4.3	Concept of EM Energy Harvesting Based on Focusing	62
4.4	Principle of Operation of the Novel Harvester	63
4.4.1	Generalized Phase Law and Design Procedure of the Focusing Metasurface	64
4.4.2	Metasurface Focusing Point Using Ansys HFSS	68
4.5	The P2110 Power-Harvesting System- Off the Shelf Commercialized Technologies	69
4.5.1	Description	69
4.5.2	Contents of P2110b Kit	69
4.5.3	Power Harvester's Efficiency	69
4.5.4	P2110b Setup, Testing and Installation	71
4.6	Realization, Measurements and Validation of the Novel Concept	72
4.6.1	Measurements of the Metasurface Focal Point	73
4.6.2	Implementation of the Focusing Metasurface with the Commercial P2110b Energy Harvester	77
4.7	Conclusion	79
5	Assessment of The Focusing Metasurface Harvesting System in the Railway Environment	82
5.1	Introduction	82
5.2	Description of the railway environment	83
5.3	Description of the experimental set-up	84
5.4	On-Site measurement results	86
5.4.1	Site Measurements Using the concept of the focusing metasurface	86
5.4.2	Antenna implementation along side a metallic plate	87
5.4.3	Measurements using the commercialized receiving antenna alone	88
5.4.4	Focusing metasurface implementation at a different position without facing the base station	89
5.5	Comparisons and discussions	89
5.6	Conclusion	91

6	Tracking and Localizing Efficiency Enhancement Using Multi-Angle Retrodirective Metasurfaces: Application for Wireless Power Transfer	93
6.1	Introduction	93
6.2	Concept: Application Aspect	94
6.3	Metasurfaces and Anomalous Wave Control	95
6.4	From the Generalized Phase Law of Reflection to Retrodirectivity	97
6.4.1	Design of a Retrodirective Super-Cell: Principle of Operation	98
6.4.2	Lossless Reflection Condition	99
6.4.3	Design of Retrodirective Metasurfaces for various angles of incidence	100
6.4.4	Design of Dual Polarized Retrodirective Metasurfaces	105
6.5	Design of a Multi-Angle Cascaded Retrodirective Metasurface based on Superposition	108
6.5.1	Comparison between the C-MIARM and the Conventional Corner Dihedral .	110
6.5.2	Experimental Measurements for the C-MIARM	112
6.6	Multi-Angle Retrodirective Metasurfaces from Non Reciprocal to Reciprocal: Impedance Modulation for High Super-cell Periodicity Designs	113
6.6.1	Relation between Periodicity L_x and Wavelength λ	114
6.6.2	High Periodicity Reciprocal Metasurface Design Procedure: Surface Impedance Modulation Technique	115
6.6.3	Metasurface Design and Results	117
6.6.4	Fano Resonance Based Multiple Angle Retrodirective Metasurface	119
6.6.5	Metasurface Experimental Measurements	123
6.7	Conclusion and Future Work	123
7	Metamaterial Energy Harvesters Based on Absorption: Challenges at Low MHz Frequencies For Railway Applications	125
7.1	Introduction	125
7.2	Proposal of High Efficient Metamaterial Energy Harvesters at Low MHz Frequencies	126
7.2.1	Challenges	126
7.2.2	Principle of Operation and Concept	127
7.2.3	Design of a Single Band Metamaterial Energy Harvester	127
7.2.4	Design of a Multi-Band Metamaterial Energy Harvester	131
7.3	Conclusion and Future Work	135
	Conclusion of the thesis and Future Work	136
	Main contributions of the thesis	136
	Bibliography	142

List of Figures

1	Application to supply low input power devices in the railway environment using EM energy harvesting technologies and WPT. Challenges and proposed solution using the physical properties of metasurfaces.	4
1.1	Electric power supply needed for different devices in the railway system. [1]	10
1.2	Sources of energy in the railway environment. [1]	10
1.3	Architecture Diagram of the system under test. [2]	12
1.4	System model of wireless sensor nodes implemented along a railway track using sinks powered by AC supply and Energy harvesting power sensors. [3]	12
1.5	a) Components and b) energy model of a wireless sensor node powered by an energy harvester. [3]	12
1.6	Overall Proposed Architecture of an IOT solution for Smart Railways [4].	13
1.7	View of high-speed train with WPT system [5].	14
1.8	a) Proposed transformer for charging on-board battery for a railway system, b) Miniature experimental illustration of coil transformer [6].	15
1.9	Piezoelectric element place under the rail which produces voltage due to strain along its length and the field test where the orange clamps hold the device during glue up. [7]	15
1.10	Illustration of bogie rail harvester scales(left); enlarged view of clamped cantilevered piezoelectric beam configuration(right). [8]	16
1.11	a) Proposed mechanical design for the electromagnetic converter. b) Electromagnetic converter architecture based on a mechanical spring and magnetic spring. [9]	17
1.12	a),c) applied random excitation for the converter, b),d) generated voltage from the converter. [9]	17
1.13	On the left we have the drawing of the MMR based harvester prototype and on the left the finished and deployed MMR harvester prototype. [10]	18
1.14	3D schematic of solar Photovoltaic panels on train setup. [11]	18
1.15	3D schematic of solar Photovoltaic panels on train setup. [11]	19
1.16	Table: System configuration details. [11]	19
1.17	a) Model of the Helmholtz resonator. b) The mass-spring model. [12]	20
1.18	Electric circuit and illustration of the acoustic energy harvesting system. [12]	20
1.19	Prototype and installation of the noise barrier. [12]	21
1.20	The frequency response and amplification ratio for the acoustic energy harvesting system. [12]	21
1.21	Catenary line, pantograph and rail return current to feed the train electrical traction chain. [13]	23
1.22	a) Biconical antenna responsive teletrico the polarized electric field for receiving an field component. b) Magnetic loop parallel to the loop catenary wire rail [13].	23
1.23	Configuration of the measurement setup using a vector network analyzer [13]	24
1.24	Received signal a) during the absence of a train and b) during the passage of a train at frequencies between 9 kHz to 300 MHz. [13]	24

1.25	Measurements of the field radiation in the railway environment, where the curves A, B and C show the radiation emission limits. For more details refer to the standard EN 50121-3-1. [14]	25
1.26	Measurements of the E-field magnitude (dBuV) with respect to frequency carried out by SNCF in Belfort in the railway environment	26
1.27	Example of the possible energy harvesting process in the railway environment.	26
2.1	On the left shows the picture of Nikola Tesla who started WPT and on the right Guglielmo Marconi inventor of the radio.	28
2.2	Wireless Power Transfer from DC to RF through an antenna transmitter to an antenna receiver.	28
2.3	Rectenna architecture design consisting of an antenna, Rectifier circuit and storage elements. [15]	29
2.4	Different Wireless Power Transfer technologies and timeline over the past history. [16]	30
2.5	a) An integrated sensor node by Solmu Technologies. b) Prototyped antenna for energy transmission. [17]	30
2.6	a) Internet of things on deep space exploration. b) vector modular active beam forming antenna array used. [18]	31
2.7	Map of different locations of london underground for the study of ambient sources of energy.(Imperial Colledge London)	31
2.8	Spectrum analyzer and omnidirectional antenna for a band of frequency from 0.3 GHz - 3 GHz.(Imperial Colledge London)	32
2.9	Power energy obtained for London underground ambient sources study at different bands of frequency.(Imperial Colledge London)	32
2.10	a) RFID tag presented bu Murata Electronic North America technologies for a frequency of 13.5 MHz. b) Block diagram of the RFID tag.	33
2.11	The M24LR Discovery Kit with RF energy harvesting EEPROM. [19]	34
2.12	a) The P1110B designed by POWERCAST design and pins b) P1110B block diagram	34
2.13	Block diagram of a rectenna design. [20]	35
2.14	Reference circuit with 50 Ohm input impedance (top); and fully optimized rectifier with non-50 Ohm impedance (bottom). [20]	35
2.15	a) The realized reference circuit with 50 Ohm input impedance (top) and fully optimized rectifier (bottom). b) Output Voltages of the given designs. [20]	36
2.16	a) Fabricated rectenna Top view of radiating patch and bottom view of rectifier circuit.b) Efficiency of the rectenna design for different input powers across a 6.2 kΩ resistance. [21]	36
2.17	a) Photographs of the 14 quasi-Yagi array top side and back side. b) Efficiencies of the Yagi design antenna array with respect to frequency for different input power levels [22].	37
2.18	Railway Electromagnetic Zones [23]	38
2.19	Illustration of the on board GSM-R system [24]	39
2.20	EM interferences caused by the catenary line and pantograph as well as GSM based stations which are received by the GSM-R antenna implemented on the rooftop of the train. [24]	39
2.21	Tunnel Environment for high speed rails. [25]	40
2.22	Railway communications scenarios (Renfe AVE train and train station pictures are under Creative Commons License). Color meaning: pink (train-to-infrastructure communications), blue (inter-car communications), light-green (intra-car communications), yellow (communications inside the station), purple (infrastructure-to-infrastructure communications), and dark green (wireless sensor networks). [26]	41
2.23	Summary of the conclusion of part one on the railway application and existing technologies.	42

3.1	Sketch of the concept considered by the group of F. Cappasso in [27], where a metasurface positioned at the interface between two ordinary media (characterized by refractive indexes n_i and n_t) describing the generalization of the laws of reflection and refraction.	48
3.2	a) SEM image of a metasurface consisting of an array of V-shaped gold optical scatterers patterned on a silicon wafer. It creates a constant gradient of phase jump along the metasurface for the control of the propagation direction of light transmitted through or reflected from the metasurface. b) 3D top view of the metasurface and the super-cell periodicity. [27]	49
3.3	a) Schematic of a metasurface design consisting of gold patch elements separated from a gold back plane by an MgF2 spacer with subwavelength thickness. [28] b) Fabricated microwave metasurface design consisting of H-unit cell elements separated from a metallic back plane by a dielectric spacer. [29]	49
3.4	a) Illustration of the three-channel beam splitter. The incident beam is split into three transmitted beams. b) The structure profile of the gradient metasurface. There are three phase gradient directions along the arrows, and each triangles drawn with black dotted line represent nanocylinders with same phase delay. [30]	50
3.5	Comparison between the reflection of an incident wave from an engineered topology and metallic surface.	50
3.6	Photograph of the fabricated prototype that consists of 5×6 unit cells with overall dimensions of 7.2×6.0 cm [31].	52
3.7	N-port isolating mirror. The wave incoming from different angles is reflected back to the source for various angles of incidence. [32]	52
3.8	Geometry of a generic optically thin absorbing layer (left) and its equivalent model as a set of two current sheets (right). [33]	53
3.9	a) Electric resonator and cut wire from different angle views . b) Reflection in green, Absorption in red and Transmission in blue with respect to frequency of the designed element. [34]	53
3.10	a) Proposed metamaterial element for miniaturized designs. b) The metasurface structure of such element operating at 400 MHz. [35]	54
3.11	a) Split ring resonators using multi-layer technique. b) Reflection coefficient of the metamaterial design. [36]	54
3.12	a) Dual ring metamaterial absorber unit cell element design. b) Absorption with respect to frequency. [37]	55
3.13	Metamaterial unit cell energy harvester design. [38]	55
3.14	Metamaterial unit cell energy harvester design. [38]	56
3.15	3D design of an unit cell element structure and top view at THz frequencies for EM focusing. [39]	57
3.16	a) Focusing metasurface design. b) Desired phases for the unit cell scatterers with respect to frequency. c) Focusing intensity of the metasurface design at different frequencies. [39]	57
3.17	a) Geometry of a tri-dipole unit cell element. b) Focusing metasurface design with periodic unit cell tri-dipole elements each with a specific phase. [40]	58
3.18	a) Prototype fabrication and measurements in the near field. b) Electric field intensity of the x-y plane at the distance of the focal point. [40]	58
4.1	Fabricated proposed energy harvesting antenna. (a) Perspective view. (b) Side-view. (c) Top view. [41]	62
4.2	Concept of an EM energy harvesting system based on focusing	63
4.3	Functionality of a Thin Metalens compared to that of a bulky lens system for light focusing (The photo is referenced to EM Lab UTEP)	64
4.4	Concept of Wave focusing using engineered topologies.	64
4.5	Metamaterial unit cell structures	65

4.6	Geometry and dimensions of the unit cell Jerusalem cross design operating at frequency 900 MHz.	65
4.7	a) Jerusalem cross dimensions and a factor a to vary the element dimensions from initial to each with a specific reflection phase b) The phase of the reflection coefficient with respect to the factor a at a frequency of 900MHz.	66
4.8	Phase of each element (21×21) of the metasurface design in the x and y planes at 900 MHz.	67
4.9	Focusing metasurface of 21×21 unit cell elements of dimensions $81.4 \text{ cm} \times 81.4 \text{ cm}$ operating at 900 MHz Using Ansys HFSS.	67
4.10	a) Electric field distribution of the incident wave illuminated towards the metasurface b) Electric field distribution of the reflected wave from the metasurface in the x - z plane operating in the far-field at 900MHz.	68
4.11	Electric field distribution of the reflected wave in the a) y - z plane b) x - z plane and c) x - y plane	69
4.12	The P2110b Power Harvester Development Kit for Wireless Sensors.(P2110b Owner's Manual)	70
4.13	Table showing the items in the P2110b Kit and descriptions of each. (P2110b Owner's Manual)	70
4.14	Powerharvester efficiency with respect to input RF power in a)dBm and b)mW (P2110b Powerharvester Datasheet)	71
4.15	Powerharvester efficiency with respect to Frequency in MHz for an input power of a)250 and 500 μW and b)1000 and 5000 μW (P2110b Powerharvester Datasheet)	71
4.16	Powerharvester P2110b setup for testing at the Lab	72
4.17	Example of the output data illustrated by the power harvester using the hyperterminal.	72
4.18	Table explaining each item displayed on the screen and the valid range of data.	73
4.19	Realized metasurface of dimensions $81 \text{ cm} \times 81 \text{ cm}$	74
4.20	Setup for the measurement of the focal point of the metasurface design.	74
4.21	Grid sheet fixed 30 cm away from the metasurface design.	75
4.22	P2110b powercast energy harvester set-up connected to MPlab PC for calculating the received power at the focal point.	75
4.23	Dipole antenna measuring at each point 30 cm away from the metasurface at the fixed grid sheet.	76
4.24	Power received in mW in the x - y plane at the focal point 30 cm away from the metasurface.	76
4.25	Averaging of the Power received at the focal point 30 cm away from the metasurface.	77
4.26	Vivaldi transmitting antenna at 900 MHz.	78
4.27	General setup of the concept of the novel energy harvesting system in far field measurements in an anechoic chamber at 900 MHz.	78
4.28	Commercial Energy harvester configuration set-up with the metasurface fixed 30cm away in the far-field.	79
4.29	Commercial Energy harvester configuration set-up with a metallic plate fixed 30cm away in the far-field.	79
4.30	Commercial Energy harvester configuration set-up alone at the same position.	80
4.31	Power received in mW by the energy harvester over a continuous time for three different configurations of the commercial energy harvester with a metasurface, metallic plate and alone. (Antenna horizontal polarization)	80
4.32	Power received in mW by the energy harvester over a continuous time for three different configurations of the commercial energy harvester with a metasurface, metallic plate and alone. (Vertical polarization)	81
5.1	A passing train in the railway infrastructure with a GSM-R base station situated next to the railway track. (SNCF Reseau Paris, France)	84

5.2	Setup of our focusing metasurface and harvesting device at a far distance from the railway system, including all components.	85
5.3	VNA to measure the received power by the Powercast P2110b dipole antenna.	86
5.4	Power received in dBm by the antenna implemented along side the focusing metasurface, measured using the VNA with respect to frequency (MHz).	87
5.5	Receiving P2110b antenna along side the metallic plate.	87
5.6	Power received in dBm by the antenna implemented along side the metallic plate, measured using the VNA with respect to frequency (MHz).	88
5.7	Receiving antenna implemented alone in the far-field away from the GSM-R base station.	88
5.8	Power received in dBm by the antenna implemented alone, measured using the VNA with respect to frequency (MHz).	89
5.9	Setup of our focusing metasurface and harvesting device without facing the GSM-R base station in the far-field.	90
5.10	Power received in dBm by the antenna implemented along side the focusing metasurface without facing the base station, measured using the VNA with respect to frequency (MHz).	91
5.11	Power received versus frequency comparing the three configurations	91
6.1	Wireless Power Transfer concept for tracking an IOT device to supply along with the usage of a retrodirective metasurface from the application aspect.	95
6.2	Concept for a metasurface where an incident plane wave is controlled in arbitrary directions [42]	96
6.3	An incident wave reflecting back from an engineered gradient metasurface in the same direction of incidence	97
6.4	Super cell divided into subwavelength unit cells of dimensions L_x and L_y	98
6.5	Phase of the reflection coefficient for a TM polarized wave at 14.7 GHz with respect to the dimensions of the strip-lines d_y	99
6.6	The normal component of the Poynting vector with respect to θ_i for a metasurface design at 30°	100
6.7	a) Metasurface design at 30° Using Ansys HFSS, b) Metasurface prototype of 7×9 super-cells printed on a Teflon substrate of dimensions $14.3 \text{ cm} \times 9.2 \text{ cm}$ and thickness 1.57 mm	101
6.8	Monostatic RCS (dB) with respect to the incident angles (degrees) for a 30° metasurface design of 7×9 super cells and dimensions $14.3 \text{ cm} \times 9.2 \text{ cm}$ compared to that of a metallic flat plate of similar dimensions.	101
6.9	Monostatic RCS (dB) with respect to the incident angles (degrees) for a 25° metasurface design of 6×5 super-cells and dimensions $6.1 \text{ cm} \times 12 \text{ cm}$ compared to that of a Flat metallic plate of similar dimensions.	103
6.10	Monostatic RCS (dB) with respect to the incident angles (degrees) for a 20° metasurface design of 7×5 super-cells and dimensions $7.1 \text{ cm} \times 15 \text{ cm}$ compared to that of a flat metallic plate of similar dimensions.	103
6.11	Monostatic RCS (dB) with respect to the incident angles (degrees) for a 15° metasurface design of 7×5 super-cells and dimensions $7.14 \text{ cm} \times 19.7 \text{ cm}$ compared to that of a metallic flat plate of similar dimensions.	105
6.12	Monostatic RCS (dB) with respect to the incident angles (degrees) for a 10° metasurface design of 6×4 super-cells and dimensions $6.12 \text{ cm} \times 23.5 \text{ cm}$ compared to that of a metallic flat plate of similar dimensions.	105
6.13	A metasurface design with two opposite directions structure at 10° using Ansys HFSS. 106	
6.14	Monostatic RCS of the 10° metasurface proposed structure of 12×4 super-cells(Figure 6.13) of dimensions $12.224 \text{ cm} \times 23.5 \text{ cm}$ compared to that of a flat metallic plate of similar dimensions.	106

6.15	Monostatic RCS of the 15° metasurface proposed structure of 14×5 super-cells of dimensions $14.28 \text{ cm} \times 19.7 \text{ cm}$ compared to that of a flat metallic plate of similar dimensions.	107
6.16	Normalized monostatic RCS with respect to the incident angles of the experimental measurements compared to that of the simulation results for a 30° metasurface prototype.	107
6.17	Super cell of dimensions L_x and L_y divided into subwavelength patch structured unit cells	107
6.18	Super cell of dimensions L_x and L_y divided into subwavelength cross structured unit cells	108
6.19	Cross Structure metasurface of 4×3 super-cells.	108
6.20	Patch Structure metasurface of 4×3 super-cells.	108
6.21	Normalized monostatic RCS in dB10norm with respect to the incident angles for a cross metasurface structure at TM and TE polarizations	109
6.22	Normalized monostatic RCS in dB10norm with respect to the incident angles for a patch metasurface structure at TM and TE polarizations	109
6.23	Prototype of a cross metasurface structure for measurements carried on in an anechoic chamber.	109
6.24	Normalized monostatic RCS measurements compared to that of the simulation results for TE polarization for the cross metasurface at 14.7 GHz.	110
6.25	Normalized monostatic RCS measurements compared to that of the simulation results for TM polarization for the cross metasurface at 14.7 GHz.	110
6.26	Cascaded Multiple Incident Angle Retrodirective Metasurface (C-MIARM) with the superposition of 4×8 30° , 25° and 20° super-cells each with 15° and 10° metasurfaces using the mirror image form, where the MIARM has an overall dimension of $8.163 \text{ cm} \times 56.23 \text{ cm}$ and substrate of $\epsilon=2.2$ and thickness 1.57 mm.	111
6.27	Normalized monostatic RCS in dB of the C-MIARM with respect to the overall performances of the metasurfaces designed at 30° , 25° , 20° , 15° and 10°	111
6.28	Monostatic RCS of the C-MIARM of dimensions $8.163 \text{ cm} \times 56.23 \text{ cm}$ compared to that of a conventional corner dihedral of dimensions $8 \text{ cm} \times 15.5 \text{ cm} \times 7.75 \text{ cm}$	112
6.29	Fabricated prototype of the C-MIARM of dimensions $8.163 \text{ cm} \times 56.23 \text{ cm}$	112
6.30	Normalized Monostatic RCS with respect to the incident angles of the simulation results compared to that of the measurements at 14.7GHz for the C-MIARM.	113
6.31	a) Super-cell periodicity $L_x \leq \lambda$, retro-reflection is obtained in the desired direction θ_i , the reciprocal direction and at normal incidence. b) Super-cell periodicity $\lambda < L_x < 2\lambda$, retro-reflection is obtained in the desired direction θ_i and the reciprocal direction, whereas for normal incidence is absent. c) Super-cell periodicity $L_x \geq 2\lambda$, retro-reflection is obtained only in the desired direction θ_i , whereas the conventional properties of the metasurface are lost in the reciprocal and normal incidence directions.	114
6.32	Nominal super cell design discretized into 10 patch cells of dimensions d_y (given in table (6.6)) following the generalized phase law of reflection.	115
6.33	Optimized Super-cell after tuning the patches to the proper reactive surface impedance of dimensions d_y (given in table (6.6)).	116
6.34	Phase of the reflection coefficient with respect to the patch dimensions d_y in mm for a given frequency at 14.7 GHz	116
6.35	a) Metasurface design using Ansys HFSS of 5×4 nominal super-cells b) Metasurface design of 5×4 optimized super-cells	117
6.36	Normalized Monostatic RCS of the optimized metasurface (Figure 6.35b) after implementation of the impedance modulation compared to that of the nominal design (Figure 6.35a) following the generalized phase law of reflection operating at 14.7 GHz and of similar dimensions $5.1 \text{ cm} \times 23.5 \text{ cm}$	118

6.37	Monostatic RCS (dB) of the optimized metasurface design(Figure 6.35b) compared to that of flat metallic plate with respect to the given incident angles at 14.7 GHz of similar dimensions $5.1 \text{ cm} \times 23.5 \text{ cm}$	119
6.38	Unit cell dolmen structure of 3 elements, two sub-radiant modes in the x-direction of dimensions L_1 and W_1 , and one super-radiant mode in the y-direction of dimensions L_2 and W_2 . With a gap g between the two sub-radiant modes and the super-radiant mode.	120
6.39	Phase of the reflection coefficient with respect to that of Factor X which is multiplied with the dimensions of the sub-radiant modes at 24 GHz.	120
6.40	Metasurface design using the optimized dimensions of 4×3 super-cells, of dimensions $25 \text{ mm} \times 215 \text{ mm}$, with a ground plane and substrate of permittivity $\epsilon_r=2.2$ and thickness 1.6 mm	121
6.41	Monostatic RCS (dB) of the metasurface design in blue compared to a flat metallic plate of similar dimensions in dotted green, when the electric field of plane wave is in the direction of the sub-radiant modes (x-direction) at 24 GHz	122
6.42	Monostatic RCS (dB) of the metasurface design in blue compared to a flat metallic plate of similar dimensions in dotted green, when the electric field of plane wave is in the direction of the super-radiant mode (y-direction) at 24 GHz	122
6.43	Realized Metasurface prototype of 10×7 super cells of dimensions $10.2 \text{ cm} \times 41.125 \text{ cm}$	123
6.44	Normalized Monostatic RCS (dB10norm) with respect to the incident angles of the simulation results compared to that of the measurements at 14.7 GHz for the optimized metasurface.	123
7.1	Spiral structure design with the given dimensions printed on top of a substrate with a via connecting the inclusion to the ground plane.	128
7.2	Simulation Results of the reflection coefficient S_{11} (dB) with respect to frequency(MHz) using Ansys HFSS.	128
7.3	Real $\text{Re}(Z_s)$ and Imaginary $\text{Im}(Z_s)$ parts of the surface impedance Z_s of the spiral metamaterial design with respect to frequency(MHz)	129
7.4	Absorption rate of the spiral design with respect to frequency(MHz)	129
7.5	Impedance Z of the load resistance real and imaginary parts in Ohms with respect to frequency(MHz).	130
7.6	Reflection coefficient S_{11} (dB) from the load side of the design structure.	130
7.7	Power efficiency of the energy dissipated through the given load resistor with respect to frequency (MHz).	131
7.8	a) Coil spiral structure of 12 turns, width w and gap g ; b) Side view of the proposed design	132
7.9	Unit cell design of the metamaterial structure with the direction of the electric field E and magnetic field H	132
7.10	Reflection coefficient of the proposed design S_{11} in dB with respect to frequency (MHz)	132
7.11	Absorption rate of the proposed design with respect to frequency (MHz)	133
7.12	Metasurface design of 6×6 unit cell structures of dimensions $48 \text{ cm} \times 48 \text{ cm}$ and thickness 61.6 mm consisting of an FR4 substrate of thickness 1.6 mm and $\epsilon=4.4$ and an air of thickness 60 mm , as well as load resistance of 282Ω connected to each unit cell end part.	134
7.13	Power Efficiency % of the absorbed energy across the 282Ω Load Resistance.	134
7.14	Full wave rectification energy harvesting system along side the metasurface design.	135
7.15	Summary of the conclusion of part two on metasurfaces.	136
7.16	a) Active unit cell structure. b) Picture of the fabricated unit cell. c)An EM simulation model with nine cascaded unit cells. [43]	140
7.17	a) Illustration of the active metasurface design. b) Fabricated metasurface design. [44]	141

7.18 Smart radio environments: communications. [45] 141

Abbreviations

EH	E nergy H arvesting
IoT	I nternet O f T hings
GSM	G lobal S ystem for M obile C ommunications
EM	E lectro M agnetic
EMC	E lectro M agnetic C ompatibility
RF	R adio F requency
HTN	H ybrid T echnology N etworking
WSN	W ireless S ensor N etwork
WPT	W ireless P ower T ransfer
MMR	M echanical M otion R ectifier
DC	D irect C urrent
PV	P hoto V oltaic
DAC	D ata A cquisition C ontrol
PVDF	P oly V inyl-dene F luoride
GSM-R	G lobal S ystem for M obile C ommunications R ailway
AC	A lternating C urrent
WEH	W ireless E nergy H arvesting
DTV	D igital T elevision
3G	T hird G eneration
5G	F ifth G eneration
6G	S ixth G eneration
RFID	R adio F requency I dentification
NFC	N ear F ield C ommunication
HF	H igh F requency
HB	H armonic B alance
ELC	E lectric I nductive C apacitive
FSS	F requency S elective S urfaces
Q-factor	Q uality-factor
RCS	R adar C ross S ection
RWG	R ao W ilton G lisson
TE	T ransverse E lectric
TM	T ransverse M agnetic
Z_s	S urface I mpedance
VNA	V ector N etwork A nalyzer
CMIARM	C ascaded M ultiple I ncident A ngle R etrodirective M etasurface

General Introduction to Thesis Work

The growing popularity and increasing number of smart systems and devices, has been remarkable in the past few years creating lot of opportunities to solve different challenges and problems in the field of health structure monitoring, automobile tracking, communication systems, biomedical, transport, safety applications, environmental data gathering and many more. Recently, researchers have shown significant interest in smart devices and their applications such as IoT systems, WSNs and 5G communication devices. These systems and their significant number of use cases, can bring various benefits and enhance the performances of applications and technological devices.

Railway transportation has been a major and popular way of transport in many countries worldwide in the history of the transport industry. This is mainly due to its social, economical and energy efficient aspects, also its well known characteristics of low carbon mode, safety and resource efficient transport mode. With the rise of smart devices and communication systems, the need for the implementation of such devices in the railway industry for smart railway systems can be beneficial for more reliable, secure and enhanced maintenance of railway systems. Smart railway systems can be achieved by the deployment of IoT, WSNs and 5G communication systems. However, such technologies require low input power supply which can be a challenge for compact systems. Energy harvesting and wireless power transfer systems can be a key solution and key to enable autonomous and compact smart systems, specially with various energy sources that can exist in the railway environment.

Indeed, the railway environment is well-known for various sources of energy which can be considered for energy harvesting and supply of low input power devices. Many devices have been developed and deployed in the railway industry based on sources such as vibration [46, 47], acoustics [12], wind [48] and solar energy sources [11]. In the field of electromagnetic energy harvesting less harvesting technologies have been developed specially for the railway application [9, 10, 49], where most technologies are based on mechanical vibrations on railway tracks. However, in electromagnetics a high level of electromagnetic energy is present; it has been experimentally observed by Marc Heddebaut et al. [13] for frequencies as high as the microwave region, which has also been provided by SNCF Reseau. Moreover according to the EMC standard EN 50121-3-1 [14] for EM emission limits in the railway environment a high level of electromagnetic energy can exist at a wideband of frequency from 10 kHz up to 1 GHz. Different energy harvesting systems based on rectenna devices have been developed and designed, specially at RF frequencies such as 2.4 GHz [20, 21]. To propose

the design of rectenna systems for applications such as railways, can be a challenge due to its low efficiency and incompatibility at low frequencies.

Many researchers have worked on the enhancement of the antenna efficiency to increase the level of power harvested [41, 50, 51]. Although this method can be a possibility, but some limitations and challenges can still occur specially in the railway environment in terms of low ambient energy efficiency and dimensions at low microwave frequencies. In this work, our aim focuses on introducing and defining novel concepts to enhance the performances of EM energy harvesting and wireless power transfer systems, based on metamaterial and metasurface designs, in which they can be a compatible solution to existing technologies, where we can overcome the challenges and limitations for a compatible device for the railway application.

Metasurfaces [52] are the subject of intensive research nowadays for their applicative potential and the generality of their design approach [53]. They are characterized by their 2D subwavelength structure and their ability to control the wavefront of an electromagnetic wave [54, 55] with perfect, abnormal and achromatic reflections [56, 57]. Metasurfaces, being two-dimensional materials, can be easily implemented into and along side other devices [58, 59], which can be very useful in different applications. Their simplicity of design and fabrication can make them very attractive compared to 3D metamaterial structures specially in the microwave region. They are well known for their variety of characteristics and utilization in terms of application and wave control manipulation [60, 61]. The control of the reflection phase [62] of an incoming incident wave has been significant for metasurfaces following the generalized phase law [27, 63] in different sectors. With the control of the reflection phase, metasurfaces have been used as ultra thin polarization transformers [64, 65], wave front manipulation such as beam shaping [66], beam splitting [67], focusing [68], retro-reflection [69, 70], de-focusing [71], reflection and refraction. Moreover, metasurfaces based on absorption [72–74], have shown significant potential over conventional absorbers, in terms of miniaturization, efficiency, absorption bandwidth, polarization insensitivity and wider allowable incident angles. Following this concept for metasurface absorbers, metasurface energy harvesters arised, where TS Almoneef *et al.* [75–78] introduced the concept of energy conversion from electromagnetic to DC electric energy, using high efficient metasurface absorbers, and introducing a via for energy dissipation.

This work and thesis is in the framework of SNCF Reseau, france. The proposed application is under investigation by the company for future potential to use and benefit from electromagnetic energy in the railway infrastructure, for more reliable and smart railway systems. The project is also co-financed by the “*European Union with the European Regional Development Fund*”.

Objective of the Thesis

The aim of this thesis is to address the challenges and enhance the performances of EM energy harvesting and WPT systems, which can be associated and compatible for the application to low-input-power systems in the railway environment. Indeed a convenient concept and approach is needed, in order to introduce novelty and mature technology for the proposed application. In this work, we focus on the use of metasurface designs with their remarkable physical properties, to be a complementary solution to enhance the performances of existing EM Energy harvesting (EH) and WPT systems.

Various energy harvesting and wireless power transfer systems have been developed and implemented by many researchers in the past years for application in the railway environment. With the rise of

smart railway systems and subsystems using IoT and Wireless sensor network (WSN) devices, the power supply of such devices using renewable energy in the railway system has been a subject of research and development such that autonomous systems are enabled. The railway infrastructure is well known for its rich environment with different sources such as vibrations, sound energy, wind, solar and electromagnetic fields, which can be considered for harvesting and for the power supply of low-input-power devices. However, most existing harvesting technologies in the literature for such applications are based on vibration [46,47], acoustics [12], wind [48] and solar energy sources [11]. To date no mature technology in terms of electromagnetics has been introduced for railway applications. Measurements of electromagnetic energy in the railway environment, have been introduced in the literature [13] and provided by SNCF Reseau. The results have shown the potential of these sources which can be beneficial in terms of energy harvesting.

However, several challenges need to be addressed to overcome the limitations of EM EH and WPT systems in the railway applications. Some of those include: low surface and radiation efficiencies of rectenna systems and antenna receivers, large dimensions at low microwave frequencies and line of sight for WPT devices. We propose to focus on the use of metasurfaces with their exceptional physical properties, to enhance the performances and as a complementary solution to existing EM EH and WPT devices, and overcome the challenges and limitations for the railway application.

Indeed, metasurfaces and their remarkable physical properties, can be used as a solution for performance enhancement in our application. In our work, we investigate the potential of metasurfaces in terms of focusing, absorption and anomalous reflection to overcome the challenges introduced for EM EH and WPT technologies that can arise in the railway environment. A summary of our aim and aspect is given in Figure 1.

In terms of EM EH systems we introduce and investigate the potential of a novel concept to enhance the performance of rectenna systems based on focusing metasurfaces. The concept is defined by introducing a well designed miniaturized high efficient focusing metasurface following the hyperboloidal profile of the generalized phase law. The metasurface in theory can overcome the scattering of ambient EM energy in the environment where the energy in the far-field is focused at one point at a certain distance from the metasurface. A rectenna system can then be implemented at the focal point where the energy is harvested. This solution can overcome the challenge of scattered ambient energy and low efficiency performances of rectenna devices in such environments. At low microwave frequencies for the railway application, efficiency and implementation of a compact EH system can be a challenge. In [75–78] the concept of metasurface energy harvesters based on absorption is given. This solution is also proposed and can be interesting specially for low microwave frequencies in the railway environment. Metamaterial absorbing subwavelength inclusions can be used to overcome the challenge of miniaturization and efficiency for our application.

An alternative solution for power supply can be wireless power transfer. However, the main challenge specially for railway applications, is line of sight where tracking and localization can be poor specially for moving trains from the angular aspect. Backscattering engineered surfaces have shown remarkable results in terms of detection enhancement for different systems. Metasurfaces are well known for their high efficiency in terms of anomalous reflection. Retrodirectivity is defined in which a wave is re-directed back in the same direction. Following the generalized phase law of reflection, one can design a gradient metasurface which can perform retro-reflection at an oblique incident angle. The challenge is to design passive metasurfaces which can perform retro-reflection for multiple incident angles simultaneously. We propose two different approaches to achieve multi-angle retrodirective metasurfaces based on cascading and surface impedance modulation.

With the collaboration of SNCF Reseau in this work, our aim is to demonstrate, test and implement the potential of one of our concepts in the railway environment and investigate its potential in terms of EM energy harvesting. We propose to test our concept based on focusing metasurfaces on site and study its potential specially for the challenge to overcome the low efficiency of ambient EM energy harvesting.

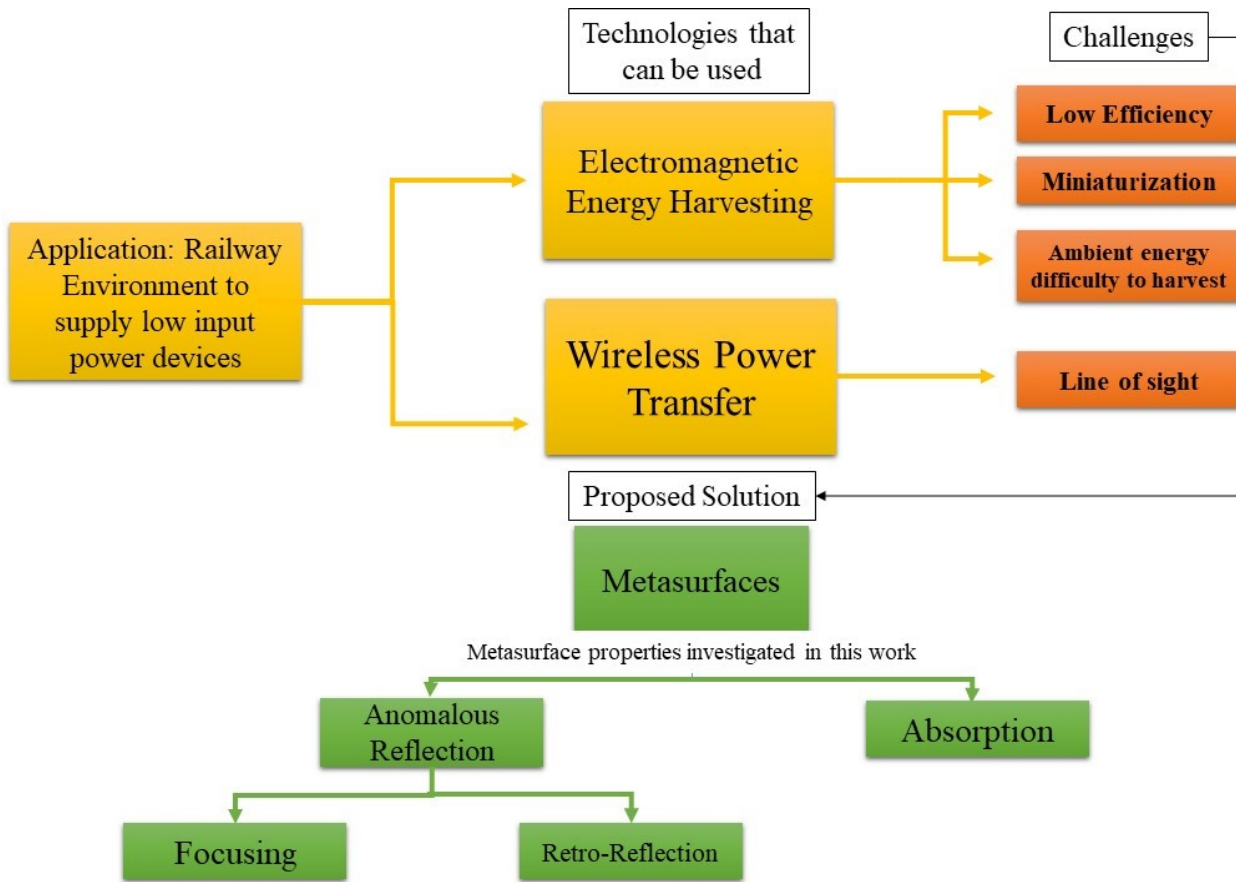


Figure 1: Application to supply low input power devices in the railway environment using EM energy harvesting technologies and WPT. Challenges and proposed solution using the physical properties of metasurfaces.

Organisation of the dissertation

In chapter 1, an overview is given on existing technologies for energy harvesting and wireless power transfer that have been developed and deployed in the railway environment. We also highlight how the railway system can be a rich environment with various sources for energy harvesting from vibrations, solar, acoustics, piezoelectric, wind and electromagnetic. Thus, with the rise of smart railway systems using IoT, WSN and 5G communication devices, one can take advantage of the various sources present to enable autonomous devices. We also highlight the potential of EM energy in the railway environment, by providing different measurements carried on in the literature and by SNCF reseau.

In chapter 2, following the overview in chapter 1, we can notice that to date, no mature EM energy harvesting system has been introduced for railway applications. Thus, we focus on electromagnetic energy from using existing WPT to WEH technologies. We explain how WPT system works and the applications where it can be useful, as well as the challenges that may arise. Ambient EM energy is also introduced, and a study by the Imperial Colledge in London for calculating the energy in the environment is introduced. Various EM energy harvesting technologies are introduced from

commercial products and radiators already existing. The main application is the implementation of such systems and technologies from WPT or WEH in the railway environment. Thus, we introduce the use cases for such devices and how they can be implemented and used.

In chapter 3, many challenges for EM EH and WPT systems can arise specially for the railway application. We propose and investigate the potential of metasurfaces as a solution to overcome these challenges and their ability to enhance their performances. Thus, in this chapter, we focus mainly on three properties of metasurfaces which can be beneficial for our application which are: focusing, anomalous reflection and absorption. We give a brief overview of the concept of the generalized phase law of reflection and refraction for phase control and design of metasurfaces. We also show different designs and research studies that have been developed over the years for metasurfaces in terms of wave reflection manipulation, absorption and focusing.

In chapter 4, we propose a novel concept to enhance the efficiency and performances of existing EM energy harvesting rectenna systems, based on focusing metasurfaces. we discuss a few relevant inventions and publications concerning rectenna devices and their disadvantages and the problem we can overcome using our system. We discuss in details the main concept, principle of operation and design procedure. The objective of the concept is to propose a solution to low efficiency and to increase the level of power collected by RF energy harvesting systems through the use of a focusing metasurface of given dimension with respect to frequencies of the ambient EM energy. We will also show how this device can be used with in addition to existing commercial off-the-shelf harvesting systems. Measurements have been carried on and a prototype has been fabricated and the concept has been tested and validated in an anechoic chamber.

In chapter 5, we implement and test our proposed concept on site using the focusing technique for EM ambient energy harvesting in the railway environment. The measurements were carried on in collaboration with SNCF Réseau in Paris. The measurements and EM energy harvesting were based on the use case of the GSM-R system present in the railway environment. We implemented the system at a far distance in the far-field to determine the potential of our system in terms of EM harvesting and the power present. When using the focusing concept with the metasurface along side the rectenna , the system has shown remarkable results in terms of enhancing the power received by the commercialized rectenna system compared to that when implemented alone. The harvesting system was able to receive 10W when implemented along side the focusing metasurface compared to that of 1 nW when using the rectenna alone, which can be an interesting result to supply low input WSNs where such power is needed to wake up and function the device.

In chapter 6, for alternative technologies to supply power such as WPT, we focus on introducing novel concepts for the design of efficient multi-angle retrodirective metasurfaces, to overcome the challenges such as line of sight. This work was published in journals and presented at different IEEE conferences. Concepts are given from technical based on superposition [69] to physical based on impedance modulation [70] and fano-resonance [79]. Prototypes and measurements have been carried out to validate the concept and results. From the applicative point of view, retrodirective metasurfaces proposed in this case, can be very useful for tracking enhancement performances in WPT for IOT devices, sensing and radar systems.

In chapter 7, other solutions using metasurface designs are proposed for EM energy harvesting that can be interesting to overcome challenges for the railway application. In this chapter, metasurface energy harvesters are given based on absorption at low microwave frequencies. This solution can be interesting to overcome the challenges of miniaturization and low efficiency specially at we investigate the potential of metamaterial energy harvesters based on absorption in terms of efficiency and miniaturization, with designs at a single frequency and multi-band frequencies.

The conclusion and future work provides a summary of the findings in this thesis, the limitations of the proposed designs and concepts discussed, as well as future perspectives of the thesis work are presented.

Part I

State of the art on energy harvesting in Railway environment

Introduction

The growth and development of the railway network has been a demanding research topic in the past years for many companies around the globe. Railway transportation has become an essential method of transport between regions for many people around the world, this specially due to its safety, economical value, low carbon mode, resource efficient transport mode and environmental friendly. Moreover, the enhancement and growth of the railway environment is essential specially with the rise of different smart technologies such as IoT, wireless sensor networks (WSN) and 5G communication systems. These technologies can help enhance the reliability, security and maintenance and give rise to smart railway systems. However, the need of power supply for systems such as WSN or IoT devices on the railway system can be a challenge, specially to enable autonomous and more reliable systems for implementation and deployment. The railway environment is said to be rich with various energy sources from vibrations, wind, acoustics, solar and electromagnetic that can be beneficial to supply such low power input devices.

In this part, we do an overview on the various existing energy harvesting and wireless power transfer technologies that have been developed and deployed over the past decade in the railway infrastructure. However, most technologies were based on vibration, acoustics and solar energy sources. Moreover, for WPT, different technologies were introduced based on inductive systems for power electric charging in the railway infrastructure. A summary is also given for the different EH technologies and the advantages and disadvantages that can arise. In terms of EM energy sources in the railway environment, recent measurements observed in the literature are highlighted, whereas other measurements provided by SNCF Reseau are given. The results have shown a high potential of power which can be beneficial and interesting to investigate in terms of harvesting, since to date no mature technology for such application for the given sources has been introduced.

Limitations and different challenges can arise for such technologies for the given application. Therefore, in chapter 2, we investigate and study existing technologies given in the literature and commercial sector, for different methods and methodologies for rectenna systems, EM energy harvesting and WPT systems. We also go through the developments that have been rising in the history of wireless technology. We explain how WPT system works and the applications where it can be useful, as well as the challenges that may arise. Ambient EM energy is also introduced, and a study by the Imperial Colledge in London for calculating the energy in the environment is given. Various EM energy harvesting technologies are introduced from commercial products and radiators already existing. The main application is the implementation of such systems and technologies from WPT or WEH in the railway environment.

Finally, the use cases of such technologies and how they can be deployed in the railway system are defined. Different use cases from implementation in railway tunnels, interaction occuring in the railway environment, GSM-R systems and the rise of smart railway systems using IoT and WSNs.

Chapter 1

Energy Harvesting and Wireless Power Transfer Systems in The Railway Environment

1.1 Introduction

Energy harvesting is the concept where energy is derived from ambient sources of energy in the environment where it is converted and stored as electric power [15, 80, 81]. Different sources of energy can exist in the environment which can vary from solar [82–84], wind [85–87], hydro and ocean energy [88–91], to electromagnetic [92–94], electrostatic, heat [95–97], thermal variations [98, 99] and mechanical vibrations [46, 47], where one can have advantages and disadvantages over the other depending on the application, cost and environment [100]. The main aim of advanced energy harvesting technologies is to power low energy electronics such as wireless power sensors without the need of batteries [101, 102].

Nowadays, energy harvesting in the railway environment has become an interesting topic for researchers [1, 8–10, 49, 103–112] with a gain of popularity for railway transportation systems. This is mainly for the railway industry requirements for electric power supply such as GSM communication systems, light signals, health monitoring, switching machines and specially with rise of smart railways using wireless sensor nodes and IOT devices, where energy harvesting can be a key solution for more autonomous, reliable and feasible system [1] (Figure 1.1). Several low power energy harvesting systems have been developed and deployed in the railway environment based on existing sources in the railway infrastructure from mechanical vibrations, wind, solar, thermal, disturbances and electromagnetic fields (Figure 1.2). The interest is supplying low power to feed sensors in wireless sensor networks which are deployed for instance for railway health monitoring thus reducing maintenance, inspection costs and constraints [2, 3, 113–116]. Many devices typically have been implemented in several research projects [117] with different energy generation goals.

Several types of energy harvesting technologies have been developed and deployed; they are popular in railway applications due to the fact that they are based on mature technologies and that the



Figure 1.1: Electric power supply needed for different devices in the railway system. [1]

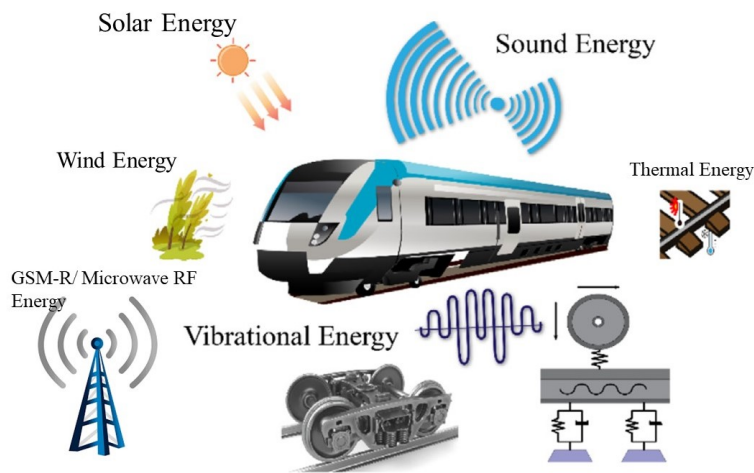


Figure 1.2: Sources of energy in the railway environment. [1]

sources present have a sufficiently high amplitude to yield the required power for feeding sensors or devices. Some of the harvesters that we can mention can vary from piezoelectric energy harvesting systems [7,118–121] to electromagnetic [89,93,109,122–124], wind energy harvesting systems [111] and solar based energy harvesting technologies for railways [11,112]. The sources present in the railway environment can vary which can have disadvantages and advantages depending on the interest of study and applications [125].

Piezoelectric harvesting systems have been developed to harvest mechanical vibrations and pressure induced by moving trains to the rail and convert it to electrical power [1,105,121,126–129]. Piezoelectric components can be made from different materials: crystal, piezoceramics, thin films, screen printable thick films based on piezoceramics and polymeric materials [130–133]. In terms of solar based energy harvesting technologies in the railway environment, a practical implementation of a solar based system for monitoring and analysis system for solar photo voltaic terrestrial vehicles has been developed in the indian railways [11,112]. The objective was to use renewable energy to decrease the use of fossil fuels and emission of carbon dioxide which causes global warming. Although

solar based energy harvesting systems might be practical but they can have some disadvantages since they depend on several factors such as sunshine hours, solar isolation, climatic conditions, speed of the train, travelling direction ...etc.

In the field of electromagnetic energy harvesting less electromagnetic energy harvesting technologies have been developed specially for the railway application [9, 9, 10, 49, 92, 109, 122], where most technologies were based on mechanical vibrations on railway tracks. However, in electromagnetics a high level of electromagnetic energy is present; it has been experimentally observed recently by Marc Heddebaut et al. [13] for frequencies as high as the microwave region. Moreover according to the EMC standard EN 50121-3-1 [14] for EM emission limits in the railway environment a high level of electromagnetic energy can exist at a wideband of frequency from 10 kHz up to 1 GHz. Different energy harvesting systems based on rectenna energy harvesting systems have been developed and designs specially at RF and 2.4 GHz [20–22, 134–137]. To propose the design of rectenna system for applications such as railways can be a challenge due to its low efficiency and incompatibility at low frequencies.

In this chapter, we show the existing technologies for energy harvesting in railway environments that have been developed and deployed. Researchers have implemented different systems based on various sources of energy. We show in this chapter energy harvesting technologies based on various sources of energy from piezoelectric, solar, wind to electromagnetic (EM) energy. In terms of EM energy, we introduce the potential sources that can exist and different measurements that have been carried on in the literature and provided to us by SNCF reseau.

1.2 Application: Power-autonomous Wireless power sensor nodes

Wireless sensor networks have been a focus of research in the freight railroad industry to enable on-board real time sensing of critical railcar parameters [2, 3, 113, 113–115]. Important railcar aspects like wheel bearing temperature, air pressure, brake failure, and the integrity of transported goods can then be monitored closely and reliably. This enables immediate preventive actions in case of impending failures and also enables trend analysis that can be used to fine tune maintenance efforts on railcars. These increase the safety, efficiency, and dependability of railroad operations. Sushanta Mohan Rakshit et al. and John Punwani et al. [2] presented the detail measurements of Hybrid Technology Networking(HTN) to determine the energy consumed by HTNMote in various operational situations that are encountered during their operations onboard freight tailcars. Figure 1.3 gives an architectural overview of the system that was tested. There are several HTNMotes acting as sensor nodes that sense and report to the cluster gateway via low-power radio wireless link. The cluster gateways relay this information towards the HTNMote in the locomotive via WiFi links. Several such clusters span the entire length of the freight train.

Thus, wireless sensor networks (WSN) have been gaining popularity with its rapid and robust assessment of structural integrity. With the recent advances in ambient energy harvesting technologies, alternative sources of energy for powering WSN can be viable. WSNs powered by ambient energy harvesting are potentially more useful and economical in the long term than traditional battery powered WSNs as they can operate for very long periods of time without the need for human involvement and paving the way towards alleviating energy constraints that continue to challenge WSNs. An example of a system model of a wireless sensor network implemented for railroad health monitoring is shown in Figure 1.4.

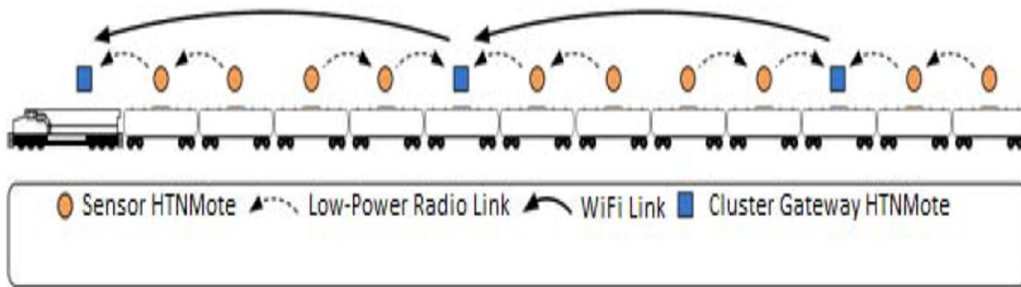


Figure 1.3: Architecture Diagram of the system under test. [2]

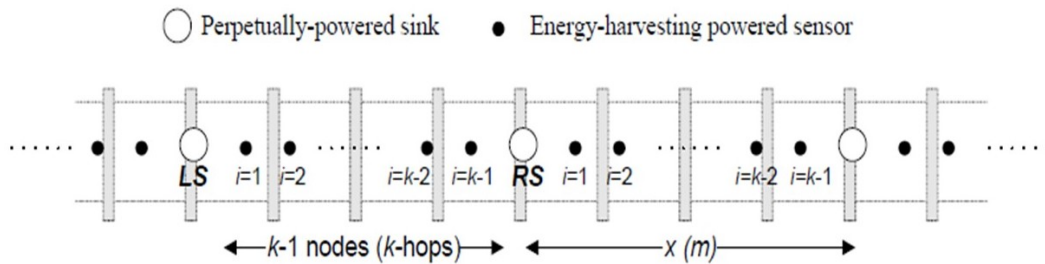


Figure 1.4: System model of wireless sensor nodes implemented along a railway track using sinks powered by AC supply and Energy harvesting power sensors. [3]

The sinks/gateways are placed at fixed intervals (x) along the railway track. These sinks form the interface between the energy harvesting powered sensors and the outside world. Over the interval between each pair of sinks, $k-1$ sensor nodes are deployed. The components of the wireless sensor nodes are shown in Figure 1.5a. The energy harvesting device converts ambient energy into electrical, where the harvested energy is stored continually in a supercapacitor with unlimited recharging cycles. Once the stored energy reaches a useful level, the energy consumers draw power to carry out the operation.

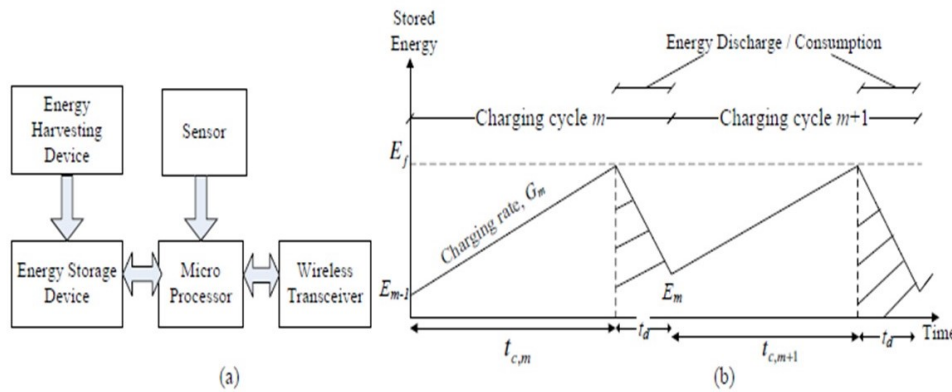


Figure 1.5: a) Components and b) energy model of a wireless sensor node powered by an energy harvester. [3]

Each wireless sensor node is configured to communicate directly with the sink, and define a simple

energy model as shown in Figure 1.5b. Each charging cycle m comprises a charging phase, characterised by a charging rate G_m and full energy level E_f . The charging time in the cycle m (t_{c_m}) depends on E_f and the characteristics of G_m . E_m represents the residual energy. For more details regarding the analysis and simulations for the given system model refer to the reference. [3]

1.3 IOT for Railways

Railways over the past years have been playing an important role in the sector of transportation. However, many challenges and issues have been rising specially those concerning safety, maintenance and giving rise to smart systems to follow up and be up to date in terms of technologies. Nowadays, many believe that by combining railway systems with IOT technologies, can allow communication, exchange of information and give rise to smart railway infrastructure [138–142]. From a technical point of view, IoT technology [143] has two parts, which are the detection and processing phases. For the detection sector, various sensors and devices collect information relating to things and equipment such as railways, trains and other infrastructure. During the access stage, the data collected to objects can be efficiently transmitted to IoT platforms using various IoT access technologies without effort. Then, the platform analyzes the data and takes a processing phase. Hence, with IOT technologies, this can give rise to the deployment of intelligent railway infrastructure. Figure 1.6 shows the overall proposed architecture of an IOT solution for smart railways [4].

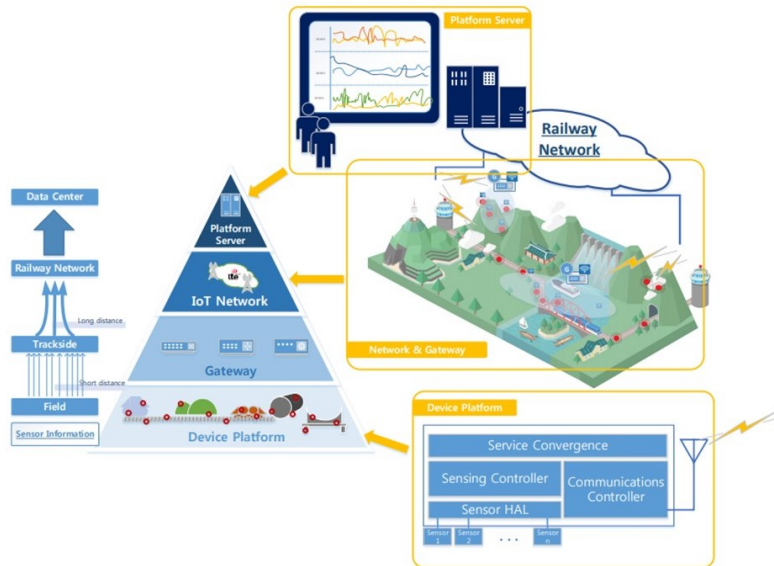


Figure 1.6: Overall Proposed Architecture of an IOT solution for Smart Railways [4].

The proposed architecture shows the efficient distribution of information around the IOT platform in the railway infrastructure. However, IOT systems can be of great potential for smart railway infrastructure, but the important part is to have an autonomous and reliable system for better implementation. In order to supply IOT devices on the railway track in a reliable manner, different solutions can be used. With the rise of wireless power transfer and energy harvesting technologies, and the great potential of different sources found in the railway environment, these technologies can be remarkable for the deployment and supplying autonomous IOT technologies.

1.4 Wireless Power Transfer in the Railway Environment

Wireless power transfer (WPT) is a rising technology which is mainly defined as the transmission of power without connecting wires [144, 145]. It has been a significant research topic over the years for different applications, specially in reducing toxic materials such as batteries and wires, and has always been interesting for the built of mature wireless power technologies [146, 147]. WPT can be classified as radiative [148–150] and non-radiative [151] depending on the system and technology used. For non-radiative WPT systems, near field (short range and mid ranges), the method of power transfer usually used can be based on inductive [152, 153] or capacitive coupling [154]. The efficiency of these systems can be high up to 95%, but with some drawbacks such as interaction with human bodies for some applications and the need of a large coupling area. However, for radiative WPT systems, far field wireless power supply, the methods carried on include basically microwave/RF technologies or laser photo electricity [155–158]. These systems can be useful for transfer of power at far distance for low power input devices such as IOT devices or wireless sensor nodes, but challenges can also occur regarding line of sight adjustments and directivity towards the fed device.

Railway systems have been known for their conventional power feeding systems using the catenary and pantograph feeding methods. However, WPT technologies are being developed in the railway systems, where research studies are being introduced for different applications [5, 159–163]. The employment of WPT systems for high speed trains (Figure 1.7), can give rise to safety, more convenient and flexible railway infrastructure, solving the problems of traditional supply methods. K Hwang et .al [162] developed a 1 MW WPT system based on inductive coupling for supplying vehicles of the railway without batteries. K Yamamoto et .al [6] from Chiba University Japan introduced the design of a high power contactless transformer for power capacity increasing in the railway environment. Their new design methodology was based for a series-series tuned resonant, large-air-gap, 300-kW, online WPT system for train applications considering efficiency, electromagnetic field radiation, output power and voltage level, and control stability. The proposed model is shown in Figure 1.8.



Figure 1.7: View of high-speed train with WPT system [5].

The high capacity coil transformer model proposed, is installed between the rails to provide power to the railway cars. The power supply of the system was able to achieve a level of 1 KW at an operating frequency of 10 KHz and with an efficiency of 73.8%. However, most WPT technologies in the railway environment proposed are based on inductive and capacitive coupling systems. With the rise of smart railway infrastructure and IOT, it can be interesting to investigate different systems and technologies for low input power supply, based on WPT or alternative solutions such as energy harvesting.

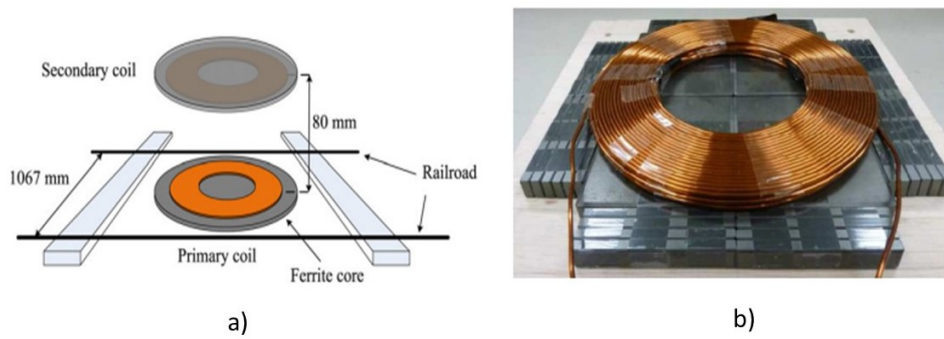


Figure 1.8: a) Proposed transformer for charging on-board battery for a railway system, b) Miniature experimental illustration of coil transformer [6].

1.5 Energy Harvesting in the Railway Environment

1.5.1 Vibration

1.5.1.1 Piezoelectric Technologies

Pierre and Jacques Curie, in 1880, were the first to develop an energy harvesting method from pressure [105]. They experimentally proved that certain crystals can exhibit a surface charge when subjected to mechanical stress. Piezoelectric materials fall within the class of materials which can generate electricity for the applications of pressure or vibrations. They can be made from different materials such as crystal, piezoceramics, thin films and polymeric materials such as polyvinylidene fluoride.

In terms of railway applications, one of those we can mention for energy harvesting technologies which are mostly common are based on piezoelectric technologies. Nelson et al. [7] introduced a piezoelectric system based on crystalline for railway applications. In which the vibration and pressure provided by the train on the rail can be harvested and converted into electricity. The Piezoelectric element and its implementation under the rail and field test are shown in Figure 1.9. They concluded that 0.05 mW is the maximum power that can be generated during every train pass over the rail which is sufficient to supply wireless sensor nodes.

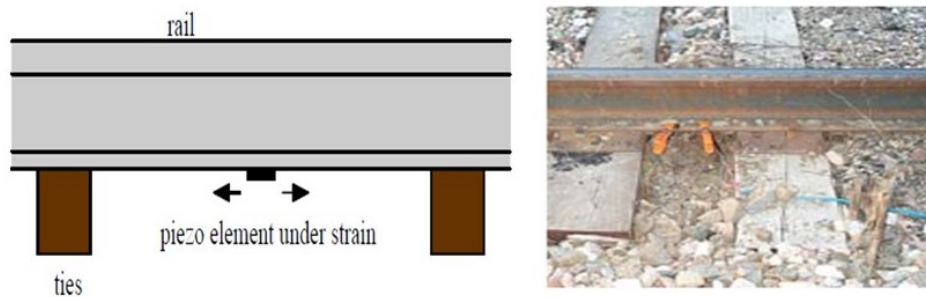


Figure 1.9: Piezoelectric element place under the rail which produces voltage due to strain along its length and the field test where the orange clamps hold the device during glue up. [7]

Other piezoelectric transducers for higher efficiency at low Hz frequencies have also been introduced [118, 126–128]. M.Y.Gao et al [8] introduced a rail-borne piezoelectric transducer for harvesting

vibration in the railway at low frequencies between 5 Hz to 7Hz. The illustration of the rail-borne transducer is given in Figure 1.10. The prototype was capable of small railway vibrations from 0.2 mm to 0.4 mm rail displacement. The output power of 4.9 mW and voltage 22.1 V with a load impedance of 100 kOhms was achieved for a piezoelectric energy harvester of total dimensions 200 mm \times 170 mm \times 80 mm.

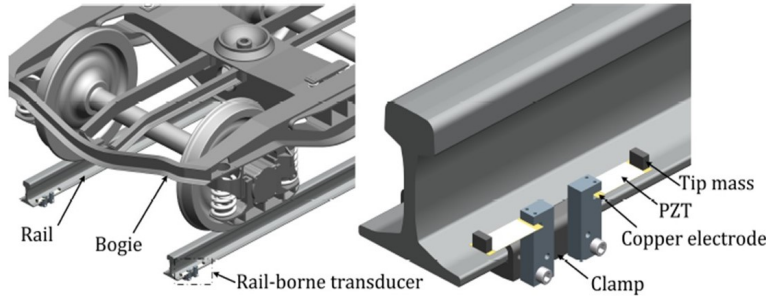


Figure 1.10: Illustration of bogie rail harvester scales(left); enlarged view of clamped cantilevered piezoelectric beam configuration(right). [8]

1.5.1.2 Electromagnetic Technologies Based on Mechanical Vibrations

Electromagnetic generators operate based on electromagnetic induction, known as Faraday's law, which states that when an electric conductor is moved relative to a magnetic field, electric current will be induced in the conductor. These can operate in direct current or alternating current, single phase or three phases. Such generators are mostly used in the big power plants based on both non-renewable sources such as nuclear and thermal, as well as those based on renewable sources such as hydropower plants, wind turbines and even wave energy technologies [80, 105].

In the field of energy harvesting, smaller electromagnetic generators have been developed over the last decade in order to convert ambient energy sources which are mostly based on mechanical vibrations [9, 10, 93, 103, 109, 122, 123]. Electromagnetic generators are different from piezoelectric systems, as they are not actuated directly by the mechanical energy of moving trains. Interfaces are applied to maximise the harvested energy, supply the electromagnetic generators with the appropriate characteristics of mechanical energy, exploit their maximum efficiency, guarantee best performances and protect them from high loads that could incur damage. The harvesting units are based on electro-mechanical systems, hydraulic or pneumatic systems, or micro- electro-mechanical systems.

In terms of railway applications for energy harvesting, some prototypes and designs have been developed based on mechanical vibrations induced by the train on the rail track. An electromagnetic energy harvester for mechanical vibrations has been proposed by S. Bradai *et al.* [9] for traveling trains between two German cities. The proposed design is given in Figure 1.11a.

The design is formed with a mechanical spring where a coil is attached. Magnets are placed inside the coil. The main advantage of this design that it can be placed in a magnetic environment, its compactness and the possibility to tune the resonant frequency by changing the stiffness spring or using an added mass. To ensure the system functionality, two main concepts are used for the converter design. The first is to use a mechanical spring where a coil or magnet is attached and moves relevant to that of the applied excitation (Figure 1.11b). The second is based on the use of magnetic spring principle to transmit the applied vibration. The coil is fixed in this case surrounding

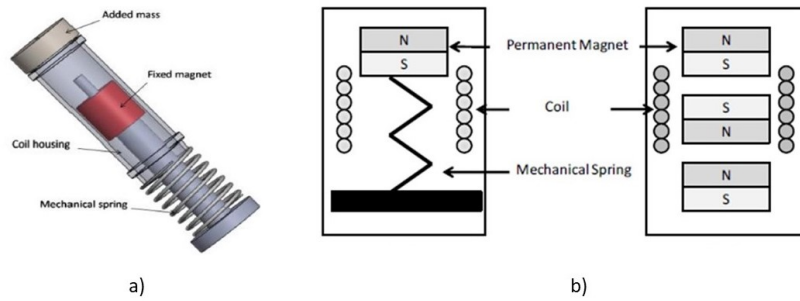


Figure 1.11: a) Proposed mechanical design for the electromagnetic converter. b) Electromagnetic converter architecture based on a mechanical spring and magnetic spring. [9]

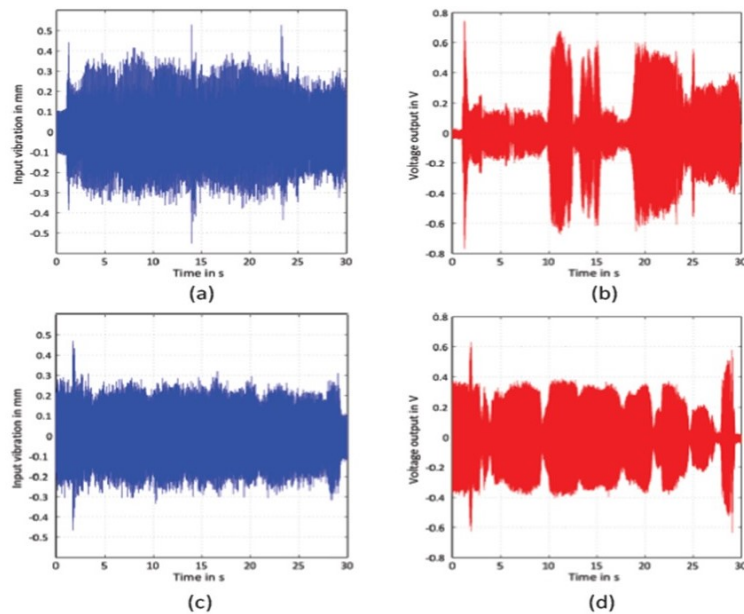


Figure 1.12: a),c) applied random excitation for the converter, b),d) generated voltage from the converter. [9]

the moving magnet from the magnetic spring (Figure 1.11b). The experimental results for the given prototype are given in Figure 1.12.

The measured profiles are characterized by an acceleration amplitude up to 10 m/s^2 and a frequency range between 20 to 40 Hz. Results indicate that a maximum of 1.7 V peak to peak voltage corresponds to a maximum of 10 mW output power which can be reached for specific cycle where the frequency is close to the resonant frequency of the converter.

Other prototypes have been developed for high efficiency and more compact applications for electromagnetic energy harvesting. One of those we can mention was presented by John Wang et al. [10] where they designed a mechanical motion rectifier (MMR) based energy harvester to harvest the

vibrational power from railroad track deflections due to passing trains. The difference between the design and existing topologies is that typical vibration energy harvester technologies are built for low power applications of milliwatts range, whereas they presented a design for higher power applications such as major track-side equipment such as warning signals, switches, and health monitoring systems which require a power supply of 10-100 Watts. The details and the finished MMR prototype are shown in Figure 1.13.

They concluded that the designed prototype shows capability of harvesting 10-50 Watts. It is also able to harvest 28 Watts for very low track oscillations of 1 cm/second. For normal track motion the efficiency was between 45-47%. The mechanical efficiencies ranged between 49% to 71% depending on the type of resistor used and the load pattern on the device. This illustrates features and benefits of the MMR based harvester, which showed reduction of continual system loading, regulation of generator speed, and capability of continuous DC power generation.

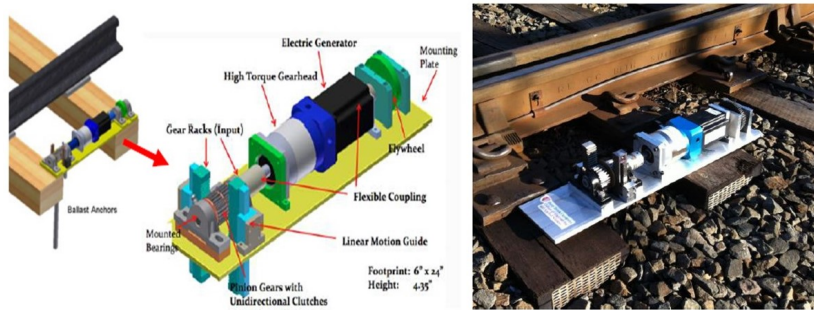


Figure 1.13: On the left we have the drawing of the MMR based harvester prototype and on the right the finished and deployed MMR harvester prototype. [10]

1.5.2 Solar Power

In terms of solar energy harvesting systems in the railway environment, a practical implementation, monitoring and analysis system for solar photovoltaic terrestrial vehicles in Indian scenarios has been tested and deployed [11]. The aim is the use of renewable sources such as solar energy which can be relevant energy to limited fossil fuel to decrease emissions of carbon dioxide and global warming. The project is to serve the proof of concept for a roof top solar energy harvesting system to contribute to the electrical power requirements of Linke Hofmann Busch coaches of a train in the Indian railways. The 3D model of the setup of solar photovoltaic panels is shown in Figure 1.14.

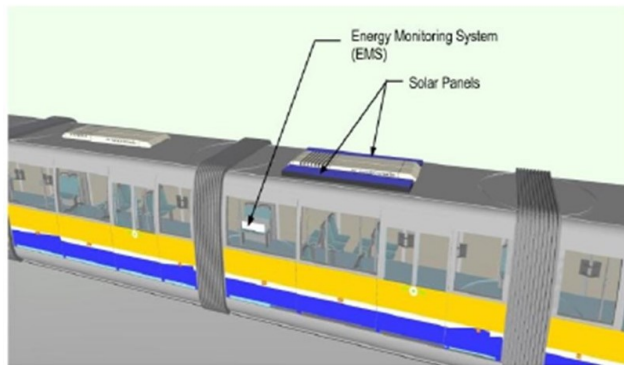


Figure 1.14: 3D schematic of solar Photovoltaic panels on train setup. [11]

The system operation of the solar photovoltaic (PV) system is shown in a schematic diagram in

Figure 1.15. The solar PV modules capture the incident solar radiation, feeding the energy to a charge controller unit that controls the charging battery bank and also powers the sample loads in the coach as shown. The Data Acquisition and Control unit (DAC) is also shown in the block diagram. The system configuration details are shown in Figure 1.16 in the table below.

They concluded that by implementing the solar energy harvesting system on all 63,511 coaches in the railways can enable 450 million units of electrical power to be harvested from solar energy which can result in savings of 11 crore litres of diesel and reduction of carbon dioxide emissions by 3 lakh tonnes every year.

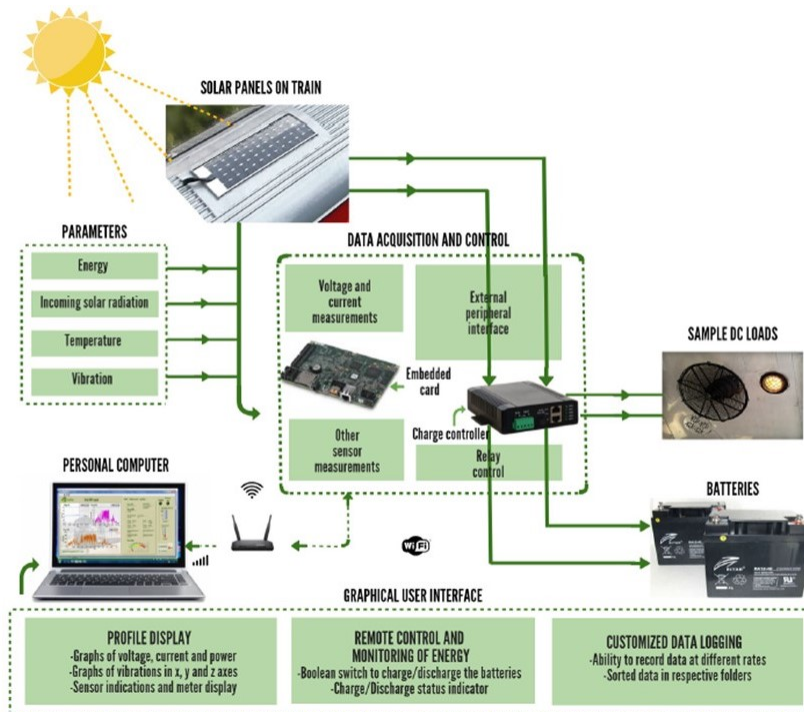


Figure 1.15: 3D schematic of solar Photovoltaic panels on train setup. [11]

Sl. No.	Parameter	Value
1	Solar Panel capacity	380W
2	System Voltage level	24V
3	Net battery current capacity	150Ah
4	Area covered by the panels	1.875m ²

Figure 1.16: Table: System configuration details. [11]

1.5.3 Acoustic Energy

Other energy harvesting technologies have also been addressed based on acoustic high speed train noises at low frequencies. Yuan Wang et al. [12] proposed a novel noise barrier that harvests alter-

native acoustic energy using a Helmholtz resonator and a Poly-vinylidene Fluoride (PVDF) film to achieve noise reduction and electricity generation. The theoretical and prototype model of the proposed Helmholtz resonator is shown in Figure 1.17.

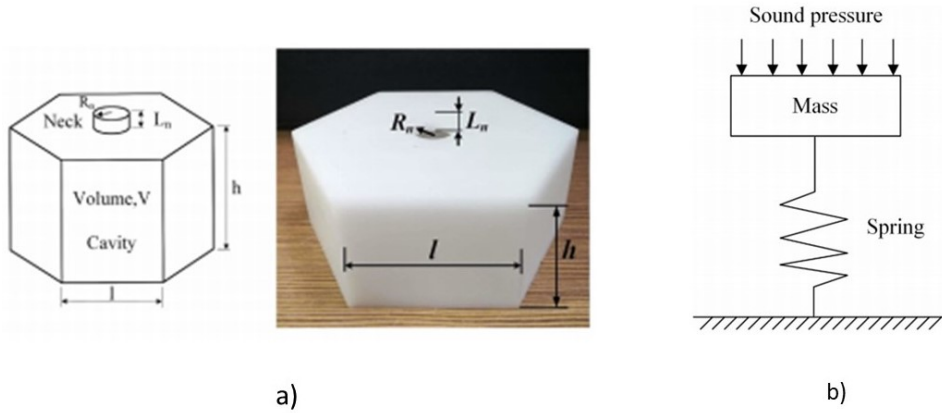


Figure 1.17: a) Model of the Helmholtz resonator. b) The mass-spring model. [12]

The resonator is then connected to a rectifying circuit. The sound incoming by the train puts pressure on the spring within the model. A proposed scenario of the system is given in Figure 1.18.

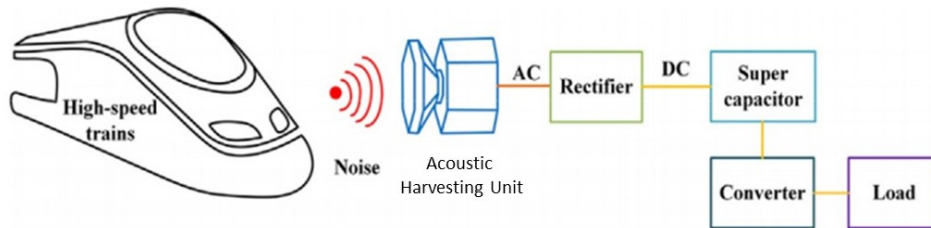


Figure 1.18: Electric circuit and illustration of the acoustic energy harvesting system. [12]

The noise or sound can be regarded as a mass vibrating with the incident sound waves, while the air in the container is expanded and shrunk due to the vibrations of the air through the neck. Then, it can be seen as a spring, and the helmontz rasonator is the same as a mass spring system which is explained in Figure 1.17b.

A prototype of the noise barrier system was fabricated and installed in the high speed railway environment. The prototype and installation are shown in Figure 1.19. The system was installed in a residential area as shown in Figure 1.19b, where it can collect the sound energy from the running high-speed trains, while also reducing the noise to the neighbourhood.

In terms of efficiency, the system was tested in a lab for measurements. The amplification ratio was calculated both for simulation and measurements between 400 and 600 Hz. The results are given in Figure 1.20. The result have shown an amplification ratio between output power and incident power of 18.13% at 440 Hz. Table 1.1 gives a summary from the literature review of some energy harvesting systems in the railway environment based on different sources of energy. It also highlights the efficiency of each system and drawbacks or disadvantages with respect to railway energy harvesting systems.

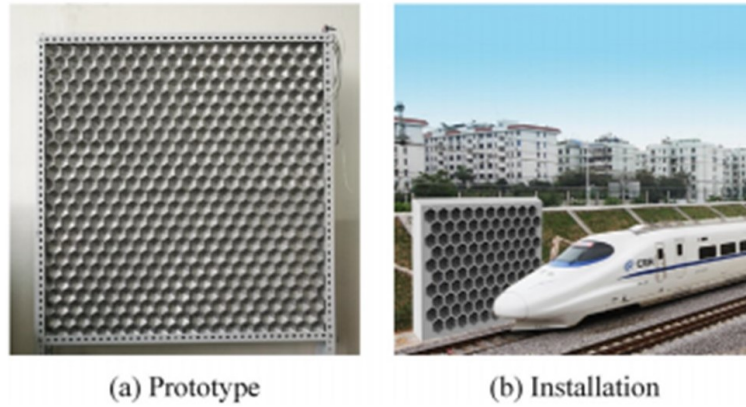


Figure 1.19: Prototype and installation of the noise barrier. [12]

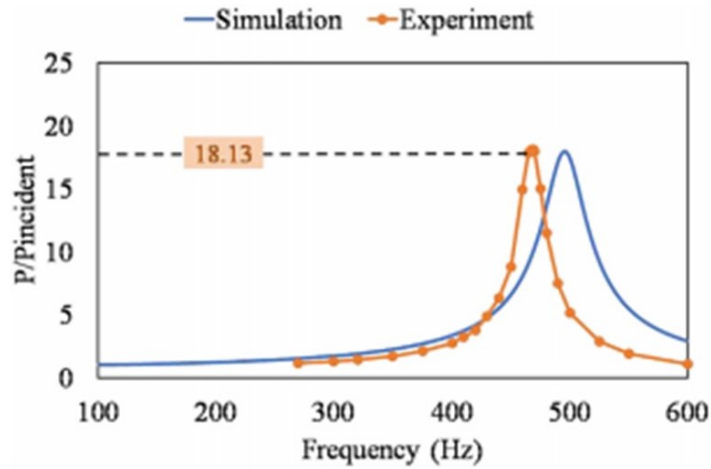

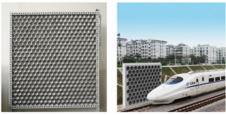
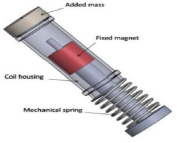
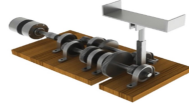
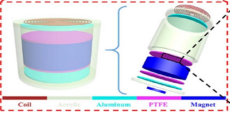
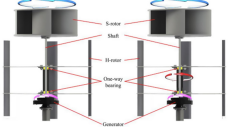
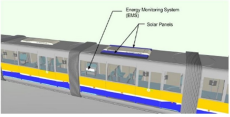


Figure 1.20: The frequency response and amplification ratio for the acoustic energy harvesting system. [12]

Table 1.1: Summary of some energy harvesting systems in the railway environment based on different sources and their efficiency and drawbacks.

Energy Harvesting System	Year	Categories	Efficiency	Drawbacks
 [10]	2013	Vibration Sources	49% to 71% depending on the type of resistor used and the load pattern on the device.	Invasive and close to the system
 [12]	2018	Acoustic Energy	20.8% amplification ratio.	Close to the system and bulky.

 [9]	2018	Vibration Sources	10mW output power at 40 Hz.	Close to the system, easy to break.
 [164]	2016	Vibration Sources	55% output power up to 6.9 W.	Close to the system and invasive.
 [165]	2020	Piezoelectric	Average output power up to 20.9 mW.	Difficult to fabricate.
 [115]	2017	Hybrid Energy Harvesting	0.34 mW/g peak power density.	High cost and difficult to fabricate.
 [48]	2019	Wind Energy Harvester	Max output power 107mW and efficiency 23.2%.	Difficult to fabricate and climate conditions dependant.
 [11]	2015	Solar Energy	380W solar panel capacity.	High cost and not railway specific.

1.6 Electromagnetic Energy Sources in the Railway Environment

The aim is to study the potential EM sources of energy found in the railway environment. A wide-band analysis of the railway catenary line radiation and new applications of its unintentional signals has been observed by Marc Heddebaut *et al.* [13] They observed that the catenary line, connected to the train pantograph through a sliding contact, arcing while transferring electrical power from the catenary line to the train traction chain. Since a huge quantity of electrical energy is transferred through this sliding contact where this phenomenon occurs frequently. In the electromagnetic spectrum, a radiation is emitted whose characteristics are directly linked to the physical phenomenon involved in the generation of electric sparks. Validation and measurements has been performed from 10 kHz to 1 GHz magnetic field noted H, and electric field noted E were performed and recorded along a high speed railway line. An example of a railway infrastructure with a high speed train running is shown in Figure 1.21.

Recently, it has been observed experimentally by Marc Heddebaut et al [13] that high levels of disturbances and electromagnetic sources can exist in the railway environment for frequencies as high as the microwave region. Measurements have been carried out for a passing train at different frequency bands. The configuration setups for the measurements are shown in figures 1.22 and 1.23.



Figure 1.21: Catenary line, pantograph and rail return current to feed the train electrical traction chain. [13]



a)



b)

Figure 1.22: a) Biconical antenna responsive to the polarized electric field for receiving an field component. b) Magnetic loop parallel to the loop catenary wire rail [13].

Figures 1.22a and 1.22b show the antenna setup implemented in the railway. The antennas used are a biconical antenna and a magnetic loop for measurements from 200 Hz up to 300 MHz using the magnetic loop and the biconical antenna for measurements in the microwave region. In Figure 1.23 we see the configuration setup for the analysis and measurements using a vector network analyzer.



Figure 1.23: Configuration of the measurement setup using a vector network analyzer [13]

1.6.1 Measurements

The measurements were carried out at a selected road bridge crossing a high speed line where the equipment were installed overhanging the railway line. Different sensors were used at different band of frequencies, as well as various measurements and results, for more details one can refer to the following reference [13]. Here we show some measurements which are interesting for us in the microwave region. Figure 1.24a shows the measurements in the frequency band between 50 MHz and 300 MHz during the absence of a passing train. The results show very low power levels with a peak of -38 dBm. However, for a passing train, higher levels were detected in the same frequency range with a peak up to -30 dBm.

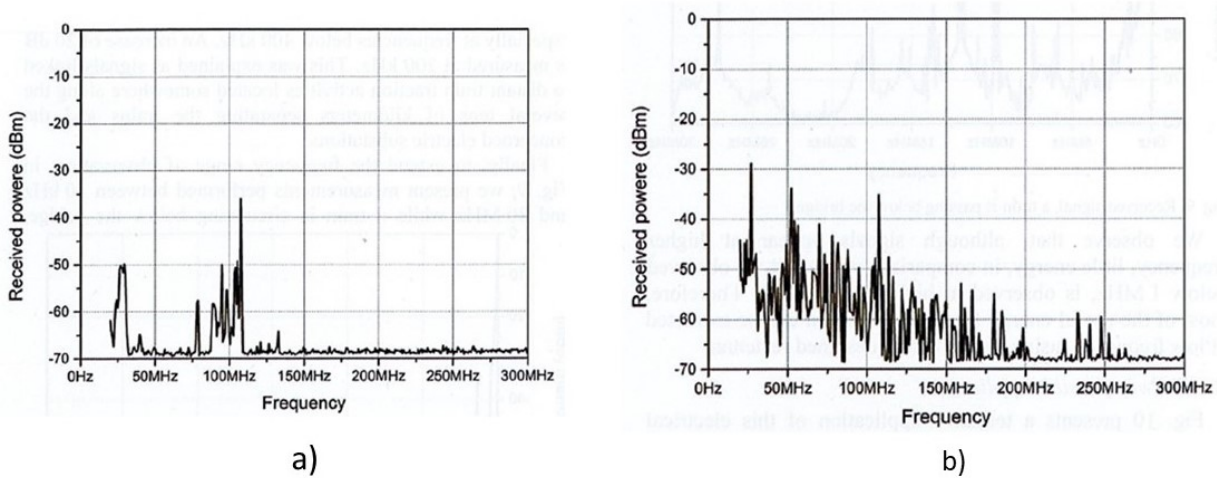


Figure 1.24: Received signal a) during the absence of a train and b) during the passage of a train at frequencies between 9 kHz to 300 MHz. [13]

Moreover according to the EMC standard EN 50121-3-1 [14], for EM emission limits in the railway environment, a high level of electromagnetic energy can exist at a wide band of frequency from 10 kHz to 1 GHz. Figure 1.25 shows the EM emission energy levels in the railway environment for the electric field region and magnetic field region with respect to frequency. It should be noted

that the gap in fields levels in the frequency bands are due to the fact the field is measured using detector with different integration times in each band. The integration time of the detectors are defined based on those present in victim EM devices available at those frequencies. For instance, for higher frequency range, devices considered are telecommunication systems and the integration time is higher resulting in a higher E-field level.

1.6.1.1 Measurements demonstrated in Belfort provided by SNCF

Measurements in terms of electric field energy at a wide band of frequency, have been carried out in Belfort France for the railway infrastructure, and provided by SNCF Reseau. High values have been shown at GSM band frequencies between 800 MHz - 850MHz and 900MHz - 950MHz. These energies are present due to the GSM-R telecommunication systems and base stations found around the railway infrastructure. The other sources of energy present between 400 MHz and 700 MHz can be due to the interactions happening in the railway environment between the catenary and the pantograph. The results are shown in Figure 1.26.

Our aim is to design an energy harvesting system based on metamaterials to recover the energies present in the GSM band frequencies and at lower MHz frequencies, for applications such as supply of wireless power sensors.

According to the observation and measurements that have been carried out for the radiation emissions in the railway environment, the possible application can be is to design an energy harvesting system to convert EM radiation into electrical which can be provided to wireless power sensors which can be used for health infrastructure monitoring and other applications. Figure 1.27 presents an example of the energy harvesting process.

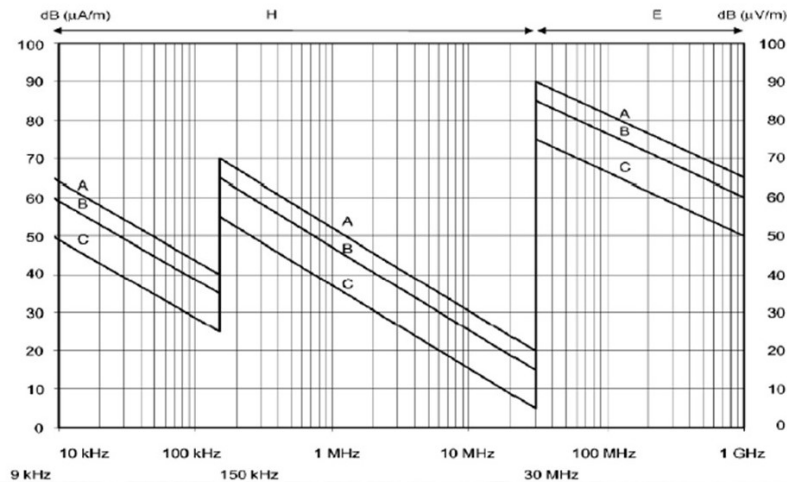


Figure 1.25: Measurements of the field radiation in the railway environment, where the curves A, B and C show the radiation emission limits. For more details refer to the standard EN 50121-3-1. [14]

1.7 Conclusion

With the rise of different novel technological systems for a future with smart infrastructure, railways have been gained popularity in this context, for more reliable, safe, secure and enhanced infrastructure. However, for autonomous reliable systems such as IOT or WSN, electric power supply is needed. Moreover, the railway system can be a rich environment with different ambient energy

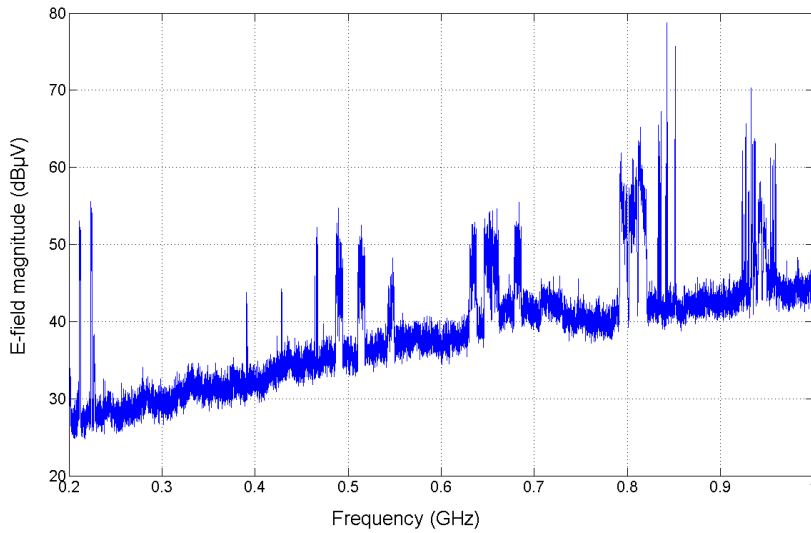


Figure 1.26: Measurements of the E-field magnitude (dBμV) with respect to frequency carried out by SNCF in Belfort in the railway environment

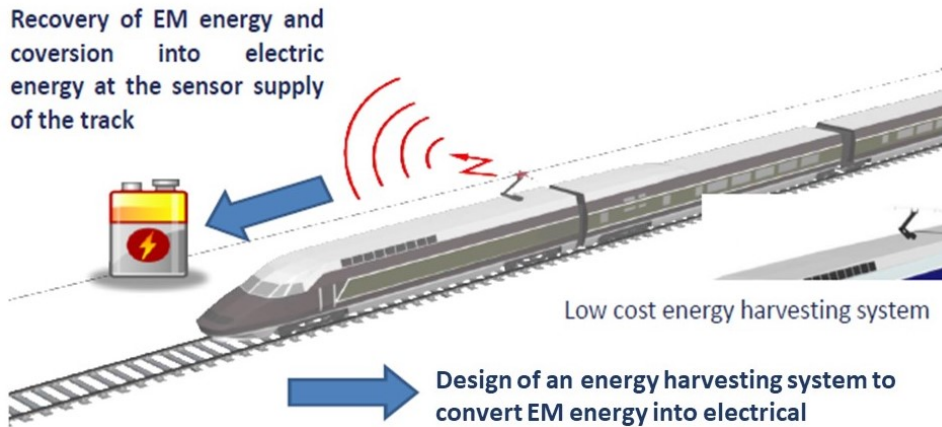


Figure 1.27: Example of the possible energy harvesting process in the railway environment.

sources from vibrations, sound energy, wind, solar to EM/Microwave RF energy. In this chapter, we examined different existing energy harvesting systems based on these sources, that have been designed and implemented for the railway system. Wireless power transfer has also been a solution for high power charging of the railway cars.

In terms of EM/ RF energy harvesting in the railway environment, to date no mature technology has been developed. However, measurements have been carried on by our team to determine the potential EM sources in the railway environment. It has been shown that high levels of EM energy can exist up to the microwave region at 1 GHz. Based on these studies, we would like to investigate the potential to design a mature and reliable EM energy harvesting, by introducing novel concepts for EM energy harvesting based on metasurfaces.

Chapter 2

Electromagnetic Energy Harvesting and Wireless Power Transfer

2.1 Introduction

Wireless Power Transfer (WPT) or electromagnetic energy transfer is the transmission [144,166–169] of energy without wires as a physical link. In a wireless power transmission system, a transmitter device, driven by electric power from a power source, generates a time-varying electromagnetic field, which transmits power across space to a receiver device, which extracts power from the field and supplies it to an electrical load [170–173]. Wireless power transfer is useful to power electrical devices where interconnecting wires are inconvenient, hazardous, or are not possible [174–178].

After 1890 inventor Nikola Tesla (Figure 2.1) experimented with transmitting power by inductive and capacitive coupling using spark-excited radio frequency resonant transformers, now called Tesla coils, which generated high AC voltages [179]. Tesla went on to develop a wireless power distribution system that he hoped would be capable of transmitting power long distance directly into homes and factories. Later, Guglielmo Marconi [180–182] (Figure 2.1) came later and began to conduct experiments in radio waves, where he proved that information can also be transmitted with an electromagnetic wave.

Wireless power transfer can have lot of advantages for different applications, where it can be an energy supply for different batteryless and autonomous devices. One of those applications we can mention are biomedical devices [183–185], IOT systems [17,186–188], wireless sensor nodes [189,190] and mobile applications [191,192]. Ambient energy harvesting systems are also other solutions and technologies that are used in different applications such as solar energy harvesters [193], piezoelectric [132], wind [194], vibration sources [195], electromagnetics and RF energy [196]. These technologies can be of remarkable use for green energy [197] and also instead of the use of batteries and wires.

Wireless Power Transmission WPT



Wireless Information Transmission WIT



Figure 2.1: On the left shows the picture of Nikola Tesla who started WPT and on the right Guglielmo Marconi inventor of the radio.



Figure 2.2: Wireless Power Transfer from DC to RF through an antenna transmitter to an antenna receiver.

Moreover, in terms of the differentiation between wireless power transfer (WPT) and wireless energy harvesting (WEH) [198], the common characteristic is that both depend on wireless energy as well as being far-field techniques. For the case of RF and electromagnetics, in WPT the antenna is designed for the transmission of energy through an energy flow to a receiver or collector, which is different compared to that of WEH where an energy harvesting system is designed for the collection of ambient energy. Figure 2.2 shows the scenario of a WPT method, where an antenna transmitter transmits energy through a channel to an antenna receiver.

In the past, WPT was used in targeting long distance and high power applications mainly driven by wireless powered aircrafts [199, 200] which require huge transmission antennas for high transmission power. In modern WPT, low power wireless systems up to few Watts are being used for moderate distances about few meters, which are being used for remotely charging of various low- to medium power devices such as wireless power sensors [189, 190]. Challenges that can be present for WPT are range, efficiency, non-line of sight, mobility support, energy consumption...etc.

However, WEH can differ from WPT in the case that an energy transmitter is absent and the receiver functions as a collector of ambient energy sources. Thus, a high efficient energy harvesting system is needed since the energy received cannot be controlled and high power is needed across the diode to feed the load in the rectifying circuit. An architecture of an energy harvesting system is shown in Figure 2.3 [15, 201].

In this chapter, we focus on electromagnetic energy from using WPT to WEH technologies. We explain how WPT system works and the applications where it can be useful, as well as the challenges

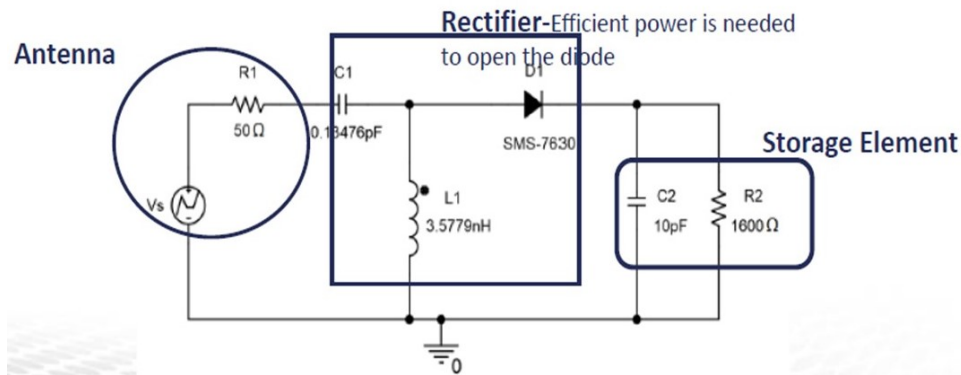


Figure 2.3: Rectenna architecture design consisting of an antenna, Rectifier circuit and storage elements. [15]

that may arise. Ambient EM energy is also introduced, and a study by the Imperial College in London for calculating the energy in the environment is introduced. Various EM energy harvesting technologies are introduced from commercial products and radiators already existing. The main application is the implementation of such systems and technologies from WPT or WEH in the railway environment. Thus, we introduce the use cases for such devices and how they can be implemented and used.

2.2 State of the Art on Wireless Power Transfer

The remarkable history of wireless power transfer (WPT) starts with Hertz to our present time. The path of wireless power transfer history to our daily times is illustrated in Figure 2.4 [16]. Prof. Hertz demonstrated in the 18th century the propagation of an electromagnetic wave through space [202]. After that, Tesla went on to develop a wireless power distribution system that he hoped would be capable of transmitting power long distance directly into homes and factories. However, using the vacuum tube oscillator to transmit power inductively was demonstrated in 1964 [144]. Furthermore, the development of microwave antennas made it possible for wireless power transfer to be used for different applications at that time specially for aircrafts [144, 199, 200].

Recent advances in the domain of wireless power transfer, specially after Prof. Marin Soljacic of Massachusetts Institute of Technology proposed the magnetic resonance wireless power transfer (WPT) in 2007, has made wireless charging possible for different applications [203–205]. Most recent and common usage and application for WPT is the rise of autonomous wireless sensor networks and IOT devices [17, 18, 206–208]. The aim is the usage of green energy based technologies and battery-less, which can be compact and better for implementation. One of the sensor nodes designed by Solmu Technologies is shown in Figure 2.5a.

The main component in this case which they focus on, is the design of an efficient antenna transmission system. The designed directional antenna used as a wireless power supplier is shown in Figure 2.5b.

However, WPT has also been investigated to power up deep space IOT sensors to reduce the weight of cables for deep space exploration [18]. Figure 2.6a shows an illustration for the deployment of IOT sensors on top of a surface of a planet or comet. It can be challenging for such applications in terms of WPT, thus they proposed a vector modular active beam forming antenna array for such applications where various numbers of sensors should be fed. The module suggested is given in Figure 2.6b.

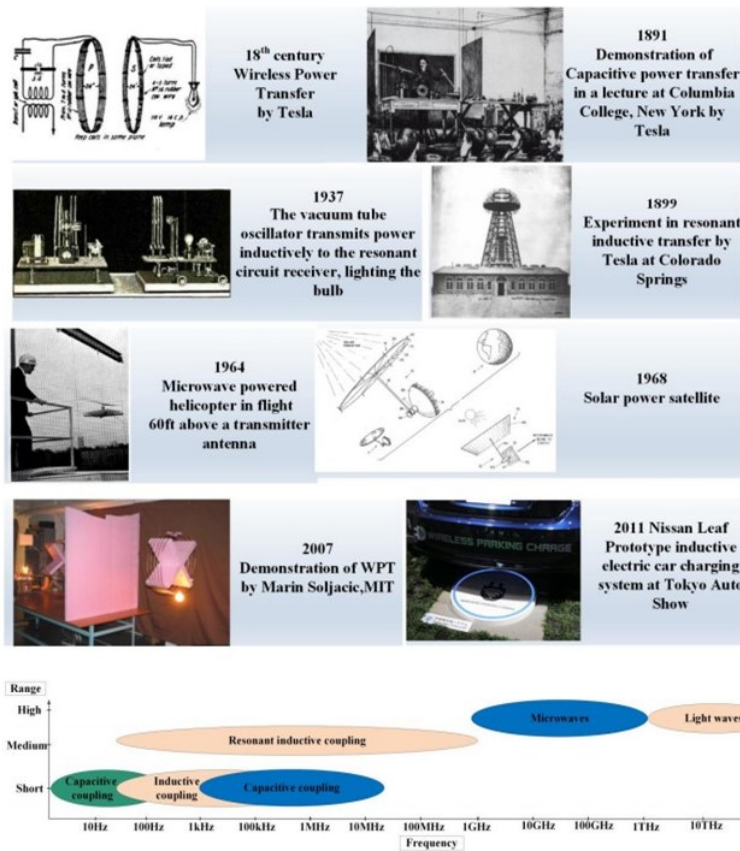
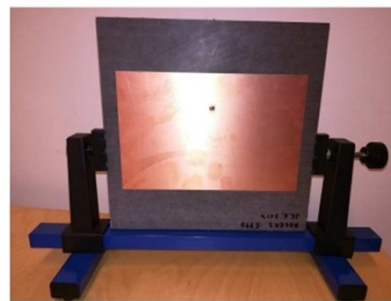


Figure 2.4: Different Wireless Power Transfer technologies and timeline over the past history. [16]



a)



b)

Figure 2.5: a) An integrated sensor node by Solmu Technologies. b) Prototyped antenna for energy transmission. [17]

2.3 Ambient Electromagnetic Energy

In terms of ambient energy in the environment of energy harvesting system, sources must be of high level and efficient enough to be collected and stored as electrical energy. A study has been done for London underground for Rf spectral survey by the Imperial College of London. The map of the

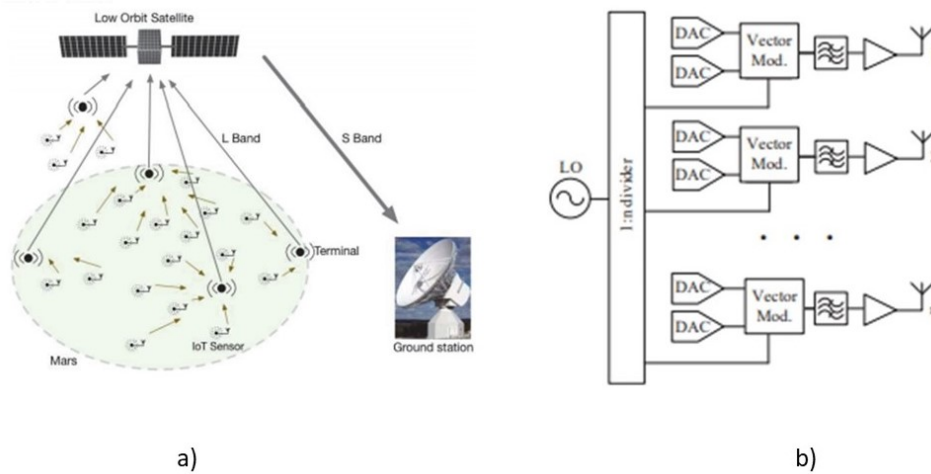


Figure 2.6: a) Internet of things on deep space exploration. b) vector modular active beam forming antenna array used. [18]

locations where ambient sources have been studied is shown in Figure 2.7.



Figure 2.7: Map of different locations of london underground for the study of ambient sources of energy.(Imperial Colledge London)

For the equipment to determine the measurements, a spectrum analyzer and omnidirectional antenna (0.3 GHz - 3 GHz) were used to carry out the study as shown in Figure 2.8.

The power levels of the ambient sources for London underground at different frequency bands are presented in the table in Figure 2.9. The study has been carried out for different frequency bands (DTV, GSM 900, GSM 1800, WiFi, 3G), where maximum power was obtained in the GSM 1800 band.



Figure 2.8: Spectrum analyzer and omnidirectional antenna for a band of frequency from 0.3 GHz - 3 GHz.(Imperial Colledge London)

Band name	Frequency (MHz)	BW (MHz)	Average P ($\mu\text{W}/\text{cm}^2$)	Maximum P ($\mu\text{W}/\text{cm}^2$)
DTV	470 - 610	140	0.89×10^{-3}	0.046
GSM 900	921 - 960	39	0.036	1.93
GSM 1800	1805 - 1876	71	0.084	6.39
WiFi	2400 - 2473	73	0.18×10^{-3}	6.47×10^{-3}
3G	2110 - 2170	60	0.012	0.24

Figure 2.9: Power energy obtained for London underground ambient sources study at different bands of frequency.(Imperial Colledge London)

2.4 State of the technology: RF harvesters - commercial products

In todays wireless connected world, ambient Radio Frequency (RF) energy is everywhere. Technically, this free-flowing energy can be captured, converted and stored for use in other applications. In fact, it is already in use in a number of ultra-low-power, battery-free applications, such as RFID tags, contactless smart cards, and wireless sensor networks. As a result of technological advances, harvested RF energy is just beginning to realize its wider potential, including charging batteries in smartphones and other portable devices. These enabling technologies include RF transceivers, power conversion circuits, and ultra-low-power microcontrollers, all of which are becoming ever more efficient.

2.4.1 Radiators

Currently, emerging technologies and recent commercial products have been developed. These include energy harvesting development kits that support RF energy harvesting [209,210].RF energy is readily available in most inhabited areas from sources such as TV, radio and cellular phone antennas as well as wireless radio (Wi-Fi) networks, base stations, routers and even portable communications devices. RF energy can be captured via a power generating circuit linked to a receiving antenna, then converted into usable DC voltage. In the same way as other energy harvesting sources, the converted power can either be stored directly in a battery, or can be accumulated in a capacitor to power circuits directly or charge a battery.

Although the power available from ambient RF energy is very low (typically measured in microwatts),

it has proven to be sufficient for a number of applications, such as RFID tags, wireless sensor networks for remote monitoring, and NFC functionality in contactless smart cards and more recently in smartphones [211].

RFID tags, for example, incorporate an integrated sensor, transmitter and antenna, which harvest just enough RF energy from the RF signal sent by the reader, to send back identification information. Evolving technology is enabling tags to be made smaller and to increase read ranges. Typically requiring just microwatts of energy to transmit ID data, the read range will vary depending on the power of the transmitter. Indeed, in any application, proximity to the transmitting antenna is critical and this, combined with the power output of the source, will define the types of applications that can be supported. An RF Tag presented by Murata Electronic North America is shown in Figure 2.10a.

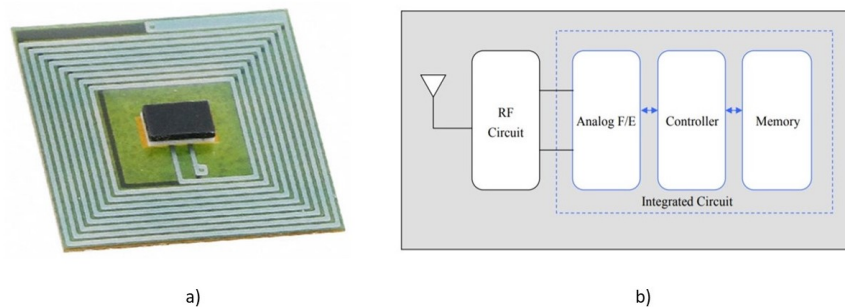


Figure 2.10: a) RFID tag presented by Murata Electronic North America technologies for a frequency of 13.5 MHz. b) Block diagram of the RFID tag.

The block diagram of the RFID tag is given in Figure 2.10b. The RF Tag operated at 13.5 MHz with an embedded antenna and using NXP NTAG213 1152bit user memory.

In the commercial world, the product choice continues to grow. A technology leader in the contactless smart card and NFC marketplace, STMicroelectronics, has recently released a development platform for its innovative contactless memories with RF energy harvesting capabilities. Designed for battery-free applications that can exchange data with (ISO15693 compatible) NFC-enabled smartphones and RFID systems, the M24LR Discovery Kit is based on the company's M24LR EEPROMs. The memory device itself features a standard interface as well as an RF interface, which can convert ambient radio waves emitted by RFID reader/writers and NFC phones, or other portable devices, to power its circuits, thereby giving it energy-autonomous, battery-free operation. The prototype of the M24LR Discovery Kit with RF energy harvesting EEPROM is shown in Figure 2.11 [19].

The kit meanwhile, includes an RF transceiver board with a 13.56 MHz multiprotocol RFID/NFC transceiver, driven by an STM32 32-bit microcontroller, which powers and communicates wirelessly with a second board equipped with the M24LR dual interface EEPROM, the STM8L, ST's ultra-low power 8-bit microcontroller and a temperature sensor.

The amount of energy available is dependent on the RF power of the source and the distance between the devices. The use of ultra-low power microcontrollers is essential, and devices in ST's STM8L range offer five different power modes, consuming just 300 nA in its lowest power mode.

Applications for the M24LR energy harvesting solution are seen in energy-autonomous data collection, asset tracking and diagnostics in a wide variety of sectors, including electronic shelf labels, home appliances, industrial automation, sensing and monitoring systems and personal healthcare products.

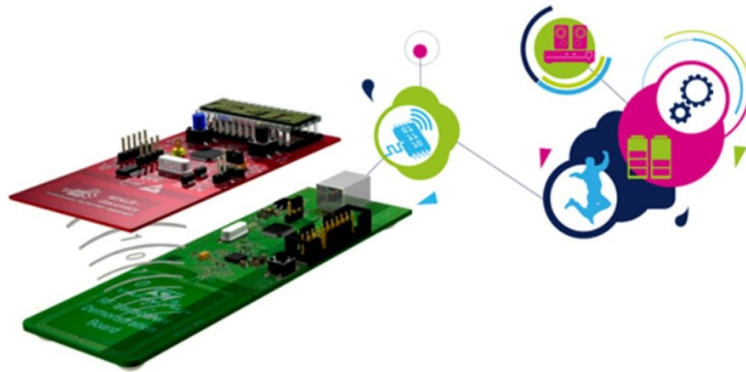


Figure 2.11: The M24LR Discovery Kit with RF energy harvesting EEPROM. [19]

2.4.2 Rectifying circuits

In terms of rectifying circuits for RF energy harvesting commercial products, different technologies and designs have been developed and introduced by different companies. One we can mention is the P1110 RF power harvester which has been introduced as POWERCAST product. The chip P1110 and its block diagram are shown in Figure 2.12a and 2.12b.

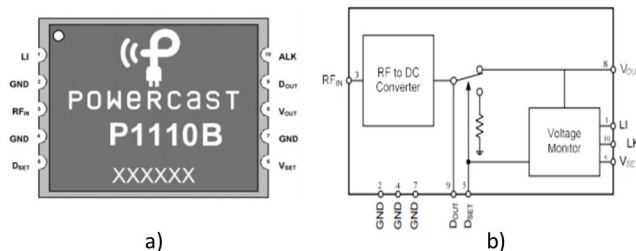


Figure 2.12: a) The P1110B designed by POWERCAST design and pins b) P1110B block diagram

The Powercast P1110B Powerharvester receiver is an RF energy harvesting device that converts RF to DC. Housed in a compact SMD package, the P1110B receiver provides RF energy harvesting and power management for battery and capacitor recharging. The P1110B converts RF energy to DC and provides the energy to the attached storage element. When an adjustable voltage threshold on the storage element is achieved, the P1110B automatically disables charging. A microprocessor can be used to obtain data from the component for improving overall system operation. The P1110B features high conversion efficiency greater than 70%, low power consumption, configurable voltage output to support Li-ion and Alkaline battery recharging, operation from 0V to support capacitor charging, received signal strength indicator, no external RF components required -internally matched to 50 ohms, wide operating range, operation down to -5 dBm input power and industrial temperature range.

2.5 State of the research on electromagnetic energy harvesters: Radiators

2.5.1 Antennas at 2.4 GHz

In terms of electromagnetic energy harvesting and power detection from RF to DC energy, different antenna and rectifying systems have been developed and designed specially at 2.4 GHz [20, 21, 134].

The design of rectenna systems for low input power less than -10 dBm are in investigated. Vlad Marian et al. [20] introduced the design of a rectifying antenna for low power detection where their performances have been evaluated through the definition of a Figure of Merit.

In RF to DC conversion circuits, circuits are built around diodes or diode-mounted transistors. Diode threshold voltage has to be overcome in order to put them in a conductive state; it is a key factor when choosing a diode for designing a rectenna. Under high power levels, diode threshold is not an issue because it is small compared to incident high frequency voltage amplitude, but losses due to diode threshold become predominant in the case of low incident power levels (below 1 mW).

In a typical rectenna circuit (Figure 2.13) incident RF power captured by the antenna is transformed into DC power by the diode based converter. A HF filter ensures impedance match between the rectifier and the antenna for optimal power transfer. The output DC filter smoothens the output DC voltage and current by attenuating high frequency harmonics present in the RF signal or generated by the highly nonlinear rectification process. They have introduced two rectifying circuits to compare the results of the output voltage across a 3 K Ω resistor. The two circuit designs are shown in Figure 2.14.

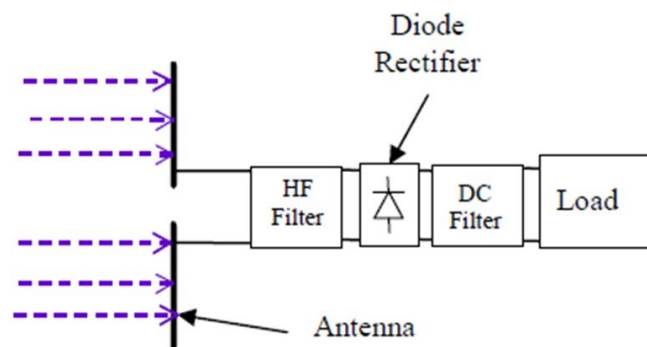


Figure 2.13: Block diagram of a rectenna design. [20]

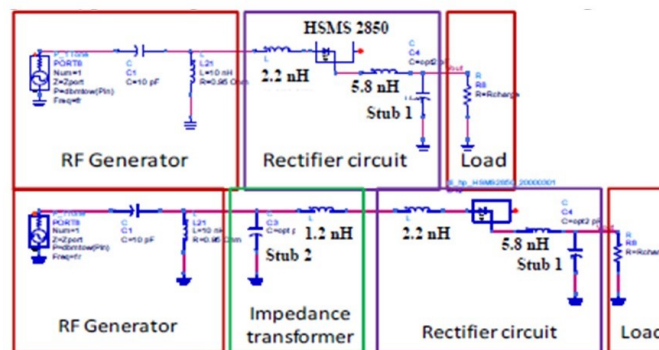


Figure 2.14: Reference circuit with 50 Ohm input impedance (top); and fully optimized rectifier with non-50 Ohm impedance (bottom). [20]

The results of Figure 2.15b validate the different guidelines applied to the design. Although maximum DC voltage level is different between simulation and measurement (around 100 mV), a relative comparison between the reference circuit and the optimized one leads to a great compliance between the predicted result and the measurement. As a whole, an improvement of output voltage of around

100 mV is observed when the antenna impedance is added to the design optimization. Notice that this last design leads to a more selective behavior of the rectenna. Rectenna system performance was given through a 3 KOhms Load Resistor where the efficiency was recorded to be equal to 25%.

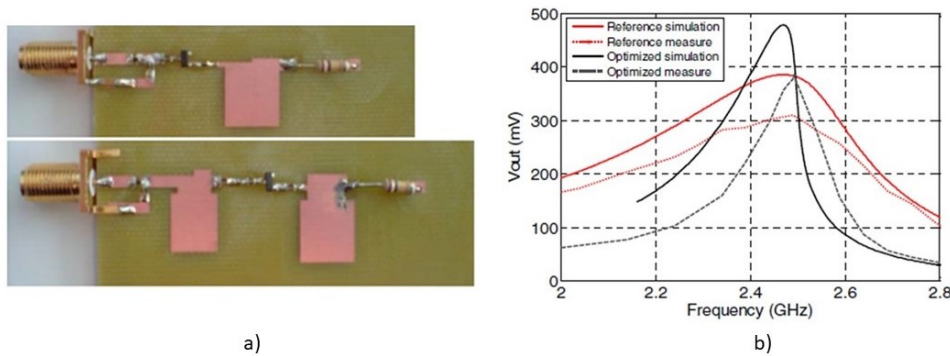


Figure 2.15: a) The realized reference circuit with 50 Ohm input impedance (top) and fully optimized rectifier (bottom). b) Output Voltages of the given designs. [20]

Rectenna designs have been also introduced by A. Georgiadis et al, [21] where they designed a rectenna system combining the methodology of electromagnetic (EM) simulation and harmonic balance (HB) analysis. It consists of applying reciprocity theory to calculate the Thevenin equivalent circuit of the receiving antenna and optimizing the rectifying circuit parameters using HB analysis. The method is demonstrated by designing a 2.45-GHz rectenna based on a square aperture-coupled patch antenna with dual linear polarizations. The design is shown in Figure 2.16a.

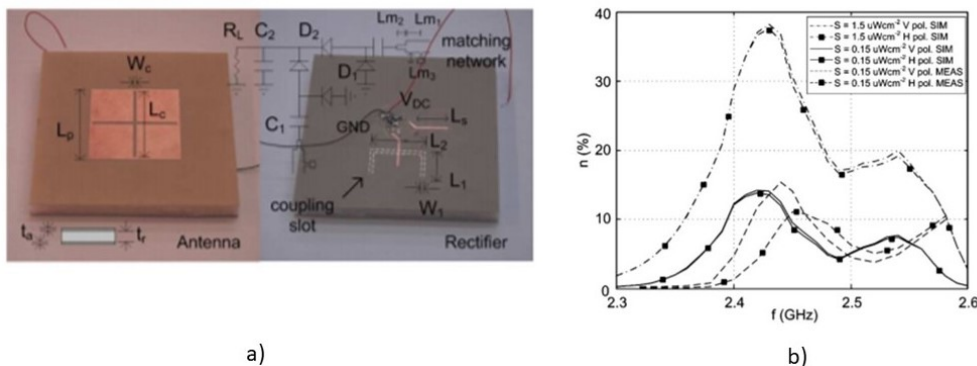


Figure 2.16: a) Fabricated rectenna Top view of radiating patch and bottom view of rectifier circuit. b) Efficiency of the rectenna design for different input powers across a 6.2 kΩ resistance. [21]

The circuit given has been optimized for low input power densities. The result of the RF to DC efficiency of the designed rectenna is given in Figure 2.16b. The results show that a simulated maximum efficiency of 38.2% was obtained for 1.5 uWcm² input RF power density at 2.43 GHz across a load resistance of 6.2 kΩ.

2.5.2 Antenna arrays

In terms of rectenna systems for energy harvesting the main elements are the antenna and the rectifier. Different rectenna systems have been developed for energy harvesting which has been

shown to be of low efficiency and narrow band [135]. Hucheng Sun et al. [22] introduced a dual band rectenna using broadband Yagi Antenna array for ambient energy harvesting. The details and prototype of the design are given in Figure 2.17a. The efficiencies of the designed Yagi antenna array are given in Figure 2.17b. The design has shown to give a maximum efficiency up to 38% at 1.85 GHz and 35% at 2.15 GHz for -18 dBm input power.

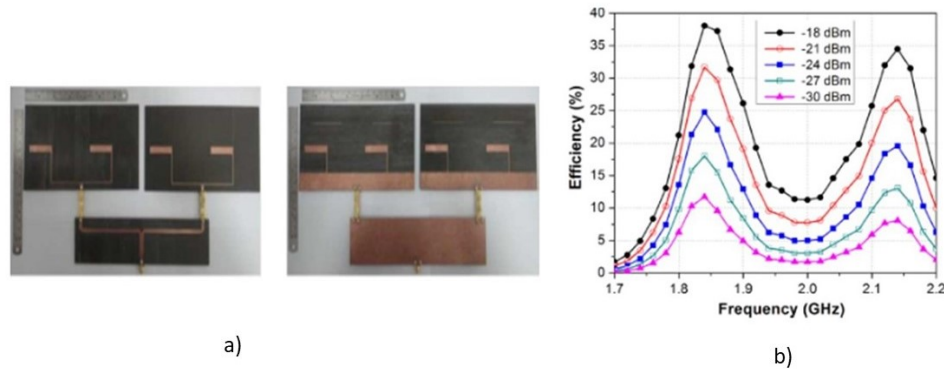


Figure 2.17: a) Photographs of the 14 quasi-Yagi array top side and back side. b) Efficiencies of the Yagi design antenna array with respect to frequency for different input power levels [22].

2.6 Use Cases for EM energy harvesters in the Railway Environment

Nowadays, the development of an intelligent rail infrastructure is said to be an important research topic for different companies in the railway industry. This requires the deployment of wireless power sensor nodes which are embedded and placed along the railway infrastructure, in order to monitor various parameters for operations, maintenance and safety. These sensors provide measurement and perception functions for the railway environment. Harnessing the data from these sensors enables infrastructure managers and operators to ensure increased resilience, which is vital for these critical infrastructures. For example, the only cost of cable theft is about 30 million euros each year on the national rail network, not to mention the consequences in terms of operating losses and image of the mode of operation. However, the operational implementation of on-board and off-road autonomous sensors is hampered by a number of technological obstacles in the highly constrained railway environment. A particular problem to be solved concerns the power supply of these sensors. Although they can be developed to require only low power consumption, they require a minimum power supply to acquire the requested data and transfer it to a control station.

Therefore, developing a network of sensors to build a smart rail infrastructure requires serious consideration to determine an effective power supply of these equipment. Thus, the objective is to design an EM energy harvesting system to supply power to wireless power sensors benefiting from the sources of EM energy which exist in the railway infrastructure. The project is being carried out in collaboration with SNCF, they have prioritized use cases and provide access to data to analyze the availability of electromagnetic energy on the network. The radiations from the sources of energy in the railway environment bypasses three zones as shown in Figure 2.18 where the energy decreases gradually as we move far from the source. The near field zone is where the energy remains fairly constant and is 1λ away from the sources of energy.

The railway main system elements consist of the vehicle, line and supply substations. They present different characteristics in terms of electromagnetic phenomena and intensities of EM energy. This

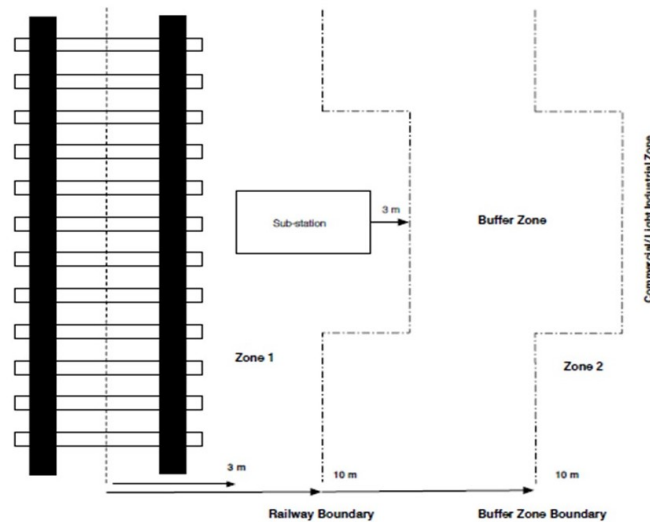


Figure 2.18: Railway Electromagnetic Zones [23]

can be due to different coupling paths produced between the catenary line and the pantographe, as well as the presence of conductive elements. In terms of use cases of an energy harvesting system in the railway environment, one should study the different EM environments present around and produced in the railway infrastructure. [24] [25] [13]

2.6.1 Train or on Board EM Environments

The Train environment refers to all the equipment installed on board, that may include signalling devices, communication apparatus, information technology equipment, etc.. It is characterized by a strong magnetic field at the traction frequency, produced by all the traction system apparatus and its connections (main transformers, filters, traction converters and motors, braking choppers, circuit breakers, etc.), and by a significant transient magnetic field in case, for example, of circuit breaker tripping. For the presence of several switching devices and radio frequency communication systems in close proximity, the expected field intensity over a wide frequency range is high; it is easy to see that over the entire MF and HF bands, ranging from tens of kHz to some or a ten of MHz, the electromagnetic emissions from static converters and other switching apparatus are in the reactive field region, so that magnetic and electric field components are both relevant and the direction of vectors as well as their ratio (the wave impedance) reduce the efficacy of electromagnetic shielding solutions.

2.6.2 Line and Track Electromagnetic Environment

The Line and track environment refers to the equipment installed at a short distance from the line or with a specific EM connection to the track and line, even at a larger distance ; examples are signalling devices and their cable connection to relays and electronic apparatus installed in protected rooms, but in connection, in terms of coupling path, to the L environment. A different approach is to be followed if the victim cable is in direct connection with the rails, since the over voltages appearing in case of a lightning stroke hits the rails (directly or in close proximity) are well above the prescribed surge test levels of the L environment (the most severe environment anyway); special countermeasures must be set up by the manufacturer or installer to bring the residual overvoltage to a safe level, compatible with the prescribed EMC tests, thus avoiding an unnecessary increase of the testing severity for the connected equipment. These sources can be beneficial for energy harvesting

systems implemented close to the railway infrastructure on the side of the train at a short distance.

2.6.3 EM sources from Telecommunication Base Stations

2.6.3.1 GSM-R Telecommunication system

The GSM-R (Global System for Mobile communication-Railways) is a wireless digital communication system (Figure 2.19), based on the public European GSM Phase 2+. This system is used to ensure the vocal exchanges and to transmit railway signalling information between trains and railway control centres. The GSM-R is used in order to maintain a continuous voice and data link between the train and the control centres, and different trains located in the same neighbourhood. In Europe, the GSM-R uplink occupies the frequencies between 876 MHz and 880 MHz and the downlink between 921 MHz and 925 MHz. These frequency bands are separated by a frequency bandwidth dedicated to public and extended GSM.

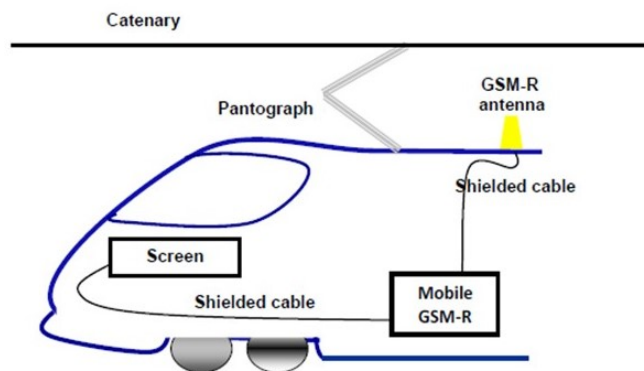


Figure 2.19: Illustration of the on board GSM-R system [24]

2.6.3.2 EM noises interfering with GSM-R signals

From an EMC point of view, the railway infrastructure is a harsh complex EM environment where cohabitation between high power and digital communication systems with numerous eventual coupling mechanisms could be hazardous for the useful signal of the GSM-R. The GSM-R system, on board moving trains, is mainly affected by transient EM disturbances occurring between the catenary and the pantograph, in addition to the permanent disturbances coming from the public GSM base stations as illustrated in Figure 2.20.

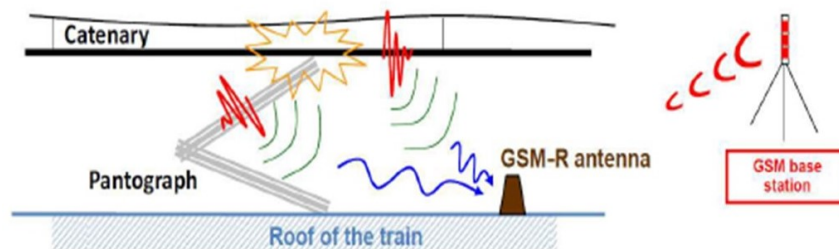


Figure 2.20: EM interferences caused by the catenary line and pantograph as well as GSM based stations which are received by the GSM-R antenna implemented on the rooftop of the train. [24]

2.6.3.3 Use case of EM noises and GSM signals for Energy harvesting

The presence of unintentional signals in the railway environment from GSM signals to sparks appearing between the catenary and the pantograph, which are considered as EM noises for GSM-R antennas, can be beneficial sources for EM energy harvesting systems in the railway environment specially at GSM frequencies where a high level of energy can exist. The miniaturization process can also be more relevant at GSM frequencies compared to that of other sources present in the railway infrastructure at lower frequencies.

2.6.4 Tunnel Environments

Tunnel is an artificial underground passage for high speed railway environments as is shown in Figure 2.21. The presence of tunnel ensures the high speed of train operation in rolling terrain. The sectional view of tunnel in high speed railways is usually vaulted or semicircle, with a height of 5 to 10 m and a width of 10 to 20 m. The length of the tunnel mostly ranges from few to several kilometers.



Figure 2.21: Tunnel Environment for high speed rails. [25]

Generally, two main base stations are placed at the beginning and the end of the tunnel. Dependent on the length of the tunnel, several sub-base stations are placed inside the tunnel, installed in the wall. These help to provide great wireless coverage inside the tunnel. Due to the smooth walls and the close structure of the tunnel, there are high level of reflections and scattering components inside the tunnel, which introduce the wave guide effect dominating the radio wave propagation inside the tunnel. This phenomenon makes the prediction of wireless signal in tunnel totally different from other propagation scenarios.

In terms of energy harvesting systems, the implementation of an electromagnetic energy harvesting system in the scenario of tunnel environments can be beneficial specially due to the presence of high level of electromagnetic waves, caused by the high level of reflections and scattering inside the tunnel. EM energy harvesting systems can also have an advantage over other systems specially in the scenario of tunnel environments such as solar based energy harvesting systems.

2.6.5 IOT use cases for Railways

The deployment and implementation of IOT devices for the railway infrastructure is the future of this industry, which can give rise towards the internet of smart trains. The future of the railway industry is expected to be based on smart transportation systems that to reduce its life-cycle cost,

integrate new services, such as integrated security, asset management, and predictive maintenance, in order to improve timely decision-making for issues like safety, scheduling, and system capacity. Figure 2.22 represents the communication system using IOT devices for a railway infrastructure [26]

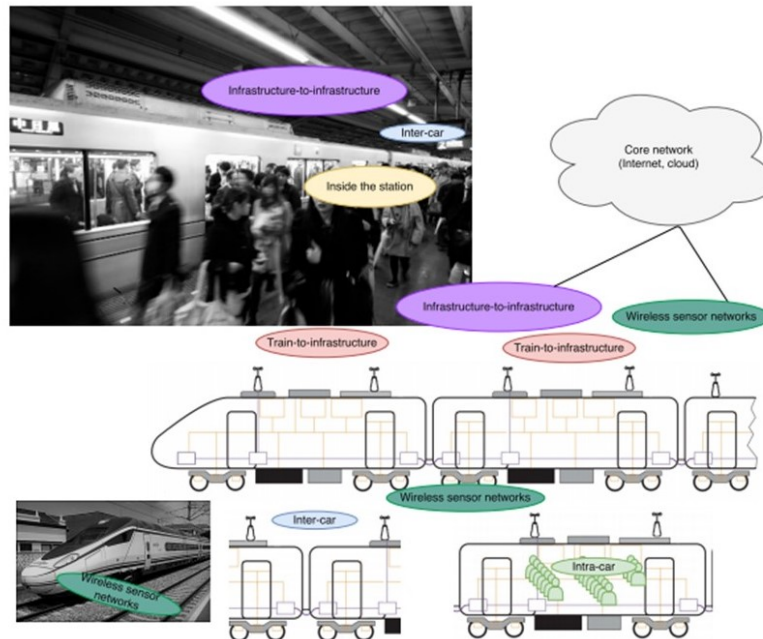


Figure 2.22: Railway communications scenarios (Renfe AVE train and train station pictures are under Creative Commons License). Color meaning: pink (train-to-infrastructure communications), blue (inter-car communications), light-green (intra-car communications), yellow (communications inside the station), purple (infrastructure-to-infrastructure communications), and dark green (wireless sensor networks). [26]

For better deployment of such IOT devices, and to make them more reliable, autonomous and compact, WPT and energy harvesting technologies can be of great use for such applications, which we are investigating in this work.

2.7 Conclusion

In this chapter, we introduced the definition and history of wireless power transfer and EM energy harvesting. The progress in technologies and research studies have been remarkable over the years for both technologies. State of the art on some studies and applications for WPT have been given and shown in this chapter. Different studies and experimental work have been followed to study the potential of ambient electromagnetic energy which have been carried out by the Imperial College of London. The aim is to benefit from these existing potential sources, to build energy harvesting systems for the supply of different technologies which can make them more compact and autonomous. In terms of EM energy harvesters, different technologies from commercial to research topics, were developed mostly based on rectenna designs and RF harvesters.

These technologies have been of great use for rising autonomous WSN and IOT devices. In our application specially for railways, these devices can be highly useful for the development of smart

railway infrastructure. To date, no mature device and technology based on WPT and EM energy harvesting for railways have been deployed, specially for the supply of autonomous WSN and IOT. Rectenna systems can be of low efficiency and bulky with the antenna design at low frequencies in terms of EM energy harvesting. WPT systems can also have some challenges in terms of line of sight implementation and efficiency. Thus, in the following chapters, we investigate the potential of novel concepts in terms of EM energy harvesting and WPT based on metamaterials and metasurfaces, for more efficient, compact and reliable devices.

Conclusion of the Part

In this part, we presented and highlighted the various existing energy harvesting technologies that have been deployed and developed for the railway environment. The application is to implement smart devices for a more reliable and sustainable railway infrastructure. Technologies such as energy harvesting and wireless power transfer can be a key for autonomous and compact devices. The railway environment is rich with various sources of energy which can be beneficial. Recently, electromagnetic sources have shown to have a high potential in the railway environment. This can be interesting to investigate in terms of EH specially that no mature technology to date for such application has been developed. A summary is shown in Figure 2.23.

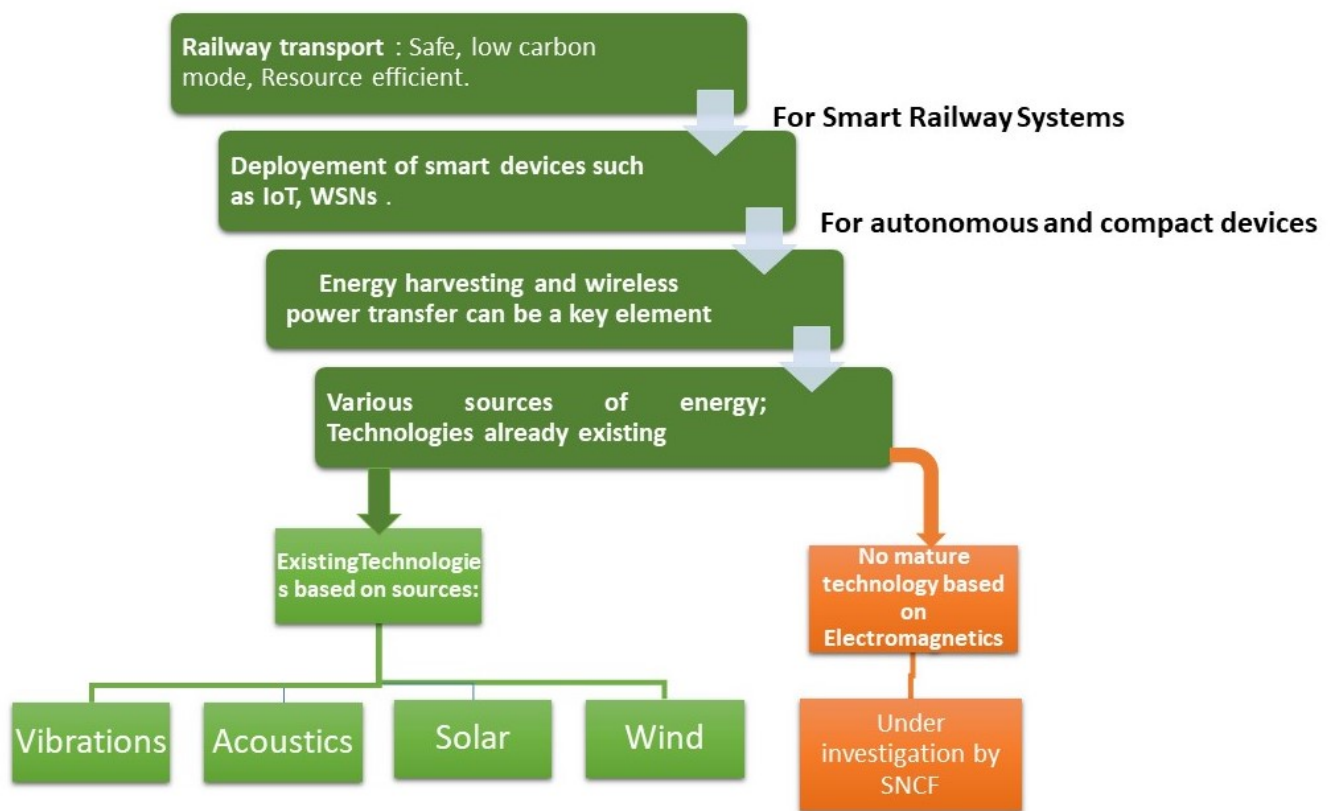


Figure 2.23: Summary of the conclusion of part one on the railway application and existing technologies.

Our goal is to introduce a mature system and energy harvesting technology based on electromagnetics. Many challenges can arise specially for the application of the railway system. In the next part,

we investigate the potential of metasurfaces to develop a mature and reliable EM EH and WPT systems compatible for railway systems, and overcome the challenges such as efficiency, miniaturization and line of sight that can arise in our application.

Part II

Metasurface solutions for EM energy harvesting and WPT performance enhancement in Railway environment

Introduction

Metasurfaces have gained remarkable interest in the field of electromagnetics for many researchers in the past years. This is many for their exceptional physical properties, characteristics and wide generality design approach, specially in terms of wave control and manipulation in various manner depending on the engineered design and application needed. They are characterized by their 2D subwavelength thickness and structure, which make them very attractive compared to 3D metamaterials, mainly for ease of fabrication and implementation. A wide range of characteristics in terms of wave control have been given in the literature for metasurface designs, from anomalous wave control, beam splitting, focusing, wavefront manipulation, absorption, energy harvesting, retro-reflection and many more.

In the previous part, we defined the application, problematic and objective of our thesis. Since various energy harvesting technologies have been presented for the railway application based on different sources from vibrations, wind, solar to acoustics, and with high potential of EM energy proven to be present in the railway system no mature technology for energy harvesting based on these EM sources has been introduced. Our aim is to introduce high efficient, mature, compact and miniaturized EM energy harvesting systems following novel concepts based on metasurface designs.

For the railway application, many challenges and limitations can arise for EM energy harvesting devices. Rectenna systems for low microwave frequencies, can be of low efficiency and difficult to implement. Therefore, in this part we use the different characteristics of metasurface designs from focusing, anomalous reflection to absorption where give a brief overview on these properties in chapter 3. We investigate the potential of these properties to enhance the performances of EM energy harvesting and wireless power transfer systems, in order to overcome the challenges and limitations for such application.

In chapter 4, we introduce a novel concept and approach in terms of EM EH, for enhancing the performances of rectenna systems. The concept is based on focusing metasurfaces in which a well designed, high efficient and miniaturized metasurface focuses the EM energy present in the far field at a focal point at a distance from the metasurface. An off the shelf rectenna system is then implemented at the spot to harvest the energy. This concept can be a remarkable approach to overcome the challenge and limitation of low efficient ambient EM energy in the surrounding environment, and enhance the performances of low efficient rectenna systems.

Our goal is introduce a device compatible for the railway application, in which it can be implemented and tested on site in the railway environment, in the presence of a GSM-R base station to investigate its potential. In chapter 5, we introduce the measurements and performance of our concept based on focusing, by implementing a rectenna system alone and alone side the focusing metasurface and comparing their performances on terms of harvesting for GSM-R frequencies.

An alternative solution for power supply for low input power devices can be WPT technologies. However, line of sight can be a major challenge for such applications. In chapter 6, we introduce the design of retrodirective metasurfaces following the generalized phase law of reflection, which can be remarkable in terms of tracking and localization enhancement specially from the oblique angular aspect. However, the challenge is to design passive metasurfaces operating for multiple angles simultaneously. Thus, we introduce different approaches and concepts based on the cascading method and surface impedance modulation, which have shown unprecedented properties in terms of backscattering enhancement.

In chapter 7, we propose other solutions for EM EH based on absorbing metasurfaces [212], which can be compatible for our application at low microwave frequencies. We use the concept introduced in [212], by designing single to multi-band metasurface energy harvesting absorbers for low microwave frequencies. This solution can be interesting to overcome the challenge of low efficient collectors in rectenna systems specially at low microwave frequencies, where using the property of subwavelength metamaterial inclusions can be of great use.

Chapter 3

An Overview on Metasurfaces; Focusing, Anomalous reflection and Absorption: Applications and Physics

3.1 Introduction

Metamaterials [213, 214] are engineered subwavelength materials, they are constructed of arranged scatterers, in a 3D configuration, in order to achieve physical properties not normally found in nature. However, the same definition and concept can be referred to 2D structures of metamaterials, which are basically a surface or single layer interface known as metasurfaces [52, 215, 216].

Metasurfaces [52] are the subject of intensive research nowadays for their applicative potential and the generality of their design approach [53, 217]. They are characterized by their 2D subwavelength structure and their ability to control the wavefront of an electromagnetic wave [54, 55, 218] with perfect, abnormal and achromatic reflections [56, 57, 219]. Metasurfaces, being two-dimensional materials, can be easily implemented into and along side other devices [58, 59], which can be very useful in different applications. Their simplicity of design and fabrication can make them very attractive compared to 3D metamaterial structures specially in the microwave region. However, any 2D engineered periodic structure whose thickness and periodicity are subwavelength with respect to the propagating wave in the media, can be defined as a metasurface [220].

Metasurfaces are well known for their variety of characteristics and utilization in terms of application and wave control manipulation [60, 61]. The control of the reflection phase [62] of an incoming incident wave has been significant for metasurfaces following the generalized phase law [27, 63] in different sectors. With the control of the reflection phase, metasurfaces have been used as ultra

thin polarization transformers [64, 65], wave front manipulation such as beam shaping [66], beam splitting [67], focusing [68, 221, 222], retro-reflection [69, 70], de-focusing [71], reflection and refraction. Moreover, metasurfaces based on absorption [72–74, 223, 224], have shown significant potential over conventional absorbers, in terms of miniaturization, efficiency, absorption bandwidth, polarization insensitivity and wider allowable incident angles. Following this concept for metasurface absorbers, metasurface energy harvesters arised, where TS Almonneef et al. [75–78] introduced the concept of energy conversion from electromagnetic to DC electric energy, using high efficient metasurface absorbers, and introducing a via for energy dissipation.

With the variety of characteristics mentioned for metasurface designs, metasurfaces have shown remarkable potential in terms of physics, applications, efficiency, use cases and interest in different domains of studies. However, with the rise of different technologies such as IoT [225], wireless sensor networks and 5G [226–228], reconfigurable metasurfaces [229–232] are being developed and used to overcome different challenges in this sector in terms of complexity, design, efficiency and the control of wave propagation in the environment. This shows that metasurfaces can provide a bright future in terms of wave propagation control in the environment and can be essential for rising developing technologies.

In this chapter, we give a brief overview of the concept of the generalized phase law of reflection and refraction for phase control and design of metasurfaces. We also show different designs and research studies that have been developed over the years for metasurfaces in terms of wave reflection manipulation, absorption and focusing.

3.2 Metasurfaces Anomalous Wave Control

Manipulation and control of an electromagnetic (EM) wave, has attracted many interest by researchers, specially using engineered topologies such as metasurfaces, to alter the amplitude, reflection phase, polarization state, wavefront and beam steering, all depending on the desired physics and application use case. Metasurfaces which are 2D metamaterial structures, are well known with their design of periodic subwavelength scatterers to manipulate a wave in a desired manner. In terms of anomalous reflection and refraction for metasurfaces, the designing is based on the generalized Snell's law of reflection and refraction.

3.2.1 Generalized Snell's Law of Reflection and Refraction

According to the conventional Snell's law, for a wave propagating between two homogeneous media with different refractive indices, the wave is divided into a reflected wave in the medium of incidence and a refracted wave in the other. However, when introducing a metasurface design between the two media, the phase of the reflected and transmitted waves will be altered, and the propagation of wave will be anomalously reflected and refracted, depending on the introduced designed metasurface. Figure 3.1 shows the concept of a metasurface design.

Figure 3.1 shows the concept of an incident wave propagating towards a metasurface, which is positioned at an interface between two media with different refracted indices. The concept was introduced by the group of F. Cappasso [27], where the plane wave targets the surface at an angle θ_i with respect to the normal of the metasurface, thus leading to a reflected and refracted angles θ_r and θ_t respectively. The generalized phase law of reflection and refraction [233] introduces an additional term (the phase gradient) with respect to the conventional Snell's law as shown in Eq. (3.1) and (3.2). This is consistent with the well-known grating equation. [234]

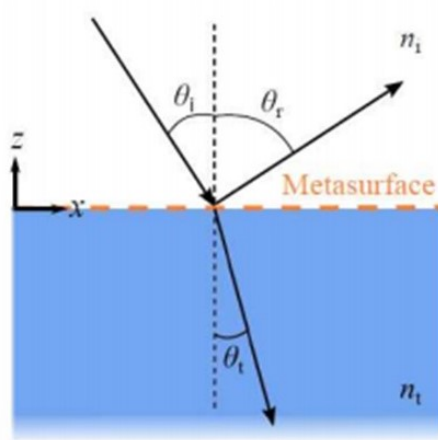


Figure 3.1: Sketch of the concept considered by the group of F. Cappasso in [27], where a metasurface positioned at the interface between two ordinary media (characterized by refractive indexes n_i and n_t) describing the generalization of the laws of reflection and refraction.

$$\sin \theta_r - \sin \theta_i = \frac{\lambda_0}{2\pi} \frac{\partial \phi}{\partial x}, \quad (3.1)$$

$$n_t \sin \theta_t - n_i \sin \theta_i = \frac{\lambda_0}{2\pi} \frac{\partial \phi}{\partial x}, \quad (3.2)$$

Equation (3.1) shows the generalized phase law of reflection where θ_r is the angle of reflection, θ_i is the angle of incidence, λ_0 the free space wavelength and $\partial \phi / \partial x$ is the phase gradient. Equation (3.2) shows the generalized phase law of refraction where θ_t is the angle of transmission, θ_i is the angle of incidence, λ_0 the free space wavelength and $\partial \phi / \partial x$ is the phase gradient, n_t and n_i are the refractive indices of media 1 and 2. However, particularly for reflection where transmission is neglected, by introducing a phase gradient between scatterers on top of an engineered metasurface design, an electromagnetic wave is reflected to a desired anomalous direction. Based on the above concept and law for anomalous reflection and refraction, the design of metasurfaces for wave manipulation has been an interesting topic for many researchers over the last decade. Metasurfaces have significantly received a lot of attention where a lot of advances in this field have been carried on.

3.2.2 Demonstration of the Generalized Phase Law

After defining the concept of anomalous reflection and refraction, and the generalized phase law, one has to demonstrate a design to validate and verify the theoretical aspect. In order to validate the concept of the generalized phase law, scatterers of subwavelength dimensions and different shapes, can be designed and integrated in a periodic array structure of a surface design, each with a specific phase depending on the desired application.

It was first demonstrated in the optical spectrum by the group of F. Cappasso [27] and Ni Xingie *et al.* [235] using V-shaped optical unit elements. The described metasurface structure is shown in Figure 3.2.

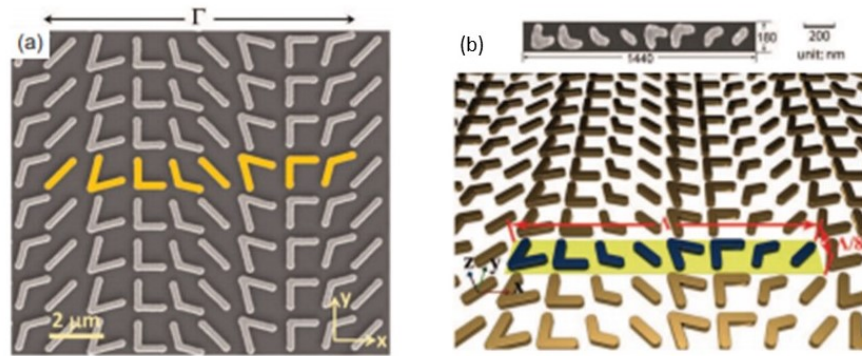


Figure 3.2: a) SEM image of a metasurface consisting of an array of V-shaped gold optical scatterers patterned on a silicon wafer. It creates a constant gradient of phase jump along the metasurface for the control of the propagation direction of light transmitted through or reflected from the metasurface. b) 3D top view of the metasurface and the super-cell periodicity. [27]

The V-shaped elements are altered and designed in a way to respect the generalized phase law of reflection and refraction for anomalous beam control. In this case the metasurface was used for the application of polarization wave control. The generalized phase law of reflection has also been demonstrated for gradient metasurfaces and reflect arrays for anomalous reflection [28, 29, 236–238]. An example of demonstrated gradient metasurfaces following the generalized phase law of reflection introduced by the group of professor S. Sun in the optical and microwave regions is shown in Figure 3.3.

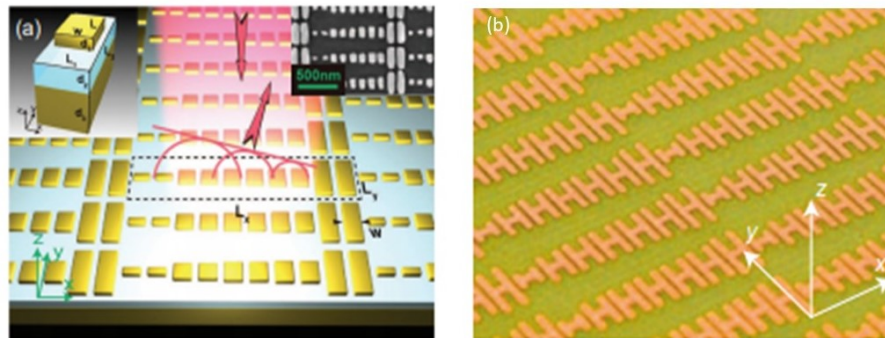


Figure 3.3: a) Schematic of a metasurface design consisting of gold patch elements separated from a gold back plane by an MgF2 spacer with subwavelength thickness. [28] b) Fabricated microwave metasurface design consisting of H-unit cell elements separated from a metallic back plane by a dielectric spacer. [29]

It has also been used and demonstrated for multi channel beam splitters gradient metasurfaces [30]. Jun Wang et al. used dielectric based metasurfaces to achieve multi-beam splitting systems at multiple channels. The design of the beam splitting metasurface is shown in Figure 3.4.

Jun Wang et al. [30] illustrated a new technique using the triangles drawn with black dotted line, which consist of nanocylinders with the same phase delay, and the adjacent triangles are composed of nanocylinders with $\pi/2$ phase difference. This leads to three phase gradient directions along the orange arrows in the interface. Thus, with normally incident wave, the beam is divided at the

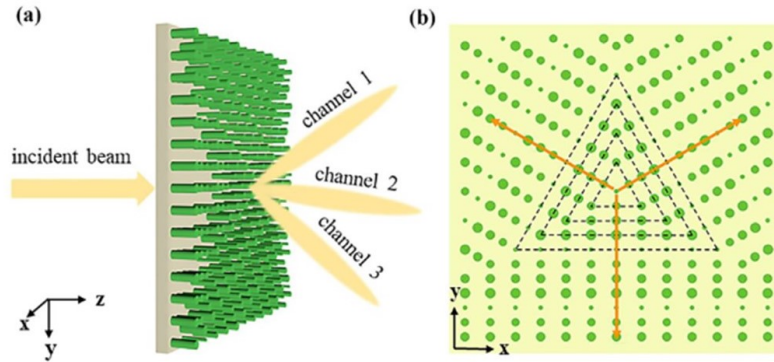


Figure 3.4: a) Illustration of the three-channel beam splitter. The incident beam is split into three transmitted beams. b) The structure profile of the gradient metasurface. There are three phase gradient directions along the arrows, and each triangles drawn with black dotted line represent nanocylinders with same phase delay. [30]

metasurface, resulting in the split of the transmitted light. The transmitted beams are expected to refract into three directions along each phase gradients direction. The angles of split- beam can be obtained according to the generalized Snell's law [27,28].

3.2.3 Retro-Reflection

Retrodirectivity or Retro-reflection has also been an interesting feature to validate the concept of the generalized phase law of reflection, by introducing the design of retrodirective metasurfaces and reflect arrays. For an incident incoming wave hitting a metallic surface, the wave is supposed to reflect in the specular direction according to the conventional law of physical optics. However, by introducing a specific phase gradient for an engineered topology following the generalized phase law of reflection, the wave can be redirected back in the same direction of incidence, which can be an important feature for many applications. The concept is illustrated in Figure 3.5.

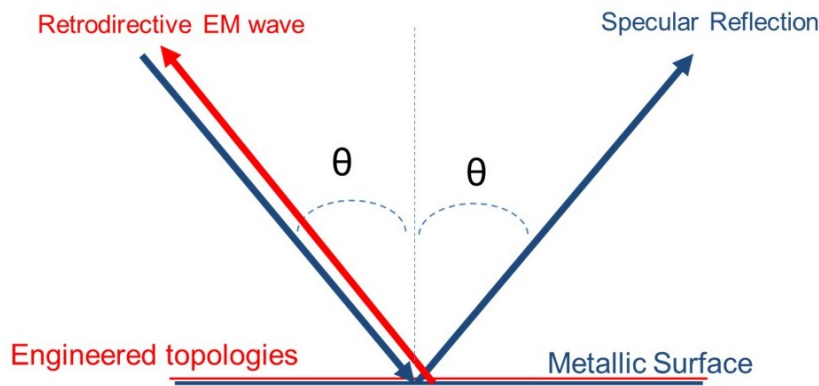


Figure 3.5: Comparison between the reflection of an incident wave from an engineered topology and metallic surface.

The idea of retrodirectivity comes from the concept of the conventional Snell's law of reflection when a wave is reflected from a mirror or metallic surface at normal incidence. However, by introducing a phase gradient for retroreflection, the wave can be manipulated in way it can experience various

virtual mirrors at oblique incident angles. Particularly for the case of retro-reflection, the incident angle $\theta_i = -\theta_r$ where θ_r is the angle of reflection. To ensure control of the full wavefront of the propagating wave, the integration (from 0 to 2π) of the generalized phase law of reflection is applied. In this case the periodicity of the gradient super-cell defines the full control of the propagating wave in a desired direction. Thus, for the case of retrodirectivity, the periodicity L_x is defined as follows:

$$L_x = \frac{\lambda}{2 \sin \theta_i} \quad (3.3)$$

L_x in Equation (3.3) defines directly the principle to design a retrodirective metasurface. Where the performance of retro-reflection for the metasurface design, depends directly on the relation between the periodicity L_x and the wavelength λ , where θ_i varies according to the incident angle desired for retro-reflection. To design a retrodirective reflective surface, a periodic design of super-cells is introduced. Each super-cell is constructed of scatterers with a specific phase gradient depending on the desired wave control of interest. The phase gradient [52] is given in Eq.(3.4).

$$\phi_{N+1} - \phi_N = 2K_0 d_x \sin \theta_i \quad (3.4)$$

d_x refers to the periodicity of the unit cell containing the scatterer element, which is defined as $d_x = L_x/N$ and K_0 is the wave number. In the case of retrodirectivity Eq.(3.3). is derived into Eq.(6.4). to determine the phase gradient for a retrodirective super-cell which is repeated in a periodic manner to form the metasurface. The phase gradient is given in Eq.(3.5).

$$\phi_{N+1} - \phi_N = \frac{2\pi}{N} \quad (3.5)$$

E. Doumanis et al. introduced the design of retrodirective surfaces based on the reflect array approach [31]. The aim was to design a reflective interface which can validate the concept of the generalized phase law of reflection, using metallic grounded designs. They designed a retrodirective surface at one specific desired angle. The design of the reflect array they introduced is shown in Figure 3.6.

The design shown in Figure 3.6 is basically a periodic structure of super-cells each divided into subwavelength scatterers with a phase gradient to achieve retro-reflection at a desired angle. E. Doumanis et al. defined the design as a reflect array, based on having a periodicity of $\lambda/2$. However, it is also well known that for a designed surface with subwavelength thickness and design, it can also be known as a metasurface, specially that the unit cell elements are of subwavelength dimensions up to $\lambda/24$.

Later on, V. S. Asadchy et al. [32] introduced the concept of multi-channel retrodirective metasurface. The concept was based on implementing a surface impedance optimization or modulation, in which a purely imaginary retro-reflective super-cell design can be achieved.

$$Z_{si} = j \frac{Z_{TM}}{\tan(\frac{\phi_i}{2})} \quad (3.6)$$

Equation (3.6) defines the surface impedance Z_{si} needed for each element where ϕ_i defines the phase of the reflection coefficient. This is applied for periodicities of dimensions which are greater than λ , thus giving rise to the ability to re-direct an incident wave back in the same direction at various angles simultaneously, thus giving remarkable unprecedented physical properties to the physics of metasurfaces (Figure 3.7).

Retro-reflection can be a remarkable feature where localization, tracking, sensing and radar cross section needs to be enhanced and more efficient. Following the given concepts of the generalized phase law and impedance modulation, metasurfaces can be remarkable in terms of retro-reflection, specially with their passive features, ease of fabrication and implementation.

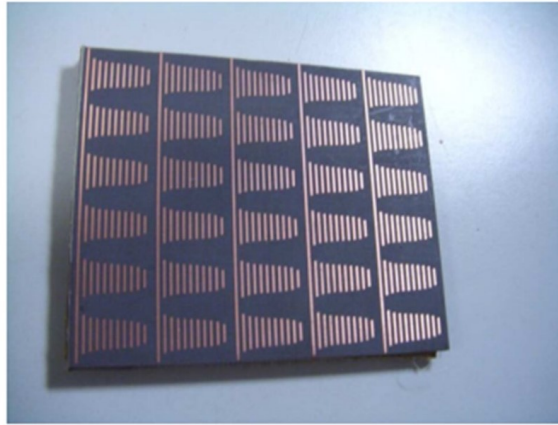


Figure 3.6: Photograph of the fabricated prototype that consists of 5×6 unit cells with overall dimensions of 7.2×6.0 cm [31].

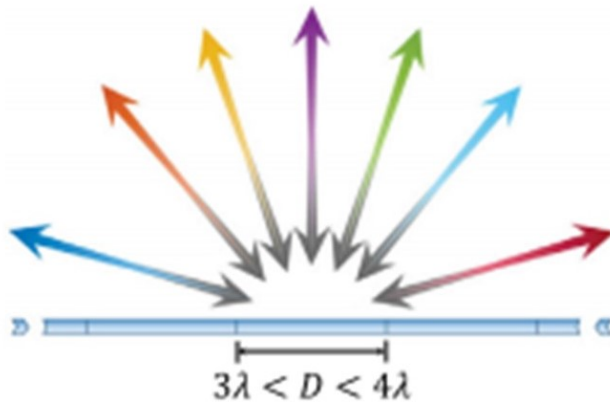


Figure 3.7: N-port isolating mirror. The wave incoming from different angles is reflected back to the source for various angles of incidence. [32]

3.3 Metamaterials and Metasurfaces Based on Absorption

With the variety of applications and characteristics for metasurfaces, high efficient absorbing metamaterials and metasurfaces have been an important topic for many researchers, specially for applications from acoustics, radio to optical frequencies where absorption is needed and useful. Many researchers defined metamaterial absorbers as perfect absorbers, in which zero energy is reflected back from the designed surface [74, 239, 240]. They are usually consisted of resonant subwavelength elements with thin thickness, which are repeated in a periodic manner to form a metasurface design. They are well matched at the desired resonant frequency, to ensure high efficient absorption. Different techniques have been presented to achieve high efficient absorption [35] such as using bending shapes [241], high resonance metamaterial structures with narrow band absorption [242], as well as other techniques for multi-band [243] and ultra-wideband absorbing metamaterial designs using multi-layer structures [244] and designs with a low quality factor [245].

From the theoretical point of view and derivation of Maxwell's equations, Y. Ra'Di *et al.* [33], introduced the derivations and theoretical analysis of the current distribution for such metasurface

designs, and explained the operation principle for absorbing surfaces. For more details of the operation principle and the derivation of Maxwell's equations please refer to the following reference [33].

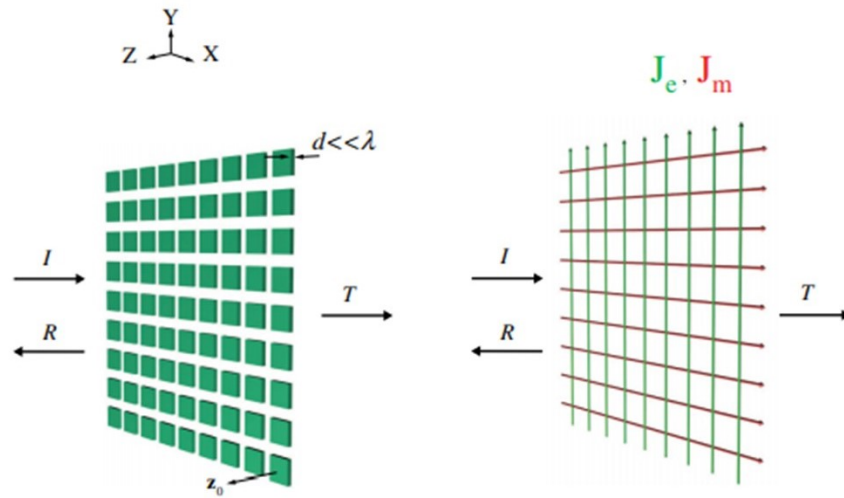


Figure 3.8: Geometry of a generic optically thin absorbing layer (left) and its equivalent model as a set of two current sheets (right). [33]

Figure 3.8 shows the generic view of a metasurface absorber with a normally incident plane wave. With the assumption of having an optically thin periodic structure, the surface generates a magnetic and electric surface current density as shown in Figure 3.8. With the use of different element components such as split ring resonators, patches or other metamaterial inclusions, each element acts as a resonant structure, which then forms a perfect absorbing designed surface.

The design of a metasurface absorber characteristics can differ, from single band absorbers to multi-band and wide band frequency designs. Different designs and techniques have been introduced in the literature which mostly depend on the characterization and optimization of the unit cell metamaterial resonating structure. N.I.Landy et al. [34] introduced the design of a perfect metamaterial absorber based on an electric resonator with a cut wire. The unit cell element is shown in Figure 3.9a.

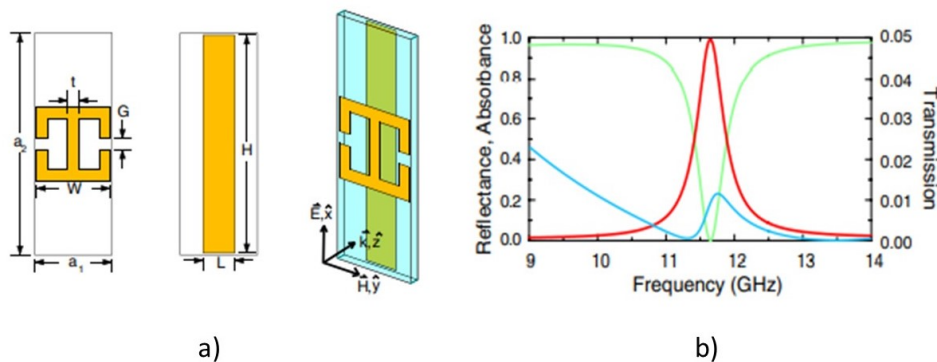


Figure 3.9: a) Electric resonator and cut wire from different angle views. b) Reflection in green, Absorption in red and Transmission in blue with respect to frequency of the designed element. [34]

The metamaterial element design depends on the coupling between the structures of the cut wire and the electric resonating element. This however, gives rise to the perfect absorbing element. As shown in Figure 3.9b, the metamaterial absorber shows a high level of absorption at 11.7 GHz.

Other size efficient metamaterial absorbers have also been introduced for ease of fabrication and implementation at low frequencies [35]. The design is basically based on structures with high inductance and capacitance, this is in order to shift the resonant frequency of the metamaterial element to lower frequencies, maintaining the miniaturized and compact design in terms of dimensions. An example of such design is shown in Figure 3.10.

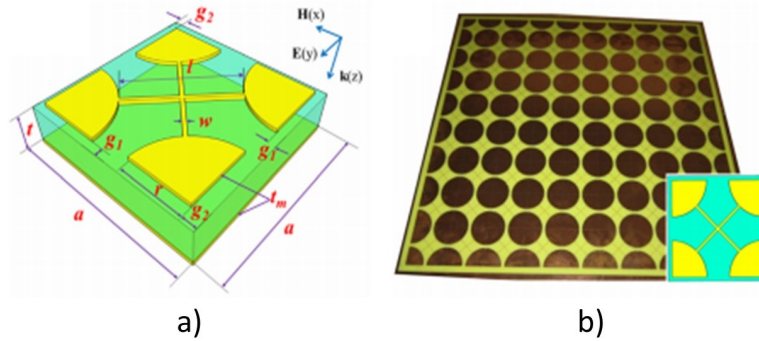


Figure 3.10: a) Proposed metamaterial element for miniaturized designs. b) The metasurface structure of such element operating at 400 MHz. [35]

The dimensions of the given design in Figure 3.10a in terms of wavelength is $\lambda/12$ and of thickness $\lambda/94$. The proposed design is a great solution for applications at low frequencies, specially in terms of miniaturization and ease of fabrications. Moreover, in terms of frequency bandwidth, various designs and techniques have been introduced for wide-band metamaterial absorbers. Jingbo Sun *et al.* [36] introduced a well known technique using multi layer metamaterial unit cell elements, in order to achieve a wide-band metasurface absorber design. An example of the design is shown in Figure 3.11.

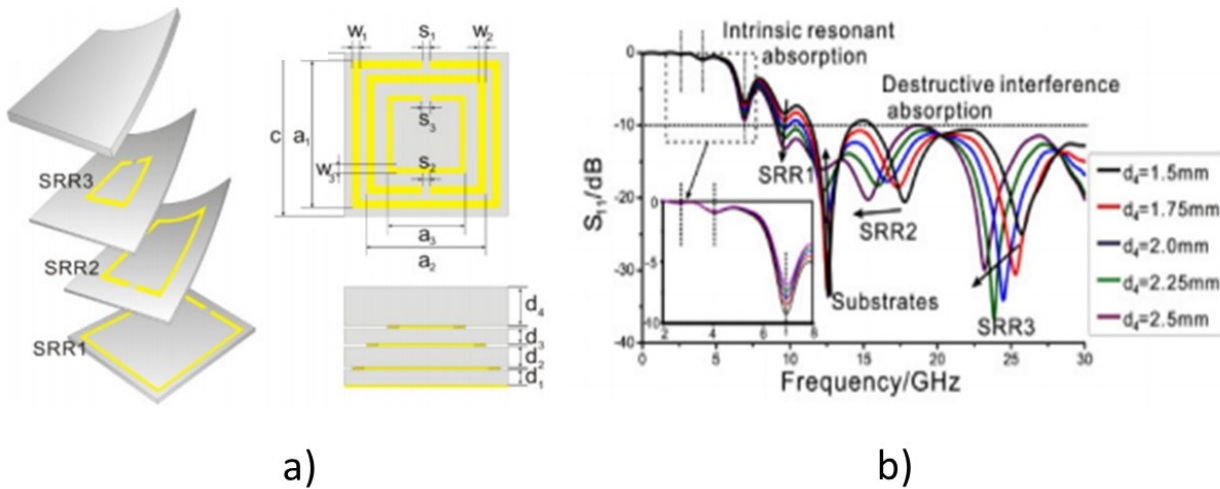


Figure 3.11: a) Split ring resonators using multi-layer technique. b) Reflection coefficient of the metamaterial design. [36]

Figure 3.11 shows the design of a multi-band absorber metamaterial element using the stacking or multi-layer technique. Absorption at a wide band of frequencies was achieved as shown in Figure 3.11b between 10 GHz up to 30 GHz. Other techniques have also been used such as ultrathin opposite ring designs to achieve wide-band absorption [37].

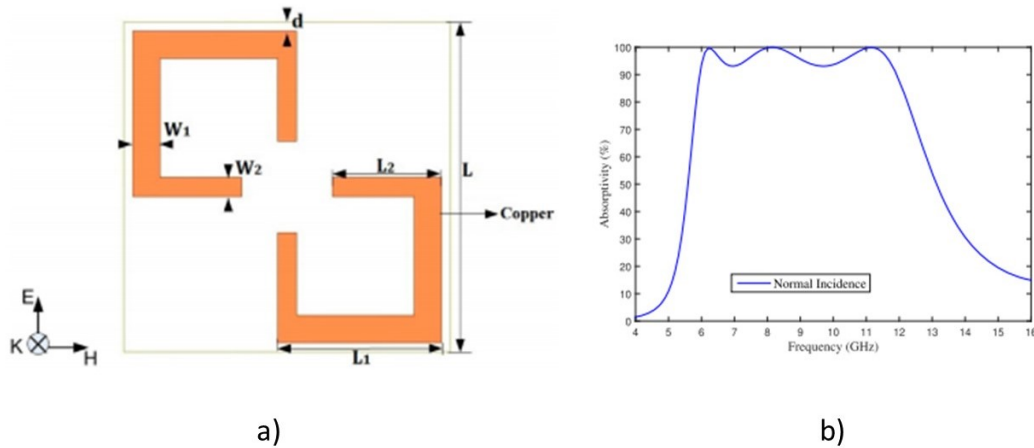


Figure 3.12: a) Dual ring metamaterial absorber unit cell element design. b) Absorption with respect to frequency. [37]

Figure 3.12 shows the design of a dual ring element absorber design, a perfect high level of absorption was achieved at a wide band of frequencies between 6 GHz to 10 GHz.

3.4 Metasurface Energy Harvesters

Electromagnetic energy harvesting based on metamaterials has been a significant topic for researchers nowadays, specially with the rise of challenges for antenna and rectenna systems, such as low efficiency, miniaturization, fabrication and implementation at low frequencies for GSM bands. The group of professor Omar Ramahi [38, 212, 246–249] have introduced a novel technique for metamaterial energy harvesters based on the concept of absorption. The concept is to design a high efficient metamaterial absorber design, and introduce a via between the designed element and a ground metallic plane through a substrate, where a load resistance matching the metamaterial structure design in terms of impedance, is inserted at the bottom end of the via. In this way, the energy absorber by the metasurface absorber is dissipated through the via towards the load resistor. An example of the concept design is shown in Figure 3.13.

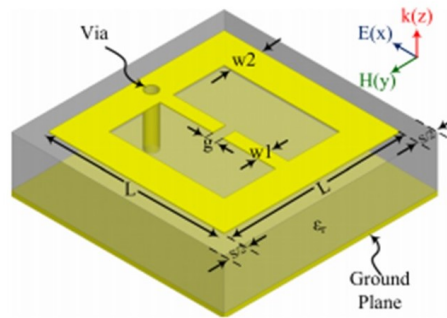


Figure 3.13: Metamaterial unit cell energy harvester design. [38]

Figure 3.13 shows an unit cell element of an ELC (Electric Inductive Capacitive) resonator metamaterial structure. A via is introduced between the ELC and the ground plane through a Rogers TMM10i dielectric substrate of relative permittivity $\epsilon=9.9$. A load resistance is the inserted at the

bottom end of the via of 82Ω where the absorbed energy is dissipated. The results of the design are shown in Figure 3.14.

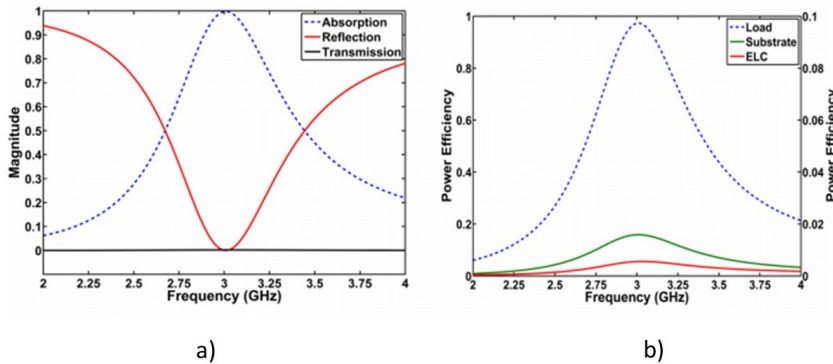


Figure 3.14: Metamaterial unit cell energy harvester design. [38]

The results in Figure 3.14a show a high level of absorption for the metamaterial design up to unity with zero reflection, and zero transmission due to the presence of the ground plane. In Figure 3.14b, the power efficiency is calculated where it is given that the energy is mostly dissipated through the load resistance.

3.5 Metasurface Lenses: Wavefront Shaping and Focusing

Metasurfaces have shown remarkable physical properties in terms of wave control and manipulation for desired applications. Moreover, metasurfaces can be also of great potential for wavefront designing and beam focusing at microwave and optical frequencies. However, in order to design a focusing lens or metasurface, to control the wavefront of an EM wave, the reflection phase should follow a hyperboloidal profile of the generalized phase law given in equation (3.7).

$$\phi(x, y) = \frac{2\pi}{\lambda} (f - \sqrt{(x^2 + y^2) + f^2}) \quad (3.7)$$

This concept is achieved by introducing subwavelength scatterers each with a specific phase to achieve the phase profile given in equation (3.7), where f is the focal point away from the designed metasurface. Thus this can be interesting to achieve using flat engineered surfaces rather than spherical parabolas which can be useful for certain applications. Flat metasurface lenses for wave focusing have been demonstrated at THz [39] and microwave frequencies for different applications [40]. The focusing metasurface was designed using different unit cell structure elements. An example of a metasurface unit cell element is shown in Figure 3.15.

Using the unit cell element structure in Figure 3.15, a focusing metasurface was designed at THz frequency to focus the propagation of light in a desired direction, following the hyperboloidal profile of the generalized phase law. The designed metasurface is shown in Figure 3.16a, it can be seen that the dimensions of the unit cell elements differentiate each with a specific phase. The phase and dimension of each unit cell is chosen using the phase of the reflection coefficient. In Figure 3.16c, the focusing intensity is given for the metasurface at various frequencies. Focusing metasurfaces have

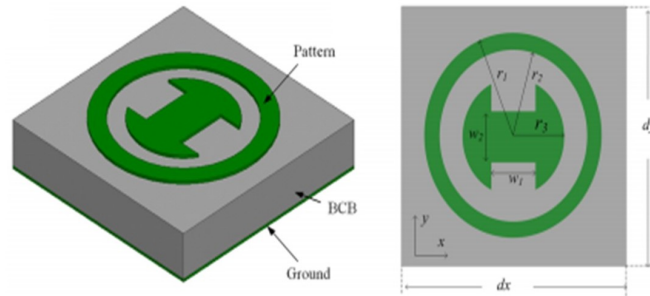


Figure 3.15: 3D design of an unit cell element structure and top view at THz frequencies for EM focusing. [39]

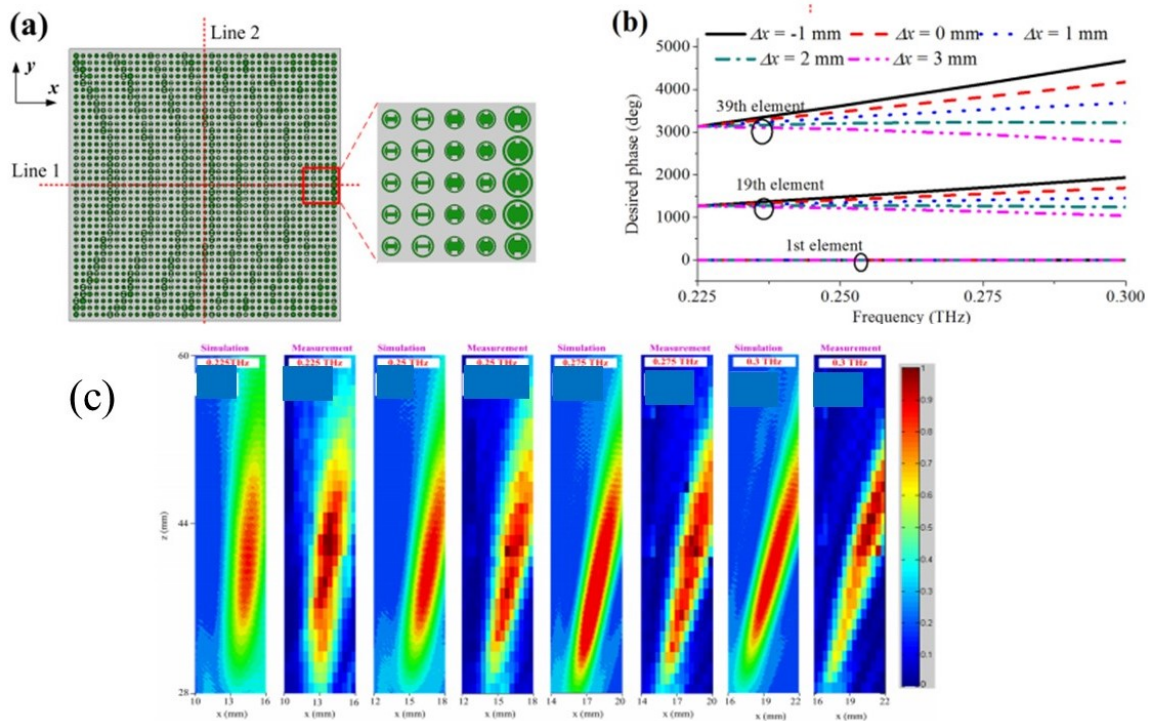


Figure 3.16: a) Focusing metasurface design. b) Desired phases for the unit cell scatterers with respect to frequency. c) Focusing intensity of the metasurface design at different frequencies. [39]

also been used for other applications such as satellite telecommunication systems [40]. This is for communication applications, where the desired wave is focused at a single point for better transfer of energy. An example of the design is given in Figure 3.17.

Figure 3.17a shows the geometry of a tri-dipole unit cell element designed for communication applications at 5.8 GHz. The structure is then distributed periodically to form the focusing metasurface design as shown in Figure 3.17b. To calculate and validate the functionality of the metasurface, a prototype is fabricated and the electric field intensity is calculated at the distance of the focal point. The designed prototype and electric field intensity is shown in Figure 3.18.

Figure 3.18a shows a prototype of the fabricated focusing metasurface with measurements carried on in the near field. The results in Figure 3.18b show that the metasurface focuses the energy at the

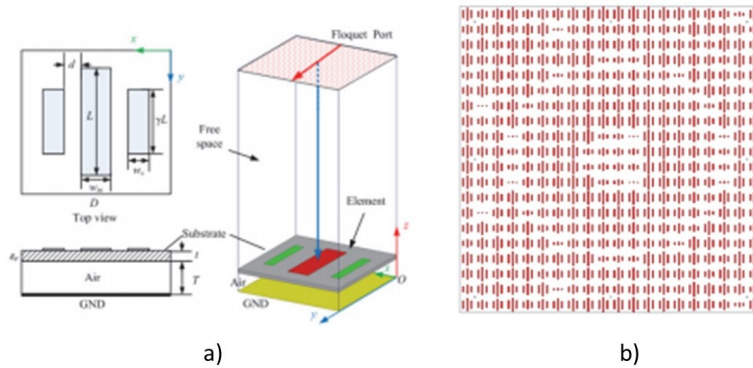


Figure 3.17: a) Geometry of a tri-dipole unit cell element. b) Focusing metasurface design with periodic unit cell tri-dipole elements each with a specific phase. [40]

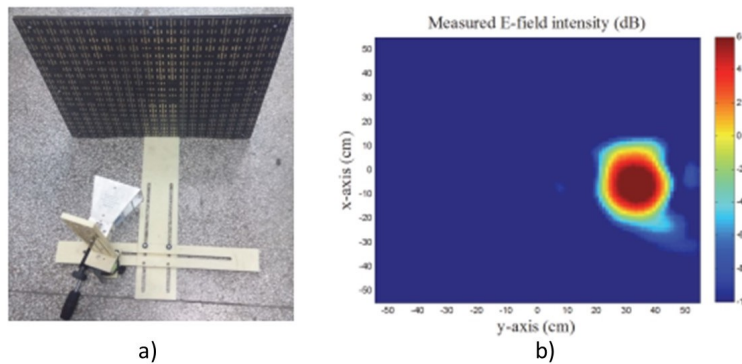


Figure 3.18: a) Prototype fabrication and measurements in the near field. b) Electric field intensity of the x-y plane at the distance of the focal point. [40]

focal point in the desired direction at the specular reflection angle where the electric field intensity is shown to be high.

3.6 Conclusion and Future Work

Metasurfaces have shown remarkable physical properties over the past decade with their characteristics and design approach, for wave control and manipulation. Metasurfaces can vary in terms of wave manipulation depending on the design approach and application needed. Anomalous reflection to a desired direction, is a well known property for metasurfaces depending on the chosen profile following the concept of the generalized phase law. It has also been shown that metasurfaces can be high efficient absorbers where absorption is needed in different applications. Moreover, in term of energy harvesting, metasurfaces with high absorption rate, can be used as significant EM energy harvesters when introducing a via for energy dissipation through a rectenna system. The progress and demand for EM wave control in the environment, have pressed researchers to overcome limitations and challenges for passive metasurfaces. Reconfigurable active metasurfaces were introduced for enhancements in terms of design limitations and efficiency, specially with the rise of various technologies such as IoT and 5G communication systems. In this chapter, we introduced a brief overview on metasurfaces with respect to their characteristics and physical properties. Some existing research work was given for some of the main properties of metasurfaces in terms of anomalous

reflection, wavefront forming, focusing, retro-reflection, energy harvesting and active metasurfaces. In the following chapters, we focus on the benefits and significance that metasurfaces can bring with their remarkable physical properties, for enhancement of the performance of energy harvesting and wireless power transfer systems in the railway environment.

Chapter 4

Novel Concept for EM Energy Harvesting Based on Focusing Metasurfaces

4.1 Introduction

Energy harvesting is a process in which energy is captured and stored as electric energy. This energy can vary from solar [193], heat [250], wind [251], hydro [252], mechanical vibrations [253] and electromagnetic [254–256], which can be useful to feed different devices such as wireless autonomous technologies and sensors. In the field of electromagnetic energy harvesting, various research topics and inventions have been introduced for different applications. Some of the existing EM energy harvesters include applications based mainly on piezoelectric [47, 257–259], rectenna systems [260–264] and metamaterial absorbers [38, 78, 265–268].

Nowadays at radiofrequencies, rectenna systems are used for energy harvesting and wireless power transfer [263]. This commonly used technology, which consists of a classical antenna at the front end (dipole, microstrip lines, antenna arrays... etc) whereby the antenna is known as the collector of the transmitted energy, is then connected to a rectifying circuit where EM energy is converted to DC and stored in a storage element. Rectenna systems have been used for different applications and inventions. One of those we can mention are methods for enhancing subsurface recovery of fluid [269], wireless power transfer [270], RF energy harvesting [271], rectenna solar energy harvesters [272]. However, the antenna part of the rectenna system, which has the function of capturing the EM energy, should be as efficient as possible to ensure an adequate designed rectenna system. On the other hand, the ambient energy at frequencies between 900-950 MHz can have a very low level and thus either become difficult to harvest or insufficient to consider for its use in industrial applications.

Several research works have focused on the design of high-efficiency antennas to achieve EM energy harvesting. Moon and Jung [41] proposed an antenna design for RF energy harvesting based on two

radiators: the main one with a printed dipole and the other with a loop structure. The antenna design is suitable to receive energy from all directions. On the other hand, Xie et al. [273], designed a hexagonal microstrip patch antenna which operates at 915 MHz, to achieve maximum possible RF energy harvesting. The main objective is to increase the efficiency of the EM energy harvesting system and overcome the low efficiency of the collector which is the main part of the rectenna system.

In our novel concept, we propose and investigate a new solution based on the concentration and focusing of EM energy in a small zone. It consists of a focusing device together with a method to associate the latter with existing RF energy harvesting systems. The focusing surface is designed based on metamaterials, it is a 2D surface which is known as a focusing metasurface. Manipulating the properties of an electromagnetic wave is the main function of metamaterials [213]. Metasurfaces which are 2D structures of metamaterials, are more compact, less lossy and easy to fabricate engineered topologies [52, 274]. Based on different concepts for the manipulation of an electromagnetic wave, from anomalous wave manipulation [69, 70], absorption [38, 275, 276], focusing [277–280], polarization control [281], multifrequency [282] and multifunctional antennas [283], metasurfaces can be a good candidate in different applications [61].

However, in our concept based on the properties of focusing metasurfaces, the focal “point” is located at a given distance from the surface, depending on the operating frequencies. A rectenna system is then placed at this focal point. Moreover, the antenna collects the concentrated EM energy which is then converted to DC through a rectifying circuit. The energy level concentrated depends on the design of the focusing surface and its optimization but a gain of 5 times the amplitude can be reached. This novel concept and system, can be a good candidate for applications such as power supply for autonomous wireless sensor nodes .

In this chapter, we will discuss a few relevant inventions and publications concerning rectenna devices and their disadvantages and the problem we can overcome using our system. We will discuss in details the main concept, principle of operation and design procedure. The objective of the concept is to propose a solution to low efficiency and to increase the level of power collected by RF energy harvesting systems through the use of a focusing metasurface of given dimension with respect to frequencies of the ambient EM energy. We will also show how this device can be used with in addition to existing commercial off-the-shelf harvesting systems. Measurements have been carried on and a prototype has been fabricated and the concept has been tested and validated in an anechoic chamber.

4.2 Rectenna Systems

In this part, we will discuss a few relevant inventions and publications concerning rectenna devices and their disadvantages and the problem we can overcome using our system.

4.2.1 Antenna efficiency improvement and metamaterial RF harvesters

One of the aims of the focusing metasurface is to increase the efficiency of the RF harvester. Another possibility to reach this aim is to consider the use of more efficient antennas as disclosed by patents [50], [51] and the publications [41], [273]. J.I Moon et al. [41] have introduced designs for high efficient antennas for energy harvesting. The antenna design they presented in shown in Figure 4.1.

The antenna has shown interesting results in terms of matching and efficiency [41]. In [284, 285], EM energy harvester based on metamaterials are introduced. The design is based on an array of unit cells, which are then connected to load at the end part of the via. The advantage of this design, that it can be more efficient than other types of antennas (microstrip, patch, dipoles... etc). However, multiple rectifying systems will be needed and it can be difficult to implement at RF frequencies which can be a challenge. In our case, we overcome the problem of using multiple rectifiers, by using only one rectenna system with an efficient antenna. The concept is that, the focusing metasurface concentrates the energy where the rectenna can easily collect and convert into DC energy.

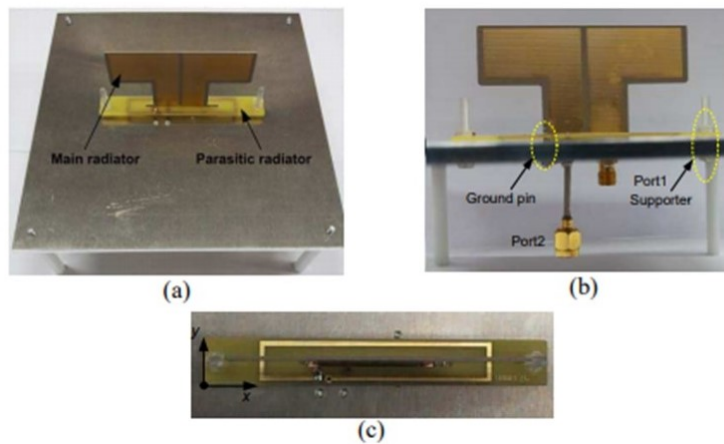


Figure 4.1: Fabricated proposed energy harvesting antenna. (a) Perspective view. (b) Side-view. (c) Top view. [41]

4.2.2 Technologies Commercialized

RF energy is transmitted around the world from different base stations and antennas (GSM, GSM-R in Railway environments, RF Base station transmitters, television... etc). These energies are free ambient energy that we can take advantage of by RF harvesting and enabling wireless charging giving rise to autonomous systems and easier implementations.

RF energy harvesting commercialized technologies such as the Powercast's Powerharvester (P2110) receivers convert RF energy to DC current. These technologies can be good candidates to harvest energy for a wide range of operating conditions and tracking the maximum energy in the ambient environment. In our invention, we propose a Focusing Metasurface which can concentrate the energy at one point for more efficient electromagnetic energy harvesting.

Any rectenna technology can be implemented with this concept to maximize energy harvesting and increase the efficiency available. The proposal is a complementary, passive and low-cost solution increase the power delivery from RF energy harvesting device in a given environment.

4.3 Concept of EM Energy Harvesting Based on Focusing

Rectenna systems [136] are formed of a classical antenna which are developed for electromagnetic energy harvesting. They also provide the ability for wireless power transfer at microwave [286] and terahertz [287] frequencies. However, the rectenna system efficiency is low, they make use of traditional antennas which have a proportional dimension with respect to the operating wavelength [288]. Different methodologies have been applied to enhance the efficiency of the rectenna design for RF energy harvesting. Those we can mention which have been defined in the state of the art, are inventions which disclose RF energy harvesters based on metamaterials and antenna arrays [284, 285, 289–292], and other researchers have worked on increasing the efficiency of the antenna itself for better energy harvesting [41, 51, 273]. In terms of commercialized technologies, several products exist. One of them we mention here is the Powercast's Power energy harvester (P2110) receivers which are used to convert RF energy to DC current. These technologies can be a good

candidate to harvest for a wide range of operating conditions and tracking the maximum energy in the ambient environment.

In our novel system and concept, we propose a new technique to increase the efficiency of RF energy harvesting systems including the existing commercial ones. The method is based on the implementation of a focusing device to be a complementary solution with existing RF energy harvesting devices. The device is based on metamaterials which is well known as metasurfaces. Metasurfaces [52, 274] have gained remarkable interest from researchers, especially for their ability to manipulate an electromagnetic wave in an unconventional manner. Recently, Long Li et al. [293] have given a review and perspective on the progress of metasurfaces and their potential for ambient RF energy harvesting. Hence, we apply a novel phenomenon based on focusing to improve the efficiency of RF energy harvesting devices. The concept is illustrated in Figure 4.2.

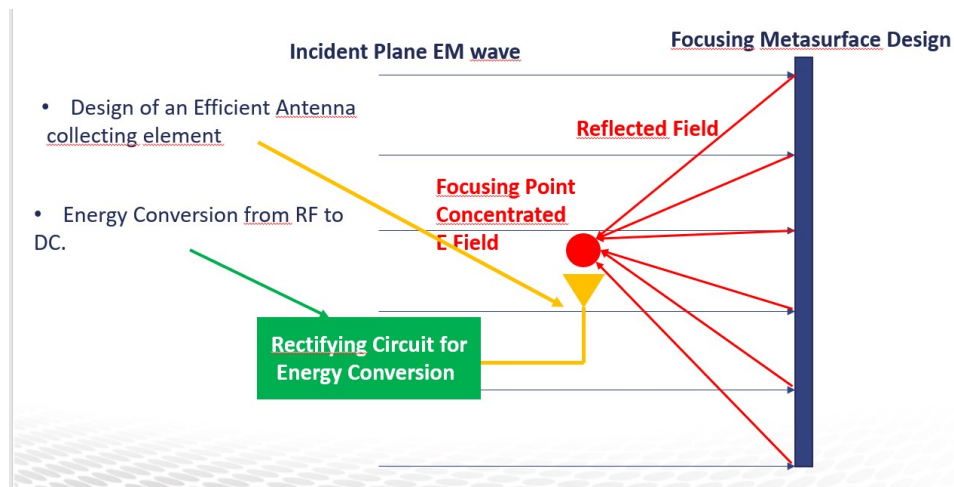


Figure 4.2: Concept of an EM energy harvesting system based on focusing

It is based on focusing EM waves radiated from ambient sources such that they are redirected to a focal point where a collector/antenna is positioned. This antenna is then linked to a state-of-the-art RF rectifying circuit.

4.4 Principle of Operation of the Novel Harvester

Metasurfaces have gained remarkable interest from researchers, especially for their ability to manipulate an electromagnetic wave in an unconventional manner. Among them, are focusing metasurfaces [39, 278, 294–296]. Focusing metasurfaces are 2D arrays of subwavelength scatterers that are designed to alter the characteristics of an EM wave, such as its wavefront, polarization, distribution intensity or spectrum. Despite having negligible thicknesses, metasurfaces can have a strong control on the behaviour of an EM wave or light, leading to reflected and transmitted electric fields, whose phase and amplitude are given by the designed metasurface as shown in Figure 4.3.

However, wave focusing is defined in which the wavefront of the reflected incident EM wave is reflected back from an engineered surface design and changed into a parabolic manner where the energy is concentrated at a focal point as shown in Figure 4.4.

Hence, in this part we investigate this feature using focusing metasurfaces, to examine its potential for enhancing the performance EM energy harvesters rectifying systems.

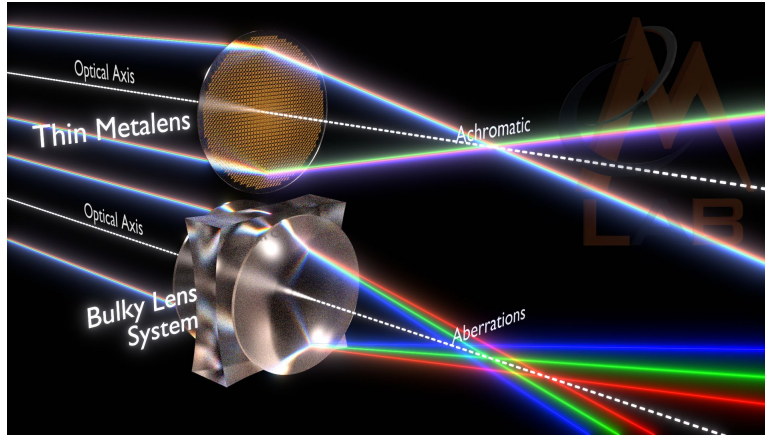


Figure 4.3: Functionality of a Thin Metalens compared to that of a bulky lens system for light focusing (The photo is referenced to EM Lab UTEP)

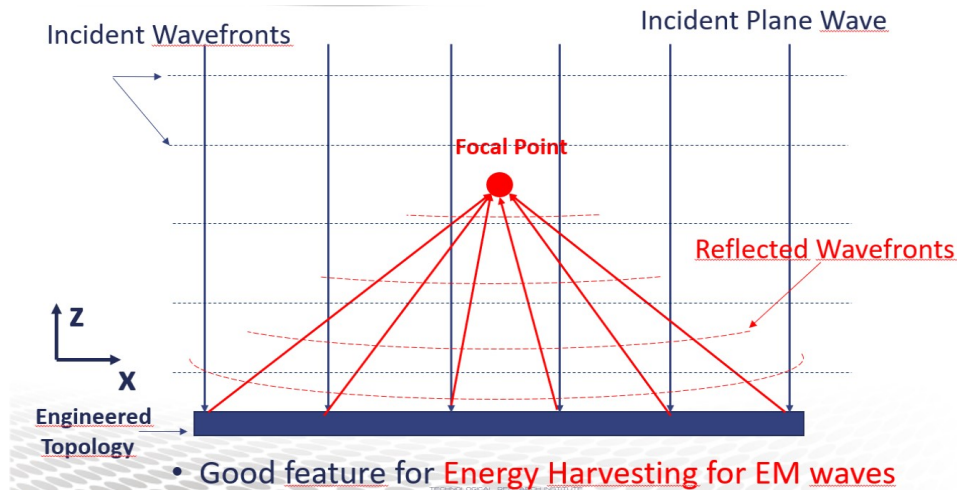


Figure 4.4: Concept of Wave focusing using engineered topologies.

4.4.1 Generalized Phase Law and Design Procedure of the Focusing Metasurface

The starting point of our concept and main part for the novel EM energy harvesting system is the design of the focusing metasurface. The considered focusing metasurface has an exceptional property where the phase of the reflected EM field is adjusted according to a phase within the 2π range, and maintaining high reflectivity from the designed structure. This is done by varying the dimensions and aspect ratio of the subwavelength scatterers chosen for the design. This approach is said to be convenient, since the phase of each scatterer is weakly influenced by its neighbor element in terms of reflection of the EM field, giving a total value in terms of wave control. This phenomenon was shown to be acceptable and proven for gradient index metasurfaces [27, 297]. However, for a flat based metasurface focusing in the x - z and y - z planes, the phase of the reflection coefficient should follow the hyperboloidal profile of the generalized phase law [40] given as follows in equation (4.1):

$$\phi(x, y) = \frac{2\pi}{\lambda} (f - \sqrt{x^2 + y^2 + f^2}) \quad (4.1)$$

ϕ is the phase of the reflection coefficient, f defines the focal point position away from the metasurface design, x and y the position of each unit cell elements and λ is the wavelength. The next step is to choose the most sufficient metamaterial unit cell for our application. In the our case for EM energy harvesting specially at GSM frequencies (900MHz), the dimensions of the resonant unit cells can be of large dimensions and a bit difficult for fabricating and testing. Various unit cell designs can exist for metamaterials in the literature one of those we can mention [216] such as cross structures, patches, circular unit cells and Split ring resonators as shown in figure 4.5.

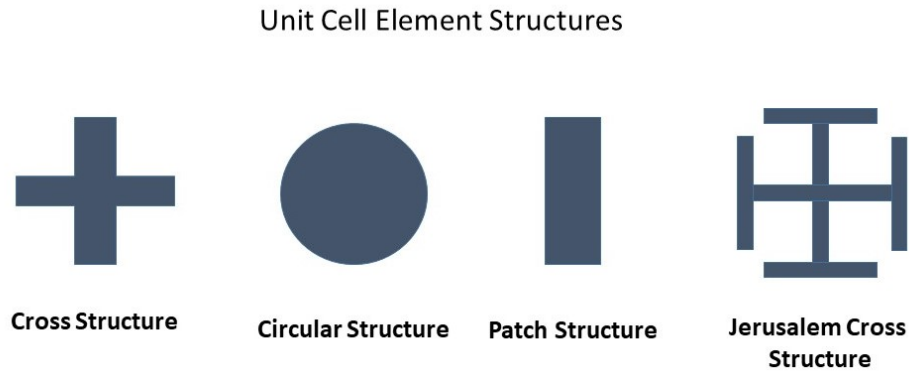


Figure 4.5: Metamaterial unit cell structures

However, for our design we have chosen the Jerusalem Cross unit cell element, this is mainly due to its miniaturized properties and maintain a good performance in terms of wave reflection and reflection phase profile with a subwavelength scale close to $\lambda/8$ compared to other structures which resonate at $\lambda/2$. The unit cell Jerusalem cross element and its dimensions designed using Ansys HFSS are shown in Figure 4.6.

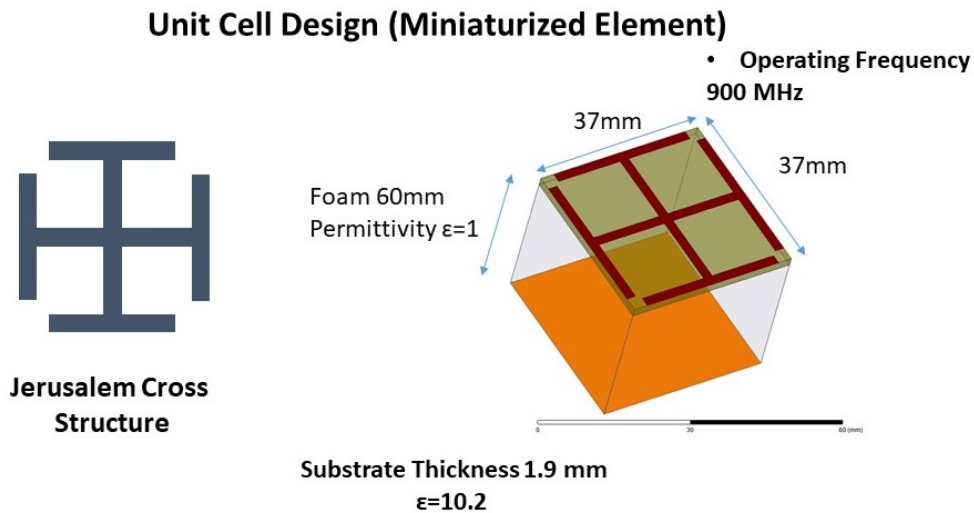


Figure 4.6: Geometry and dimensions of the unit cell Jerusalem cross design operating at frequency 900 MHz.

Figure 4.6 shows the geometry of the designed Jerusalem cross unit cell element operating at 900 MHz which is of dimensions $\lambda/9$ at the given frequency. Each unit cell element of the metasurface

is printed on top of substrate of dimensions 37 mm x 37 mm and thickness 1.9 mm and permittivity $\epsilon=10.2$. Behind the substrate there is a Foam layer of thickness 60 mm and a metallic ground plane.

For the analysis and design of the Focusing metasurface, a factor a is given to vary the dimensions between the scatterer elements of the metasurface design where each dimension refers to a specific phase as shown in Figure 4.7a. It is important to be able to accurately predict the phase of the reflection coefficient of the unit cell structure. Thus, to be able to calculate the phase, an infinite periodic model using Floquet boundary condition on Ansys HFSS to analyze the phase of the Jerusalem cross element at an operating frequency of 900MHz. We study the phase at normal incidence and for both TM and TE polarizations which have the same result. The phase of the reflection coefficient for the designed unit cell is shown in Figure 4.7b.

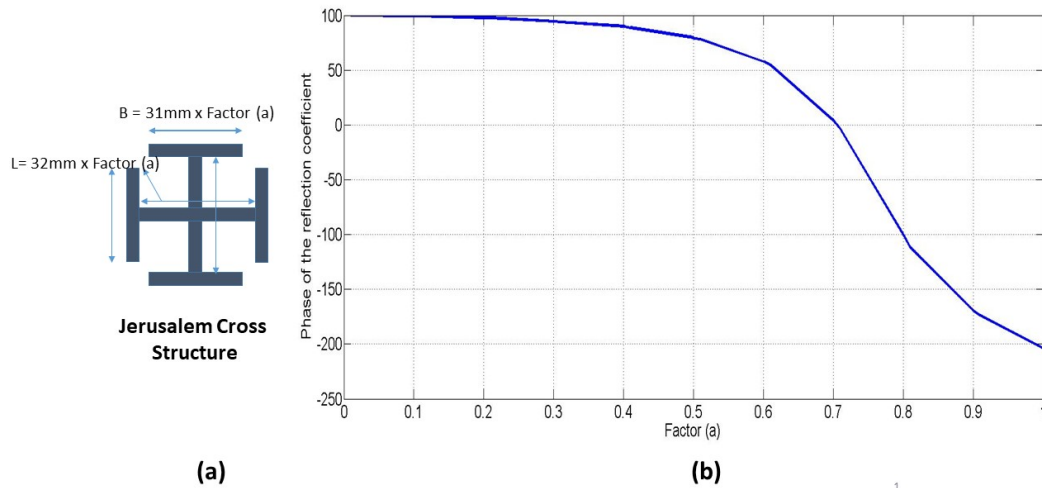


Figure 4.7: a) Jerusalem cross dimensions and a factor a to vary the element dimensions from initial to each with a specific reflection phase b) The phase of the reflection coefficient with respect to the factor a at a frequency of 900MHz.

The simulation results show a good and expected phase response over the profile range of 310° which can be used to determine the dimensions of each unit cell element of the metasurface design with a specific phase following the hyperboloidal profile for focusing. The metasurface design is composed of 21×21 unit cell elements in the x and y planes. The focal point is chosen to be equal to 30 cm away from the metasurface. The phase ϕ of each element is calculated according to equation (4.1). Figure 4.8 shows the calculation of the phase of each element in the x and y planes.

Thus, according to Figure 4.8, we are able to determine the phase of each unit cell element of the metasurface design following the hyperboloidal profile to achieve focusing. The dimensions are then determined using the phase profile of the Jerusalem cross in Figure 4.7b, where each phase corresponds to a Factor a giving the dimension of the unit cell element. Finally, after determining the dimensions of the unit cell elements, the unit cell elements are given on top of a Rogers duroid substrate of thickness 1.9 mm and permittivity $\epsilon=10.2$. Behind the substrate is a Foam gap layer of thickness 60 mm with a metal ground at the bottom. The metasurface design is shown in Figure 4.9 using Ansys HFSS.

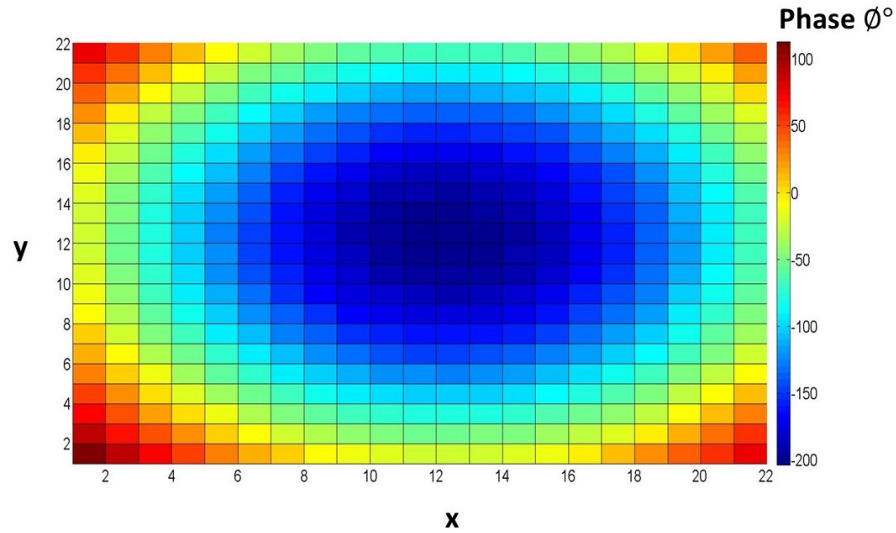


Figure 4.8: Phase of each element (21×21) of the metasurface design in the x and y planes at 900 MHz.

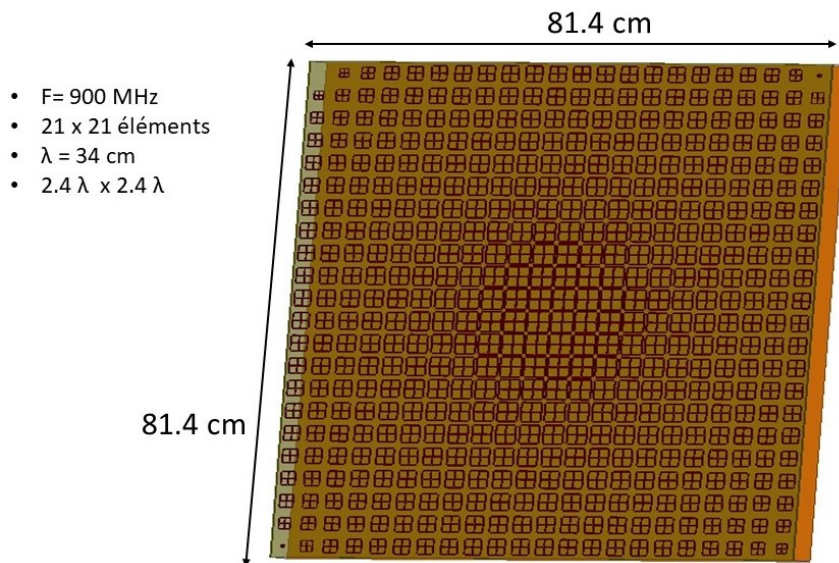


Figure 4.9: Focusing metasurface of 21×21 unit cell elements of dimensions $81.4 \text{ cm} \times 81.4 \text{ cm}$ operating at 900 MHz Using Ansys HFSS.

Figure 4.9 shows the focusing metasurface design on Ansys HFSS with 21×21 Jerusalem cross elements with each of a specific dimension and phase. The dimensions of the metasurface at the operating frequency 900 MHz are $81.4 \text{ cm} \times 81.4 \text{ cm}$ ($2.4\lambda \times 2.4\lambda$ with respect to λ). The thickness of the metasurface is composed of the substrate of 1.9 mm and a Foam gap of 60 mm with a metallic ground plane at the bottom.

4.4.2 Metasurface Focusing Point Using Ansys HFSS

The focusing metasurface has been simulated using Ansys HFSS. A Far-field plane wave has been illuminated at the operating frequency of 900 MHz. The electric field distribution of the incident and reflected waves have been calculated and illustrated on Ansys HFSS. The results of the electric field distribution are shown in Figure 4.10.

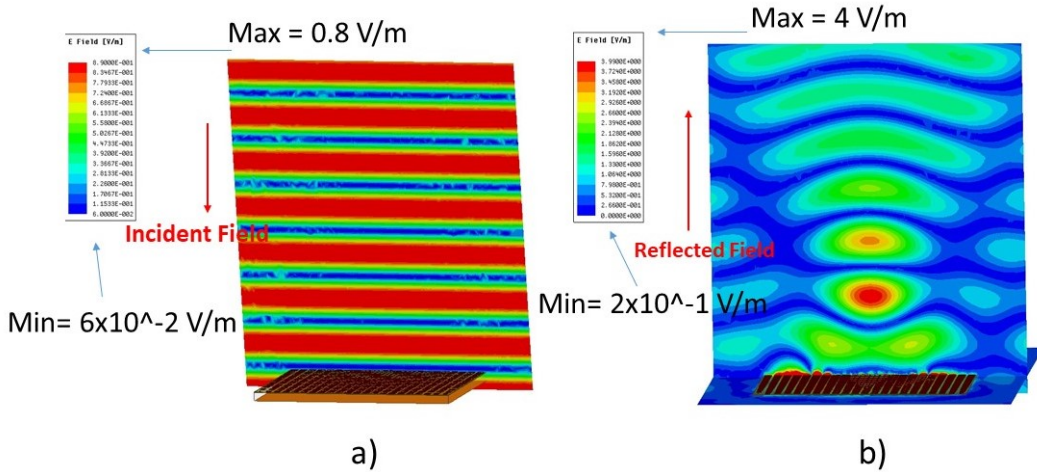


Figure 4.10: a) Electric field distribution of the incident wave illuminated towards the metasurface
 b) Electric field distribution of the reflected wave from the metasurface in the x-z plane operating in the far-field at 900MHz.

Figure 4.10a shows the distribution of the electric field for the incident plane wave towards the metasurface design. As it is illustrated, the wavefront of the electric field shows a max value in the horizontal direction at 0.8 V/m at an operating frequency of 900 MHz. In Figure 4.10b, the electric field distribution of the reflected wave from the metasurface design is shown. The results show a high concentration of electric field at the focal point 30 cm away from the metasurface. The max value of electric field distribution has been given to be 4 V/m which is a gain of 5 upon focusing compared to the incident field. It is also shown how the wavefront of the incident field is changed in a parabolic manner which is due to the hyperboloidal profile of the engineered metasurface. Table 4.1 shows the values comparing the max E-field in V/m between the incident and reflected wave and the gain upon focusing which up to 5.

Incident wave Max E-field	Reflected wave Max E-field	Gain upon focusing (in linear)
0.8 V/m	4 V/m	5

Table 4.1: Comparison of the max values of the electric field between the incident and reflected waves and the gain achieved upon focusing

In Figure 4.11 we show the distribution of the electric field of the focal point from different angles and planes at the operating frequency 900 MHz, reflected from the metasurface design.

From different angles in Figure 4.11 for the electric field distribution of the focal point where the energy is concentrated, the focal point is almost shaped as a 3D rugby ball 30 cm away from our flat designed focusing metasurface.

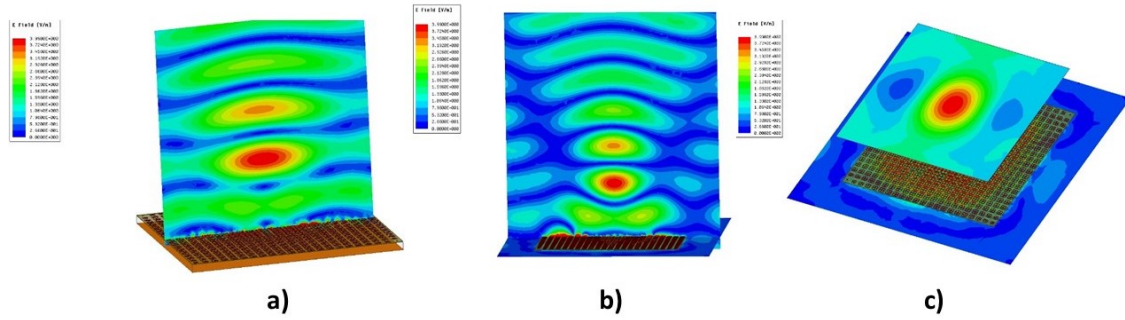


Figure 4.11: Electric field distribution of the reflected wave in the a) y-z plane b) x-z plane and c) x-y plane

After defining the design procedure and determining the results of our focusing metasurface, the next step is to validate our concept in terms of EM energy harvesting and investigate its usage, and how it can be sufficient for efficiency and potential enhancement for EM energy harvesting systems. In the next part we define an existing off the shelf existing EM energy harvesting system and how we can use our system to be a complementary to such devices.

4.5 The P2110 Power-Harvesting System- Off the Shelf Commercialized Technologies

In this part we define the main components, efficiency, set-up and applications usage of the P2110b Power harvester. (For a detailed reference please check the owner’s manual and datasheet of the P2110b Powerharvester).

4.5.1 Description

The Powercast P2110b Powerharvester is an RF energy harvesting device that converts RF to DC. Housed in a compact SMD package, the P2110B receiver provides RF energy harvesting and power management for battery-free, micro-power devices. RF energy is converted into DC and stored in a capacitor. When sufficient charge is stored the regulated output of the P2110 provides power to the wireless sensor board until the operation is completed by the node or until the power is turned off at the low-voltage threshold on the capacitor. The included wireless sensors measure temperature, humidity and light, and have an interface for an external sensor. The rectifying system of the P2110b harvester has great features in general, with high conversion efficiency, converts low-level RF signals enabling long range applications, wide RF operating range and operation down to -12 dBm input power.

4.5.2 Contents of P2110b Kit

The contents of the kit are shown in Figures 4.12 and 4.13 below. The kit includes an RF transmitter, RF energy harvesting receiver boards and antennas, wireless sensor boards, a PIC MCU-based development board and radio, and a programming tool.

4.5.3 Power Harvester’s Efficiency

The efficiency of the power harvester is important specially at our desired frequency for our application. The efficiency of the Power harvester P2110b with respect to input power and frequency are



Figure 4.12: The P2110b Power Harvester Development Kit for Wireless Sensors.(P2110b Owner’s Manual)

Qty	Item	Description
1	Power and Data Transmitter (TX91501-3W-ID)	FCC approved, 3-watt, 915 MHz transmitter for power and data with integrated 8dBi antenna and two power jacks. Sends a pre-programmed transmitter ID that is received by the P2110 Powerharvester component and is decoded by the MCU on the Wireless Sensor Board
2	P2110 Evaluation Board (P2110-EVB)	Evaluation board (Rev. B) for P2110 Powerharvester Receiver. This board has an SMA connector to connect the antennas and a 10-pin connector for the Wireless Sensor Board
2	Patch antenna	915MHz directional antenna with 120-degree reception pattern (included with the P2110 evaluation board)
2	Dipole antenna	915MHz omni-directional antenna with 360-degree reception (included with the P2110 evaluation board)
2	Wireless Sensor Board (WSN-EVAL-01)	Sensor for Temp/Humidity/Light and an external input. Plugs into P2110 evaluation board, and sends data to the access point (Microchip 16-bit XLP Development Board)
1	Access Point (WSN-AP-01)	Custom receiver board featuring Microchip’s PIC24F MCU that is pre-programmed to operate as an access point for receiving data from the Wireless Sensor Boards.
1	PICkit™ 3 programmer / debugger (PG164130)	Programming tool for updating code on the Wireless Sensor Boards and the 16-bit XLP Development Board. USB cable included in package.

Figure 4.13: Table showing the items in the P2110b Kit and descriptions of each. (P2110b Owner’s Manual)

shown below in Figures 4.14 and 4.15.

In Figure 4.14, the curves show that the powerharvester starts having an efficiency up to 40% at an input power of -10 dBm for a frequency of 915 MHz which is suitable for our application. However, in Figure 4.15 the harvester seems to have a high efficiency at a wide range of frequencies between 700-1200 MHz when the input power is as high as 5000 μ W as shown in Figure 4.15b, and functions quite well at the desired frequency of 900 MHz even for low input powers such as 250 μ W given in Figure 4.15a.

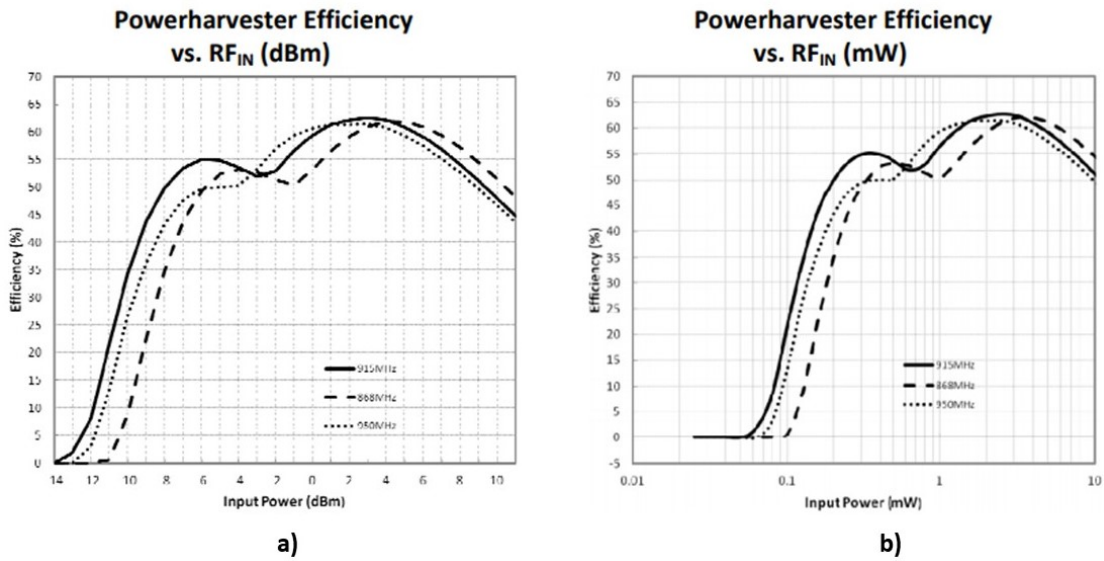


Figure 4.14: Powerharvester efficiency with respect to input RF power in a)dBm and b)mW (P2110b Powerharvester Datasheet)

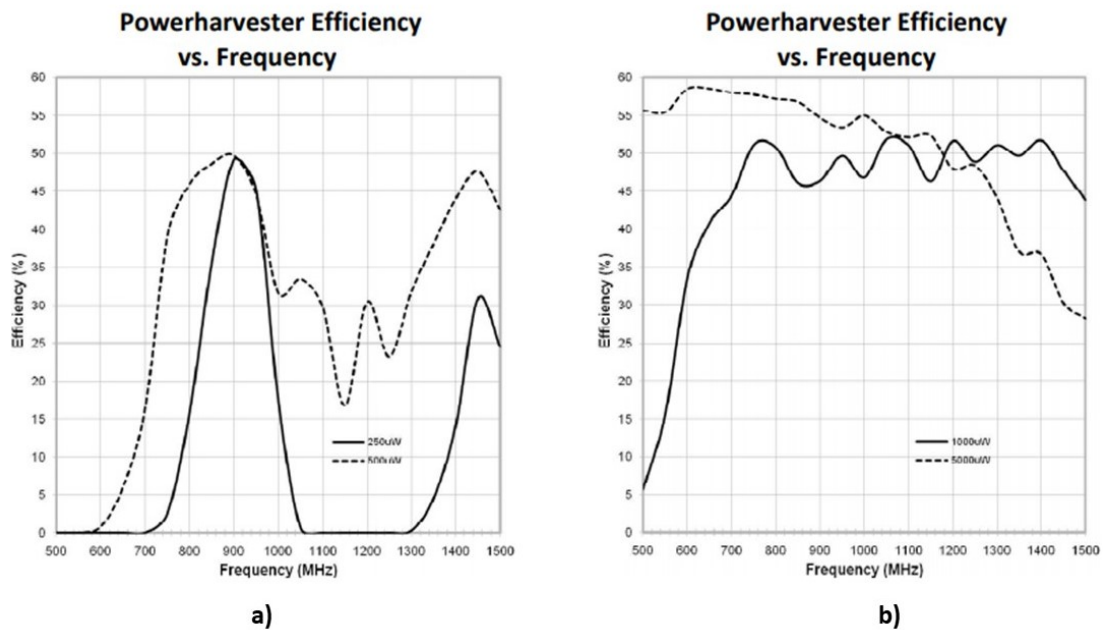


Figure 4.15: Powerharvester efficiency with respect to Frequency in MHz for an input power of a)250 and 500 μ W and b)1000 and 5000 μ W (P2110b Powerharvester Datasheet)

4.5.4 P2110b Setup, Testing and Installation

For the testing and installation of the device, the dipole antenna is attached to one of the P2110 evaluation boards. The access point is connected to a PC where the output results are illustrated and calculated. The MpLab program is installed and used to send the input program to the evaluation

board via the access point. A hyperterminal with the good inputs is used to illustrate the results for testing. The set up for testing and installation and example of the output data illustration of the calculated results by the harvesting system are shown in figures 4.16 and 4.17.

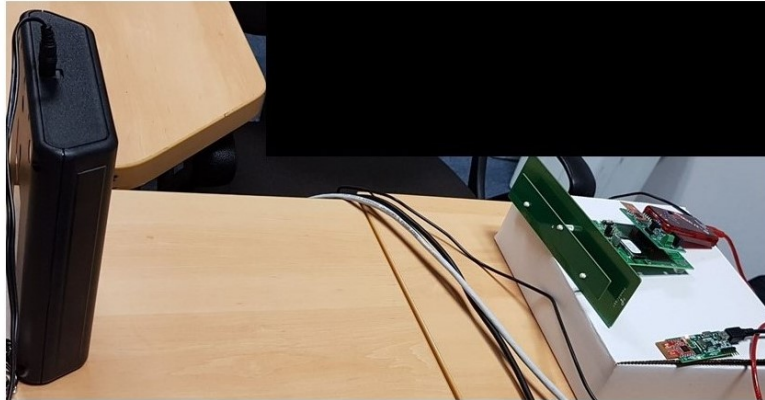


Figure 4.16: Powerharvester P2110b setup for testing at the Lab

Figure 4.17 shows the output data illustration given by the power harvester and the description of each term is given in the table in Figure 4.18. In our application and project our main focus is the received power in mW given by the P2110b power harvesting system.

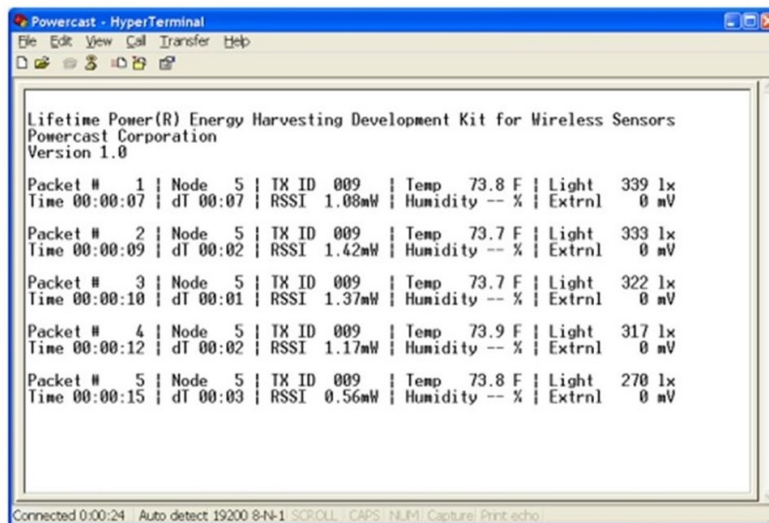


Figure 4.17: Example of the output data illustrated by the power harvester using the hyperterminal.

4.6 Realization, Measurements and Validation of the Novel Concept

After defining the concept of the novel energy harvesting system, and the design procedure of the metasurface design, in this part the main objective is the realization and validation of our concept, in which our theory and system can be used as a complementary with off the shelf low input power energy harvesting technologies, by increasing their potential and efficiency in terms of EM energy

Parameter	Description	Range
Packet#	Packet counter (reset when S1 is pressed)	1 to 99999 – number is incremented with each packet received
Time	Relative time counter (reset when S1 is pressed)	00:00:00 (HH:MM:SS) up to 99:59:59
dT	Time differential between received packets. A separate counter is used for each node	00:00 (MM:SS) up to 99:59
TX ID	The ID number broadcasted by the TX91501 transmitter (factory programmed).	1 – 254 “---” otherwise (error)
Node	Wireless Sensor Board identifier*	0 – 7 (configured by DIP switches)
RSSI	Received Signal Strength Indicator – the received signal strength from an RF power source	0.04 – 50 mW “---” otherwise
Temp	Temperature (Fahrenheit)	25 - 125°F “---” otherwise
Humidity	Relative Humidity	15 – 85 % rh “---” otherwise
Light	Ambient luminance (Lux)	10 – 99999 lux “---” otherwise
Extrnl	External sensor reading	0 – 3000mV

Figure 4.18: Table explaining each item displayed on the screen and the valid range of data.

harvesting.

4.6.1 Measurements of the Metasurface Focal Point

The first point is to study and validate the functionality of the metasurface design in terms of EM focusing. In Figure 4.19, a realized prototype of the focusing metasurface of dimensions 81 cm x 81 cm is given. The metasurface is formed of jerusalem crosses unit cell elements printed on top of a Rogers Duroid substrate of thickness 1.9 mm and relative permittivity 10.2. The metasurface is also separated from a metallic ground plane with a foam gap of 60 mm. The metasurface mounting has been carried on at Université Gustave Eiffel/ IFSTTAR.

Afterwards, to study the focal point of the realized design, experimental verification of the metasurface prototype is carried out at an anechoic chamber for validation of the theoretical and simulation results (The experiments were done at the Université de Lille 1 P3). The Setup and configuration of the realized metasurface are shown in Figures 4.20 and 4.21.

In Figure 4.20, the metasurface is implemented on a stand in an anechoic chamber, situated 3 m away in the far field from a double rigid horn antenna at 900 MHz with transmitting power equal to 20 dBm (100 mW). A laser is used for centering between the antenna and metasurface. To be able to visualize the focal point in our measurements, a grid sheet was fixed 30 cm away from the metasurface as shown in Figure 4.21, where in theory is said to be the position of the focal point according to our design and simulation results.

To carry on with the measurements of the focal point, the P2110b Power-Harvester electronic device has been used to calculate the received power in mW at each point of the grid sheet over a period of time. The power harvester setup is shown in Figure 4.22.

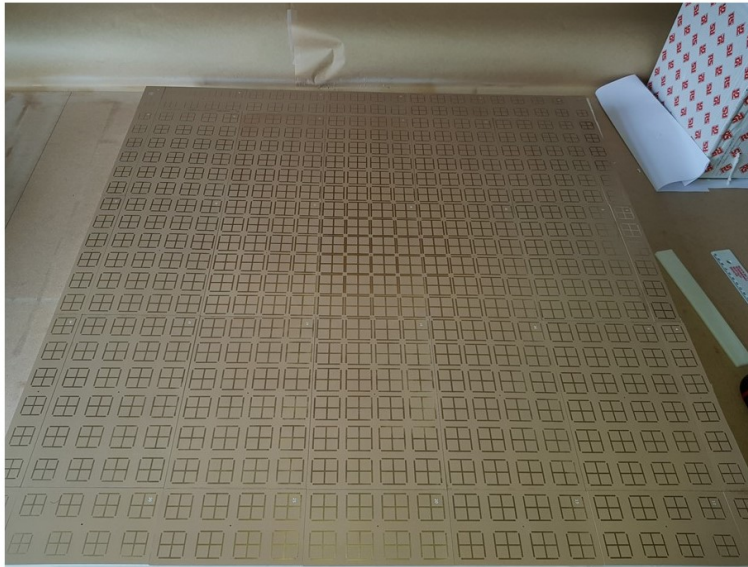


Figure 4.19: Realized metasurface of dimensions 81 cm x 81 cm.

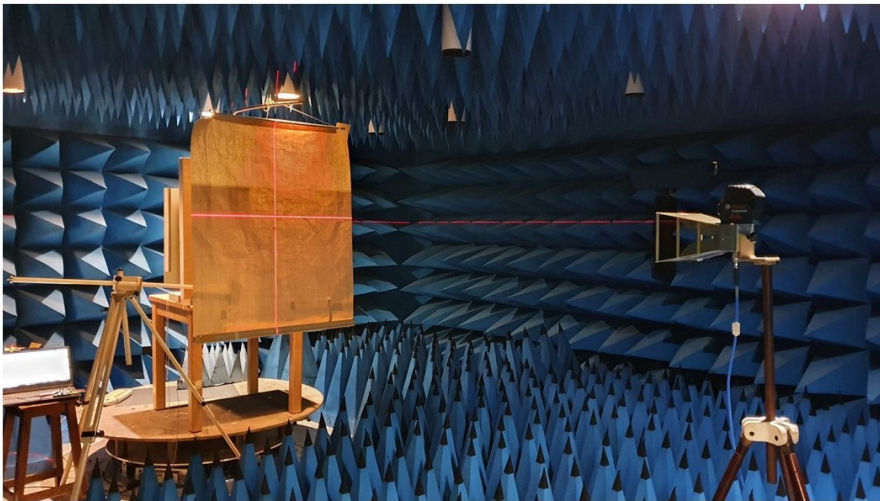


Figure 4.20: Setup for the measurement of the focal point of the metasurface design.

A dipole antenna connected to the electronic device is attached to a non metallic stick on an elongating stand, which can elaborate away from the metasurface at the fixed grid sheet, was used to measure the power received at each point as shown in Figure 4.23.

The measurement calculated results have been carried on in the x-y plane of the metasurface design. The power received has been measured at 15×15 points along the x-y plane from the design over a period of 30 seconds at each point. The measurement results of the received power in mW are shown in Figure 4.24.

The results in Figure 4.24, show that the received power 30 cm away from the metasurface is mostly concentrated at the center of the metasurface design. The results are given which a max up to

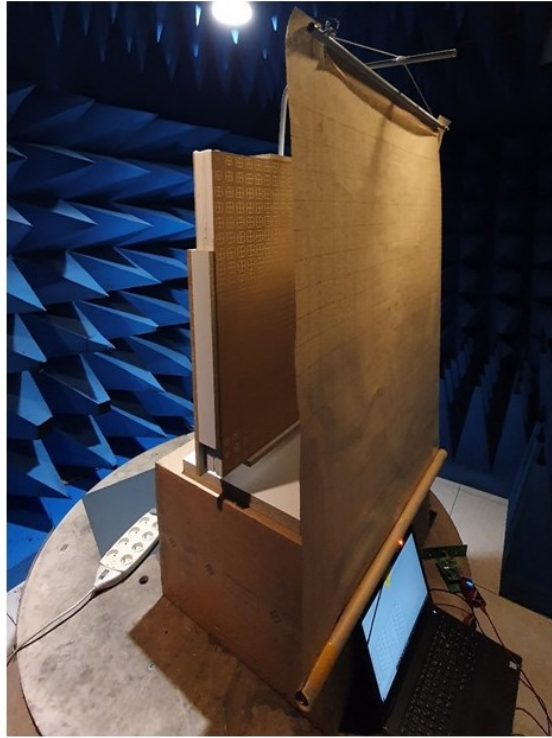


Figure 4.21: Grid sheet fixed 30 cm away from the metasurface design.

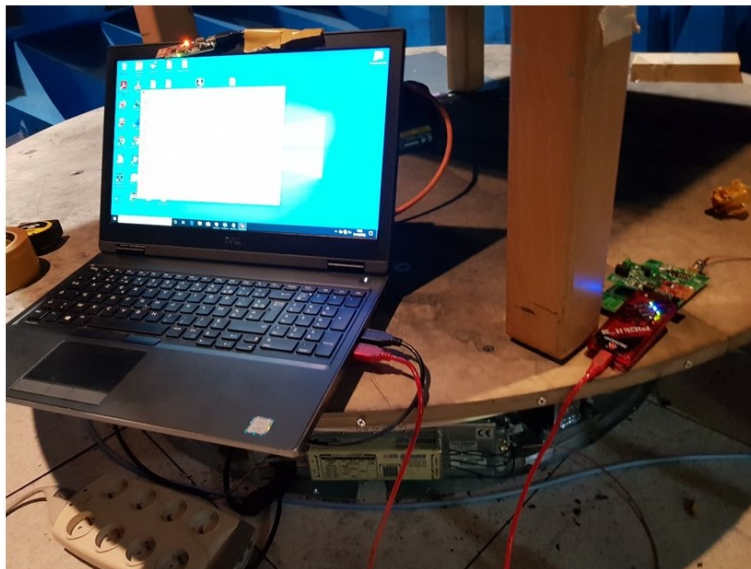


Figure 4.22: P2110b powercast energy harvester set-up connected to MPlab PC for calculating the received power at the focal point.

11 mW and a minimum down to 0.3 mW around the focal point. This indicates that the energy transmitted towards the Focusing metasurface, is reflected and focused at one point 30 cm away from the surface, thus validating our theoretical and simulation results.



Figure 4.23: Dipole antenna measuring at each point 30 cm away from the metasurface at the fixed grid sheet.

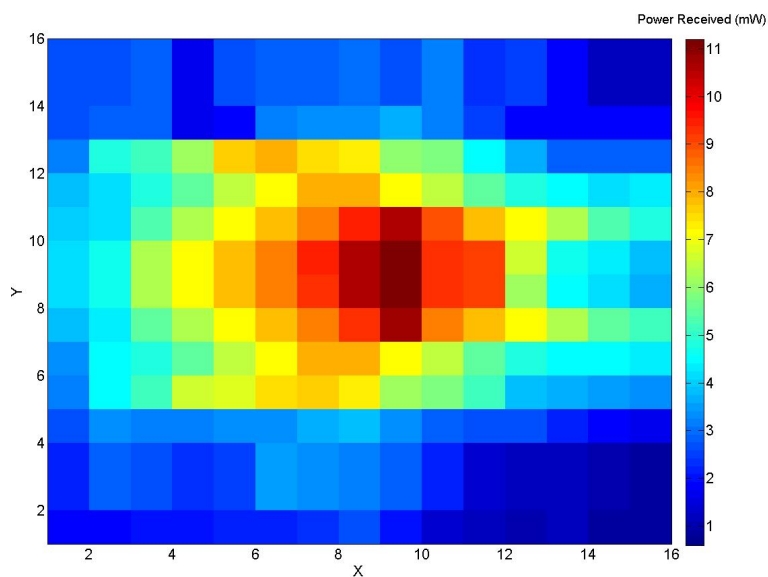


Figure 4.24: Power received in mW in the x-y plane at the focal point 30 cm away from the metasurface.

To make the result more clear from noises and show a smooth visual of the concentrated energy at the focal point, the smooth function on MatLab has been used. The result and visualization is shown in Figure 4.25.

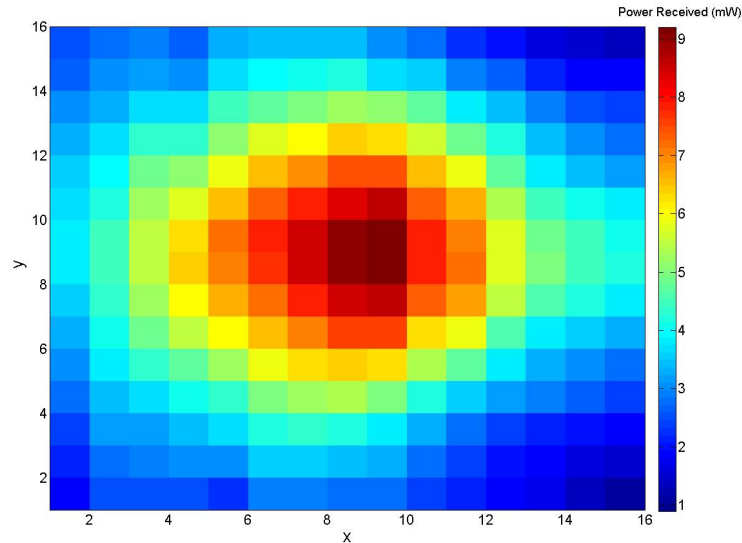


Figure 4.25: Averaging of the Power received at the focal point 30 cm away from the metasurface.

4.6.2 Implementation of the Focusing Metasurface with the Commercial P2110b Energy Harvester

The main objective and concept of the novel system is to determine and show how metasurfaces can be a complementary for EM energy harvesting systems, in terms of better potential, performances and efficiency. Following that, measurements to validate the concept, have been carried on in an anechoic chamber. A vivaldi transmitting antenna at 900 MHz in the far field has been used as shown in Figure 4.26. We have implemented the P2110b Harvesting system along side our design in the far field 3 meters away from the vivaldi transmitting antenna at power of 10 dBm (10 mW), the dipole antenna of the energy harvesting system has been situated 30 cm away from the metasurface design at the focal point as shown in Figure 4.27.

To study the potential of our concept, the Power Electronic harvester has been tested in three configurations. First the commercial energy harvesting system with the metasurface (Figure 4.28), second with a metallic plate (Figure 4.29) and the energy harvesting system alone (Figure 4.30) at the same position respectively. The antenna was given in horizontal polarization.

The received power in mW by the Energy harvesting system, is calculated using the MpLab program where the output data is visualized on the PC. The received power is calculated over a continuous period of time every 5 sec for the three configurations given. The results are given for the dipole antenna in both vertical and horizontal polarization in Figures 4.31 and 4.32.

The results in Figures 4.31 and 4.32, show the received power for the three configurations. As given, the received power by the commercial energy harvester in horizontal polarization (Figure

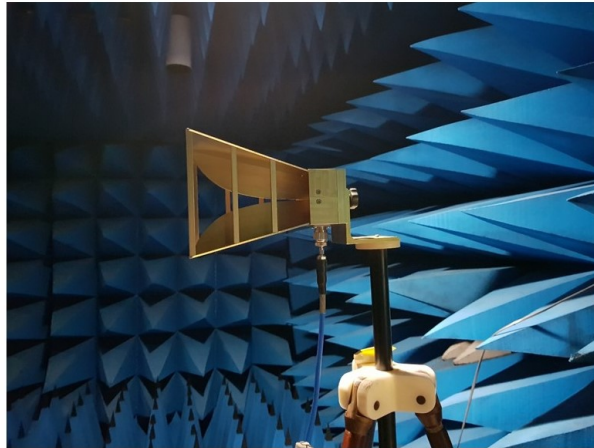


Figure 4.26: Vivaldi transmitting antenna at 900 MHz.

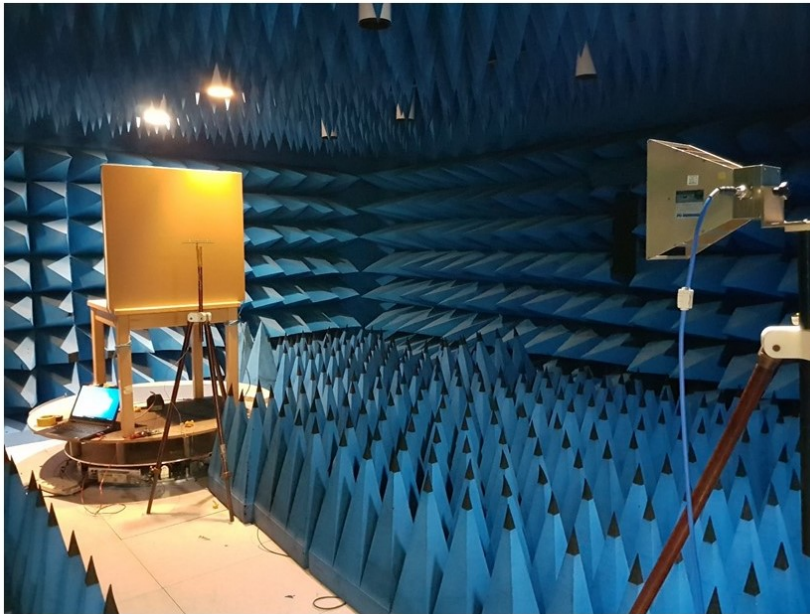


Figure 4.27: General setup of the concept of the novel energy harvesting system in far field measurements in an anechoic chamber at 900 MHz.

6.31) along side the metasurface design reaches a value up to 1.8 mW compared to that when the commercial harvester is implemented with a metal plate or alone giving a result of 0.6 mW and 0.2 mW respectively over a continuous period of time which is 55 sec in this case. As well as, the same performances have been achieved for the case of vertical polarization (Figure 4.32). This indicates that by implementing the metasurface alongside the harvester, a gain up to 9 in linear of received power has been achieved, which itself proves and validates our concept that the metasurface can enhance the potential, performance and efficiency of EM energy harvesting systems when implemented alongside the harvester in the environment.

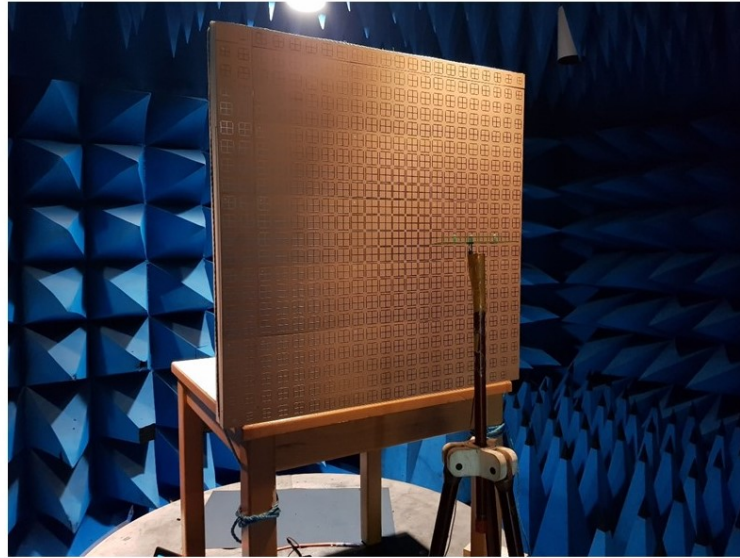


Figure 4.28: Commercial Energy harvester configuration set-up with the metasurface fixed 30cm away in the far-field.

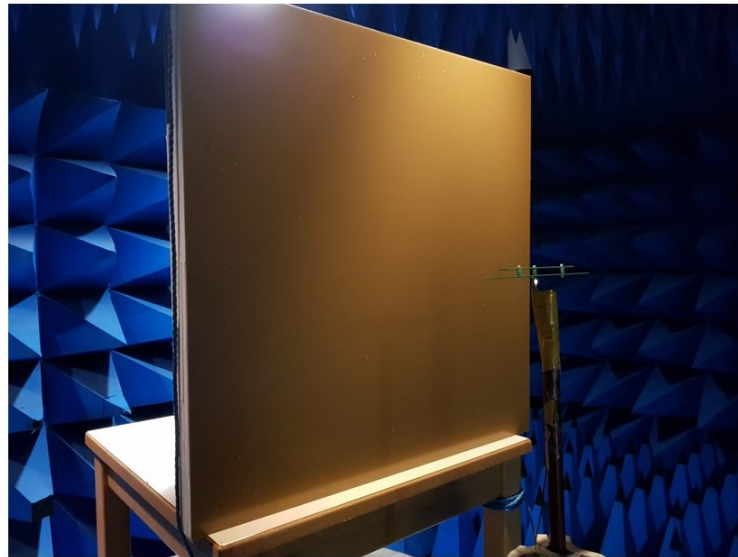


Figure 4.29: Commercial Energy harvester configuration set-up with a metallic plate fixed 30cm away in the far-field.

4.7 Conclusion

In this chapter, we introduced a novel concept for EM energy harvesting based on focusing. The main aim was to investigate the potential of metasurfaces to be a complementary solution for low input power energy harvesting technologies, and their capability in enhancing their performances, potential and efficiency. Different innovations in this chapter from state of the art on rectenna systems were introduced. We stated how the innovations can be compared to our concept in terms of efficiency improvement and how we are able to overcome some disadvantages.

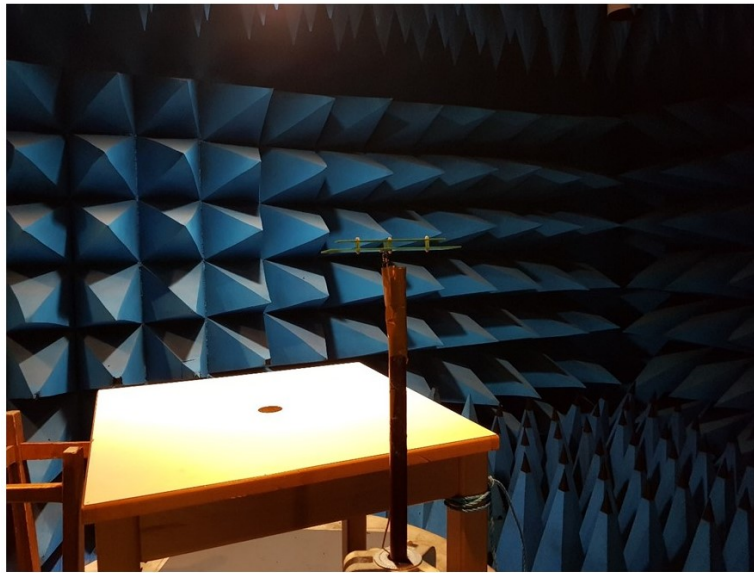


Figure 4.30: Commercial Energy harvester configuration set-up alone at the same position.

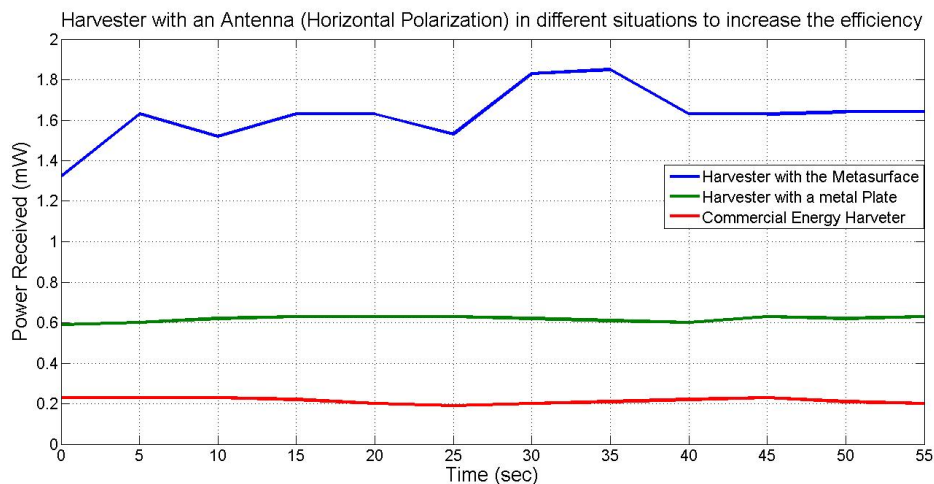


Figure 4.31: Power received in mW by the energy harvester over a continuous time for three different configurations of the commercial energy harvester with a metasurface, metallic plate and alone. (Antenna horizontal polarization)

The concept is based on designing a flat focusing metasurface, where the energy is concentrated at one point in a small zone. A rectenna system is then implemented at this point where the energy is collected. The principle of operation and design procedure of the focusing metasurface was defined in details, where a miniaturized Jerusalem cross element has been used and designed based on the hyperboloidal profile of the generalized phase law. Realization of a metasurface prototype was given, where measurements have been carried on in an anechoic chamber, to validate the potential of the metasurface in terms of focusing. The metasurface showed great performance where the energy was concentrated at the center focal position 30 cm away from the surface as expected according to theory and our simulation results.

We also carried on with the validation of the novel concept for EM energy harvesting. An off the shelf

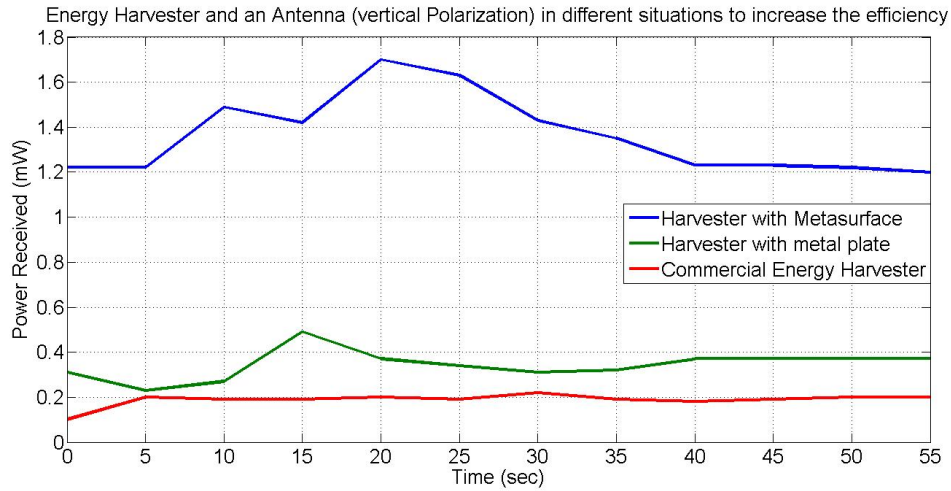


Figure 4.32: Power received in mW by the energy harvester over a continuous time for three different configurations of the commercial energy harvester with a metasurface, metallic plate and alone. (Vertical polarization)

P2110b power harvester was used to investigate and validate our concept. Testing and realization of the concept were carried on in an anechoic chamber. The rectenna system was implemented at the focal point of the metasurface, and the received power from a transmitting vivaldi antenna at 900 MHz, was calculated over a continuous period of time. The energy harvesting system was set in three different configurations (with metasurface, with metallic plate and the commercial harvester alone) to study the potential of the design and concept. The harvester was able to harvest for a gain of 9 times better in terms of power received along side the metasurface, compared to that when the harvesting system was implemented alone.

This concept and theory that we have introduced in this chapter can be of great potential in the future for the field of EM energy harvesting systems and specially rectenna designs. The design and theory has shown remarkable potential in enhancing the performance of EM energy harvesting systems, in terms of efficiency, reliability, and can also solve the problem for enhancing of the antenna aperture in complex EM energy harvesting system applications. On the other hand, for application usage, the concept can be very reliable for low input harvesting systems at GSM frequencies, can also be used in railway environments where GSM-R systems are implemented and for autonomous smart wireless sensor nodes that are being implemented nowadays in different applications. In chapter 5, we will show the assessment and implementation of our system on site measurements in the railway environment, which have been done in collaboration with SNCF reseau.

Chapter 5

Assessment of The Focusing Metasurface Harvesting System in the Railway Environment

5.1 Introduction

The growth and development of the railway network has been a demanding research topic in the past years for many companies around the globe. Railway transportation has become an essential method of transport between regions for many people around the world, this specially due to its safety, economical value, low carbon mode, resource efficient transport mode and environmental friendly. Moreover, the enhancement and growth of the railway environment is essential specially with the rise of different smart technologies such as IoT, wireless sensor networks (WSN) and 5G communication systems. These technologies can help enhance the reliability, security and maintenance and give rise to smart railway systems. However, the need of power supply for systems such as WSN or IoT devices on the railway system can be a challenge, specially to enable autonomous and more reliable systems for implementation and deployment. The railway environment is said to be rich with various energy sources from vibrations, wind, acoustics, solar and electromagnetic that can be beneficial to supply such low power input devices.

Various existing technologies for energy harvesting and wireless power transfer have been developed and implemented for different applications, one of them is for railway systems. In our research study, the thesis is in collaboration with SNCF Réseau which is France's national state-owned railway company. The aim of the PhD thesis is to investigate the potential of electromagnetic energy harvesting in the railway environment. Many energy harvesting systems have already been studies and implemented based on different sources in the railway system. However, for EM energy harvesting systems, to date no mature technology has been developed. High sources of electromagnetic energy have been proven to exist in the railway infrastructure, which can beneficial for renewable energy to supply low power input devices such as WSN. Many challenges and limitations can rise

specially at low microwave frequency ranges for railway EM energy harvesting and wireless power transfer technologies in terms of efficiency, reliability and implementation.

The application is to be able to supply low input power devices such as IoT and WSNs. WPT can be a solution for such technologies, however in the railway environment many challenges can rise such as line of sight, localization and tracking. In chapter 5, we proposed a solution for such challenges using retrodirective metasurfaces that can help enhance the efficiency and performance for such technologies in case they are used. In terms of EM energy harvesting, it can be challenge to harvest specially for ambient energy where it can be scattered in the railway environment and not very efficient to supply and wake up WSNs. GSM-R systems can be a use case to harvest and supply low input devices. Using commercialized off the shelf rectenna systems to harvest ambient energy can be a challenge specially with the energy scattered and the low power that will be received by the antenna. In chapter 6 we proposed a solution for such challenges and problems that can occur by introducing a novel concept which can be a complementary solution for such technologies. The concept is by using engineered designed focusing metasurfaces along side the EM energy harvesting systems. The system showed remarkable results when tested in the anechoic chamber, with a linear gain up to 8 in terms of received power when using the focusing metasurface along side a commercialized EM rectenna system compared to that using a rectenna system alone.

In this chapter, we implement and test our proposed concept on site using the focusing technique for EM ambient energy harvesting in the railway environment. The measurements were carried on in collaboration with SNCF Réseau in Paris. The measurements and EM energy harvesting were based on the use case of the GSM-R system present in the railway environment. We implemented the system at a far distance in the far-field to determine the potential of our system in terms of EM harvesting and the power present. When using the focusing concept with the metasurface along side the rectenna , the system has shown remarkable results in terms of enhancing the power received by the commercialized rectenna system compared to that when implemented alone. The harvesting system was able to receive $10\mu\text{W}$ when implemented along side the focusing metasurface compared to that of 1 nW when using the rectenna alone, which can be an interesting result to supply low input WSNs where such power is needed to wake up and function the device.

5.2 Description of the railway environment

The railway environment is one of the greener modes of transport and having a higher share of passenger and freight journeys performed by trains. The railway industry has been a major transport method from economical to social benefits to link countries in Europe through out transport history. Many railway companies are working on enhancing the performance and functionality of railway systems. In our work, the thesis and research study is in the framework of SNCF Réseau which is a major railway transport company in France. The company is investigating the use of different smart devices to make the railway system more reliable and with higher performances. Electromagnetic energy harvesting is one of the major topics being investigated for the railway application specially that to date no mature technology in this field has been presented.

The railway environment consists of the a rail, the passing rail car body, pantograph and catenary system. when passing trains are present, different interactions can occur specially between the catenary line and pantograph. This yield to electromagnetic sparks and signals specially at low microwave frequencies. This is shown in Figure 1.26 (chapter 1) which have been provided by SNCF Réseau showing many high values in terms of electromagnetics at low microwave frequencies which

can be related to such interactions. However, for signals and high values of EM waves at frequencies up to 900 MHz, this is mainly referred to the present of GSM-R base stations implemented in the railway environment.

Global System for Mobile Communications – Railway (GSM-R) is a radio communication system which offers a wide range of voice and data services needed for daily operation of railways. GSM-R provides telephony, SMS and data services, as do public GSM networks. GSM-R facilitates the communication between train driver and traffic control centres, by providing specific features such as group communication, location dependent addressing, priority levels, railway emergency calls and shunting communication. An example of the railway environment with a GSM-R base station is given in Figure 5.1.



Figure 5.1: A passing train in the railway infrastructure with a GSM-R base station situated next to the railway track. (SNCF Reseau Paris, France)

Figure 5.1 is a photo taken during our site field measurements at SNCF Reseau in Paris. The figure shows a passing train and a GSM-R base station situated next to the rail track. For the environment given, we expect to have RF activity and electromagnetic energy around 900 MHz which can be beneficial for EM energy harvesting and the validation of our concept and device potential and performance. The maximum transmitted electromagnetic power for GSM-R frequencies according to the “*Assessment report on GSM-R current and future radio environment*”, by the international union of railways is -10 dBm. Measurements for GSM-R frequencies have been applied where the maximum received power by a conventional antenna system is -40 dBm [298–300]. The aim is to increase the performance and efficiency of a conventional EM rectenna system for such frequencies following our focusing concept, where EM energy harvesting in such low power ambient environment can be a challenge.

5.3 Description of the experimental set-up

The system was deployed in the far-field away from the railway system and GSM-R base station. The GSM-R base station is transmitting continuously in the range of 920 MHz with a maximum power of -10 dBm. Our system consists of:

- P2110b powercast harvester rectenna system. The powercast harvester consists of the rectifying circuit, dipole antenna and access point for receiving the data from the rectifying system and displaying the data using MpLab program on a PC.
- The focusing metasurface which was implemented along side the rectenna system. The surface's ground plane was also used as a metal plate to compare between different scenarios.
- A portable vector network analyzer (VNA) was used to measure low received power which is not received by the P2110b.
- Some equipment such as a table and stick were used to fix and hold the system.

The setup of the system is shown in Figure 5.2.



Figure 5.2: Setup of our focusing metasurface and harvesting device at a far distance from the railway system, including all components.

Figure 5.2 shows all the components used during the measurement setup. The max transmitting power by the GSM-R base station is -10 dBm. However the minimum received input power needed for our Powercast P2110b harvester is -14 dBm. Different scenarios were used to measure the received power.

- The first setup was using the rectenna system alone with the dipole antenna. For better detection of the power received since -14dBm is needed to display measurements, the antenna of the P2110b system was connected to the VNA.
- The rectenna system was implemented along side the focusing metasurface. Moreover, the received power was also measured using the VNA for this scenario.
- A metallic plate was also given along side the rectenna device and measurement were taken.

5.4 On-Site measurement results

5.4.1 Site Measurements Using the concept of the focusing metasurface

The system was set as shown in Figure 5.2. The first measurements were taken using the P2110b powercast rectenna device along side the focusing metasurface. In terms of harvesting, the rectenna system was able to receive 0.05 mW at some points in time during the measurements were taken which is equivalent to -13 dBm. However, since the max value of transmitting base station of the GSM-R system is -10 dBm, the power received at the input of the rectifier is low compared its needed minimum level. Thus, an alternative rectifying can be used in this case with higher efficiency for better EM harvesting.

The aim is to study the potential of the focusing metasurface and concept to increase the efficiency of the receiving system. Thus, we used a VNA as shown in Figure 5.3, in order to detect and analyze the level of power for the different scenarios specially that the VNA is capable of measuring low received input power .



Figure 5.3: VNA to measure the received power by the Powercast P2110b dipole antenna.

The first configuration is shown in Figure 5.2. The receiving device is situated and fixed on a stick 30 cm away from the focusing metasurface where the focal point is located. The measurement are in far-field at a far distance away from the railway and GSM-R base station. The measurements were taken carefully over a period of 5 to 6 min with a fixed configuration. The results of the measurements of the first scenario are given in Figure 5.4.

Figure 5.4 shows the results of the setup with the first configuration using the concept of the focusing metasurface. The measurements were taken using a portable VNA as shown in Figure 5.3 over a period of time. However, using the focusing metasurface, there were instants where we received -13 dBm or 0.05 mW which was enough to be harvested by the rectifying system. However, for a long period of time a more efficient rectifier or antenna would be needed. The received power was measured over a range of frequency between 890 MHz to 945 MHz using the VNA to a constant and global measurement. When using the focusing metasurface the power received by the receiving antenna was measured with a peak to be equal to -20 dBm at 922 MHz and -22 dB at 924 MHz. This is significant specially with the low efficient power in the ambient environment with a GSM-R base station transmitting at -10 dBm. Low levels of power were detected in the frequency band between 890 MHz to 920 MHz with a peak up to -55 dBm at 914 MHz.

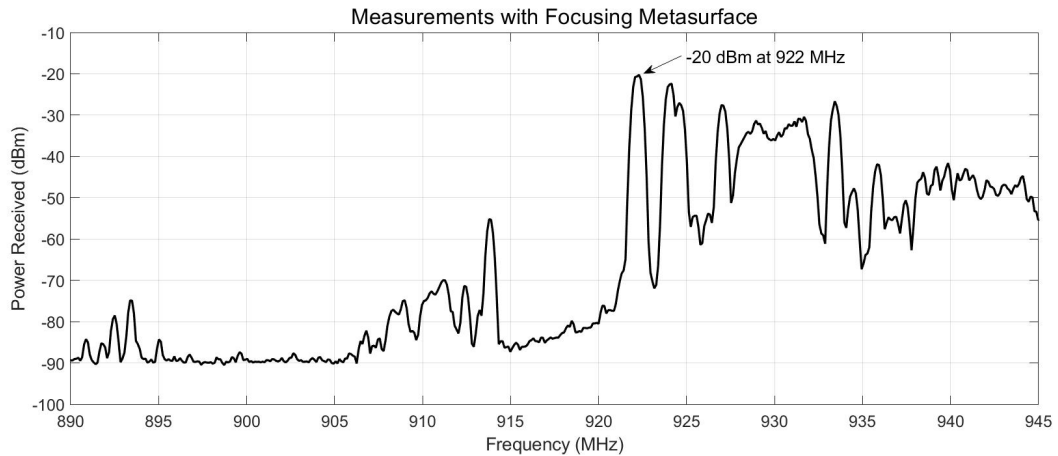


Figure 5.4: Power received in dBm by the antenna implemented along side the focusing metasurface, measured using the VNA with respect to frequency (MHz).

5.4.2 Antenna implementation along side a metallic plate

For comparison with different scenarios and to validate the potential of the focusing metasurface, the antenna of the Powercast P2110b was implemented along side a metallic plate. Since the metasurface is designed with a metallic ground plane, it is used to highlight the concept. The second configuration is shown in Figure 5.5.



Figure 5.5: Receiving P2110b antenna along side the metallic plate.

Figure 5.5 shows the receiving antenna of the P2110b powercast fixed on a stick at the same position compared to that of the first configuration with the focusing metasurface in Figure 5.2, but only by reversing the metasurface to the metallic plate side. The measurements of the received power were done following the same strategy over the same period of time using the VNA. The results of the given scenario are shown in Figure 5.6.

In Figure 5.6, the received power is calculated using the VNA with the antenna implemented along

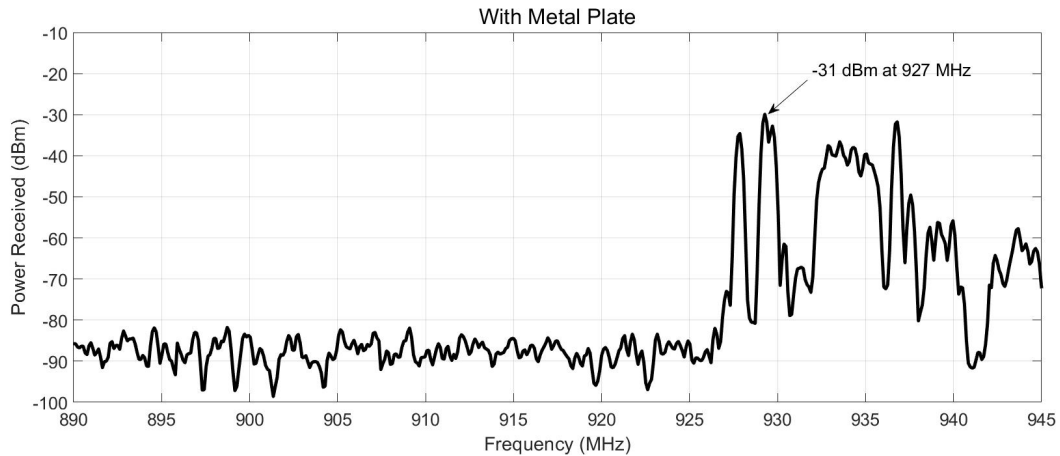


Figure 5.6: Power received in dBm by the antenna implemented along side the metallic plate, measured using the VNA with respect to frequency (MHz).

side the metallic plate. The measured received power is given at a frequency band between 590 MHz to 945 MHz. A peak of -30 dBm was determined at 927 MHz and -32 dBm at 937 MHz. Low values of power were observed in the frequency band between 890 MHz to 926 MHz.

5.4.3 Measurements using the commercialized receiving antenna alone

To validate the potential of the focusing metasurface in terms of power receiving enhancement, the receiving antenna of the Powercast P2110b device was situated alone at the same position compared to that of previous configurations, by removing the metasurface from its position. The received power was similarly calculated over a period of time using the VNA. Figure 5.7 shows the antenna implemented in the far-field away from the base station, situated on the stick without changing its initial position. The results of the received power are given in Figure 5.8.



Figure 5.7: Receiving antenna implemented alone in the far-field away from the GSM-R base station.

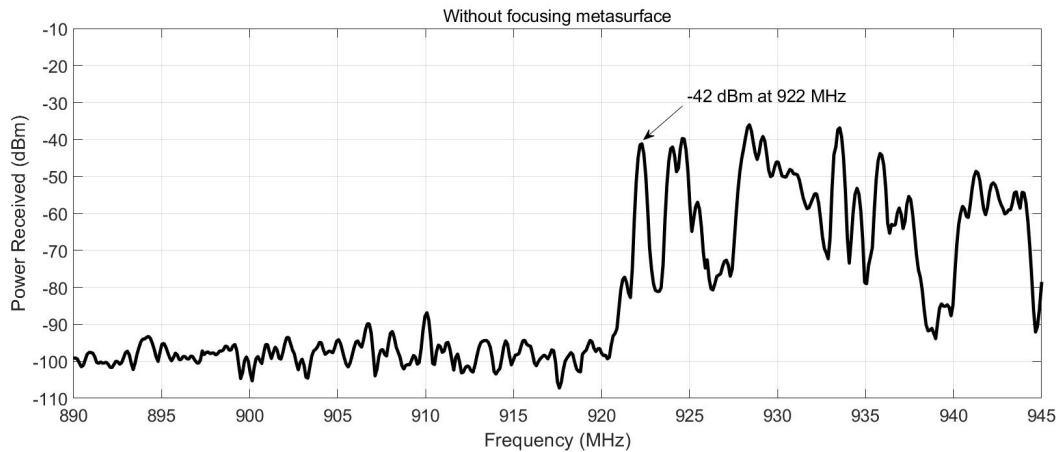


Figure 5.8: Power received in dBm by the antenna implemented alone, measured using the VNA with respect to frequency (MHz).

In Figure 5.8, the received power determined by the antenna was measured over a period of time using the VNA. The antenna is situated alone in the far-field away from the base station. We can observe that a very low power is received almost null between 890 MHz to 920 MHz. A max peak of -42 dBm was detected at 922 MHz as well as 924 MHz, 927 MHz and 934 MHz. This shows the low efficiency that can be received using a conventional antenna or rectenna system in an ambient environment such as the railway infrastructure with the GSM-R communication system.

5.4.4 Focusing metasurface implementation at a different position without facing the base station

For more technical validation, the receiving antenna along side the focusing metasurface were implemented at a different position without facing the GSM-R base station in the far-field. The setup is shown in Figure 5.9. Measurements of the received power were also carried out using the same procedure and set-up with the VNA over a period of time. The results of the received power are shown in Figure 5.10.

The results in Figure 5.10 show low level of received power between 890 MHz to 920 MHz. We observed a max peak of received power of -22 dBm at 924 MHz. The idea of this set-up is show and validate the potential of the focusing metasurface in the far-field and be able to operate at different positions while maintaining similar results.

5.5 Comparisons and discussions

The aim is to validate the potential of the focusing concept in terms of enhancing the performance of commercialized rectenna or receiving antenna collectors in an ambient environment where power efficiency can be low and difficult to harvest. The focusing metasurface showed remarkable and interesting results for enhancing the efficiency of the commercialized P2110b device. We were able to harvest at certain moments power up to 0.05 mW GSM-R base station transmitting at 0.1 mW in the far field. However, for long period and average time with the focusing metasurface, the antenna was able to receive -20 dBm equivalent to 10 μ W. In comparison to other scenarios, the device received lower levels when implemented with a metallic plate and alone with a max received power of -30 dBm (1 μ W) and -40 dBm (0.1 μ W) respectively. The comparison of the three configurations



Figure 5.9: Setup of our focusing metasurface and harvesting device without facing the GSM-R base station in the far-field.

in terms of received power in dBm is shown in Figure 5.11, and the values in μW are given in Table 5.1.

Figure 5.11 shows the results of the received power levels for the three configurations and scenarios. We can observe very clearly that the focusing metasurface has given significant enhancement in terms of improving the performance of such receiving or harvesting devices. Moreover, compared to other measurements in the literature [298–300], the max received power for GSM-R systems using conventional antennas was given to be -40 dBm. This shows the value of the concept and physical properties of focusing metasurfaces, which can be beneficial to overcome difficulties and challenges in ambient EM energy harvesting environment specially performances of rectenna devices and efficiency. However, for higher values of received power, an antenna with higher gain and better aperture to harvest the focused energy can be used such as a vivaldi antenna, in order to increase the level of harvested power.

Commercialized antenna with focusing metasurface	Commercialized antenna with metallic plate	Commercialized antenna alone
10 μW	1 μW	0.1 μW

Table 5.1: Comparison of the max received power in μW for each configuration when using the focusing metasurface, metallic plate and commercialized antenna system alone.

In terms of application with the achieved power level using the focusing metasurface. It is known that wireless sensor nodes which can be implemented in the railway system, need a minimum input power of $10 \mu\text{W}$ to wake up the sensor. This can be relevant specially with the power achieved, and with a more efficient rectifying system, the focusing concept can be significant to enhance the efficiency and provide the needed power for such low power input devices. Moreover, for 5G communication systems in the railway environment, the dimension of the focusing metasurface can be smaller making it more significant at higher frequencies in terms of implementation and deployment.

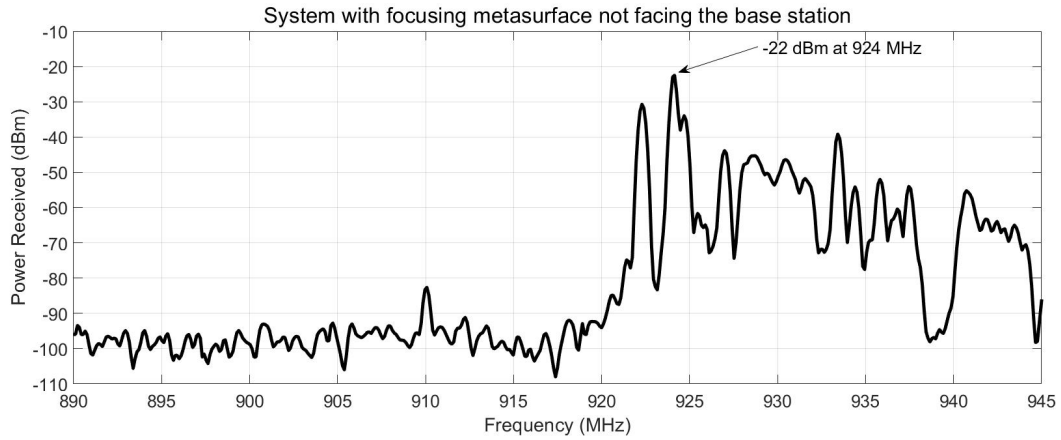


Figure 5.10: Power received in dBm by the antenna implemented along side the focusing metasurface without facing the base station, measured using the VNA with respect to frequency (MHz).

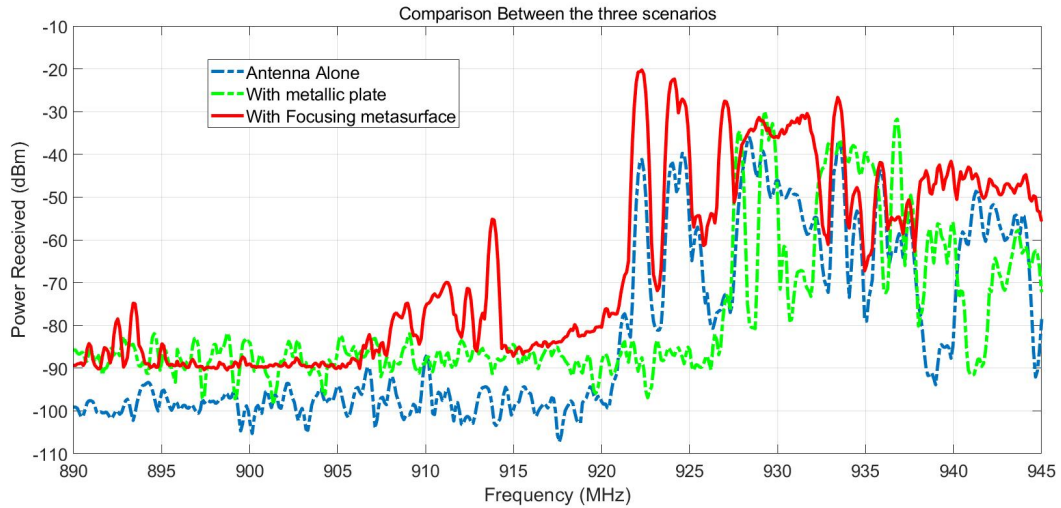


Figure 5.11: Power received versus frequency comparing the three configurations

5.6 Conclusion

The demand for more reliable and smart railway systems has been an interesting topic to investigate for many researchers and industrial companies over the past years, specially with the rise of smart technologies and devices such as IoT and WSNs. However, for autonomous and reliable systems, energy harvesting can be a key element to supply such low input power devices. Various technologies based on different sources have been presented in the railway infrastructure, however to date no mature technology and research study has been investigated for such an application based on EM energy. In this chapter we tested on site the potential of our concept based on focusing metasurfaces to enhance the performance of off the shelf rectenna systems, and overcome the challenges of low efficient ambient EM energy harvesting specially at GSM frequencies. The system was deployed in three configurations: The receiving antenna along side the focusing metasurface, the antenna along side a metallic plate and the antenna alone. The focusing concept showed remarkable results compared to the other configurations with a receiving power up to $10 \mu\text{W}$ compared to that of the antenna with a metal plate and alone of $1 \mu\text{W}$ and $0.1\mu\text{W}$ respectively. The level of $10 \mu\text{W}$ however

can be relevant for the application to supply WSNs which is the minimum required input power for such devices. For higher performances, an antenna with higher gain and aperture can be used to harvest the focused energy along side an efficient rectifying circuit.

Chapter 6

Tracking and Localizing Efficiency Enhancement Using Multi-Angle Retrodirective Metasurfaces: Application for Wireless Power Transfer

6.1 Introduction

Wireless power transfer (WPT) [144, 145] has gained remarkable interest nowadays for many researchers and manufacturers, this is due to its convenient, safe and autonomous properties that can be beneficial and important for many applications. WPT or electromagnetic energy transfer is the transmission of energy or power to a target without any physical link or connection. It has been an active topic for many applications such as medical implants [185, 301, 302], wireless charging systems for portable devices [303–305], electric vehicles [306–309], wireless sensor nodes [310–314] and internet of things (IOT) technologies [315–319].

Particularly, the idea of autonomous (also known for batteryless) Wireless Sensor Networks (WSN) and IOT devices [320–323], is an interesting topic and under investigation by many researchers, specially with their properties of low input power needed. The main idea is to be able to supply or feed the device without any batteries or cables when implemented. With the rise of technologies for Energy harvesting (EH) [324] and WPT the idea of autonomous devices became reality. However, Energy harvesting [325] is the usage of surrounding energy that can be found in the environment from solar [326], vibrations [327], wind [328] and electromagnetic [329], and convert it electric DC power. WPT can be another solution where power can be transmitted to the IOT or WSN device without the usage of any connections [330–332].

In some applications for WPT such as railways, vehicle communication systems and IOTs, tracking and localization [319] of the wireless sensor or IOT device can be essential for efficient and high performance WPT. Many research topics have focused on the development and improving the efficiency of the transmitting device for better WPT such as algorithm improvements [333], impedance matching [334], magnetic resonant coupling [335] and autonomic resonant frequency tracking devices [336]. Although it can be interesting and useful to focus on designing an efficient WPT system, however tailoring or controlling the surrounding of the environment of your system, for better performances and higher efficiency, is indeed an attractive solution and interesting to investigate. Metasurfaces [52] are the subject of intensive research nowadays for their applicative potential and the generality of their design approach [53, 217]. They are characterized by their 2D subwavelength structure and their ability to control the wavefront of an electromagnetic wave [54, 55, 218] with perfect, abnormal and achromatic reflections [56, 57, 219]. One of the common metasurfaces are phase-gradient surfaces [278] designed to tailor or manipulate a reflected and transmitted electromagnetic wave [56, 337]. Other applications have been introduced recently for metasurfaces including polarization conversion [338], antennas broadband diffusion of terahertz waves [339], hologram [340], Huygens' metasurfaces [57], multi-functional metasurfaces [219, 341], transformation of propagating waves into surface waves [53, 342] and total control or beam steering [343] metasurfaces at optical and microwave frequencies [344].

In WPT, for tracking an IOT device or a sensor node, a pilot signal is normally sent, a receiving pilot signal is then sent back to the transmitting device from the position of the IOT system. The autonomous IOT or sensor node, after detecting its location, is fed by the transmitting device. In cases where tracking can be a challenge specially from the angular perspective or moving devices, metasurfaces and especially retrodirective engineered metasurfaces, can be a solution and of great applicative potential for better tracking and localization when implemented along side the IOT or wireless sensor device. Indeed retro-reflection [345] can be obtained from diffraction in blazed grating [346–348], such as in a Littrow configuration [234]. More recently, flat metal-dielectric surfaces for retro-reflection or more generally for anomalous reflection [53], have been designed based on generalized phase law [233] and reflect-array approach [349]. However, it can be a challenge and interesting to investigate the potential of metasurfaces and their performances, in terms of retro-reflection for multiple incident angles simultaneously, which can be of remarkable usage in different applications for tracking and localization enhancement specially from the angular perspective.

In this chapter, we focus on introducing novel concepts for the design of efficient multi-angle retrodirective metasurfaces which we have published in journals and presented at different IEEE conferences. Concepts are given from technical based on superposition [69] to physical based on impedance modulation [70] and fano-resonance [79]. Prototypes and measurements have been carried out to validate the concept and results. From the applicative point of view, retrodirective metasurfaces can be very useful for tracking enhancement performances in WPT for IOT devices, sensing and radar systems.

6.2 Concept: Application Aspect

Wireless power transfer has gained remarkable attention nowadays, in the domain of wireless power supply, specially for applications such as WSN and IOT devices. WPT can be an interesting feature where power supply is needed, in order to give rise to autonomous (batteryless) and smart systems. IOT devices are largely being implemented in different applications nowadays and in future projects [350] such security and blockchains [321], industrial and environmental fields [351], 5G [352], railways [353] and vehicle tracking systems [354]. In applications where tracking of the device is needed in

order to be fed, it can be a challenge where line of sight is needed, specially if the target is moving or at different angular positions away from the power supplier. Many researchers have focused on enhancing the WPT systems itself for better efficiency supply [333–335]. However, controlling the environment and surrounding of the system can be an interesting and more reliable aspect for enhancing and improving the WPT system. Metasurfaces, specially in terms of wave control [62, 355, 356], have proved to be remarkable due to their unprecedented physical properties that are not usually found in nature and other engineered physical topologies. Retrodirective metasurfaces on the other hand, have proven to be of great use specially for applications where tracking enhancement efficiency and localization is needed [69]. Figure 6.1 shows how retrodirective metasurfaces can be used as a complementary solution for applications such as WPT.

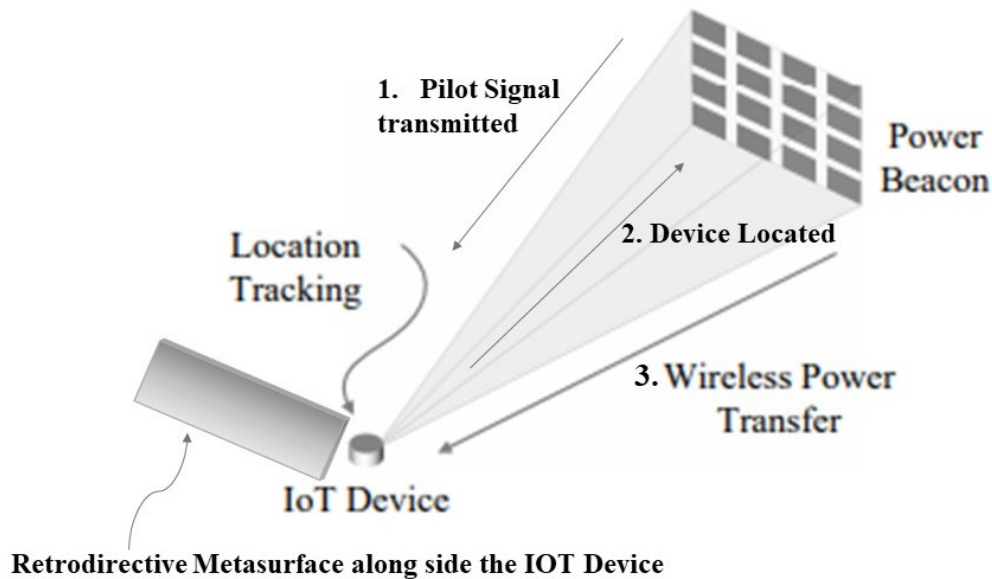


Figure 6.1: Wireless Power Transfer concept for tracking an IOT device to supply along with the usage of a retrodirective metasurface from the application aspect.

Figure 6.1 shows the functionality of a WPT system for feeding an IOT device. The power supplier starts by sending a pilot signal to locate the IOT device, when the signal is then sent back to the supplier, the location of the target is known and the device is fed. However, in some applications the localization of the IOT device can be a challenge specially from the angular aspect if the target is moving or far. In this case multi-angle retrodirective metasurface can be a complementary solution when implemented along side the target device for better tracking and localization. In the next part we define the principle of operation, design procedure and challenges to design multi-angle retrodirective metasurfaces.

6.3 Metasurfaces and Anomalous Wave Control

An electromagnetic wave propagating between two media of different refractive indices, usually results in a reflective and refractive waves in both media [42]. However, for a homogeneous media the wave obeys the simple reflective and refractive conventional Snell’s law. This can differ for engineered topologies such as metasurfaces, which is characterized by a non homogeneous media, thus giving rise to unprecedented physical properties to control the wave anomalously for the reflected and refracted waves. The principle is shown in Figure 6.2.

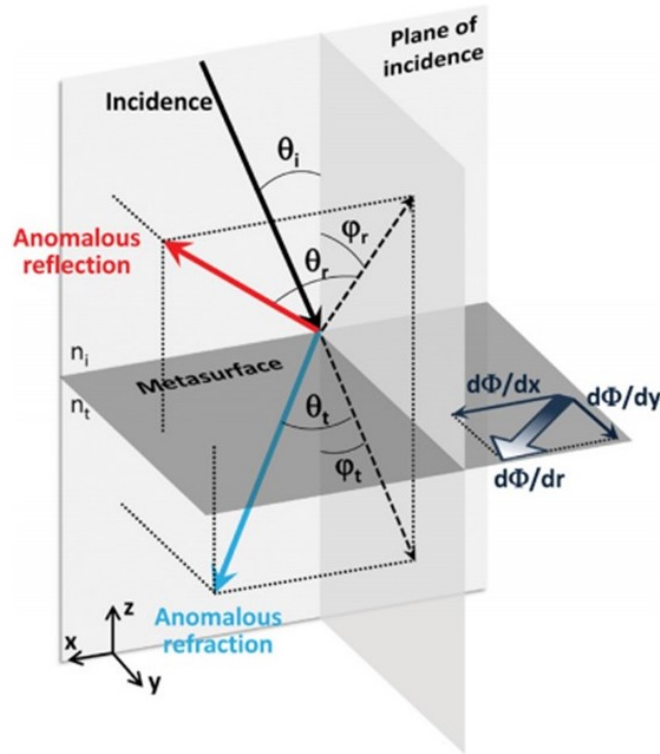


Figure 6.2: Concept for a metasurface where an incident plane wave is controlled in arbitrary directions [42]

Figure 6.2 shows that a propagating EM wave through a metasurface, reflects and refracts the wave in anomalous directions, in a way which is different then that compared to the conventional physical laws. For gradient metasurfaces [53] which we will focus on in this chapter, are well known for their potential of manipulating and controlling of an electromagnetic wave, such as beam steering and anomalous reflection. The design of a gradient metasurface is based on the generalized phase law of reflection and refraction [233], where an additional term (the phase gradient) is given with respect to the conventional Snell's law as shown in Eq. (6.1) and (6.2). This is consistent with the well-known grating equation. [234]

$$\sin \theta_r - \sin \theta_i = \frac{\lambda_0}{2\pi} \frac{\partial \phi}{\partial x}, \quad (6.1)$$

$$n_t \sin \theta_t - n_i \sin \theta_i = \frac{\lambda_0}{2\pi} \frac{\partial \phi}{\partial x}, \quad (6.2)$$

Equation (6.1) shows the generalized phase law of reflection where θ_r is the angle of reflection, θ_i is the angle of incidence, λ_0 the free space wavelength and $\partial \phi / \partial x$ is the phase gradient. Equation (6.2) shows the generalized phase law of refraction where θ_t is the angle of transmission, θ_i is the angle of incidence, λ_0 the free space wavelength and $\partial \phi / \partial x$ is the phase gradient, n_t and n_i are the refractive indices of media 1 and 2. However, particularly for reflection where transmission is neglected, by introducing a phase gradient between scatterers on top of an engineered metasurface design, an electromagnetic wave is reflected to a desired anomalous direction.

6.4 From the Generalized Phase Law of Reflection to Retrodirectivity

Retrodirectivity has been an interesting property for metasurfaces, which is defined by reflecting an incoming wave back in the same direction of incidence [32]. The idea of retrodirectivity comes from the concept of the conventional Snell's law of reflection when a wave is reflected from a mirror or metallic surface at normal incidence. In case of a retrodirective designed gradient metasurface, the wave is reflected back from a virtual surface (mirror) which is tilted by an angle θ as shown in Figure 5.3, this shows that after introducing a phase gradient δ between unit cells, the wave is reflected back from a virtual surface where the initial reference is tilted by an angle θ_i , re-directing back in the same direction similar to that of the conventional case for a mirror or flat plate at normal incidence.

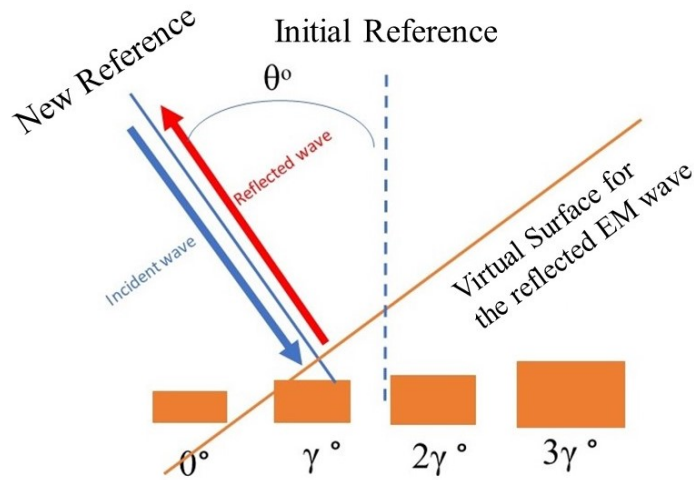


Figure 6.3: An incident wave reflecting back from an engineered gradient metasurface in the same direction of incidence

For the design of a gradient metasurface for wave control we follow the generalized phase law of reflection defined in Equation 6.1. However, particularly for the case of retro-reflection, the incident angle $\theta_i = -\theta_r$ where θ_r is the angle of reflection. To ensure control of the full wavefront of the propagating wave, the integration (from 0 to 2π) of the generalized phase law of reflection is applied. In this case the periodicity of the gradient super-cell defines the full control of the propagating wave in a desired direction. Thus, for the case of retrodirectivity, the periodicity L_x is defined as follows:

$$L_x = \frac{\lambda}{2 \sin \theta_i} \quad (6.3)$$

L_x in Equation (6.3) defines directly the principle to design a retrodirective metasurface. Where the performance of retro-reflection for the metasurface design, depends directly on the relation between the periodicity L_x and the wavelength λ , where θ_i varies according to the incident angle desired for retro-reflection.

6.4.1 Design of a Retrodirective Super-Cell: Principle of Operation

In this part we show briefly and in details the design procedure for a retro-directive super-cell. We have published this work in the Journal of applied physics entitled “ Multi Angle Retrodirective Cascaded Metasurface” [69]. The same procedure and principle is used for all the designs which will follow but only by changing the desired angle of incidence θ_i . Thus following the generalized phase law and after determining the periodicity for a retrodirective super-cell L_x , the super-cell is then divided into N unit cells with a phase gradient $d\phi/dx$ between the unit cell scatterers as shown in Figure 6.4. In this case we give a first example of a super-cell design.

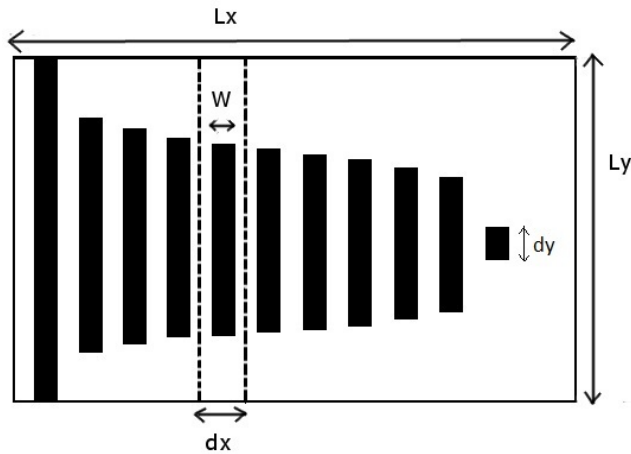


Figure 6.4: Super cell divided into subwavelength unit cells of dimensions L_x and L_y

In this case, strip lines metallic patches are used as a unit cell for their subwavelength structure and to ensure low periodicity between the scatterers giving rise to a magnetic coupling for high efficient performance [53]. The unit cells are tuned to obtain a progressive phase shift covering the range of the phase of the reflection phase coefficient for the control of the wavefront. The phase gradient [52] is given in Eq.(6.4).

$$\phi_{N+1} - \phi_N = 2K_0 d_x \sin \theta_i \quad (6.4)$$

d_x refers to the periodicity of the unit cell which is defined as $d_x = L_x/N$ and K_0 is the wave number. In the case of retrodirectivity Eq.(6.3). is derived into Eq.(6.4). to determine the phase gradient for a retrodirective super-cell which is given in Eq.(6.5).

$$\phi_{N+1} - \phi_N = \frac{2\pi}{N} \quad (6.5)$$

The phase gradient in Eq.(6.5) is shown to be dependent on the number of subwavelength unit-cells N . The dimensions of the unit cells are determined following the reflection phase coefficient and

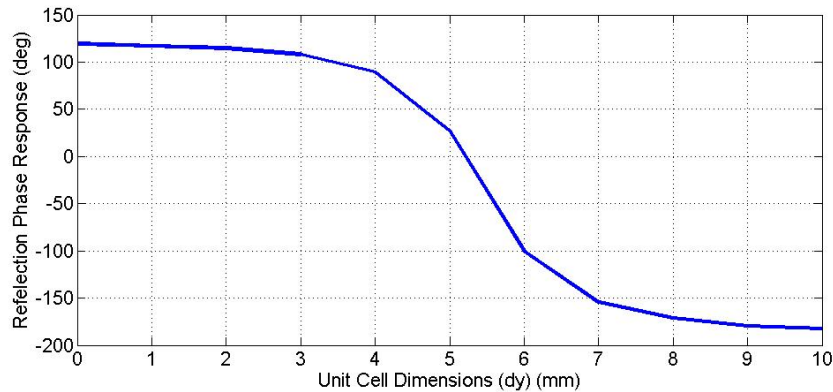


Figure 6.5: Phase of the reflection coefficient for a TM polarized wave at 14.7 GHz with respect to the dimensions of the strip-lines d_y .

Eq.(6.5). An example of a super-cell design is given for $\theta_i = 30^\circ$. The reflection phase coefficient is calculated using Floquet harmonic boundaries for a unit cell of periodicity d_x and length L_y , with the strip-line of width w and length d_y as shown in Figure 6.5. In this case an example is given for a design at $\theta = 30^\circ$ and $\lambda = 20\text{mm}$ (Frequency 14.7 GHz) (Note that: the frequency chosen at 14.7 GHz is just for better demonstration and ease of fabrication, where the concept can be transposed to any frequency depending on the concept), with $N = 12$, $w = 0.71\text{mm}$ and $L_y = \lambda/2$. The metallic strip-lines are printed on a grounded substrate of permittivity $\epsilon = 2.2$, $\tan(\delta) = 1 \times 10^{-3}$ and thickness 1.57 mm.

Following the curve of the reflection phase coefficient given in Fig.6.5. and Eq.(6.5), the phase gradient is given as $d\phi/dx$ equal to 30° . The dimensions of the strip lines are given in Table (6.1). Eleven strip lines are given in this case due to the fact that the phase of the last strip line corresponds to zero.

Phase Coefficient (degrees)	Dimensions d_y (mm)
-182.6812	10.2
-152.6812	7.1
-122.6812	6.5
-92.6812	6.06
-62.6812	5.82
-32.6812	5.6
-2.6812	5.34
27.3188	5.1
57.3188	4.6
87.3188	4.12
117.3188	1
147.3188	0

Table 6.1: Reflection phases with respect to the dimensions of the strip-lines d_y with a phase gradient ϕ_N equal to 30°

6.4.2 Lossless Reflection Condition

In order to ensure a high efficient retrodirective wave, the lossless reflection condition should be validated. It has been shown [357] that in order to obtain a high efficient reflected signal, the

normal component of the Poynting vector should be less than or equal to zero $P_n \leq 0$ which is satisfied when the reflected electric field E_r is equal to that of the incident electric field E_i ($E_r = E_i$). P_n is defined as follows:

$$P_n = \frac{E_i^2}{2\eta_1} (\cos \theta_r - \cos \theta_i) [1 + \cos \phi_r(z)] \quad (6.6)$$

where ϕ_r defines the reflection phase. Taking the example of the design at 30° , P_n has been calculated as shown in Figure 6.6.

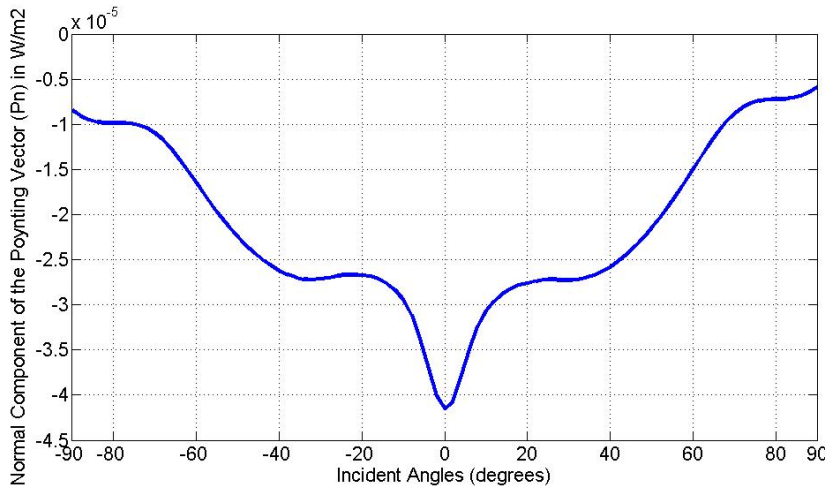


Figure 6.6: The normal component of the Poynting vector with respect to θ_i for a metasurface design at 30° .

The result in Figure 6.6 shows that P_n is less than zero for all incident angles, this indicates that the condition of Eq.(6.6) is validated and the retro-reflector is lossless.

6.4.3 Design of Retrodirective Metasurfaces for various angles of incidence

Following the design procedure and the general principle of operation for a super-cell design at 30° that we have just defined, different metasurfaces are designed at 25° , 20° , 15° and 10° each with a different periodicity with respect to λ following the same principle and procedure.

To determine the retrodirectivity performances of each metasurface from the angular aspect, we calculate the monostatic Radar cross section (RCS) of each design. The monostatic RCS is defined as the wave's energy which is sent and re-directed back to the at the same angle of incidence, which is basically a similar case to that which is used in WPT as a pilot signal for tracking and localization [319]. Moreover, each metasurface is compared to that of a flat metallic plate, this is basically for efficiency studies and having the metallic flat plate as a reference which is well known for its performance for retrodirectivity at normal incidence.

6.4.3.1 Monostatic RCS Performance for a Retrodirective Metasurface at 30°

After the design of a retrodirective super-cell following the general principle of operation at 14.7 GHz, an array periodic structure of 7×9 super-cells is printed on top of a Teflon substrate of

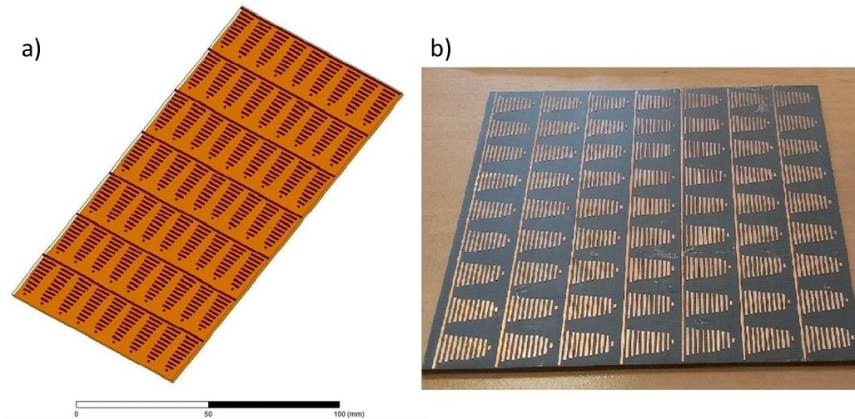


Figure 6.7: a) Metasurface design at 30° Using Ansys HFSS, b) Metasurface prototype of 7×9 super-cells printed on a Teflon substrate of dimensions $14.3 \text{ cm} \times 9.2 \text{ cm}$ and thickness 1.57 mm .

relative permittivity $\epsilon = 2.2$ as shown in Fig. 6.7. The dimensions of the strip lines are given in Table 6.1.

For $\theta = 30^\circ$ the periodicity L_x is equal to λ according to Eq.(6.3). The monostatic RCS for the design is given in Figure. 6.8 and compared to that of a conventional metallic flat plate.

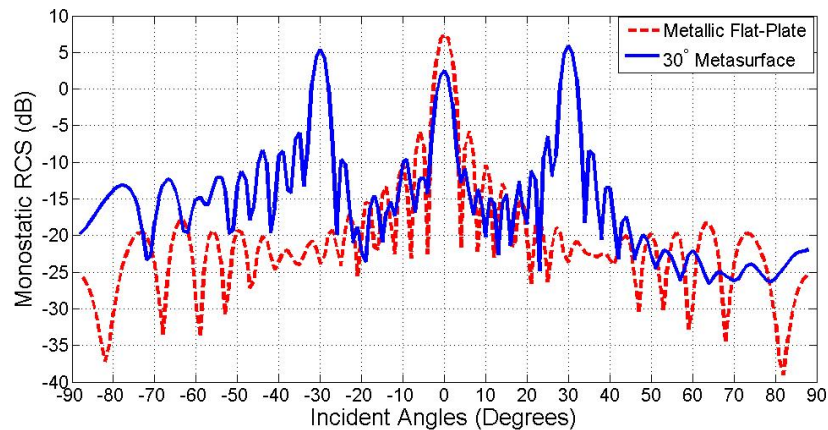


Figure 6.8: Monostatic RCS (dB) with respect to the incident angles (degrees) for a 30° metasurface design of 7×9 super cells and dimensions $14.3 \text{ cm} \times 9.2 \text{ cm}$ compared to that of a metallic flat plate of similar dimensions.

The result in Figure 6.8 shows a high value of retroreflection at the desired angles as well as at -30° and normal incidence, the symmetrical response of the metasurface is expected, this is due to the similar response in both directions of the phase of the reflection coefficient from 117° to -182.68° and from -182.68° to 117° which is given in Figure 6.5 .

6.4.3.2 Monostatic RCS Performance for Retrodirective Metasurface designs at 25° and 20°

The same procedure is followed for the designs at 25° and 20° given to that at 30° . The periodicity L_x is 1.18λ and 1.462λ at 25° and 20° respectively. The dimensions of the strip lines of the unit cells

for 25° and 20° are given in Table (6.2) and (6.3) respectively. The monostatic RCS of the given designs is shown in Figures 6.9 and 6.10 respectively.

Phase Coefficient (degrees)	Dimensions d_y (mm)
-182.6812	10.2
-152.6812	7.12
-122.6812	6.618
-92.6812	6.12
-62.6812	5.87
-32.6812	5.63
-2.6812	5.38
27.3188	5.13
57.3188	4.63
87.3188	4.12
117.3188	1.56
147.3188	0

Table 6.2: Reflection phases with respect to the dimensions of the strip-lines d_y with a phase gradient ϕ_N equal to 25° for the super-cell design at 25°

Phase Coefficient (degrees)	Dimensions d_y (mm)
-182.6812	10.2
-152.6812	7.63
-122.6812	6.78
-92.6812	6.25
-62.6812	5.93
-32.6812	5.68
-2.6812	5.43
27.3188	5.17
57.3188	4.7
87.3188	4.16
117.3188	2
147.3188	0

Table 6.3: Reflection phases with respect to the dimensions of the strip-lines d_y with a phase gradient ϕ_N equal to 30° for the super-cell design at 20°

In Figure 6.9 a high value of retroreflection is given at 25° as well as at -25° due to the symmetrical response of the metasurface design, whereas an absence at normal incidence compared to that for the 30° design which is the result of a periodicity $L_x > \lambda$. In this case higher orders of diffraction are present (at -58°) as the periodicity increases higher than λ , as expected according to Floquet-Bloch analysis [358]. Figure 6.10 shows the result of retroreflection for the design at 20° giving a high value at 20° and -20° with a diffracted order at -44° with a significant value in terms of retrodirectivity.

6.4.3.3 Monostatic RCS Performance for Retrodirective Metasurface designs at 15° and 10°

The design of a retrodirective metasurface is given in this case where the periodicity L_x is equal to 2λ and 2.88λ at 15° and 10° respectively. The dimensions of the unit cell elements of the given designs are given in Tables (6.4) and (6.5). The monostatic RCS of the given designs is shown in Figures 6.11 and 6.12 respectively.

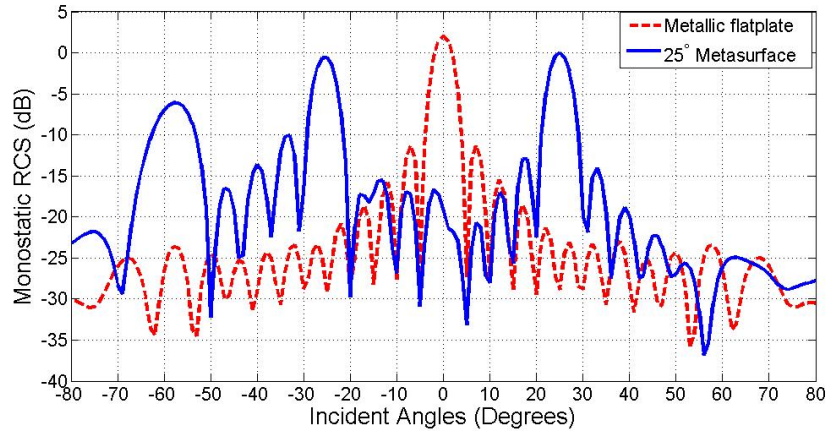


Figure 6.9: Monostatic RCS (dB) with respect to the incident angles (degrees) for a 25° metasurface design of 6×5 super-cells and dimensions $6.1 \text{ cm} \times 12 \text{ cm}$ compared to that of a Flat metallic plate of similar dimensions.

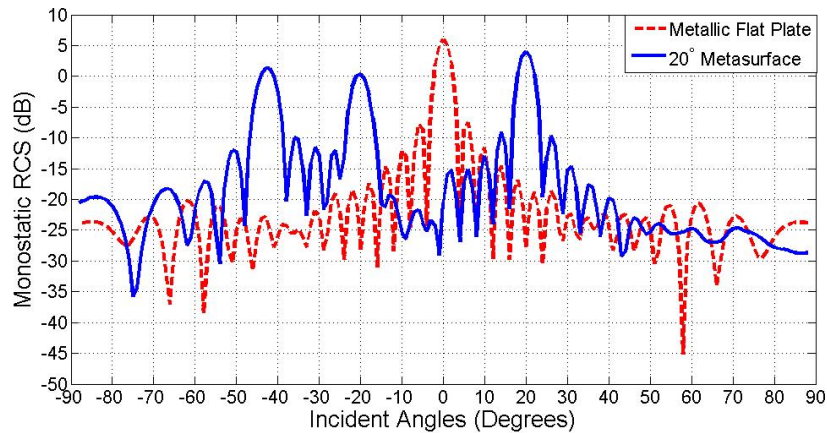


Figure 6.10: Monostatic RCS (dB) with respect to the incident angles (degrees) for a 20° metasurface design of 7×5 super-cells and dimensions $7.1 \text{ cm} \times 15 \text{ cm}$ compared to that of a flat metallic plate of similar dimensions.

The result in Figure 6.11. shows a high value of monostatic RCS at 15° . It can be shown in this case, that the symmetrical response in the opposite direction at -15° is lost, although the phase of the reflection coefficient remains with the same response compared to that at 30° , 25° and 20° . Two diffracted orders are present in this case showing a high value of monostatic RCS at -32° and -50° as shown in Figure 6.11. The symmetrical response in terms of retrodirectivity for the metasurface design is lost due to the high periodicity L_x in this case, being $\geq 2\lambda$ and the presence of the higher orders of diffraction [358]. Figure 6.12. shows the result of the monostatic RCS for a 10° designed metasurface with a periodicity $L_x=2.88\lambda$. A high value of monostatic RCS is present at the desired angle with the absence of retrodirectivity in the opposite direction at -10° and two significant values at the diffracted orders at -44° and -60° .

Phase Coefficient (degrees)	Dimensions d_y (mm)
-182.6812	10.2
-152.6812	7.8
-122.6812	6.88
-92.6812	6.39
-62.6812	6
-32.6812	5.75
-2.6812	5.5
27.3188	5.24
57.3188	4.83
87.3188	4.29
117.3188	2.22
147.3188	0

Table 6.4: Reflection phases with respect to the dimensions of the strip-lines d_y with a phase gradient ϕ_N equal to 30° for the super-cell design at 15°

Phase Coefficient (degrees)	Dimensions d_y (mm)
-182.6812	10.2
-152.6812	7.83
-122.6812	6.9
-92.6812	6.46
-62.6812	6.05
-32.6812	5.8
-2.6812	5.54
27.3188	5.29
57.3188	4.93
87.3188	4.33
117.3188	2.76
147.3188	0

Table 6.5: Reflection phases with respect to the dimensions of the strip-lines d_y with a phase gradient ϕ_N equal to 30° for the super-cell design at 10°

6.4.3.4 Metasurfaces with Symmetrical Responses at -15° and -10° for periodicity greater than 2λ

As mentioned before, the metasurface design for a periodicity $\geq 2\lambda$ shows a loss in the symmetrical response of the metasurface design. Thus, a different design structure is proposed for the metasurfaces at 15° and 10° by introducing a metasurface with two opposite directions as shown in Figure 6.13. The results for the monostatic RCS for the proposed design structure at 15° and 10° are given in Figures 6.14 and 6.15.

Figures 6.14 and 6.15 show the comparison between the proposed metasurface designs at 10° and 15° to that of a flat metallic plate respectively. The results of the retroreflection in Figures 6.14 and 6.15, show a recovery of the loss in the symmetrical directions at -10° and -15° for the desired angles of incidence using the proposed structure design for both cases with lower efficiency with respect to that of the flat metallic plate, compared to that of the metasurfaces which show a high value only for the angles at 10° and 15° , but regaining the loss of the symmetrical response of the metasurface in this case.

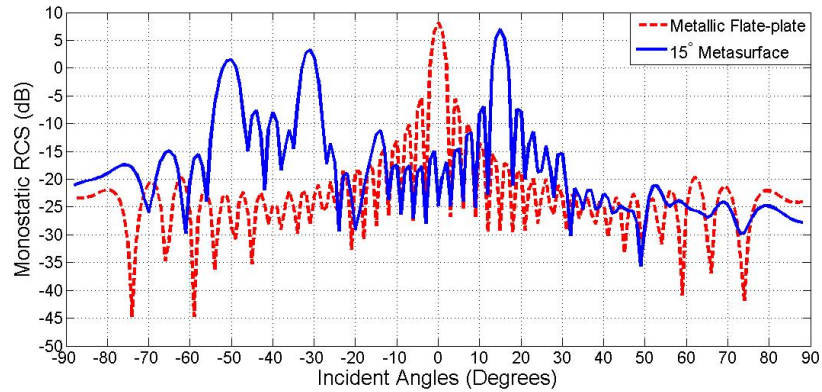


Figure 6.11: Monostatic RCS (dB) with respect to the incident angles (degrees) for a 15° metasurface design of 7×5 super-cells and dimensions 7.14 cm × 19.7 cm compared to that of a metallic flat plate of similar dimensions.

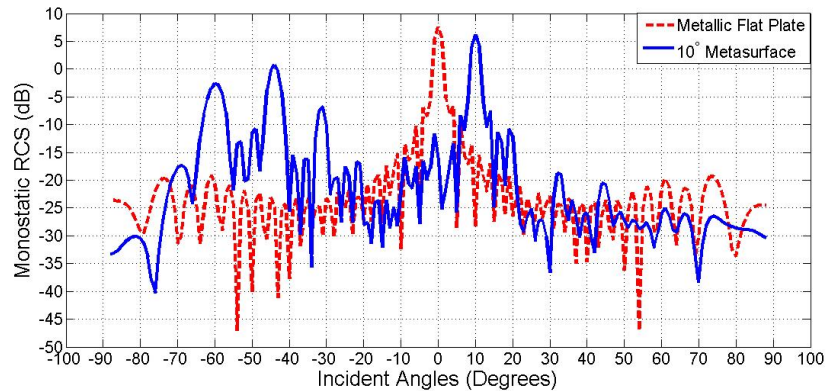


Figure 6.12: Monostatic RCS (dB) with respect to the incident angles (degrees) for a 10° metasurface design of 6×4 super-cells and dimensions 6.12 cm × 23.5 cm compared to that of a metallic flat plate of similar dimensions.

6.4.3.5 Experimental Measurements for a 30° Metasurface Prototype

For the validation of the numerical analysis of a 30° metasurface, a prototype has been fabricated as shown in Figure 6.7b. with 7×9 periodic array of super-cells of dimensions 14.3 cm × 9.2 cm, printed on top of a Teflon grounded substrate of relative permittivity $\epsilon=2.2$ and thickness 1.6mm. The measurements were carried out in an anechoic chamber at an operating frequency of 14.7 GHz. The results have been compared to the simulation results as shown in Figure 6.17.

Figure 6.16 shows that the measurement results are in good agreement with the numerical results.

6.4.4 Design of Dual Polarized Retrodirective Metasurfaces

In some applications dual polarization can be essential. In this part we introduce the design of dual polarized retrodirective metasurfaces following the same design procedure and principle of operation explained before, the only change to be in the unit cell element chosen. This part has been presented at the 2018 IEEE Radio and Antenna Days of the Indian Ocean (RADIO) Conference [359].

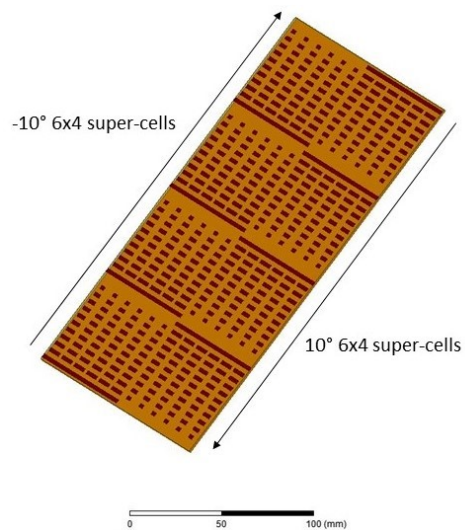


Figure 6.13: A metasurface design with two opposite directions structure at 10° using Ansys HFSS.

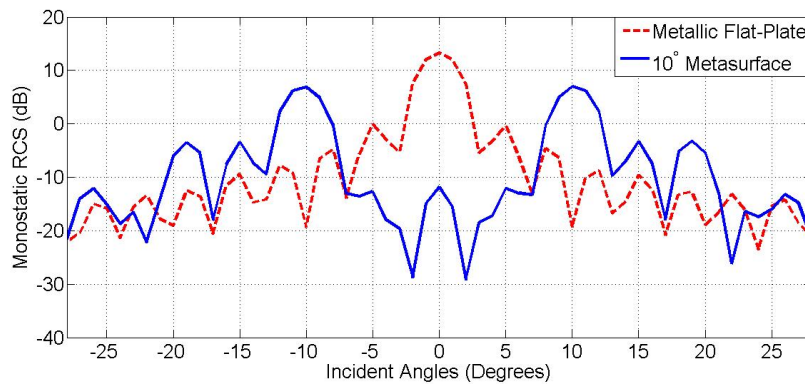


Figure 6.14: Monostatic RCS of the 10° metasurface proposed structure of 12×4 super-cells (Figure 6.13) of dimensions $12.224 \text{ cm} \times 23.5 \text{ cm}$ compared to that of a flat metallic plate of similar dimensions.

A design for an incident angle at 5° is given in this part for demonstration. L_x is equal to 5.76λ , $N = 12$ unit cells at a frequency equal to 14.7 GHz and printed on top of a grounded substrate of permittivity $\epsilon = 2.2$. The super-cell designs are shown in Fig. 5.17 and 6.18. Fig 5.17 shows the patch structure with two degrees of freedom P_x and P_y , whereas in Fig 6.18 the cross has been designed having three degrees of freedom C_x, C_y and w which are determined following the reflection phase coefficient and the phase gradient in (5.5). L_x and L_y define the dimensions of the super-cell and d_x for that of the unit cell in both cases.

6.4.4.1 Numerical Results for A Dual-Polarized Retrodirective Metasurface Design

A cross structure and patch metasurface of 4×3 super-cells are given as shown in Figure 6.19 and 6.20 respectively.

The monostatic RCS for both metasurfaces is calculated for a propagating wave at 14.7 GHz . The results of the normalized monostatic RCS are shown in Figure 6.21 and 6.22 for the cross and patch metasurfaces respectively.

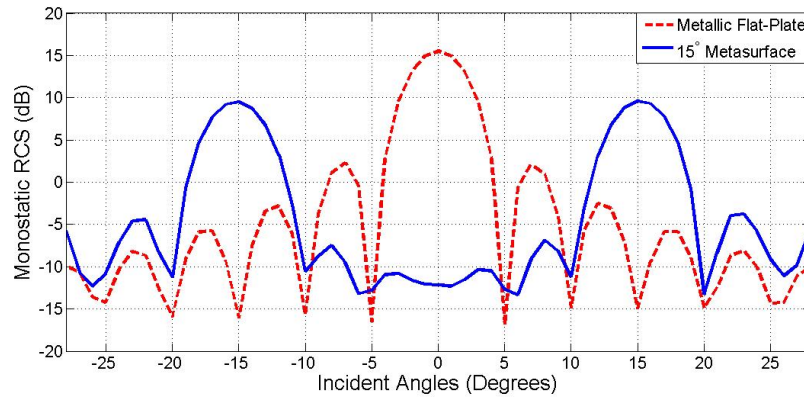


Figure 6.15: Monostatic RCS of the 15° metasurface proposed structure of 14×5 super-cells of dimensions 14.28 cm × 19.7 cm compared to that of a flat metallic plate of similar dimensions.

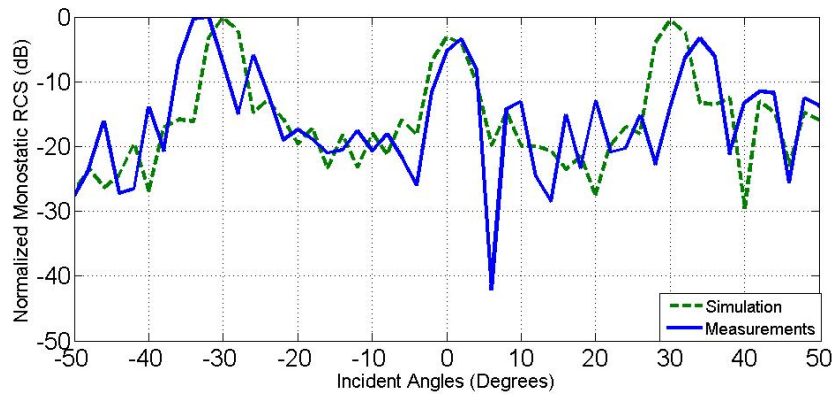


Figure 6.16: Normalized monostatic RCS with respect to the incident angles of the experimental measurements compared to that of the simulation results for a 30° metasurface prototype.

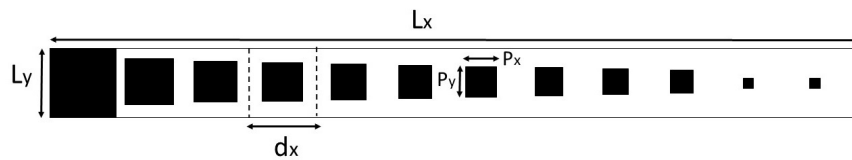


Figure 6.17: Super cell of dimensions L_x and L_y divided into subwavelength patch structured unit cells

The results in Figures 6.21 and 6.22 show a high level of retroreflection at the 5° desired angle for both polarization TM and TE, this indicates that this results in tracking enhancement for both polarizations at oblique incidence. Measurements have been carried out for a cross structure metasurface in an anechoic chamber at 14.7 GHz. The prototype is shown in Figure 6.23.

Measurements for both TM and TE polarizations have been carried out for the cross prototype metasurface. The results of both TE and TM measurements compared to the simulation results are given in Figures 6.24 and 6.25.

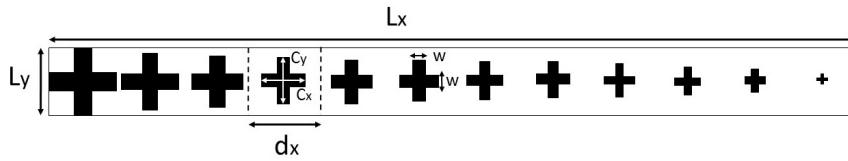


Figure 6.18: Super cell of dimensions L_x and L_y divided into subwavelength cross structured unit cells

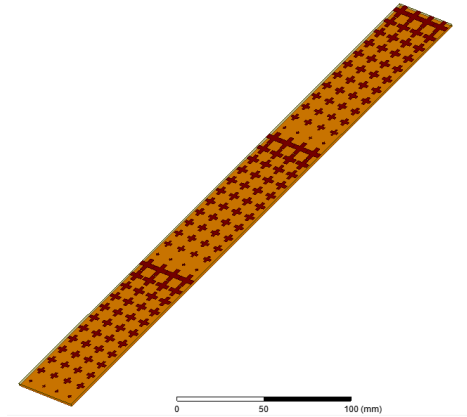


Figure 6.19: Cross Structure metasurface of 4×3 super-cells.

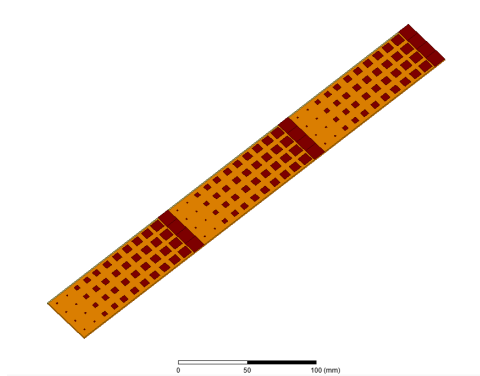


Figure 6.20: Patch Structure metasurface of 4×3 super-cells.

The results in both figures 6.24 and 6.25 for TE and TM measurements of the cross metasurface agree almost perfectly with the simulation results, thus validating the results.

6.5 Design of a Multi-Angle Cascaded Retrodirective Metasurface based on Superposition

The aim of our study is to design retrodirective metasurfaces which can operate at wide range of incident angles. This is to enhance the potential of tracking and localization from the angular aspect of a target to provide wireless power for example in the application of WPT, specially for extreme oblique incident angles. The Cascaded Multiple Incident Angle Retrodirective Metasurface (C-MIARM) is designed based on superposing different designed metasurfaces at various angles. In

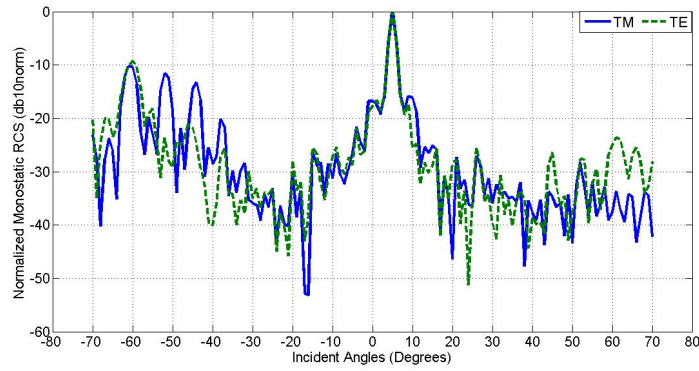


Figure 6.21: Normalized monostatic RCS in dB10norm with respect to the incident angles for a cross metasurface structure at TM and TE polarizations

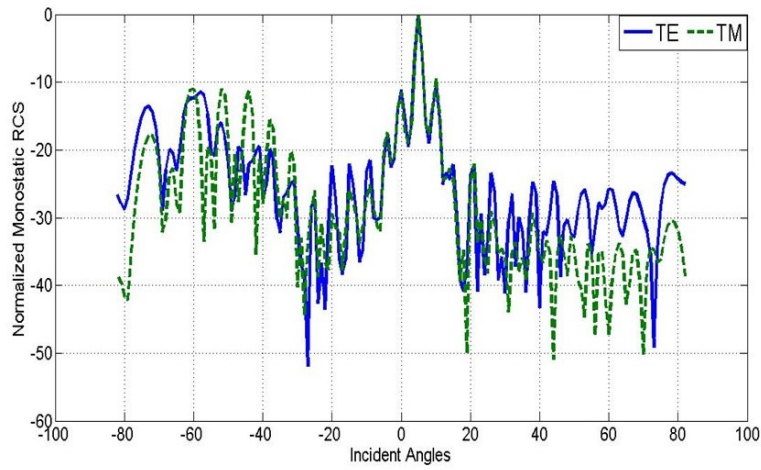


Figure 6.22: Normalized monostatic RCS in dB10norm with respect to the incident angles for a patch metasurface structure at TM and TE polarizations

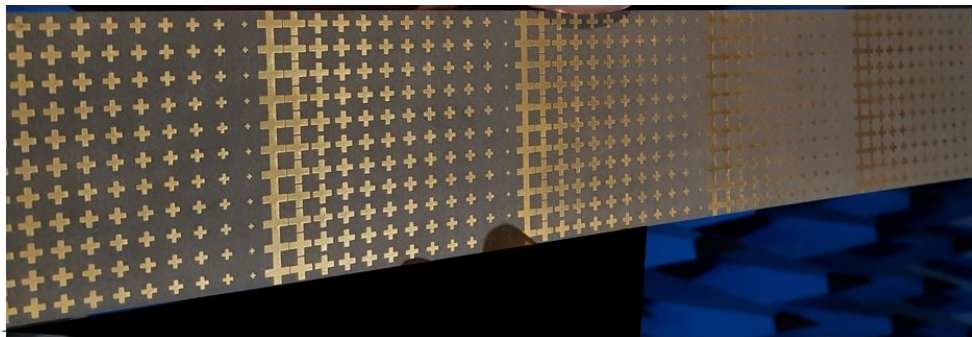


Figure 6.23: Prototype of a cross metasurface structure for measurements carried on in an anechoic chamber.

this case, the metasurface is designed by superposing designs at 30° , 25° , 20° , 15° and 10° , and using the opposite metasurface structure for the designs at 15° and 10° as shown in Figure 6.13.

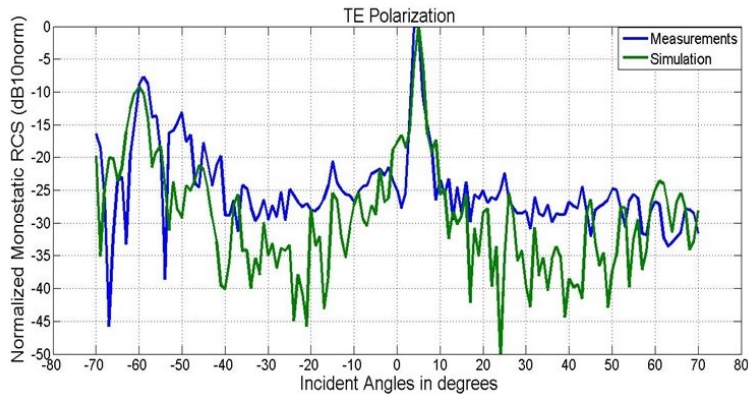


Figure 6.24: Normalized monostatic RCS measurements compared to that of the simulation results for TE polarization for the cross metasurface at 14.7 GHz.

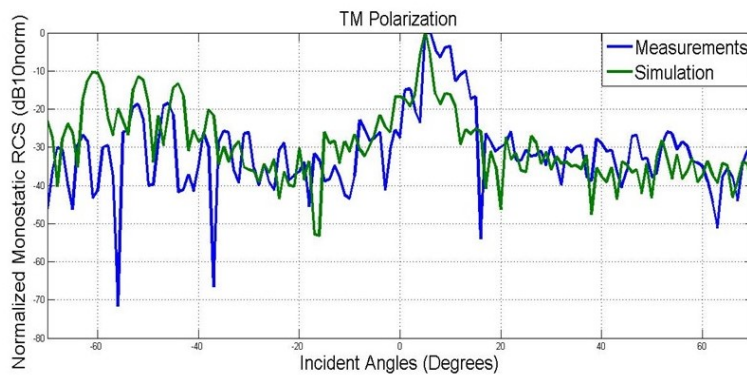


Figure 6.25: Normalized monostatic RCS measurements compared to that of the simulation results for TM polarization for the cross metasurface at 14.7 GHz.

The C-MIARM design is shown in Figure 6.26.

The overall dimensions of the C-MIARM are $8.163 \text{ cm} \times 56.23 \text{ cm}$. The normalized monostatic RCS with respect to the metasurfaces at various angles is given in order to determine the overall retro-reflective performance of the designed metasurface as shown in Figure 6.27.

The results in Figure 6.27, have shown a wide range of retroreflection with respect to various incident angles in the ranges between -30° to -10° and from 10° to 30° . A low value is present in the range between -10° to 0° which can be said to be due to the absence of a metasurface design at 5° for the simplicity of the numerical analysis, whereas an intermediate value was shown between 0° and 10° .

6.5.1 Comparison between the C-MIARM and the Conventional Corner Dihedral

Different topologies of retrodirective reflectors have been shown in the literature including the corner dihedral [360]. For performance and efficiency comparison purposes, The results and performance

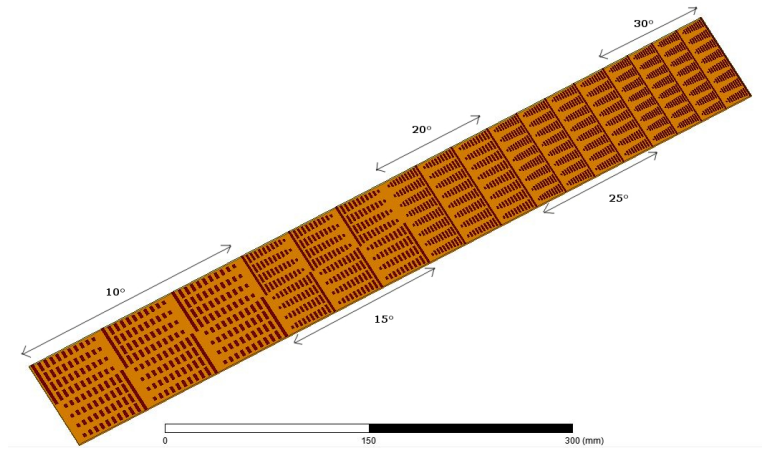


Figure 6.26: Cascaded Multiple Incident Angle Retrodirective Metasurface (C-MIARM) with the superposition of 4×8 30° , 25° and 20° super-cells each with 15° and 10° metasurfaces using the mirror image form, where the MIARM has an overall dimension of $8.163 \text{ cm} \times 56.23 \text{ cm}$ and substrate of $\epsilon=2.2$ and thickness 1.57 mm .

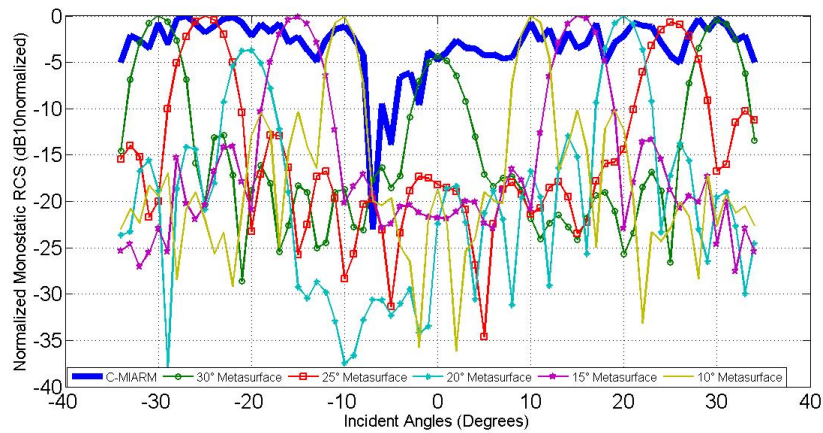


Figure 6.27: Normalized monostatic RCS in dB of the C-MIARM with respect to the overall performances of the metasurfaces designed at 30° , 25° , 20° , 15° and 10° .

of the C-MIARM with respect to retroreflection is compared to that of the corner dihedral as shown in Figure 6.28.

The results in Figure 6.28 show a 50 dB gain of monostatic RCS for the C-MIARM with respect to the corner dihedral of dimensions $8 \text{ cm} \times 15.5 \text{ cm} \times 7.75 \text{ cm}$ in the range between -30° to -20° and 20° to 30° , whereas the corner dihedral was limited between -20° to 20° where the C-MIARM showed a wide range between -30° to -10° and 10° to 30° . Giving a value up to 5 dB of monostatic RCS, the C-MIARM was able to achieve this value with dimensions $8.163 \text{ cm} \times 56.23 \text{ cm}$ compared to that of a 3D structured corner dihedral of dimensions $8 \text{ cm} \times 15.5 \text{ cm} \times 7.75 \text{ cm}$. The advantage of the

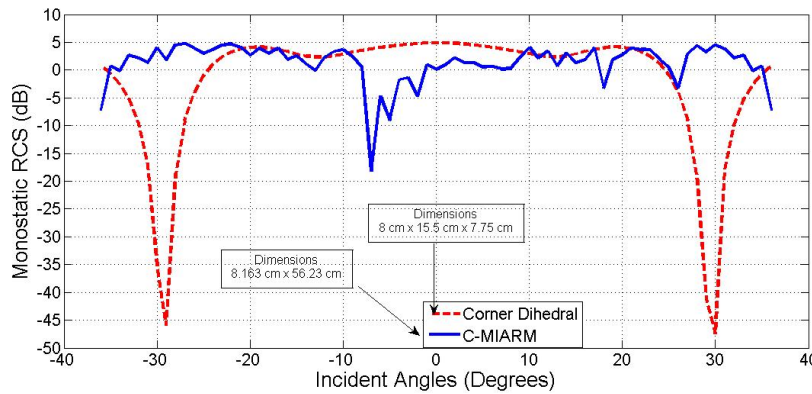


Figure 6.28: Monostatic RCS of the C-MIARM of dimensions $8.163 \text{ cm} \times 56.23 \text{ cm}$ compared to that of a conventional corner dihedral of dimensions $8 \text{ cm} \times 15.5 \text{ cm} \times 7.75 \text{ cm}$.

C-MIARM is having a 2D structure making it easy for implementation for different application and addressing extreme incident angles, and can be a complementary solution for such topologies.

In terms of frequency, the corner dihedral is broadband and can perform for a wide-band of frequencies. On the other hand, the C-MIARM is narrow-band and can be sufficient at the given frequency of 14.7 GHz, as well as a tolerance of 150 MHz around the selected frequency. This can be significant for applications such as automotive radar systems. However, for applications where broadband is needed, other type of unit cells [361] can be proposed to ensure a stable distribution of the reflection phase at a wide-band of frequencies.

6.5.2 Experimental Measurements for the C-MIARM

A prototype of the C-MIARM has been fabricated and tested as shown in Figure 6.29. The dimensions of the prototype are $8.163 \text{ cm} \times 56.23 \text{ cm}$. The measurements were carried out in an anechoic chamber using two Vivaldi antennas (transmitter and receiver) operating at 14.7GHz. The measurements and simulation results have been compared as shown in Figure 6.30.

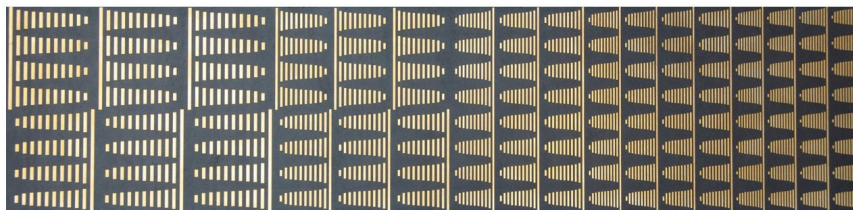


Figure 6.29: Fabricated prototype of the C-MIARM of dimensions $8.163 \text{ cm} \times 56.23 \text{ cm}$.

The measurement results in Figure 6.30, are said to follow and be in good agreement compared to that of the simulated results with some losses at the angles of 8° and -23° which can be due to mechanical inaccuracies, as well as the coupling and phase shift present between the two Vivaldi antennas.

The C-MIARM has shown remarkable results in terms of retroreflection at a wide range of incident angles. It can be a complement solution for tracking and localization enhancement where it can be needed such as WPT for IOT devices.

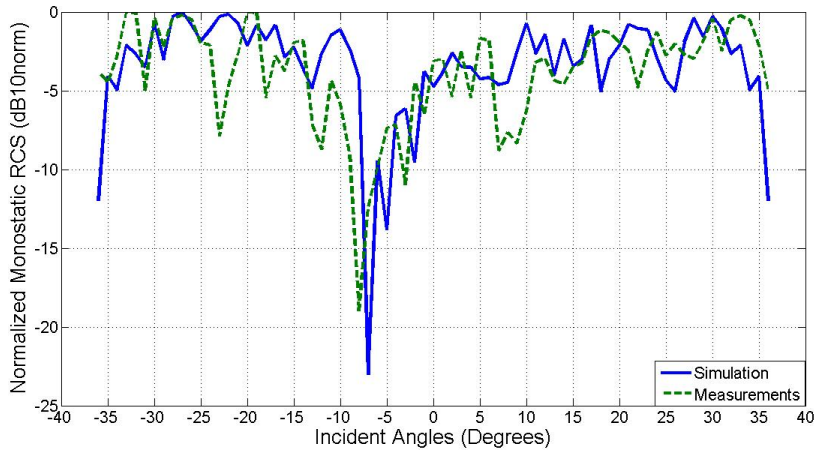


Figure 6.30: Normalized Monostatic RCS with respect to the incident angles of the simulation results compared to that of the measurements at 14.7GHz for the C-MIARM.

6.6 Multi-Angle Retrodirective Metasurfaces from Non Reciprocal to Reciprocal: Impedance Modulation for High Super-cell Periodicity Designs

In this part we introduce a different technique to design multi-angle retrodirective metasurfaces based on impedance modulation. This work has been published in the journal Applied Physics A, Springer entitled “Retrodirective metasurfaces from non-reciprocal to reciprocal using impedance modulation for high-super-cell-periodicity designs” [70]. Indeed, retro-reflection can be achieved at a given incident angle, and it is well known that it can be directly achieved in the opposite or reciprocal direction as given in equation (6.3) and in [53,349,362]. We recall in the work we presented in previous sections that the design of retrodirective metasurfaces for various angles of incidence at different super-cell periodicity designs [69], we have shown that, for retrodirective metasurface designs with subwavelength super-cell periodicities L_x , the metasurface can perform retro-reflection for both the desired direction and the opposite reciprocal direction as well as at normal incidence [53, 69, 349, 362]. However, according to Floquet-Bloch harmonic analysis [32, 358], with an increase of periodicity higher than the wavelength λ , higher orders of diffraction can exist for the super-cell design, which creates more apertures for wave propagation at different angles of incidence. For a super-cell periodicity between λ and 2λ , retro-reflection for the metasurface at normal incidence is shown to be lost [69] as we recall which is shown in Figures 5.9 and 5.10. On the other hand, for periodicities greater than 2λ , the metasurface loses its conventional reciprocal property for retro-reflection [69], which can be due to the existence of higher orders of diffraction and apertures where the wave is propagating as was shown in Figures 6.11 and 6.12.

V.S. Asadchy et al. have introduced the concept of the surface impedance modulation [357], to design multi-channel reflectors [32], under the assumption of lossless and reciprocal reflectors at a periodicity of 1.064λ . Although this concept has been demonstrated for an incident angle of 28° , it can be interesting to study the design of retrodirective metasurfaces addressing lower incident angles such as 10° where the periodicity can reach a level up to 2.88λ . The main challenge is to retain the conventional reciprocal property of a retrodirective metasurface at high super-cell periodicity designs and achieve efficient retro-reflection at the higher orders of diffraction. In contrast to what we have introduced in previous sections, where the concept of cascading has been introduced [69]

and the design of opposite super-cell designs (Figures 6.26 and 6.13), we would like in to optimize the association for several retrodirective metasurfaces without the loss of their performance, where the cascaded metasurface [69] can be bulky and of large dimensions for some applications.

In this part, we demonstrate the possibility to design a retrodirective metasurface with a high super-cell periodicity up to 2.88λ using the surface impedance modulation technique, this is, by retaining its conventional reciprocal property at 10° and normal incidence with high efficiency using a single designed super-cell. Furthermore, taking advantage of the high number of diffraction orders at these periodicities and with a proper engineered surface impedance, one can extend the retrodirective metasurface to operate at multiple incident angles simultaneously which can be a great complementary solution for tracking enhancement and of compact dimensions for ease of implementation.

6.6.1 Relation between Periodicity L_x and Wavelength λ

The performance of retro-reflection for the metasurface design depends directly on the relation between the periodicity L_x and the wavelength λ , where θ_i varies according to the incident angle desired for retro-reflection as given in Equation (6.3). In this case, since L_x is the periodicity of the super-cell design, thus it can only be a positive value. Hence, in theory the metasurface should perform retro-reflection for the desired angle θ_i and reciprocal angle $-\theta_i$ simultaneously. This has been proved in previous work at subwavelength periodicity designs [32, 53, 349, 362]. However, with an increase of periodicity beyond λ , the performance of the retrodirective metasurface differs and shows direct relation between the periodicity L_x and wavelength λ as shown in Figure 6.31.

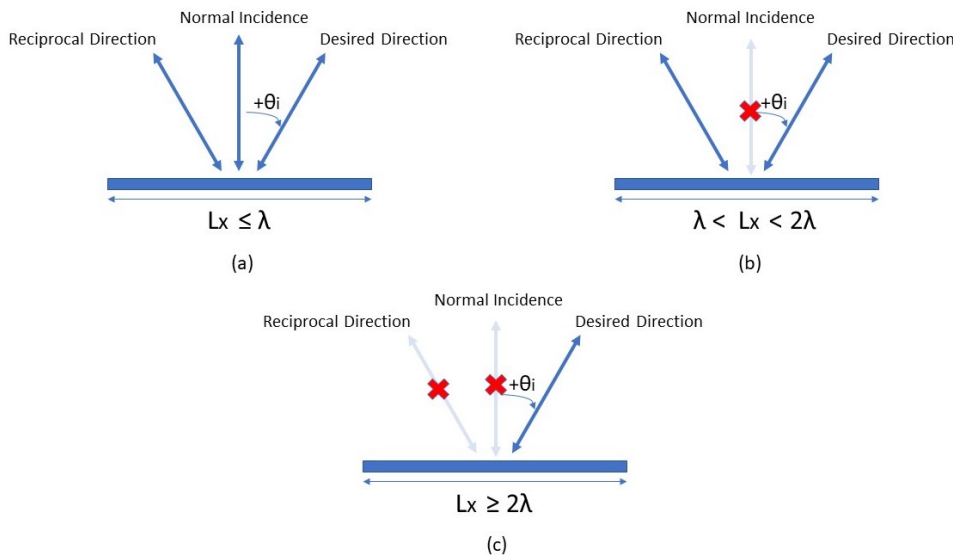


Figure 6.31: a) Super-cell periodicity $L_x \leq \lambda$, retro-reflection is obtained in the desired direction θ_i , the reciprocal direction and at normal incidence. b) Super-cell periodicity $\lambda < L_x < 2\lambda$, retro-reflection is obtained in the desired direction θ_i and the reciprocal direction, whereas for normal incidence is absent. c) Super-cell periodicity $L_x \geq 2\lambda$, retro-reflection is obtained only in the desired direction θ_i , whereas the conventional properties of the metasurface are lost in the reciprocal and normal incidence directions.

For a periodicity $L_x \leq \lambda$, retroreflection is obtained at the desired angle, reciprocal direction and normal incidence as shown in Figure 6.31a (demonstrated in Figure 6.8). However, for $\lambda < L_x < 2\lambda$,

the metasurface loses its performance for retro-reflection at normal incidence [69] as shown in Figure 6.31b (Demonstrated in Figures 6.9 and 6.10). On the other hand, with an increase of periodicity beyond 2λ ($L_x \geq 2\lambda$), the retrodirective metasurface loses its conventional reciprocal property and retroreflection is obtained only at the desired angle [69] as shown in Figure 6.31c (Demonstrated in Figures 6.11 and 6.12). According to Floquet-Bloch analysis [358], for a metasurface design of periodicity larger than λ , higher orders of diffraction and open apertures can exist. This can explain the loss of retro-reflection in the reciprocal direction and normal incidence, which is due to the the existence of open apertures which allow the propagation of the wave in other directions. However, the direction of the open apertures or higher orders of diffractions can be obtained as follows:

$$\theta_{rn} = \arcsin \frac{n\lambda}{L_x} \quad (6.7)$$

where n defines the number of open apertures or diffraction orders and θ_{rn} the direction of the diffraction orders.

6.6.2 High Periodicity Reciprocal Metasurface Design Procedure: Surface Impedance Modulation Technique

The main challenge in this work is to retain the conventional reciprocal property for a retrodirective metasurface as well as at normal incidence. However, following the surface impedance modulation technique, with a proper engineered surface impedance, for super-cell periodicities higher than 2λ , one can achieve efficient retro-reflection at the directions of the higher orders of diffraction. In this section, we explain briefly the design procedure of a reciprocal retrodirective metasurface for a periodicity design of 2.88λ operating at 14.7 GHz. We define the nominal super-cell following the generalized phase law of reflection and the optimized super-cell design after introducing the surface impedance modulation technique.

The retrodirective metasurface consists of optimized super-cells which are designed in two steps. The starting point for the design of a gradient metasurface, is by defining a configuration based on the generalized phase law of reflection. The designed nominal super-cell is shown in Figure 5.32.

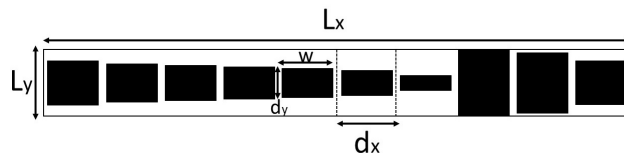


Figure 6.32: Nominal super cell design discretized into 10 patch cells of dimensions d_y (given in table (6.6)) following the generalized phase law of reflection.

The periodicity L_x and L_y of the nominal super-cell define the length and width of the super-cell respectively as shown in Figure 6.32. L_x is determined according to Equation (6.3). The patch dimensions d_y are determined following the phase of the reflection coefficient which are tuned with respect to a phase gradient. In the second step the surface impedance optimization of the nominal super-cell design is implemented. It has been shown [357] that in order to ensure efficient retro-reflection of the designed metasurface, the surface impedance Z_{s_i} should be purely reactive at each patch element i with respect to the given periodicity, where the incident electric field E_i is equal to

that of the reflected electric field E_r [32,357]. Assuming a given TM polarized wave $Z_{TM} = \eta \cos \theta_i$, Z_{si} is given as:

$$Z_{si} = j \frac{Z_{TM}}{\tan(\frac{\phi_i}{2})} \quad (6.8)$$

Equation (6.8) defines the surface impedance Z_{si} needed for each patch element where ϕ_i defines the phase of the reflection coefficient. To achieve a purely reactive impedance of the super-cell design, post processing optimization using Floquet Periodic Boundary condition of the nominal super-cell patch dimensions is followed. The process is done by tuning the nominal patch dimensions d_y to obtain the best combination with a purely reactive surface impedance. Figure 6.33 shows the super-cell design after numerical optimization of the patch cells to a proper reactive surface impedance.

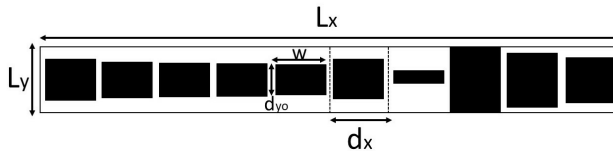


Figure 6.33: Optimized Super-cell after tuning the patches to the proper reactive surface impedance of dimensions d_y (given in table (6.6)).

The nominal and optimized super-cells are divided into N unit cells where $N = 10$ in this case, $d_x = L_x/N$, with the width of the patches being constant $w = d_x - 0.5$ mm. d_y defines the dimension of the nominal patches which are tuned with respect to a phase gradient. The dimensions of the patches are determined following the phase of the reflection coefficient ϕ_i shown in Figure 6.34.

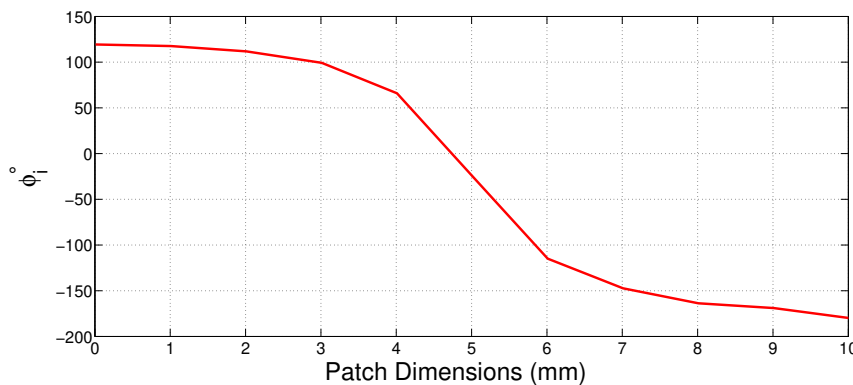


Figure 6.34: Phase of the reflection coefficient with respect to the patch dimensions d_y in mm for a given frequency at 14.7 GHz

For a given frequency of 14.7 GHz and $\theta_i = 10^\circ$, a progressive phase shift equal to 40.5° is introduced between each patch element, to achieve the whole phase distribution given in Figure 6.34 for the super-cell design. The periodicity $L_x = 2.88\lambda$ and $L_y = \lambda/2$. Table (6.6) shows the nominal

dimensions of the metallic patches with respect to ϕ_i , which are printed on a grounded substrate of permittivity $\epsilon = 2.2$, $\tan(\delta) = 1 \times 10^{-3}$ and thickness 1.57 mm as shown in Figure 6.32.

The surface impedance of the nominal super-cell shown in Figure 6.32 has been calculated at the given frequency 14.7 GHz and incident angle 10° for a TM polarized wave where $Z_s = 11.5 - j524.25$ using Floquet Periodic Boundary Condition. The patches are tuned to a level where the real part of Z_s is approximately equal to zero, this is determined by post processing numerical optimization using Ansys HFSS and finding the best combination between the designed grounded patches for the super-cell design using Floquet boundary conditions. The optimized dimensions d_{yo} have been given in Table (6.6). The surface impedance of the optimized super-cell design in Figure 5.33 has been optimized to a value of $Z_s = 0.9 - j267.3$ at 14.7 GHz, where the real part is approximately equal to zero thus eliminating the ohmic losses of the designed super-cell.

ϕ_i°	Nominal Dimensions d_y (mm)	Optimized Dimensions d_{yo} (mm)
-134.27	6.73	6.38
-93.7	5.88	5.61
-53.2	5.408	5.306
-12.7	4.969	5.102
27.8	4.489	4.898
68.3	3.979	5.915
108.8	2.306	2.04
-210.7	10.2	10.2
-170.2	9.28	8.673
-129.7	6.53	6.73

Table 6.6: The nominal dimensions d_y (mm) of the patch cells following the generalized phase law and the phase of the reflection coefficient ϕ_i° shown in Figure 5.34 with a phase gradient equal to 40.5° , as well as the optimized dimensions d_{yo} after implementation of the surface impedance modulation.

6.6.3 Metasurface Design and Results

Two metasurfaces have been designed with similar dimensions $5 \text{ cm} \times 23 \text{ cm}$ using Ansys HFSS; The first one of 5×4 nominal super-cells(Figure 6.32) as shown in Figure 5.35a and the second using 5×4 optimized super-cells(Figure 6.33) given in Figure 6.35b.

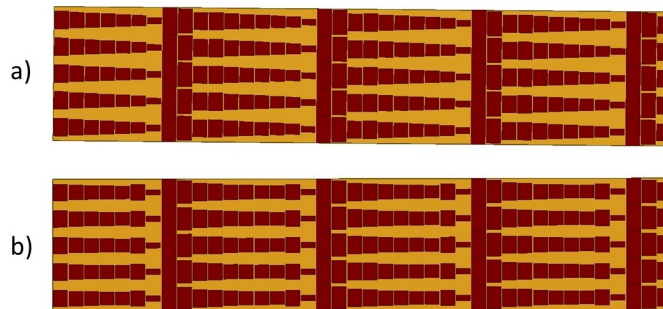


Figure 6.35: a) Metasurface design using Ansys HFSS of 5×4 nominal super-cells b) Metasurface design of 5×4 optimized super-cells .

To compare the performances in terms of retrodirectivity of both metasurfaces, the normalized

monostatic RCS is determined to calculate the energy which is redirected back to the direction of the transmitter as shown in Figure 6.36.

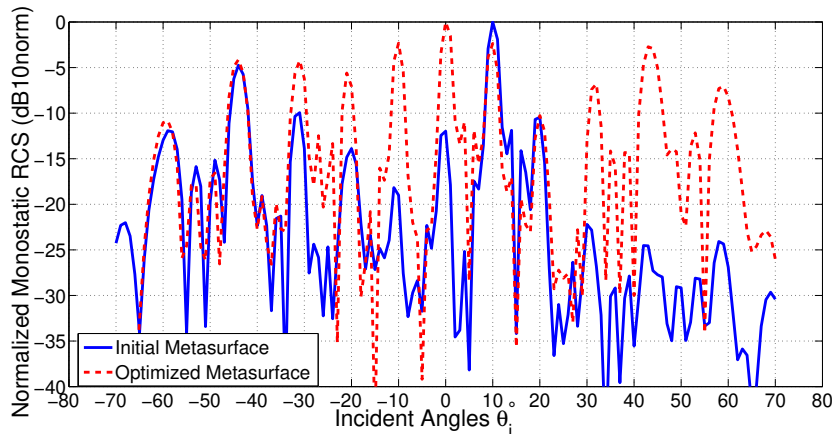


Figure 6.36: Normalized Monostatic RCS of the optimized metasurface (Figure 6.35b) after implementation of the impedance modulation compared to that of the nominal design (Figure 6.35a) following the generalized phase law of reflection operating at 14.7 GHz and of similar dimensions $5.1 \text{ cm} \times 23.5 \text{ cm}$.

First for the case of the nominal or initial metasurface design in Figure 6.35a, the results in Figure 6.36 show a high a level of retro-reflection for the nominal metasurface at 10° due to the proper periodicity and desired angle chosen. Other peaks in terms of retro-reflection are present but with low efficiency compared to the desired angle of incidence (10°) such as, -20° , -44° , -32° and -60° . This is expected, since according to Floquet Bloch analysis in Equation (6.7), higher diffraction orders can exist and the direction of the apertures can be calculated. Thus, for $L_x = 2.88\lambda$, the range of values of n are limited to $n = 0, \pm 1, \pm 2$. Hence, five open apertures or higher orders of diffraction are expected at $\theta_i = 0, \pm 20.3^\circ, \pm 44^\circ$. The presence of two other higher orders of diffraction at $\pm 32^\circ, \pm 60^\circ$ can be due to the level of periodicity which is approximately equal to 3λ . However, we can observe that, the reciprocal direction at -10° and normal incidence are absent and of very low efficiencies, which is due to the propagation of the wave in the direction of the higher diffraction orders which are said to be uncontrollable.

Second for the case of the optimized metasurface design in Figure 5.35b, after the implementation of the surface impedance modulation technique, we can observe from Figure 6.36 that the retro-reflection in the reciprocal direction at -10° and normal incidence have been retained and achieved with high efficiency. This is due to the control of the high diffraction orders by optimizing the surface impedance, as well as, retro-reflection was also obtained with higher efficiency compared to that of the nominal case, in the direction of the diffraction orders at $\pm 20.3^\circ, \pm 32^\circ, \pm 44^\circ$ and $\pm 60^\circ$. To determine the efficiency of retro-reflection for the optimized metasurface at the eleven angles of incidence, the metasurface is compared to that of a metallic flat plate of similar dimensions $5.1 \text{ cm} \times 23.5 \text{ cm}$, which well known for its high efficiency in terms of retro-reflection at normal incidence. The simulated results comparing both performances are shown in Figure 6.37.

The results show a high level of monostatic RCS or retrodirectivity for the optimized metasurface design for the following incident angles at normal incidence and $\pm 10^\circ, \pm 20.3^\circ, \pm 32^\circ, \pm 44^\circ, \pm 60^\circ$ compared to that of the metallic flat plate which only re-directs the wave back in the same direction

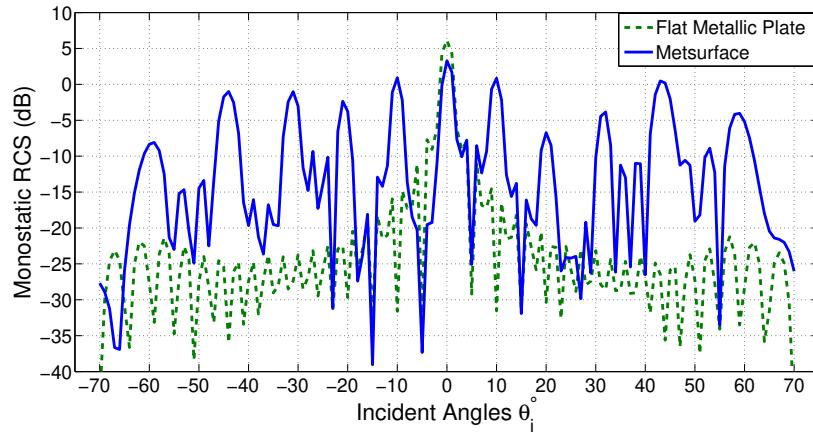


Figure 6.37: Monostatic RCS (dB) of the optimized metasurface design (Figure 6.35b) compared to that of flat metallic plate with respect to the given incident angles at 14.7 GHz of similar dimensions $5.1 \text{ cm} \times 23.5 \text{ cm}$.

at normal incidence which is 6 dB in this case. The gain (dB) of monostatic RCS for each incident angle of the optimized metasurface compared to that of the metallic flat plate are given in Table (6.7). Some angles such as that at $+20.3^\circ$, are subject to more attenuation due to the surface resistance. In terms of frequency and polarization, the metasurface is said to operate at 14.7 GHz, as well as a tolerance of $\pm 100 \text{ MHz}$ around the operating frequency. On the other hand, for applications where broadband and dual polarization is needed other unit cell designs can be considered [359,361].

θ_i°	Gain (dB)
-60	+17
-44	+23
-32	+22
-20.3	+21
-10	+32
0	-4
+10	+32
+20.3	+23
+32	+24
+44	+27
+60	+21

Table 6.7: Gain in dB of monostatic RCS of the optimized metasurface compared to that of a flat metallic plate of similar dimensions $5 \text{ cm} \times 23 \text{ cm}$ for the given incident angles θ_i at 14.7 GHz.

6.6.4 Fano Resonance Based Multiple Angle Retrodirective Metasurface

In this section, we use dolmen fano-resonating structures [363,364], which are based on spectrum engineering for highly sensitive devices, and introducing a phase gradient by tuning the sub-radiant modes following the generalized phase law of reflection, particularly for retro-reflection, while fixing the super-radiant mode. The unit cell structure is shown in Fig. 6.38.

The dimensions of the dolmen unit cell are given as follows: the two sub-radiant modes are of same dimensions in the x-direction, $L_1 = 6.5 \text{ mm}$ and $W_1 = 1 \text{ mm}$. Whereas, for the super-radiant mode

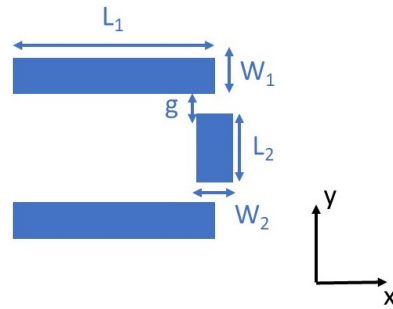


Figure 6.38: Unit cell dolmen structure of 3 elements, two sub-radiant modes in the x-direction of dimensions L_1 and W_1 , and one super-radiant mode in the y-direction of dimensions L_2 and W_2 . With a gap g between the two sub-radiant modes and the super-radiant mode.

in the y-direction, $L_2 = 2\text{mm}$ and $W_2 = 1\text{mm}$, with a gap $g = 1\text{mm}$ between the sub-radiant modes and the super-radiant modes.

In this case, θ is chosen at 5° for a frequency of 24 GHz, thus L_x is equal to 5.74λ . According to Floquet Bloch analysis [358] for a metasurface design of periodicity larger than λ , a high number of open channels can exist where retrodirectivity can be achieved in addition to choosing the desired angle. For a periodicity of 5.74λ , the design becomes very lossy and complex in terms of optimization. The usage of a Fano-resonance structure can be a good candidate to suppress the losses for super-cells with high periodicities. The super-cell is divided into 8 unit cells, where the dimensions of the sub-radiant modes L_1 are both tuned similarly in the x-direction. The phase gradient $\phi = 2\pi/8 = 45^\circ$. The dimensions of the sub-radiant modes are determined following the phase of the reflection coefficient which is shown in Fig. 6.39.

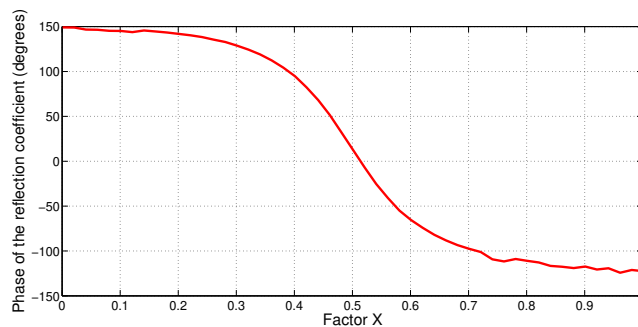


Figure 6.39: Phase of the reflection coefficient with respect to that of Factor X which is multiplied with the dimensions of the sub-radiant modes at 24 GHz.

The tuned dimensions are given as $L_{1(initial)} \times \text{Factor X}$ with $L_{1(initial)} = 6.5\text{mm}$, which is determined in Fig.6.39 with respect to a phase gradient 45° . The Factors X and the dimensions of the tuned cells are given in Table 6.8.

In order to achieve high efficient retro-reflection at the open channels, the surface impedance should be properly engineered and optimized to be purely reactive. The initial surface impedance of the dimensions given in Table 6.9 was calculated to be $Z_s = 15 - j326$ using Floquet boundary conditions

ϕ_i°	Factor X	L_1 (mm)
-122.4	1	6.5
-77.4	0.6	3.9
-32.4	0.55	3.575
12.6	0.5	3.25
57.6	0.44	2.86
102.6	0.37	2.405
147.6	0.1	0.65
-167.4	1	6.5

Table 6.8: Dimensions of the sub-radiant modes L_1 (mm) tuned with a phase gradient equal to 45° following the phase of the reflection coefficient in Fig. 6.39, where the dimensions $L_{1(initial)} = 6.5$ mm are multiplied by Factor X to form a gradient metasurface.

Initial Dimensions L_1 (mm)	Optimized Dimensions L_1 (mm)
6.5	6.5
3.9	4.095
3.575	3.705
3.25	3.38
2.86	3.055
2.405	3.9
0.65	1.3
6.5	6.5

Table 6.9: Optimized and initial dimensions of the sub-radiant modes L_1 following the surface impedance optimization and modulation to a pure imaginary value.

for one super-cell design. The surface impedance has been optimized by tuning the initial dimensions to achieve a purely reactive surface impedance determined as $Z_s = 1 - j133$ where the resistance is almost tuned to zero. The optimized dimensions are given in Table 6.9.

A metasurface of 4×3 super-cells of dimensions $25 \text{ mm} \times 215 \text{ mm}$ is designed using the optimized dimensions given in Table 6.9. The dolmen structures are printed on top of a grounded substrate of relative permittivity $\epsilon_r=2.2$ and thickness 1.6 mm operating at 24 GHz. The metasurface is shown in Fig 6.40.

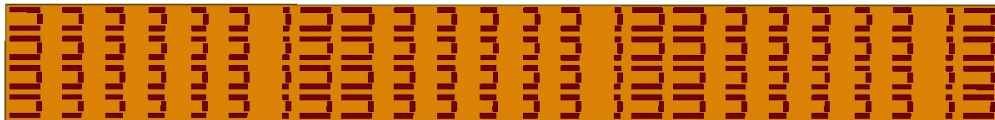


Figure 6.40: Metasurface design using the optimized dimensions of 4×3 super-cells, of dimensions $25 \text{ mm} \times 215 \text{ mm}$, with a ground plane and substrate of permittivity $\epsilon_r=2.2$ and thickness 1.6 mm.

The metasurface has been excited with a plane wave with the electric field in the X-direction of the sub-radiant modes, at a range of incident angles from -70° to 70° . The monostatic RCS has been calculated to determine the performance of the metasurface Fano-resonance based design in terms of retro-reflection. The monostatic RCS of the metasurface has been compared to that of a flat metallic

plate with similar dimensions to highlight the efficiency of the metasurface for retrodirectivity. The result is shown in Fig.6.41.

The result shows high level of retrodirectivity for almost 17 different incident angles ($-60^\circ, -52^\circ, -44^\circ, -38^\circ, -32^\circ, -21^\circ, -18^\circ, -10^\circ, -5^\circ$, normal incidence, $+5^\circ, +18^\circ, +21^\circ, +25^\circ, +32^\circ, +44^\circ, +52^\circ$) which is due to the high periodicity of the super-cell design and high sensitivity of the designed Fano-resonant dolmen structure for high efficiency and accuracy.

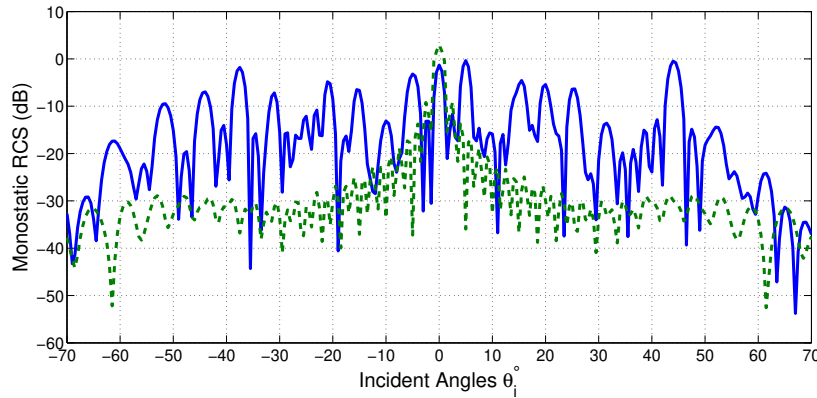


Figure 6.41: Monostatic RCS (dB) of the metasurface design in blue compared to a flat metallic plate of similar dimensions in dotted green, when the electric field of plane wave is in the direction of the sub-radiant modes (x-direction) at 24 GHz .

The metasurface has also been excited with a plane wave with the electric field in the direction of the fixed super-radiant mode in the y-direction. The monostatic RCS has been calculated and compared to that of a metallic flat plate.

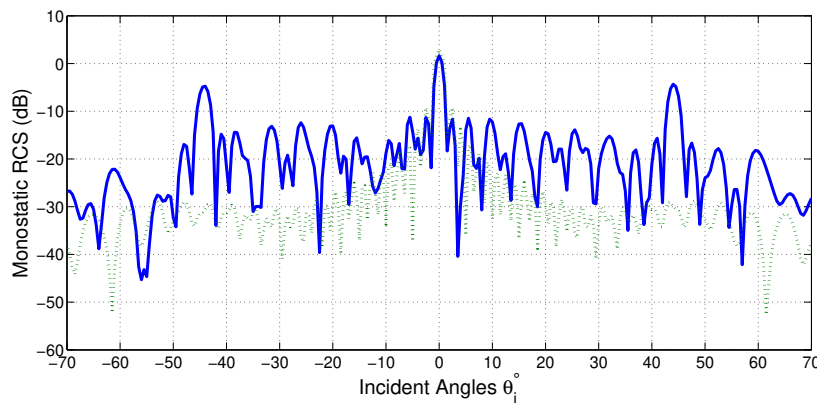


Figure 6.42: Monostatic RCS (dB) of the metasurface design in blue compared to a flat metallic plate of similar dimensions in dotted green, when the electric field of plane wave is in the direction of the super-radiant mode (y-direction) at 24 GHz .

The result in Figure 6.42, shows a high level of retro-reflection at three angles of incidence -44° , normal incidence and 44° compared to that of a flat plate of similar dimensions. This is due to the coupling present between the sub-radiant modes and the super-radiant mode, giving rise for retro-reflection for different angles with independent polarization for specific angles of incidence.

6.6.5 Metasurface Experimental Measurements

To validate the feasibility of our metasurface design, a prototype of the optimized metasurface of 10×7 super-cells and dimensions $10.2 \text{ cm} \times 41.125 \text{ cm}$ has been fabricated. The surface design has been printed on top of a Roger Duroid 5880 grounded substrate of dielectric constant $\epsilon=2.2$ and thickness 1.6 mm . The prototype is shown in Figure 6.43. The measurements were carried out in an anechoic chamber using two vivaldi antennas, one acting as a transmitter and the other as a receiver. The antennas were placed next to each other and isolated using absorbing material to eliminate the coupling. The operating frequency of the antennas was 14.7 GHz . The metasurface design was placed on top of a rotating mechanical platform and both antennas were fixed at a distance of 3 meters from the target. The far-field monostatic RCS has been calculated. Since the metasurface prototype used for measurements was of larger dimensions compared to that of simulated design (for less computational time analysis), the normalized monostatic RCS of the measurements have been compared to that of the simulation results in order to highlight the performance of the design in terms of retro-reflection at each angle of incidence as given in Figure 6.44.

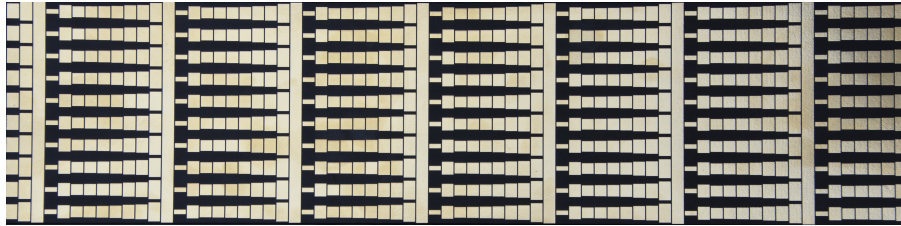


Figure 6.43: Realized Metasurface prototype of 10×7 super cells of dimensions $10.2 \text{ cm} \times 41.125 \text{ cm}$.

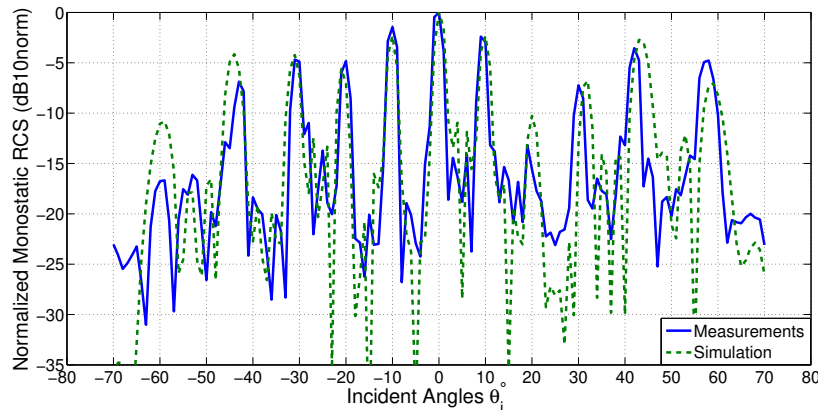


Figure 6.44: Normalized Monostatic RCS (dB10norm) with respect to the incident angles of the simulation results compared to that of the measurements at 14.7 GHz for the optimized metasurface.

The experimental measurement have shown very good agreement compared to that of the simulation results and good performance in terms of retro-reflection of the optimized metasurface at multiple incident angles ($\pm 10^\circ$, $\pm 20.3^\circ$, $\pm 32^\circ$, $\pm 44^\circ$, $\pm 60^\circ$ and normal incidence) as shown in Figure 6.44.

6.7 Conclusion and Future Work

In this chapter, we have introduced the application aspect and concept for wireless power transfer, where tracking and localization can be essential such as that for IOT devices and wireless sensor nodes. We have shown that many researchers have focused on enhancing the efficiency of the

WPT system for better tracking and power supply. In our case, we introduced a novel concept for tracking enhancement, where we control the surrounding and environment of the device, this is by implementing retrodirective metasurfaces along side the device which is being fed.

Wave control and manipulation in the environment, has gained lot of attention by researchers recently specially based on metasurfaces, this is due to their substantial physical properties, high efficiency and reliability. Retrodirectivity on the other hand, has shown to be a great feature for backscattering and localization enhancement for different targets. Moreover, in this chapter, we basically focus on investigating the potential of designing multi-angle retrodirective metasurfaces and study their reliability in terms of retro-reflection enhancement at a wide range of incident angles, where it can be of great usage for applications where tracking and localizing enhancement is needed from the angular aspect.

We have introduced the design of retrodirective metasurfaces at various angles of incidence for retro-reflection. The starting point was the generalized phase law of reflection, which states that for a non homogeneous surface design, an EM wave can be controlled in an anomalous direction. The main challenge was to achieve a design or metasurface topology which can operate at multiple incident angles simultaneously in terms of retro-reflection. A design based on superposition of multiple unit cells, each designed for a specific angle of incidence, was proposed. The retrodirective metasurface showed remarkable results in terms of retro-reflection for a range of incident angles, and was compared to a conventional corner dihedral. On the other hand, another study for multi-angle retrodirective metasurfaces was also presented, to investigate more efficient, reliable and compact design. The study was based on impedance modulation of the surface impedance of the retrodirective super-cell design. A retrodirective metasurface for eleven angles simultaneously was achieved. As well as, using this technique, we were able to retain the conventional properties of a retrodirective metasurface for high periodicity designs specially in terms of reciprocity and retro-reflection at normal incidence. Prototypes of different designs were fabricated and tested in an anechoic chamber to validate the concept and simulation results.

Retro-directive metasurfaces have shown interesting and unprecedented physical properties in terms of retroreflection specially for multiple and a wide range of incident angles. The metasurface designs have shown remarkable results in terms of retroreflection, specially from the angular aspect compared to any conventional topology. The importance of these designs specially in terms of application, that they can be used for tracking and localization enhancement, and a very reliable solution specially with their passive, compact and easy implementation properties. Form the application aspect, for WPT, they can be of great use when implemented along side a target needed to be fed, for better redirecting a pilot signal back to the system specially for applications where the target can be at extreme oblique incidence away from the supplier. In Future work, it would be interesting to demonstrate such topologies for WPT applications, specially for IOT and WSN in the railway environment which is a topic under investigation nowadays, where WPT can be an alternate solution that can be used along side energy harvesting.

Chapter 7

Metamaterial Energy Harvesters Based on Absorption: Challenges at Low MHz Frequencies For Railway Applications

7.1 Introduction

Nowadays, energy harvesting in the railway environment has become an interesting topic for researchers [8–10, 49, 103–110] with a gain of popularity for railway transportation systems. Several low-power energy harvesting systems have been developed and deployed in the railway environment [92, 365, 366] based on the existing sources in the railway infrastructure from mechanical vibrations [367], disturbances and electromagnetic fields [123]. The interest is supplying low power to feed sensors in wireless sensor networks [2, 113] deployed for instance for railway health monitoring thus reducing maintenance, inspection costs and constraints. [3, 125, 368].

Several types of energy harvesting technologies have been deployed; they are popular in railway applications due to the fact that they are based on mature technologies and that the sources present have a sufficiently high amplitude to yield the required power for feeding sensors or devices. Some of the harvesters that we can mention can vary from piezoelectric energy harvesting systems [118] to electromagnetic [89] and solar-based energy harvesting technologies for railways [11]. Piezoelectric harvesting systems have been developed to harvest mechanical vibrations and pressure induced by the moving trains to the rail and convert it to electrical power [7, 119, 127, 369]. In the field of electromagnetic energy harvesting systems in the railway environment, different systems have been deployed which are mostly based on mechanical vibrations at very low frequencies. [9, 10, 49, 92, 109, 122].

However, in electromagnetics a high level of electromagnetic energy is present; it has been experimentally observed recently by Marc Heddebaut et al [13] for frequencies as high as the microwave

region. Moreover according to the EMC standard EN 50121-3-1 [14] for EM emission limits in the railway environment, a high level of electromagnetic energy can exist at a wideband of frequency from 10 kHz up to 1 GHz. To propose the design of a rectenna system [20,21,134] for such application can be a challenge due to its low efficiency and incompatibility at low frequencies.

To date no mature technology has been proposed for such applications and frequency range. We are interested in proposing the design of a novel electromagnetic energy harvesting system based on metamaterials, and investigate their potential in terms of efficiency and miniaturization at low MHz frequencies. Metamaterials [370] have become a subject of interest for researchers nowadays, specially of their exceptional and unprecedented physical properties that can be applied for different applications, due to the generality of their design techniques and methods [371,372]. They are characterized by their subwavelength and periodic structures, as well as the ability to control an electromagnetic wave in different manners such as abnormal reflection [27] [69], cloaking [373], enhancing the performance of antennas [374], collimating orbital angular momentum vortex waves at microwave frequencies [375], absorption [376,377] and energy harvesting [38].

Particularly, for metamaterial absorbers, different techniques have been presented to achieve high efficient absorption [35] such as using bending shapes [241], high resonance metamaterial structures with narrow band absorption [242], as well as other techniques for multi-band [243] and ultra-wideband absorbing metamaterial designs using multi-layer structures [244] and designs with a low quality factor [245]. On the other hand, metamaterial energy harvesters do not just require full absorption, but also the dissipation of the absorbed energy across a load resistance [38]. Therefore, it is interesting to investigate the potential of metamaterial energy harvesters for the range of frequencies between 300 MHz - 1 GHz, specially for the application of railway environment.

In this chapter, we introduce other concept that can be interesting and compatible for our application, specially at low microwave frequencies, to overcome the challenges of low efficiency and miniaturization. Thus, we investigate the potential of metamaterial energy harvesters based on absorption, with designs at operating at a single frequency and multi-band frequencies. The results show high efficiency at the given frequencies specially for power dissipation to the load resistance.

7.2 Proposal of High Efficient Metamaterial Energy Harvesters at Low MHz Frequencies

In this part, we propose an EM energy harvester based on metamaterials at low MHz frequencies, specially for that which is compatible with our application and measurements which have been provided by SNCF Reseau in chapter 1 Figure 1.31. The aim is to overcome the challenges of low efficiency and bulkiness that existing EM energy harvesting systems can have. This work has been presented at the 13th European Conference on Antennas and Propagation (EuCAP2019) [378] and the International Workshop on Antenna Technology (iWAT2020) [379].

7.2.1 Challenges

Rectenna systems are well known existing technologies used for EM energy harvesting and wireless power transfer. A simple rectenna system consists of a dipole antenna with an RF diode connected across the dipole elements. In terms of railway applications, where electromagnetic sources are proved to exist at low kHz and MHz frequency bands, the aim is to design an electromagnetic energy harvesting system which is compact and highly efficient. The implementation of a rectenna energy harvesting system [134] can be a challenge where antennas can have a large size as well as poor efficiency and hard to implement for such applications. We propose and investigate the potential of metamaterial energy harvesters at low MHz frequencies in terms of efficiency and miniaturization which can be compatible for the railway applications.

7.2.2 Principle of Operation and Concept

Metamaterials [213] and metasurfaces have become a remarkable subject of interest nowadays for many researchers, this specially due to their unprecedented physical properties in terms of wave control [69,380], cloaking [381], focusing [382] and high efficiency absorption [383–385].

Particularly, an important feature for metamaterials is perfect absorption [34], in which a media is designed neither to transmit nor reflect an incoming EM wave. A metamaterial absorber is usually designed in a way composed of a metamaterial inclusion printed on top of a substrate with a metallic ground plane on the bottom of the design to prevent transmission. Since transmission is neglected with the presence of the ground plane, for perfect absorption and zero reflection, the metamaterial inclusion should be designed and optimized where the surface impedance is equal to that of the impedance of air $\eta = 377 \Omega$.

However, for EM energy harvesting, starting from the design of a perfect metamaterial absorber, the energy should be dissipated and collected for energy conversion. A concept has been introduced by Thamer S. Almonneef and Omar M. Ramahi [38], where a via is inserted connecting the metamaterial inclusion to a load resistance placed at the ground plane, thus dissipating the energy absorbed by the metamaterial in which a rectenna system can be placed at the bottom part of the metamaterial collector.

In our application, for railways, we want to investigate the potential of metamaterial energy harvesters for low MHz frequencies in terms of efficiency and miniaturization. The choosing of the right metamaterial inclusion and its optimization can be a challenge. To be able to have a design operating at low MHz frequencies this is directly related to the inductance and capacitance of our design as defined in equation (7.1).

$$f = \frac{1}{2\pi\sqrt{LC}} \quad (7.1)$$

where f represents the resonance frequency, L the inductance and C the capacitance of the metamaterial structure. We can see that with structures with high inductance and capacitance we can achieve a metamaterial design operating at low frequencies.

7.2.3 Design of a Single Band Metamaterial Energy Harvester

A spiral inclusion is designed and optimized in this case as shown in Figure 7.1. The spiral metamaterial design is chosen in this case, this is due to its loop structure having a high effective inductance resulting in resonance at low frequencies for the given dimensions which can be suitable for our application.

The spiral has been printed on a Rogers TMM4 grounded substrate of relative permittivity $\epsilon=4.4$, loss tangent 0.002 and dimensions 6 cm \times 6 cm ($\lambda/14$) and thickness $t= 10$ mm ($\lambda/100$). To ensure a highly efficient absorption at the resonance frequency, the surface impedance of the metamaterial structure should be optimized to be equal to that of air $\eta = 377 \Omega$. The structure has been designed to the following dimensions given in Figure 7.1 where $w= 0.5$ mm refers to the gap between the spiral

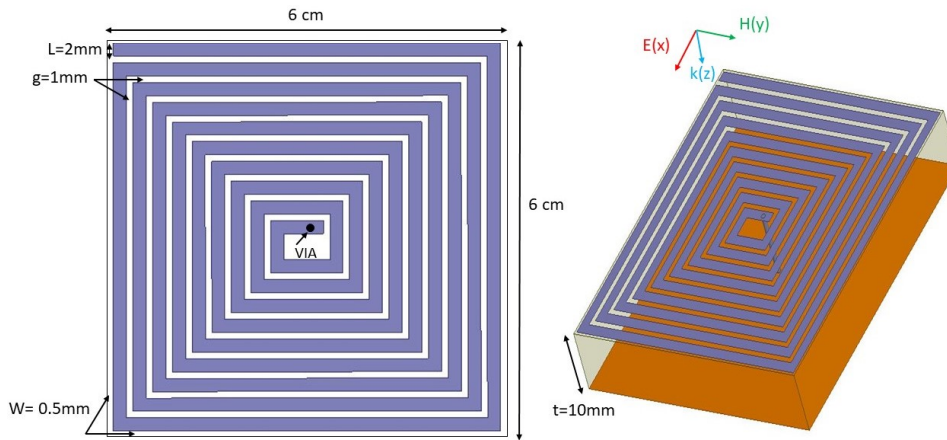


Figure 7.1: Spiral structure design with the given dimensions printed on top of a substrate with a via connecting the inclusion to the ground plane.

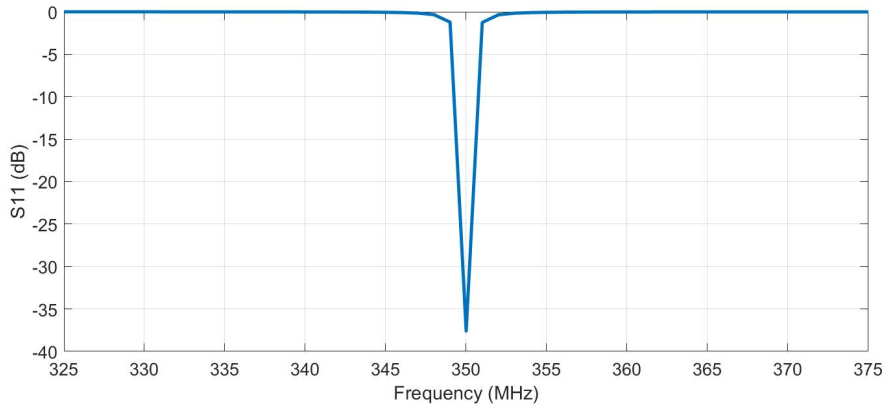


Figure 7.2: Simulation Results of the reflection coefficient S_{11} (dB) with respect to frequency(MHz) using Ansys HFSS.

and the substrate, $g= 1$ mm is the gap between the spiral lines and $L= 2$ mm is the width of the spiral. A via is inserted, in which it connects the spiral structure to the ground plane. The resonant frequency and the surface impedance have been calculated using Ansys HFSS as shown in Figure 7.2 and 7.3 where the structure has shown to resonate at 350 MHz having a surface impedance which has been optimized to a value approximately equal to 377Ω .

Figure 7.2 shows a resonance of -38 dB at 350 MHz, this indicated that the energy is perfectly absorbed at the resonant frequency. Figure 7.3 shows the surface impedance of the metamaterial structure which is approximately equal to 377 which is that of the impedance of air.

However, to obtain the amount of energy absorbed by the metamaterial design at the resonant frequency, the absorption rate is calculated according to the following equation (7.2):

$$A(w) = 1 - |S_{11}|^2 - |S_{21}|^2 \quad (7.2)$$

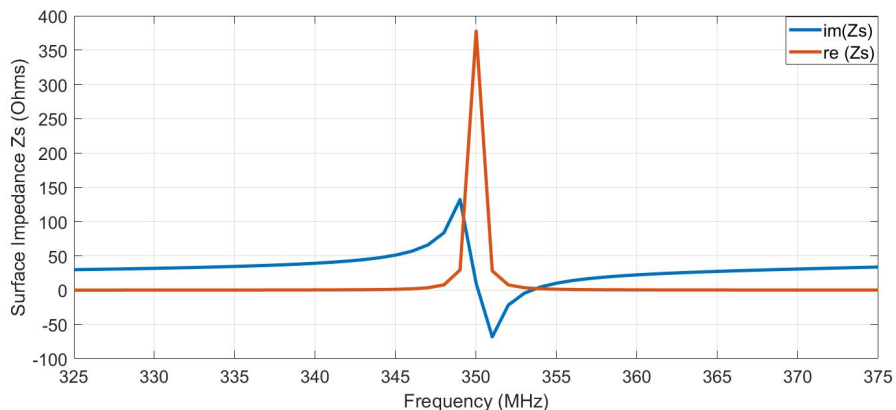


Figure 7.3: Real $\text{Re}(Z_s)$ and Imaginary $\text{Im}(Z_s)$ parts of the surface impedance Z_s of the spiral metamaterial design with respect to frequency(MHz)

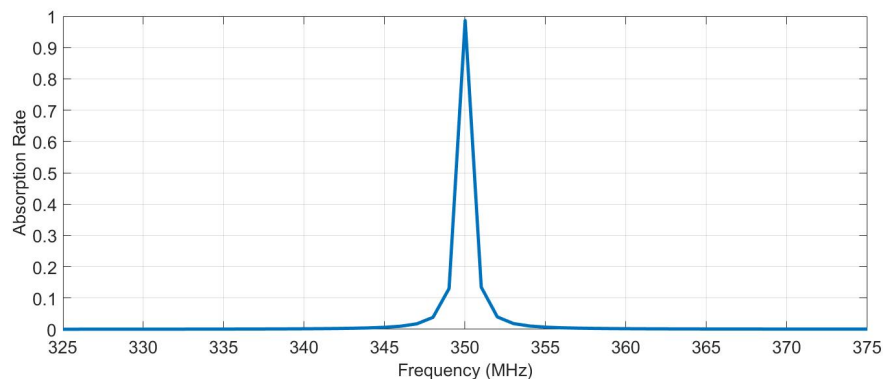


Figure 7.4: Absorption rate of the spiral design with respect to frequency(MHz)

In Eq. (7.2) S_{11} presents the reflection coefficient of the metamaterial slab, whereas S_{21} is the transmission coefficient. In this case, the structure is printed on top of a grounded substrate thus S_{21} is said to be zero. The absorption rate of the design has been calculated at the resonant frequency as shown in Fig. 7.4.

The results in Figure 7.4 show a level of absorption up to 98%, this indicates that our design is a perfect absorber at the resonant frequency 350 MHz. The second step is to have a design which can be used for energy harvesting, thus we connect a load resistor (lumped port) to the end side of the via, this is in order to calculate the amount of dissipated energy at the load with respect to the energy absorbed by the metamaterial. To ensure total power delivery to the load resistors, the impedance of the load should be matched to that of the spiral structure design. An impedance study has been done from the load side in order to calculate the appropriate value of the load resistor as shown in Fig. 7.5.

Figure 7.5 shows the impedance from the load side of the design. The results show a real value to match the metamaterial structure of $8.5 \text{ k}\Omega$ at a frequency of 382 MHz. The shift in frequency is expected due to the presence of the load resistance. Moreover, the resonant frequency from the load side has been calculated for a 4×4 array of metamaterial unit cells as shown in figure 7.6.

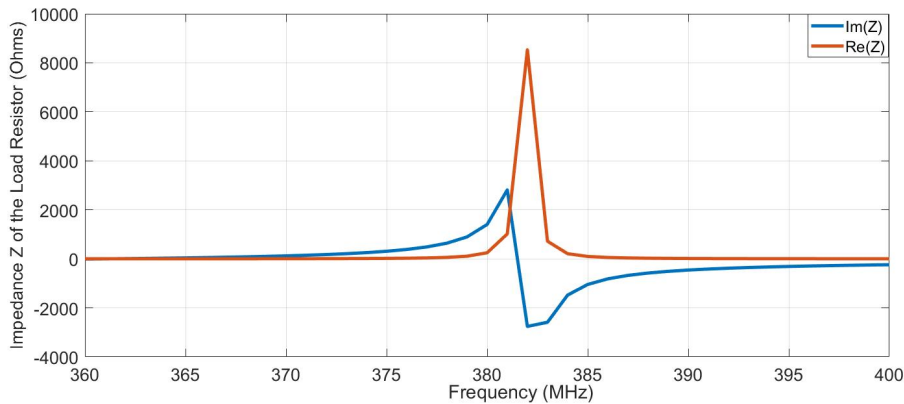


Figure 7.5: Impedance Z of the load resistance real and imaginary parts in Ohms with respect to frequency (MHz).

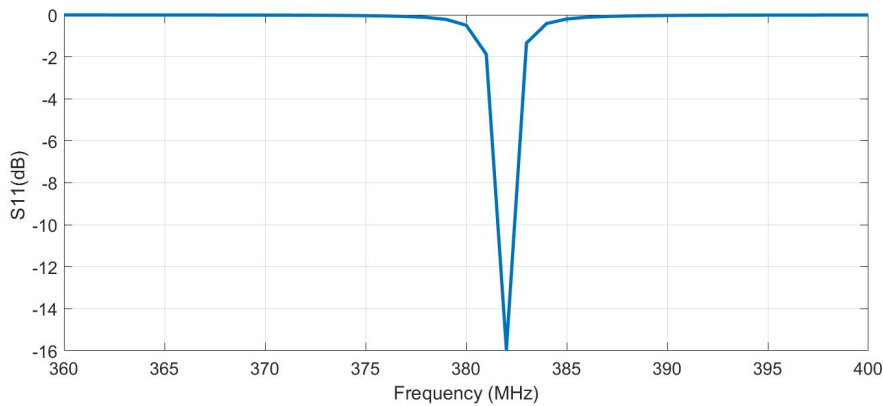


Figure 7.6: Reflection coefficient S_{11} (dB) from the load side of the design structure.

The results in Figure 7.6 indicate that the design with the load resistance is well matched at the resonant frequency 382 MHz. However, it is important to calculate the power efficiency of the energy dissipated to the load from the absorbed energy by the metamaterial design. The amount of power dissipated to the load from the absorbed energy is shown in Figure 7.7.

The results in Figure 7.7 show a power efficiency of 84% dissipated to the load resistance. This indicates that most of the energy absorbed by the metamaterial is delivered to the load.

In this part, we have given a first proposal and design of a high efficient energy harvesting system based on metamaterials at a given frequency where 84% of the absorbed energy was dissipated across an $8.5 \text{ k}\Omega$ load resistor. The design has shown to be high efficient and of low profile of unit cell dimensions $\lambda/14 \times \lambda/14$ and thickness $\lambda/100$ compared to other existing energy harvesting systems [20, 21, 38] which can be an important feature specially at low frequencies. The frequency at 350 MHz has been chosen as an example to prove the idea that metamaterial energy harvesters can be highly efficient and of subwavelength structure at low frequencies which can be a solution for applications such as railways.

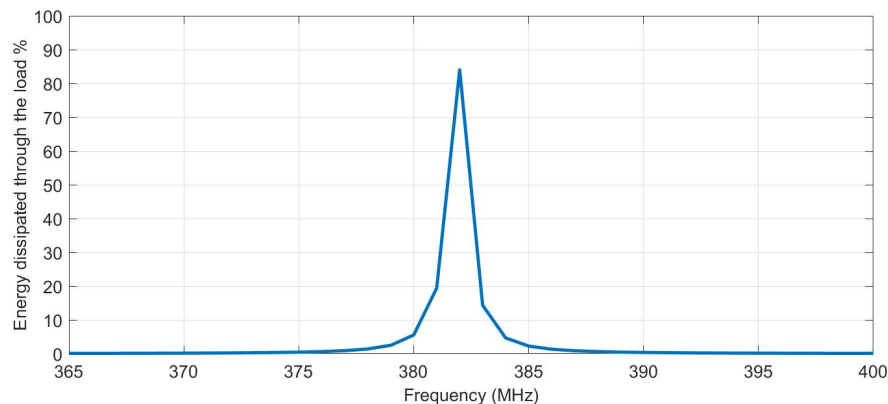


Figure 7.7: Power efficiency of the energy dissipated through the given load resistor with respect to frequency (MHz).

7.2.4 Design of a Multi-Band Metamaterial Energy Harvester

In this part, we introduce another type of metamaterial energy harvesting design based on absorption for multi-band of frequencies. We follow the same concept we introduced before for the energy harvester at a single band. Researchers have introduced different design types and concepts for multi band absorbers, where different methods have been introduced from multi-layer [244], to bending shapes [241] and low quality factor designs [245].

However, in terms of energy harvesting, we introduce a coil spiral unit cell design given in Fig. 7.8a. This type has been chosen specially due to the metamaterial structure's high inductance and ability to resonate at low MHz frequencies, which can be suitable for our application for railways. Moreover, an air gap is given between the metamaterial unit cell and the ground plane, to ensure a low quality factor design structure.

The metamaterial design is printed on top of an FR4 substrate of permittivity $\epsilon=4.4$, dimensions $80 \text{ mm} \times 80 \text{ mm}$ and thickness 1.6 mm . An air layer gap separates the metamaterial structure from a ground plane with thickness 60 mm . This is to ensure a low quality factor of the design and multi-band resonances. On the other hand, for the dissipation of the absorbed energy, a VIA is connected from the top layer to the ground plane with a load resistance of 282Ω at the end part of the VIA as shown in Fig. 7.8b. The coil spiral structure shown in Fig.4.15a consists of 12 turns, width $w = 2 \text{ mm}$, the gap between the turns $g = 0.75 \text{ mm}$ and the inner radius is equal to 1.5 mm . The unit cell design is shown in Fig.7.9.

After introducing the concept and optimization of our design structure, the resonant frequency S_{11} (dB) of the given design is calculated using Ansys HFSS. The result are given in Figure 7.10.

The results in Figure 7.10, show that our metamaterial is well matched and resonates at eight multiple frequencies simultaneously. The frequencies and the S_{11} in dB are given in Table 7.1.

The next step is to calculate the absorption rate of our design at the resonant frequencies following equation (7.2). Since our design is with a ground plane, thus transmission is neglected. The calculated absorption rates at each frequency of our design is shown in Figure 7.11. The absorption rates percentages at each frequency of the metamaterial design are given in Table 7.2.

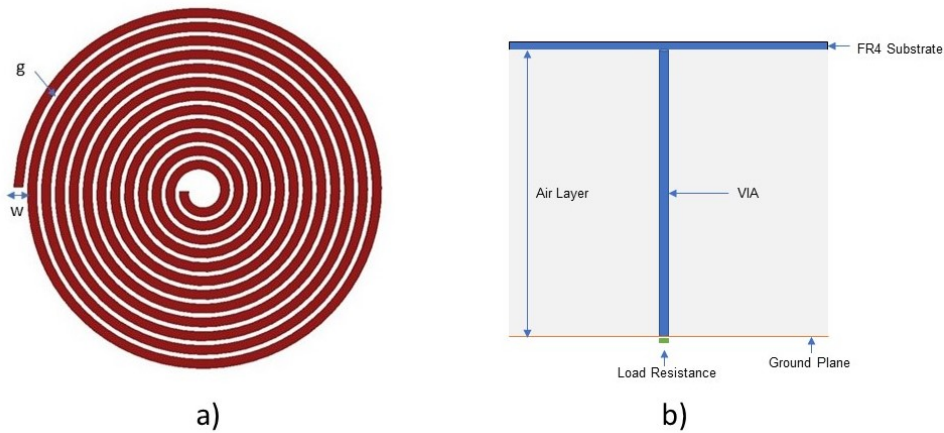


Figure 7.8: a) Coil spiral structure of 12 turns, width w and gap g ; b) Side view of the proposed design

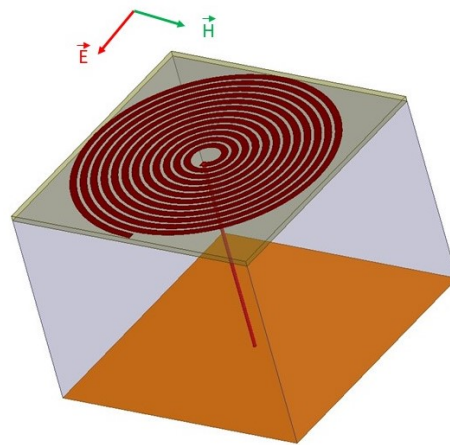


Figure 7.9: Unit cell design of the metamaterial structure with the direction of the electric field E and magnetic field H

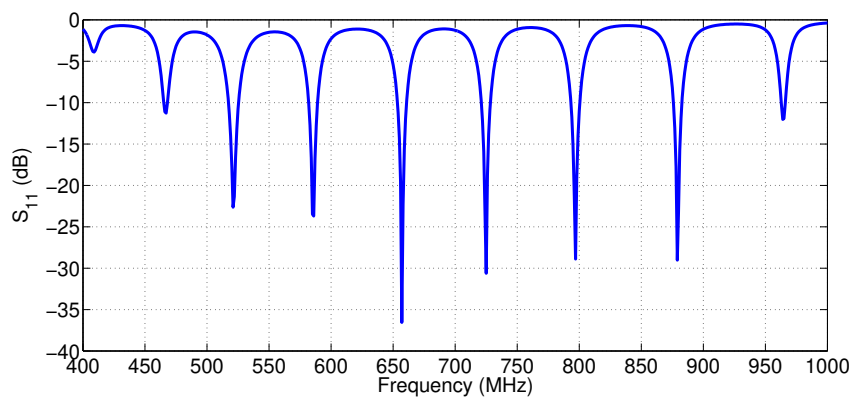


Figure 7.10: Reflection coefficient of the proposed design S_{11} in dB with respect to frequency (MHz)

Frequency (MHz)	S_{11} (dB)
462	-12
520	-23
582	-24
652	-37
725	-31
800	-28
875	-28
970	-12

Table 7.1: The resonant Frequencies in MHz and the value of the reflection coefficient S_{11} (dB)

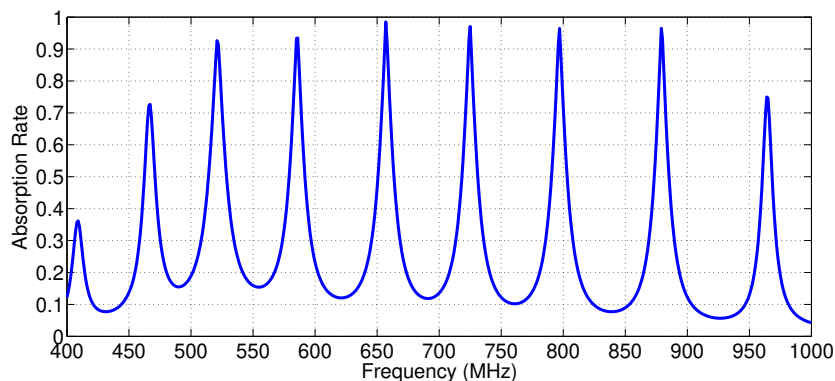


Figure 7.11: Absorption rate of the proposed design with respect to frequency (MHz)

Frequency (MHz)	Absorption Rate (%)
410	36
462	73
520	93
582	93
652	98
725	98
800	98
875	98
970	73

Table 7.2: The resonant Frequencies in MHz and the value of the Absorption Rate (%)

The results in Table 7.2 show that our design is perfect absorber at multiple frequencies simultaneously and well optimized and matched. Moreover, in order to design an energy harvesting metamaterial system, a load resistance has been inserted at the end part of the VIA. To ensure total power dissipation across the load, the resistance should match the impedance of the metamaterial design. Thus, a 282Ω was given and connected at the end part of the VIA. A 6×6 of unit cells metasurface structure has been designed as shown in Figure 7.12.

Figure 7.12 shows the metasurface of dimensions $48 \text{ cm} \times 48 \text{ cm}$ and thickness 61.6 mm . A load resistance of 282Ω is connected at each end part of the VIAs, and a plane wave has been illuminated with the given polarization. Moreover, the power dissipated from the absorbed energy by the

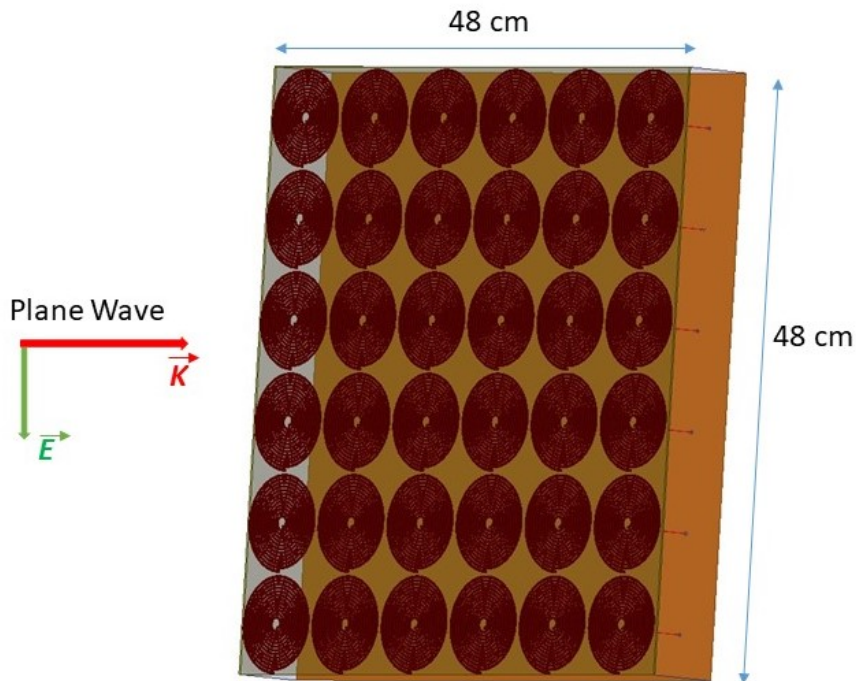


Figure 7.12: Metasurface design of 6×6 unit cell structures of dimensions $48 \text{ cm} \times 48 \text{ cm}$ and thickness 61.6 mm consisting of an FR4 substrate of thickness 1.6 mm and $\epsilon=4.4$ and an air of thickness 60 mm , as well as load resistance of 282Ω connected to each unit cell end part.

metasurface across each given load 282Ω has been calculated as shown in Figure 7.13. The results of the power dissipated at the load from the absorbed energy at each frequency are given in Table 7.3.

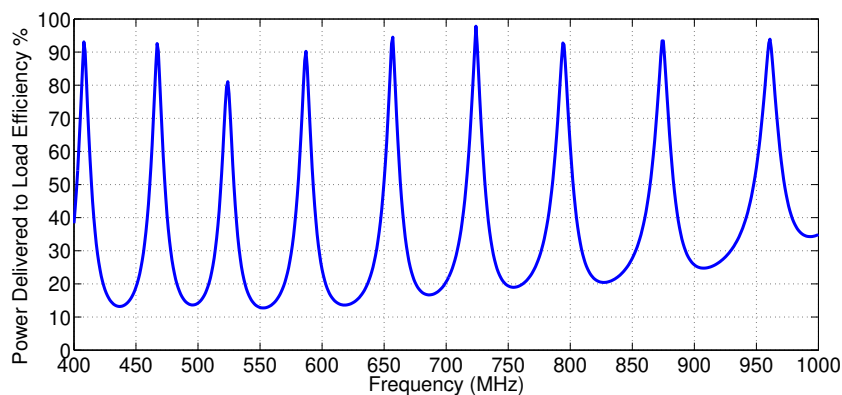


Figure 7.13: Power Efficiency % of the absorbed energy across the 282Ω Load Resistance.

The results in Table 7.3 indicate that the energy absorbed by the metasurface design is mostly dissipated at the load resistance given. This makes us conclude that our design can work as perfect EM energy harvester with high efficiency. Furthermore, the full setup of an EM energy harvester that can be introduced along with the metasurface design is shown in Figure 7.14. The concept

Frequency (MHz)	Power Efficiency Dissipated at the Load from the absorbed energy (%)
410	93
462	93
520	80
582	93
652	95
725	98
800	93
875	93
970	93

Table 7.3: The resonant Frequencies in MHz and the value of the Power efficiency Dissipated at the Load from the absorbed energy (%)

is a full wave rectification system that has been introduced by F. Erkmen et al. [386], where one rectifying system can be used for an array of unit cells.

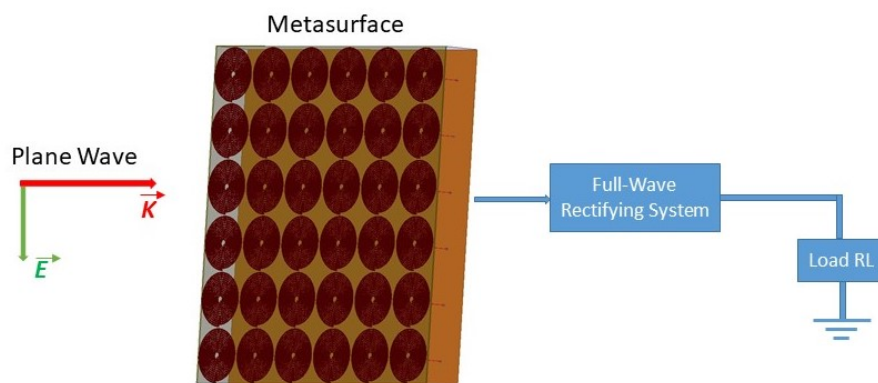


Figure 7.14: Full wave rectification energy harvesting system along side the metasurface design.

In this part, we have introduced a high efficient and miniaturized metasurface energy harvesting design, operating at multiple frequencies. This can be suitable and compatible for railway application, specially for lower MHz frequencies in the microwave region specially following the measurements and frequencies which have been introduced by SNCF Reseau in chapter Figure 1.31.

7.3 Conclusion and Future Work

Different challenges are faced from low efficiency technologies to bulkiness for EM energy harvesting in the railway environment. We proposed other interesting solutions with metasurfaces, where we investigated the potential of metamaterial energy harvesting systems based on the concept of absorption. Different designs have been given for a single band of frequency and also multiple bands. The metamaterial energy harvesting designs have shown remarkable results in terms of efficiency and miniaturization at low MHz frequencies, which can be suitable and reliable specially for railway applications. However, different designs have been introduced in the literature based on this concept [38, 212, 247]. Moreover, the fabrication and design of such metasurfaces can be complex specially with the need of multiple rectenna designs at multiple frequencies.

In future work, we can investigate wide band metamaterial absorbers have been that are introduced

[37] following different concepts in the literature. We can study the potential to design wide-band metamaterial energy harvesters following the same concept we introduced for our designs in this chapter. Moreover, fabrication of a prototype and testing will be done for validation of our results.

Conclusion of the part

In this part, we defined a solution to overcome the challenges that can arise in the railway system using conventional EM EH and WPT systems. We showed the potential of metasurfaces to be a complementary solution to existing technologies. The novel concept based on focusing metasurfaces has shown remarkable results to enhance the performances and efficiency of existing rectenna systems, specially for ambient EM energy environments. The system was test on site in the railway infrastructure in the presence of a GSM-R base station. Different configuration were tested , in which the focusing metasurface prevailed when used along side the rectenna system in terms of received power. We achieved a power of 10 μ W which can be beneficial to supply and wake up low input power devices such as WSNs. Alternative solutions were also introduced to enhance the performance of WPT systems that can also be used to supply power. We introduced multi angle retrodirective metasurfaces to enhance the system in terms of tracking and localization, which can be a great solution for challenges such as line of sight specially from the angular aspect. Metasurfaces based on absorption for multiple frequencies were also designed and introduced which showed potential results for higher efficiency and miniaturization at low microwave frequencies. A summary is shown in Figure 7.15.

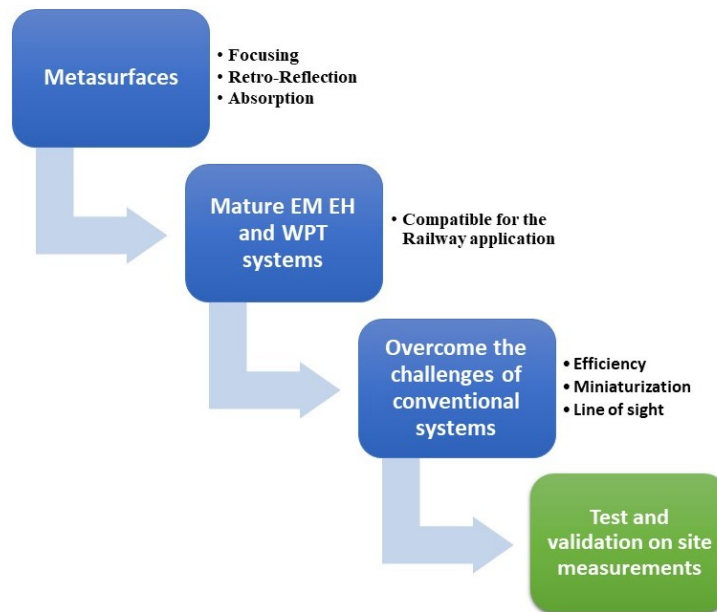


Figure 7.15: Summary of the conclusion of part two on metasurfaces.

Conclusion and Future work

Main contributions of the thesis

The aim of this thesis was to introduce novel techniques to enhance the performances of EM energy harvesting and wireless power transfer systems, based on metasurfaces, which are compatible for the application of supplying low input power devices in the railway environment. This thesis work addressed novel concepts using metasurface designs based on absorption, retro-reflection and focusing. The main goal was to use metasurfaces as a complementary solution, to enhance the performance of existing EM energy harvesting and wireless power transfer systems, as well as proposing an EM energy harvesting system that can be tested in the railway environment.

The main contributions of this work include the following:

- **Identifying existing energy harvesting and wireless power transfer systems in the railway infrastructure.** The major goal was to identify existing technologies and energy harvesting systems already implemented based on various sources from acoustics, vibrations, solar, wind to piezoelectric, and highlight their drawbacks in terms of harvesting, as well as, the study of electromagnetic sources that exist in the railway environment, and highlight that no mature technology has been integrated for such application to date.
- **Defining a solution for enhancing the performance of EM energy harvesting systems and wireless power transfer based on metasurfaces.** Many challenges can arise for EM EH and WPT systems specially for the application of the railway environment. In terms of EM energy harvesting, the scattering of ambient energy, to low frequency EM waves in the microwave region, can be a challenge for existing technologies in terms of dimensions, efficiency and ease of implementation. On the other hand, for WPT, line of sight, tracking and localization can also be a challenge in order to supply a certain device. Metasurfaces with their remarkable physical properties, can be an important solution to overcome such challenges, and give rise to better performing technologies.

- **Novel Concept for enhancing the performance of EM energy harvesters based on focusing metasurfaces.** Energy harvesting of ambient EM energy in an environment can be a challenge for different existing technologies specially rectenna systems. Moreover the low efficiency and design complications at low frequencies can be a drawback for such devices. We proposed a novel concept based on focusing metasurfaces to be a complementary solution to existing EM harvesting technologies and enhance their performances and make them more efficient. The concept is based on designing a focusing metasurface following the hyperboloidal profile of the generalized phase law. The metasurface focuses the incoming EM energy in the environment at a focal point. A rectenna system is then integrated at the focal point where the energy is focused and harvests the energy converting it to electric current. The metasurface has shown remarkable results when integrated along side the rectenna system giving a gain of up to 8 in linear compared to when a commercialized rectenna system is implemented alone. This concept can be an interesting solution in the field of EM energy harvesting specially for ambient energy environments where low power is received by the collector.

- **Integration and testing of the focusing system in the railway environment.** One of the aims of this thesis, is to test and implement a mature and novel system in terms of EM energy harvesting compatible for railway applications. Many sources of energy can exist in the railway environment. However, in our case we designed a system compatible for GSM-R frequencies existing in the railway, where the use case is to be able to charge low power input devices such as IoT and WSNs. The minimum required power to wake up WSNs is $10\mu\text{W}$ [387]. The system was implemented in the railway environment with the presence of a GSM-R base station in the far field. The measurements were carried on in Paris in collaboration with SNCF Reseau. The aim was to validate the potential of our novel concept in terms of EM energy harvesting on the field for the desired application. The rectenna system along side with the focusing metasurface was able to harvest $10\mu\text{W}$ whereas it showed low potential when implemented alone with a power of 1 nW . This is an interesting result, specially for such application for WSNs where $10\mu\text{W}$ is required as wake up energy.

- **Proposed solution for tracking and localization performance enhancement of WPT systems based on retrodirective metasurfaces.** Line of sight and tracking can be a challenge from the angular aspect for WPT systems, specially in the railway application. We proposed a solution using the remarkable physical properties of metasurfaces in terms of wave control following the generalized phase law. The aim was to design a metasurface capable of redirecting back the wave or signal in the same direction which can be useful in various applications. The challenge however is to design a passive retrodirective metasurface that can operate for multiple angles simultaneously. We introduced novel techniques to design such metasurfaces based on the cascading method [69] and surface impedance modulation for high periodicity designs [70]. We have also proved that such metasurfaces can lose their conventional property of reciprocity and introduced the technique how to regain it [70]. The metasurfaces have shown remarkable results and physical properties in both methods in terms of retro-reflection at multiple angles simultaneously. Such metasurfaces can be of great use for different application where tracking and localization need to be enhanced for different systems.

- **Proposed solution for compact and high efficient collectors at low microwave frequencies, using metasurface energy harvesters based on absorption.** Metasurface energy harvesters can be a remarkable solution when compared to low efficient and large dimension receiving rectenna systems specially at low microwave frequencies. We proposed two designs based on the concept introduced in [212, 246]. The concept is introducing a via between the metamaterial absorber and a load resistance where the energy is dissipated, which is basically equivalent to a rectenna system. We introduced a single and multi band metasurface energy harvesters at low microwave frequencies, which can compatible and a solution for the application of EM energy harvesting in the railway environment. The designs showed remarkable efficiencies in terms of energy harvesting up to 90% at multi band frequencies.

Limitations of the proposed designs

This thesis work heavily relies on the use of the physical properties and characteristics of metasurfaces from absorption, anomalous reflection to focusing for enhancing the performances of EM EH and WPT systems. Although metasurfaces can be of high potential in terms of efficiency and design for different applications, some limitations can arise such as bandwidth limitations, fabrication in some cases, dimensions and implementations. The limitations that can arise for our proposed solutions and designs in this thesis include:

- **Multi rectenna systems required at multiple frequencies for the metasurface energy harvesting absorber.** Although the metasurface energy harvester based on absorption can be an interesting solution in terms of efficiency and miniaturization at low frequencies. However, the metasurface absorber can be complex in terms of harvesting specially for multi band frequencies where multiple rectenna systems would be required which can be difficult for fabrication and design.
- **Dimensions of the multi angle retrodirective metasurfaces at low microwave frequencies.** In terms of concept and physical properties, the multi-angle retrodirective metasurfaces have shown remarkable results using the different approaches proposed which can be beneficial for various applications. However, for low microwave frequencies, the dimensions and fabrication of the multi-band retrodirective metasurfaces can be complicated.
- **Dimension of the focusing metasurface at low microwave frequencies.** Although our proposed design using the Jerusalem cross was miniaturized with respect to wavelength for a focusing metasurface design, the dimension can be a drawback a low microwave frequencies. However, for applications such as 5G communication systems the dimensions can be smaller and device can be more reliable and compact.

Future work and Perspective

Research on the topic of metasurfaces and metamaterials has been progressively and fastly developing over the past few years. However, researchers and scientists have realized some limitations of passive metasurfaces in realized applications, such as fixed wave control and manipulation properties and tradeoffs that are usually taken with design structure. Recently, many researchers have put efforts in the design of active and tunable/reconfigurable metasurfaces to externally control the EM wave with higher efficiency and a fixed manner [43, 229, 388–390]. With the high application demand and

the rise of various technologies, this gives a press for the domain of metasurfaces to progress more quickly.

Active or tunable metasurfaces are composed or consisted of artificial impedance surfaces with nonlinear circuit components. It is then designed using artificial designed subwavelength periodic unit cells. The surface impedance is designed to control or manipulate the surface waves and incoming incident waves by anomalous reflection, absorption, wavefront manipulation and various kinds of wave interactions depending on the desired application. An example of an active tunable power dependant metasurface absorber is given in Figure 7.16.

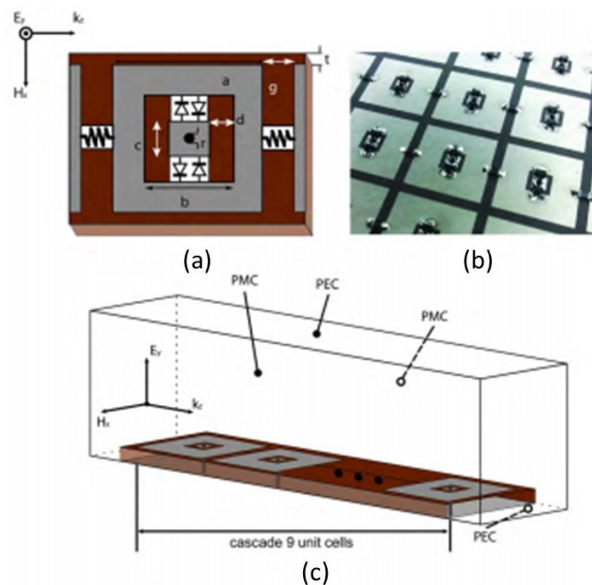


Figure 7.16: a) Active unit cell structure. b) Picture of the fabricated unit cell. c) An EM simulation model with nine cascaded unit cells. [43]

The design procedure and mechanism for active metasurfaces unit cell construction is given in Figure 7.16a. The unit cell is constructed of a metamaterial design structure with non-linear diode components attached in opposite directions. Vias are added where they are connected between the structure and ground plane. At low powers, the diodes are off, and the metasurface appears as an ordinary frequency selective surface (FSS) or metasurface absorber. The diodes turn on when illuminated by high power, and the metasurface is electrically transformed to a resistor-loaded high impedance surface, which can be highly lossy near its resonance frequency. Other type of unit cells have been introduced for active metasurfaces by the group of Prof. SN burokur [44] using varactor diodes as shown in Figure 7.17.

For passive metasurfaces, the resonance and absorption frequency is controlled by the design and structure dimensions of the unit cell and metasurface. However, this can limit the use case for different applications. In Figure 7.17, by introducing a varactor diode with the unit cell design structure, one can control the capacitance of the metasurface by introducing a different bias voltage, therefore controlling the surface impedance, and tuning the resonance frequency to the desired application in use.

With the rise of technologies such as IoT, wireless sensor nodes and 5G communication systems, recently the interest in reconfigurable smart metasurfaces has increased significantly [45, 226, 391–

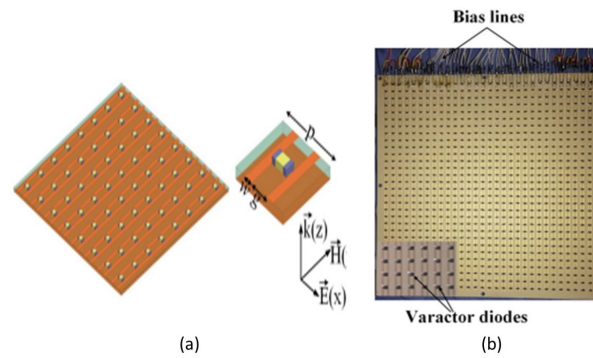


Figure 7.17: a) Illustration of the active metasurface design. b) Fabricated metasurface design. [44]

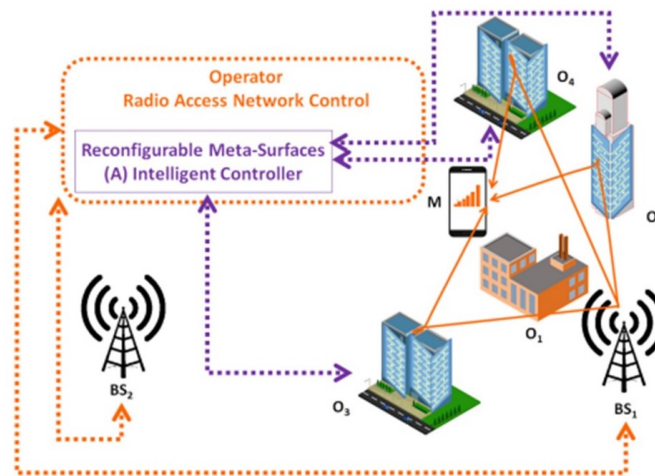


Figure 7.18: Smart radio environments: communications. [45]

[395]. The idea is to be able to introduce a smart communication environment where the propagation and scattering of the EM wave can be controlled in a desired manner. An example is shown in Figure 7.18.

With further progress in different technologies and communication systems such as IoT, WSN, 5G and the progress work on 6G communication systems [396], the control of EM and light propagation can be of great interest for smart systems.

Metasurfaces with their unprecedented physical properties have shown to be of great use for different applications, where wave control and performance enhancement for various technologies is needed. This thesis work opens up further opportunities and aspects for the potential of metasurfaces in the field of EM energy harvesting, wireless power transfer and where environmental wave control is needed. With the fast rise of smart technologies and systems such as IoT, WSNs, 5G communication systems and 6G in the near future, it will be interesting to investigate the potential of reconfigurable metasurfaces which has been a hot topic for many researchers recently. These metasurfaces can help solve some limitations found in passive metasurface designs such as bandwidth and design dependant functionality limitations. Therefore, giving rise to smart technologies where environmental wave control would be essential for such devices.

Bibliography

- [1] A. Hosseinkhani, D. Younesian, P. Eghbali, A. Moayedizadeh, and A. Fassih, “Sound and vibration energy harvesting for railway applications: A review on linear and nonlinear techniques,” *Energy Reports*, vol. 7, pp. 852–874, 2021.
- [2] S. M. Rakshit, M. Hempel, P. Shrestha, F. Rezaei, H. Sharif, J. Punwani, and M. Stewart, “Energy analysis in deploying wireless sensor networks for on-board real-time railcar status monitoring,” in *2015 Joint Rail Conference*. American Society of Mechanical Engineers, 2015, pp. 1–4.
- [3] H.-P. Tan, P. W. Lee, W. K. Seah, and Z. A. Eu, “Impact of power control in wireless sensor networks powered by ambient energy harvesting (wsn-heap) for railroad health monitoring,” in *Advanced Information Networking and Applications Workshops, 2009. WAINA’09. International Conference on*. IEEE, 2009, pp. 804–809.
- [4] O. Jo, Y.-K. Kim, and J. Kim, “Internet of things for smart railway: feasibility and applications,” *IEEE Internet of Things Journal*, vol. 5, no. 2, pp. 482–490, 2017.
- [5] H. Wang and X. Li, “Review and research progress of wireless power transfer for railway transportation,” *IEEJ Transactions on Electrical and Electronic Engineering*, vol. 14, no. 3, pp. 475–484, 2019.
- [6] K. Yamamoto, T. Maruyama, K. Kondo, and T. Kashiwagi, “A method for designing a high-power contactless power transformer considering reactive power,” *Electronics and Communications in Japan*, vol. 98, no. 4, pp. 1–10, 2015.
- [7] F. S. A. D. Nelson C, Platt S and K. V, “Regenerative power for track-health monitoring,” Tech. Rep., 2007.
- [8] M. Gao, P. Wang, Y. Cao, R. Chen, and C. Liu, “A rail-borne piezoelectric transducer for energy harvesting of railway vibration,” *Journal of Vibroengineering*, vol. 18, no. 7, pp. 4647–4663, 2016.

- [9] S. Bradai, S. Naifar, C. Viehweger, and O. Kanoun, "Electromagnetic vibration energy harvesting for railway applications," in *MATEC Web of Conferences*, vol. 148. EDP Sciences, 2018, p. 12004.
- [10] J. Wang, T. Lin, and L. Zuo, "High efficiency electromagnetic energy harvester for railroad application," in *ASME 2013 International Design Engineering Technical Conferences and Computers and Information in Engineering Conference*. American Society of Mechanical Engineers, 2013, pp. 1–10.
- [11] M. K. Darshana, K. Karnataki, G. Shankar, and K. Sheela, "A practical implementation of energy harvesting, monitoring and analysis system for solar photo voltaic terrestrial vehicles in indian scenarios: A case of pilot implementation in the indian railways," in *Electrical and Computer Engineering (WIECON-ECE), 2015 IEEE International WIE Conference on*. IEEE, 2015, pp. 542–545.
- [12] Y. Wang, X. Zhu, T. Zhang, S. Bano, H. Pan, L. Qi, Z. Zhang, and Y. Yuan, "A renewable low-frequency acoustic energy harvesting noise barrier for high-speed railways using a helmholtz resonator and a pvdf film," *Applied Energy*, vol. 230, pp. 52–61, 2018.
- [13] M. Heddebaut, V. Deniau, and J. Rioult, "Wideband analysis of railway catenary line radiation and new applications of its unintentional emitted signals," *Measurement Science and Technology*, vol. 29, no. 6, p. 065101, 2018.
- [14] E. Standard, "50121-3-1 railway applications-electromagnetic compatibility," *Rolling stock. Part*, pp. 1–3.
- [15] S. Priya and D. J. Inman, *Energy harvesting technologies*. Springer, 2009, vol. 21.
- [16] D. Patil, M. K. McDonough, J. M. Miller, B. Fahimi, and P. T. Balsara, "Wireless power transfer for vehicular applications: Overview and challenges," *IEEE Transactions on Transportation Electrification*, vol. 4, no. 1, pp. 3–37, 2017.
- [17] J. Janhunen, K. Mikhaylov, J. Petäjälä, and M. Sonkki, "Wireless energy transfer powered wireless sensor node for green iot: Design, implementation and evaluation," *Sensors*, vol. 19, no. 1, p. 90, 2019.
- [18] R. Correia, D. Belo, and N. B. Carvalho, "Iot/wpt developments in space exploration," in *2018 Asia-Pacific Microwave Conference (APMC)*. IEEE, 2018, pp. 79–81.
- [19] Y. Aleeva, G. Maira, M. Scopelliti, V. Vinciguerra, G. Scandurra, G. Cannata, G. Giusi, C. Ciofi, V. Figa, L. G. Occhipinti *et al.*, "Amperometric biosensor and front-end electronics for remote glucose monitoring by crosslinked pedot-glucose oxidase," *IEEE Sensors Journal*, vol. 18, no. 12, pp. 4869–4878, 2018.

-
- [20] V. Marian, C. Menudier, M. Thevenot, C. Vollaire, J. Verdier, and B. Allard, "Efficient design of rectifying antennas for low power detection," in *Microwave Symposium Digest (MTT), 2011 IEEE MTT-S International*. IEEE, 2011, pp. 1–4.
- [21] A. Georgiadis, G. V. Andia, and A. Collado, "Rectenna design and optimization using reciprocity theory and harmonic balance analysis for electromagnetic (em) energy harvesting," *IEEE Antennas and Wireless Propagation Letters*, vol. 9, pp. 444–446, 2010.
- [22] H. Sun, Y.-x. Guo, M. He, and Z. Zhong, "A dual-band rectenna using broadband yagi antenna array for ambient rf power harvesting," *IEEE Antennas and Wireless Propagation Letters*, vol. 12, pp. 918–921, 2013.
- [23] A. Ogunsola and A. Mariscotti, *Electromagnetic Compatibility in Railways: Analysis and Management*. Springer Science & Business Media, 2012, vol. 168.
- [24] S. Dudoyer, V. Deniau, N. B. Slimen, and R. Adriano, "Susceptibility of the gsm-r transmissions to the railway electromagnetic environment," in *Infrastructure Design, Signalling and Security in Railway*. InTech, 2012.
- [25] B. Ai, R. He, Z. Zhong, K. Guan, B. Chen, P. Liu, and Y. Li, "Radio wave propagation scene partitioning for high-speed rails," *International Journal of Antennas and Propagation*, vol. 2012, 2012.
- [26] T. M. F.-C. Paula Fraga-Lamas and L. Castedo, "Towards the internet of smart trains: A review on industrial iot-connected railways," *Sensors*, vol. 17, no. 1457, 2017.
- [27] N. Yu, P. Genevet, M. A. Kats, F. Aieta, J.-P. Tetienne, F. Capasso, and Z. Gaburro, "Light propagation with phase discontinuities: generalized laws of reflection and refraction," *science*, vol. 334, no. 6054, pp. 333–337, 2011.
- [28] S. Sun, K.-Y. Yang, C.-M. Wang, T.-K. Juan, W. T. Chen, C. Y. Liao, Q. He, S. Xiao, W.-T. Kung, G.-Y. Guo *et al.*, "High-efficiency broadband anomalous reflection by gradient meta-surfaces," *Nano letters*, vol. 12, no. 12, pp. 6223–6229, 2012.
- [29] S. Sun, Q. He, S. Xiao, Q. Xu, X. Li, and L. Zhou, "Gradient-index meta-surfaces as a bridge linking propagating waves and surface waves," *Nature materials*, vol. 11, no. 5, pp. 426–431, 2012.
- [30] J. Wang, Q. Jiang, and D. Han, "Multi-channel beam splitters based on gradient metasurfaces," *Results in Physics*, p. 104084, 2021.

-
- [31] E. Doumanis, G. Goussetis, G. Papageorgiou, V. Fusco, R. Cahill, and D. Linton, “Design of engineered reflectors for radar cross section modification,” *IEEE Transactions on Antennas and Propagation*, vol. 61, no. 1, pp. 232–239, 2012.
- [32] V. Asadchy, A. Díaz-Rubio, S. Tsvetkova, D.-H. Kwon, A. Elsakka, M. Albooyeh, and S. Tretyakov, “Flat engineered multichannel reflectors,” *Physical Review X*, vol. 7, no. 3, p. 031046, 2017.
- [33] Y. Ra’Di, C. Simovski, and S. Tretyakov, “Thin perfect absorbers for electromagnetic waves: theory, design, and realizations,” *Physical Review Applied*, vol. 3, no. 3, p. 037001, 2015.
- [34] N. I. Landy, S. Sajuyigbe, J. J. Mock, D. R. Smith, and W. J. Padilla, “Perfect metamaterial absorber,” *Physical review letters*, vol. 100, no. 20, p. 207402, 2008.
- [35] B. X. Khuyen, B. S. Tung, N. V. Dung, Y. J. Yoo, Y. J. Kim, K. W. Kim, V. D. Lam, J. G. Yang, and Y. Lee, “Size-efficient metamaterial absorber at low frequencies: Design, fabrication, and characterization,” *Journal of Applied Physics*, vol. 117, no. 24, p. 243105, 2015.
- [36] J. Sun, L. Liu, G. Dong, and J. Zhou, “An extremely broad band metamaterial absorber based on destructive interference,” *Optics Express*, vol. 19, no. 22, pp. 21 155–21 162, 2011.
- [37] P. Ranjan, A. Choubey, S. K. Mahto, R. Sinha, and C. Barde, “A novel ultrathin wideband metamaterial absorber for x-band applications,” *Journal of Electromagnetic Waves and Applications*, vol. 33, no. 17, pp. 2341–2353, 2019.
- [38] T. S. Almoneef and O. M. Ramahi, “Metamaterial electromagnetic energy harvester with near unity efficiency,” *Applied Physics Letters*, vol. 106, no. 15, p. 153902, 2015.
- [39] H. Yi, S.-W. Qu, B.-J. Chen, X. Bai, K. B. Ng, and C. H. Chan, “Flat terahertz reflective focusing metasurface with scanning ability,” *Scientific reports*, vol. 7, no. 1, pp. 1–8, 2017.
- [40] S. Yu, H. Liu, and L. Li, “Design of near-field focused metasurface for high-efficient wireless power transfer with multifocus characteristics,” *IEEE Transactions on Industrial Electronics*, vol. 66, no. 5, pp. 3993–4002, 2018.
- [41] J.-I. Moon and Y.-B. Jung, “Novel energy harvesting antenna design using a parasitic radiator,” *Progress In Electromagnetics Research*, vol. 142, pp. 545–557, 2013.
- [42] A. J. T. Hou-Tong Chen and N. Yu, “A review of metasurfaces: physics and applications,” *Reports on Progress in Physics*, vol. 79, no. 076101, p. 40, 2016.

- [43] A. Li, Z. Luo, H. Wakatsuchi, S. Kim, and D. F. Sievenpiper, "Nonlinear, active, and tunable metasurfaces for advanced electromagnetics applications," *IEEE Access*, vol. 5, pp. 27 439–27 452, 2017.
- [44] B. Ratni, A. de Lustrac, G.-P. Piau, and S. N. Burokur, "Active metasurface for reconfigurable reflectors," *Applied Physics A*, vol. 124, no. 2, pp. 1–8, 2018.
- [45] M. Di Renzo, M. Debbah, D.-T. Phan-Huy, A. Zappone, M.-S. Alouini, C. Yuen, V. Sciancalepore, G. C. Alexandropoulos, J. Hoydis, H. Gacanin *et al.*, "Smart radio environments empowered by reconfigurable ai meta-surfaces: An idea whose time has come," *EURASIP Journal on Wireless Communications and Networking*, vol. 2019, no. 1, pp. 1–20, 2019.
- [46] X. Chen, S. Xu, N. Yao, and Y. Shi, "1.6 v nanogenerator for mechanical energy harvesting using pzt nanofibers," *Nano letters*, vol. 10, no. 6, pp. 2133–2137, 2010.
- [47] M. Iqbal, M. M. Nauman, F. U. Khan, P. E. Abas, Q. Cheok, A. Iqbal, and B. Aissa, "Vibration-based piezoelectric, electromagnetic, and hybrid energy harvesters for microsystems applications: A contributed review," *International Journal of Energy Research*, vol. 45, no. 1, pp. 65–102, 2021.
- [48] H. Pan, H. Li, T. Zhang, A. A. Laghari, Z. Zhang, Y. Yuan, and B. Qian, "A portable renewable wind energy harvesting system integrated s-rotor and h-rotor for self-powered applications in high-speed railway tunnels," *Energy conversion and management*, vol. 196, pp. 56–68, 2019.
- [49] J. J. Wang, G. Penamalli, and L. Zuo, "Electromagnetic energy harvesting from train induced railway track vibrations," in *Mechatronics and Embedded Systems and Applications (MESA), 2012 IEEE/ASME International Conference on*. IEEE, 2012, pp. 29–34.
- [50] A. V. Astakhov, D. V. Tatarnikov, P. P. Shamatulsky, and A. P. Stepanenko, "Compact antenna having three-dimensional multi-segment structure," Jan. 14 2021, uS Patent App. 16/607,147.
- [51] D. Seetharamdoo, M.-h. Rabah, H. Srouf, and M. Berbineau, "Method for improving the efficiency of an electrically small antenna," Aug. 1 2019, uS Patent App. 16/311,474.
- [52] H.-T. Chen, A. J. Taylor, and N. Yu, "A review of metasurfaces: physics and applications," *Reports on Progress in Physics*, vol. 79, no. 7, p. 076401, 2016.
- [53] S. Sun, K.-Y. Yang, C.-M. Wang, T.-K. Juan, W. T. Chen, C. Y. Liao, Q. He, S. Xiao, W.-T. Kung, G.-Y. Guo, L. Zhou, and D. P. Tsai, "High-efficiency broadband anomalous reflection by gradient meta-surfaces," *Nano Letters*, vol. 12, no. 12, pp. 6223–6229, 2012, pMID: 23189928. [Online]. Available: <http://dx.doi.org/10.1021/nl3032668>

- [54] C. L. Holloway, E. F. Kuester, J. A. Gordon, J. O'Hara, J. Booth, and D. R. Smith, "An overview of the theory and applications of metasurfaces: The two-dimensional equivalents of metamaterials," *IEEE Antennas and Propagation Magazine*, vol. 54, no. 2, pp. 10–35, April 2012.
- [55] A. A. Elsakka, V. S. Asadchy, I. A. Faniayeu, S. N. Tsvetkova, and S. A. Tretyakov, "Multifunctional cascaded metamaterials: Integrated transmitarrays," *IEEE Transactions on Antennas and Propagation*, vol. 64, no. 10, pp. 4266–4276, 2016.
- [56] M. Pu, P. Chen, C. Wang, Y. Wang, Z. Zhao, C. Hu, C. Huang, and X. Luo, "Broadband anomalous reflection based on gradient low-q meta-surface," *AIP advances*, vol. 3, no. 5, p. 052136, 2013.
- [57] A. M. Wong and G. V. Eleftheriades, "Perfect anomalous reflection with a bipartite huygens' metasurface," *Physical Review X*, vol. 8, no. 1, p. 011036, 2018.
- [58] J. Gomez-Diaz, M. Tymchenko, and A. Alù, "Hyperbolic metasurfaces: surface plasmons, light-matter interactions, and physical implementation using graphene strips," *Optical Materials Express*, vol. 5, no. 10, pp. 2313–2329, 2015.
- [59] M. Teniou, H. Roussel, M. Serhir, N. Capet, G. Piau, and M. Casaletti, "Experimental validation of tensorial metasurfaces for the implementation of radiating aperture field distributions," *IEEE Transactions on Antennas and Propagation*, vol. 67, no. 7, pp. 4901–4906, 2019.
- [60] V.-C. Su, C. H. Chu, G. Sun, and D. P. Tsai, "Advances in optical metasurfaces: fabrication and applications," *Optics express*, vol. 26, no. 10, pp. 13 148–13 182, 2018.
- [61] S. S. Bukhari, J. Y. Vardaxoglou, and W. Whittow, "A metasurfaces review: Definitions and applications," *Applied Sciences*, vol. 9, no. 13, p. 2727, 2019.
- [62] L. Zhang, S. Mei, K. Huang, and C.-W. Qiu, "Advances in full control of electromagnetic waves with metasurfaces," *Advanced Optical Materials*, vol. 4, no. 6, pp. 818–833, 2016.
- [63] A. Díaz-Rubio, V. S. Asadchy, A. Elsakka, and S. A. Tretyakov, "From the generalized reflection law to the realization of perfect anomalous reflectors," *Science advances*, vol. 3, no. 8, p. e1602714, 2017.
- [64] S. Teng, Q. Zhang, H. Wang, L. Liu, and H. Lv, "Conversion between polarization states based on a metasurface," *Photonics Research*, vol. 7, no. 3, pp. 246–250, 2019.

-
- [65] C. Pfeiffer and A. Grbic, “Bianisotropic metasurfaces for optimal polarization control: Analysis and synthesis,” *Physical Review Applied*, vol. 2, no. 4, p. 044011, 2014.
- [66] Y. Sun, D. He, Y. Liu, C. Lin, W. Yuan, and Y. She, “Design of beam shaping and focusing metasurface device based on gs algorithm,” *Optical Materials*, vol. 109, p. 110247, 2020.
- [67] F. Ding, R. Deshpande, C. Meng, and S. I. Bozhevolnyi, “Metasurface-enabled broadband beam splitters integrated with quarter-wave plate functionality,” *Nanoscale*, vol. 12, no. 26, pp. 14 106–14 111, 2020.
- [68] X. Li, S. Xiao, B. Cai, Q. He, T. J. Cui, and L. Zhou, “Flat metasurfaces to focus electromagnetic waves in reflection geometry,” *Optics letters*, vol. 37, no. 23, pp. 4940–4942, 2012.
- [69] M. Kalaagi and D. Seetharamdoo, “Multiangle retrodirective cascaded metasurface,” *Journal of Applied Physics*, vol. 126, no. 10, p. 104901, 2019.
- [70] —, “Retrodirective metasurfaces from non-reciprocal to reciprocal using impedance modulation for high-super-cell-periodicity designs,” *Applied Physics A*, vol. 126, no. 4, pp. 1–7, 2020.
- [71] H. Gao, Y. Li, L. Chen, J. Jin, M. Pu, X. Li, P. Gao, C. Wang, X. Luo, and M. Hong, “Quasi-talbot effect of orbital angular momentum beams for generation of optical vortex arrays by multiplexing metasurface design,” *Nanoscale*, vol. 10, no. 2, pp. 666–671, 2018.
- [72] K. Fan, J. Y. Suen, X. Liu, and W. J. Padilla, “All-dielectric metasurface absorbers for uncooled terahertz imaging,” *Optica*, vol. 4, no. 6, pp. 601–604, 2017.
- [73] R. Alaei, M. Albooyeh, and C. Rockstuhl, “Theory of metasurface based perfect absorbers,” *Journal of Physics D: Applied Physics*, vol. 50, no. 50, p. 503002, 2017.
- [74] W. Guo, Y. Liu, and T. Han, “Ultra-broadband infrared metasurface absorber,” *Optics Express*, vol. 24, no. 18, pp. 20 586–20 592, 2016.
- [75] M. El Badawe and O. Ramahi, “Polarization independent metasurface energy harvester,” in *2016 IEEE 17th Annual Wireless and Microwave Technology Conference (WAMICON)*. IEEE, 2016, pp. 1–3.
- [76] M. El Badawe, T. S. Almoneef, and O. M. Ramahi, “A metasurface for conversion of electromagnetic radiation to dc,” *AIP Advances*, vol. 7, no. 3, p. 035112, 2017.

- [77] —, “A true metasurface antenna,” *Scientific reports*, vol. 6, no. 1, pp. 1–8, 2016.
- [78] M. El Badawe and O. M. Ramahi, “Efficient metasurface rectenna for electromagnetic wireless power transfer and energy harvesting,” *Progress In Electromagnetics Research*, vol. 161, pp. 35–40, 2018.
- [79] M. Kalaagi and D. Seetharamdoo, “Fano resonance based multiple angle retrodirective metasurface,” in *2020 14th European Conference on Antennas and Propagation (EuCAP)*. IEEE, 2020, pp. 1–4.
- [80] A.-R. El-Sayed, K. Tai, M. Biglarbegian, and S. Mahmud, “A survey on recent energy harvesting mechanisms,” in *Electrical and Computer Engineering (CCECE), 2016 IEEE Canadian Conference on*. IEEE, 2016, pp. 1–5.
- [81] M. Safaei, H. A. Sodano, and S. R. Anton, “A review of energy harvesting using piezoelectric materials: state-of-the-art a decade later (2008–2018),” *Smart Materials and Structures*, vol. 28, no. 11, p. 113001, 2019.
- [82] K. Lin, J. Yu, J. Hsu, S. Zahedi, D. Lee, J. Friedman, A. Kansal, V. Raghunathan, and M. Srivastava, “Heliomote: enabling long-lived sensor networks through solar energy harvesting,” in *Proceedings of the 3rd international conference on Embedded networked sensor systems*. ACM, 2005, pp. 309–309.
- [83] J. Gong, C. Li, and M. R. Wasielewski, “Advances in solar energy conversion,” *Chemical Society Reviews*, vol. 48, no. 7, pp. 1862–1864, 2019.
- [84] L. Ran, J. Hou, S. Cao, Z. Li, Y. Zhang, Y. Wu, B. Zhang, P. Zhai, and L. Sun, “Defect engineering of photocatalysts for solar energy conversion,” *Solar RRL*, vol. 4, no. 4, p. 1900487, 2020.
- [85] S. Li, J. Yuan, and H. Lipson, “Ambient wind energy harvesting using cross-flow fluttering,” 2011.
- [86] M. I. Mosaad, A. Alenany, and A. Abu-Siada, “Enhancing the performance of wind energy conversion systems using unified power flow controller,” *IET Generation, Transmission & Distribution*, vol. 14, no. 10, pp. 1922–1929, 2020.
- [87] J. Wang, D. Bo, X. Ma, Y. Zhang, Z. Li, and Q. Miao, “Adaptive back-stepping control for a permanent magnet synchronous generator wind energy conversion system,” *international journal of hydrogen energy*, vol. 44, no. 5, pp. 3240–3249, 2019.

-
- [88] L. Meng, L. Xu, J. Zou, J. Mi, and S. Guo, "Design and analysis of parallel interconnection hydraulic-electric energy-harvesting active radial steering bogie system," in *2017 Joint Rail Conference*. American Society of Mechanical Engineers, 2017, pp. V001T07A005–V001T07A005.
- [89] S. Guo, L. Xu, Y. Liu, X. Guo, and L. Zuo, "Modeling and experiments of a hydraulic electromagnetic energy harvesting shock absorber," *IEEE/ASME Transactions on Mechatronics*, 2017.
- [90] J. Scruggs and P. Jacob, "Harvesting ocean wave energy," *Science*, vol. 323, no. 5918, pp. 1176–1178, 2009.
- [91] A. Ramadan, M. A. Nawar, and M. Mohamed, "Performance evaluation of a drag hydro kinetic turbine for rivers current energy extraction-a case study," *Ocean Engineering*, vol. 195, p. 106699, 2020.
- [92] B. Yang, C. Lee, W. Xiang, J. Xie, J. H. He, R. K. Kotlanka, S. P. Low, and H. Feng, "Electromagnetic energy harvesting from vibrations of multiple frequencies," *Journal of Micromechanics and Microengineering*, vol. 19, no. 3, p. 035001, 2009.
- [93] X. Tang, T. Lin, and L. Zuo, "Electromagnetic vibration energy harvesting with high power density using a magnet array," in *Active and Passive Smart Structures and Integrated Systems 2012*, vol. 8341. International Society for Optics and Photonics, 2012, p. 83410Y.
- [94] L. Zhang, H. Dai, Y. Yang, and L. Wang, "Design of high-efficiency electromagnetic energy harvester based on a rolling magnet," *Energy conversion and management*, vol. 185, pp. 202–210, 2019.
- [95] V. Leonov, "Thermoelectric energy harvesting of human body heat for wearable sensors," *IEEE Sensors Journal*, vol. 13, no. 6, pp. 1–8, 2013.
- [96] S. Pandya, G. Velarde, L. Zhang, J. D. Wilbur, A. Smith, B. Hanrahan, C. Dames, and L. W. Martin, "New approach to waste-heat energy harvesting: pyroelectric energy conversion," *NPG Asia Materials*, vol. 11, no. 1, pp. 1–5, 2019.
- [97] J. H. Jung, Y. M. Ko, and Y. T. Kang, "Condensation heat transfer characteristics and energy conversion performance analysis for low gwp refrigerants in plate heat exchangers," *International Journal of Heat and Mass Transfer*, vol. 166, p. 120727, 2021.
- [98] D. Ahn and K. Choi, "Performance evaluation of thermoelectric energy harvesting system on operating rolling stock," *Micromachines*, vol. 9, no. 7, p. 359, 2018.

- [99] S. Madruga, “Modeling of enhanced micro-energy harvesting of thermal ambient fluctuations with metallic foams embedded in phase change materials,” *Renewable Energy*, vol. 168, pp. 424–437, 2021.
- [100] A. Khaligh and O. C. Onar, *Energy harvesting: solar, wind, and ocean energy conversion systems*. CRC press, 2009.
- [101] S. A. Abbas *et al.*, “Realization of autonomous sensor networks with ai based self-reconfiguration and optimal data transmission algorithms in resource constrained nodes,” *Journal of Scientific and Industrial Research (JSIR)*, vol. 80, no. 02, pp. 149–158, 2021.
- [102] O. Kanoun, S. Bradai, S. Khriji, G. Bouattour, D. El Houssaini, M. Ben Ammar, S. Naifar, A. Bouhamed, F. Derbel, and C. Viehweger, “Energy-aware system design for autonomous wireless sensor nodes: A comprehensive review,” *Sensors*, vol. 21, no. 2, p. 548, 2021.
- [103] X. Zhang, H. Pan, L. Qi, Z. Zhang, Y. Yuan, and Y. Liu, “A renewable energy harvesting system using a mechanical vibration rectifier (mvr) for railroads,” *Applied Energy*, vol. 204, pp. 1535–1543, 2017.
- [104] Y. Jiang, J. Liu, W. Tian, M. Shahidehpour, and M. Krishnamurthy, “Energy harvesting for the electrification of railway stations: Getting a charge from the regenerative braking of trains. a,” *IEEE Electrification Magazine*, vol. 2, no. 3, pp. 39–48, 2014.
- [105] F. Duarte and A. Ferreira, “Energy harvesting on railway tracks: state-of-the-art,” in *Proceedings of the Institution of Civil Engineers-Transport*, vol. 170, no. 3. Thomas Telford Ltd, 2016, pp. 123–130.
- [106] C. A. Nelson, A. Pourghodrat, and M. Fateh, “Energy harvesting from vertical deflection of railroad track using a hydraulic system for improving railroad track safety,” in *ASME 2011 International Mechanical Engineering Congress and Exposition*. American Society of Mechanical Engineers, 2011, pp. 259–266.
- [107] P. Cahill, N. A. N. Nuallain, N. Jackson, A. Mathewson, R. Karoumi, and V. Pakrashi, “Energy harvesting from train-induced response in bridges,” *Journal of Bridge Engineering*, vol. 19, no. 9, p. 04014034, 2014.
- [108] A. L. Ruscelli, G. Cecchetti, and P. Castoldi, “Energy harvesting for on-board railway systems,” in *Models and Technologies for Intelligent Transportation Systems (MT-ITS), 2017 5th IEEE International Conference on*. IEEE, 2017, pp. 397–402.
- [109] H. Park and J. Kim, “Electromagnetic induction energy harvester for high-speed railroad applications,” *International Journal of Precision Engineering and Manufacturing-Green Technology*, vol. 3, no. 1, pp. 41–48, 2016.

- [110] C. Nagode, M. Ahmadian, and S. Taheri, “Effective energy harvesting devices for railroad applications,” in *Active and Passive Smart Structures and Integrated Systems 2010*, vol. 7643. International Society for Optics and Photonics, 2010, p. 76430X.
- [111] H. L. Thadani, F. D. Zaaba, M. R. M. Shahrizal, A. S. J. A. J. Singh, Y. I. Go *et al.*, “Design and performance evaluation of vertical axis wind turbine for wind energy harvesting at railway,” *World Journal of Science, Technology and Sustainable Development*, 2021.
- [112] D. Hao, T. Zhang, L. Guo, Y. Feng, Z. Zhang, and Y. Yuan, “A high-efficiency, portable solar energy harvesting system based on a foldable-wings mechanism for self-powered applications in railways,” *Energy Technology*.
- [113] M. Macucci, S. Di Pascoli, P. Marconcini, and B. Tellini, “Derailment detection and data collection in freight trains, based on a wireless sensor network,” *IEEE Transactions on Instrumentation and Measurement*, vol. 65, no. 9, pp. 1977–1987, 2016.
- [114] C.-B. Yun and J. Min, “Smart sensing, monitoring, and damage detection for civil infrastructures,” *KSCE Journal of Civil Engineering*, vol. 15, no. 1, pp. 1–14, 2011.
- [115] L. Jin, W. Deng, Y. Su, Z. Xu, H. Meng, B. Wang, H. Zhang, B. Zhang, L. Zhang, X. Xiao *et al.*, “Self-powered wireless smart sensor based on maglev porous nanogenerator for train monitoring system,” *Nano energy*, vol. 38, pp. 185–192, 2017.
- [116] M. Gao, P. Wang, Y. Wang, and L. Yao, “Self-powered zigbee wireless sensor nodes for railway condition monitoring,” *IEEE Transactions on Intelligent Transportation Systems*, vol. 19, no. 3, pp. 900–909, 2018.
- [117] T. Lin, J. Wang, and L. Zuo, “Energy harvesting from rail track for transportation safety and monitoring,” 2014.
- [118] J. Li, S. Jang, and J. Tang, “Implementation of a piezoelectric energy harvester in railway health monitoring,” in *Sensors and Smart Structures Technologies for Civil, Mechanical, and Aerospace Systems 2014*, vol. 9061. International Society for Optics and Photonics, 2014, p. 90612Q.
- [119] G. De Pasquale, A. Somà, and F. Fraccarollo, “Piezoelectric energy harvesting for autonomous sensors network on safety-improved railway vehicles,” *Proceedings of the Institution of Mechanical Engineers, Part C: Journal of Mechanical Engineering Science*, vol. 226, no. 4, pp. 1107–1117, 2012.
- [120] M. Mishra, P. Mahajan, and R. Garg, “Piezoelectric energy harvesting system using railway tracks,” in *Innovations in Electrical and Electronic Engineering*. Springer, 2021, pp. 247–259.

-
- [121] W. Hou, Y. Zheng, W. Guo, and G. Pengcheng, "Piezoelectric vibration energy harvesting for rail transit bridge with steel-spring floating slab track system," *Journal of Cleaner Production*, vol. 291, p. 125283, 2021.
- [122] T. Lin, Y. Pan, S. Chen, and L. Zuo, "Modeling and field testing of an electromagnetic energy harvester for rail tracks with anchorless mounting," *Applied Energy*, vol. 213, pp. 219–226, 2018.
- [123] T. Lin, J. J. Wang, and L. Zuo, "Efficient electromagnetic energy harvester for railroad transportation," *Mechatronics*, vol. 53, pp. 277–286, 2018.
- [124] Y. Sun, P. Wang, J. Lu, J. Xu, P. Wang, S. Xie, Y. Li, J. Dai, B. Wang, and M. Gao, "Rail corrugation inspection by a self-contained triple-repellent electromagnetic energy harvesting system," *Applied Energy*, vol. 286, p. 116512, 2021.
- [125] G. Shafiullah, A. Gyasi-Agyei, and P. Wolfs, "Survey of wireless communications applications in the railway industry," in *Wireless Broadband and Ultra Wideband Communications, 2007. AusWireless 2007. The 2nd International Conference on*. IEEE, 2007, pp. 65–65.
- [126] J. Li, S. Jang, and J. Tang, "Modeling and analysis of a biomorph piezoelectric energy harvester for railway bridge monitoring," in *Health Monitoring of Structural and Biological Systems 2012*, vol. 8348. International Society for Optics and Photonics, 2012, p. 834827.
- [127] C. Nagode, M. Ahmadian, and S. Taheri, "Vibration-based energy harvesting systems for on-board applications," in *2011 Joint Rail Conference*. American Society of Mechanical Engineers, 2011, pp. 333–337.
- [128] M. Wischke, M. Masur, M. Kröner, and P. Woias, "Vibration harvesting in traffic tunnels to power wireless sensor nodes," *Smart Materials and Structures*, vol. 20, no. 8, p. 085014, 2011.
- [129] X. Wu, L. Qi, T. Zhang, Z. Zhang, Y. Yuan, and Y. Liu, "A novel kinetic energy harvester using vibration rectification mechanism for self-powered applications in railway," *Energy Conversion and Management*, vol. 228, p. 113720, 2021.
- [130] S. P. Beeby, M. J. Tudor, and N. White, "Energy harvesting vibration sources for microsystems applications," *Measurement science and technology*, vol. 17, no. 12, p. R175, 2006.
- [131] A. Harb, "Energy harvesting: State-of-the-art," *Renewable Energy*, vol. 36, no. 10, pp. 2641–2654, 2011.

- [132] C. Covaci and A. Gontean, "Piezoelectric energy harvesting solutions: A review," *Sensors*, vol. 20, no. 12, p. 3512, 2020.
- [133] H.-C. Song, S.-W. Kim, H. S. Kim, D.-G. Lee, C.-Y. Kang, and S. Nahm, "Piezoelectric energy harvesting design principles for materials and structures: Material figure-of-merit and self-resonance tuning," *Advanced Materials*, vol. 32, no. 51, p. 2002208, 2020.
- [134] H. Sun, Y.-x. Guo, M. He, and Z. Zhong, "Design of a high-efficiency 2.45-ghz rectenna for low-input-power energy harvesting," *IEEE Antennas and Wireless Propagation Letters*, vol. 11, pp. 929–932, 2012.
- [135] C. Mikeka, H. Arai, A. Georgiadis, and A. Collado, "Dtv band micropower rf energy-harvesting circuit architecture and performance analysis," in *RFID-Technologies and Applications (RFID-TA), 2011 IEEE International Conference on*. IEEE, 2011, pp. 561–567.
- [136] D. Surender, T. Khan, F. A. Talukdar, A. De, Y. M. Antar, and A. P. Freundorfer, "Key components of rectenna system: A comprehensive survey," *IETE Journal of Research*, pp. 1–27, 2020.
- [137] T. S. Almoneef, "Design of a rectenna array without a matching network," *IEEE Access*, vol. 8, pp. 109 071–109 079, 2020.
- [138] G. Karaduman, M. Karakose, and E. Akin, "Condition monitoring platform in railways based on iot," in *2018 International Conference on Artificial Intelligence and Data Processing (IDAP)*. IEEE, 2018, pp. 1–4.
- [139] C. Chellaswamy, A. Dhanalakshmi, V. Chinnammal, and C. Malarvizhi, "An iot-based frontal collision avoidance system for railways," in *2017 IEEE International Conference on Power, Control, Signals and Instrumentation Engineering (ICPCSI)*. IEEE, 2017, pp. 1082–1087.
- [140] J. Shahapure, A. Shinde, Y. Madwanna, V. Sontakke, and P. Laturkar, "Iot based system for passenger service in railways with secure icn architecture," in *2018 2nd International Conference on Trends in Electronics and Informatics (ICOEI)*. IEEE, 2018, pp. 819–821.
- [141] R. D. C. Leles, J. J. Rodrigues, I. W. Woungang, R. A. Rabel, and V. Furtado, "Railways networks-challenges for iot underground wireless communications," in *2018 IEEE 10th Latin-American Conference on Communications (LATINCOM)*. IEEE, 2018, pp. 1–6.
- [142] S. Muthuramalingam, A. Bharathi, N. Gayathri, R. Sathiyaraj, B. Balamurugan *et al.*, "Iot based intelligent transportation system (iot-its) for global perspective: A case study," in *Internet of Things and Big Data Analytics for Smart Generation*. Springer, 2019, pp. 279–300.

-
- [143] S. Balaji, K. Nathani, and R. Santhakumar, “Iot technology, applications and challenges: a contemporary survey,” *Wireless personal communications*, vol. 108, no. 1, pp. 363–388, 2019.
- [144] J. I. Agbinya, *Wireless power transfer*. River Publishers, 2015, vol. 45.
- [145] Z. Zhang, H. Pang, A. Georgiadis, and C. Cecati, “Wireless power transfer—an overview,” *IEEE Transactions on Industrial Electronics*, vol. 66, no. 2, pp. 1044–1058, 2018.
- [146] R. Mehrotra, “Cut the cord: wireless power transfer, its applications, and its limits,” *cse.wustl.edu*, pp. 1–11, 2014.
- [147] R. Shadid, S. Noghianian, and A. Nejadpak, “A literature survey of wireless power transfer,” in *2016 IEEE International Conference on Electro Information Technology (EIT)*. IEEE, 2016, pp. 0782–0787.
- [148] C. Lee, W. Zhong, and S. R. Hui, “Recent progress in mid-range wireless power transfer,” in *2012 IEEE Energy Conversion Congress and Exposition (ECCE)*. IEEE, 2012, pp. 3819–3824.
- [149] H. W. Pflug, H. J. Visser, and S. Keyrouz, “Practical applications of radiative wireless power transfer,” in *2015 IEEE Wireless Power Transfer Conference (WPTC)*. IEEE, 2015, pp. 1–4.
- [150] H. J. Visser, “Radiative wireless power transmission: From indoor to in-body applications,” in *2020 IEEE International Electron Devices Meeting (IEDM)*. IEEE, 2020, pp. 37–5.
- [151] S. R. Hui, “Past, present and future trends of non-radiative wireless power transfer,” *CPSS Transactions on Power Electronics and Applications*, vol. 1, no. 1, pp. 83–91, 2016.
- [152] S. L. Ho, J. Wang, W. Fu, and M. Sun, “A comparative study between novel witricity and traditional inductive magnetic coupling in wireless charging,” *IEEE Transactions on Magnetics*, vol. 47, no. 5, pp. 1522–1525, 2011.
- [153] T. Biswas, P. Ghosh, B. Manna, A. Banerji, and S. K. Biswas, “Non-radiative wireless power transfer using inductive resonance coupling,” in *2017 IEEE Calcutta Conference (CALCON)*. IEEE, 2017, pp. 479–483.
- [154] F. Lu, H. Zhang, H. Hofmann, and C. C. Mi, “An inductive and capacitive combined wireless power transfer system with lc-compensated topology,” *IEEE Transactions on Power Electronics*, vol. 31, no. 12, pp. 8471–8482, 2016.

- [155] M. Ettorre, W. A. Alomar, and A. Grbic, “2-d van Atta array of wideband, wideangle slots for radiative wireless power transfer systems,” *IEEE Transactions on Antennas and Propagation*, vol. 66, no. 9, pp. 4577–4585, 2018.
- [156] L. Ginting, H. S. Yoon, D. I. Kim, and K. W. Choi, “Beam avoidance for human safety in radiative wireless power transfer,” *IEEE Access*, vol. 8, pp. 217510–217525, 2020.
- [157] H. J. Visser, “A brief history of radiative wireless power transfer,” in *2017 11th European Conference on Antennas and Propagation (EuCAP)*. IEEE, 2017, pp. 327–330.
- [158] A. Sahai and D. Graham, “Optical wireless power transmission at long wavelengths,” in *2011 International Conference on Space Optical Systems and Applications (ICSOS)*. IEEE, 2011, pp. 164–170.
- [159] A. Kawamura, G. Kuroda, and C. Zhu, “Experimental results on contact-less power transmission system for the high-speed trains,” in *2007 IEEE Power Electronics Specialists Conference*. IEEE, 2007, pp. 2779–2784.
- [160] J. Winter, S. Mayer, S. Kaimer, P. Seitz, J. Pagenkopf, and S. Streit, “Inductive power supply for heavy rail vehicles,” in *2013 3rd International Electric Drives Production Conference (EDPC)*. IEEE, 2013, pp. 1–9.
- [161] S. R. Hui and W. W. Ho, “A new generation of universal contactless battery charging platform for portable consumer electronic equipment,” *IEEE Transactions on Power Electronics*, vol. 20, no. 3, pp. 620–627, 2005.
- [162] K. Hwang, S. Kim, S. Kim, Y. Chun, and S. Ahn, “Design of wireless power transfer system for railway application,” *International Journal of Railway*, vol. 5, no. 4, pp. 167–174, 2012.
- [163] D. Shimode, T. Murai, and T. Sawada, “Adaptation of discrete-type cores for secondary coils of wireless power transfer system for railway,” *Electrical Engineering in Japan*, vol. 201, no. 2, pp. 49–57, 2017.
- [164] X. Zhang, Z. Zhang, H. Pan, W. Salman, Y. Yuan, and Y. Liu, “A portable high-efficiency electromagnetic energy harvesting system using supercapacitors for renewable energy applications in railroads,” *Energy conversion and management*, vol. 118, pp. 287–294, 2016.
- [165] M. V. Lopes, J. J. Eckert, T. S. Martins, and A. A. Santos, “Optimizing strain energy extraction from multi-beam piezoelectric devices for heavy haul freight cars,” *Journal of the Brazilian Society of Mechanical Sciences and Engineering*, vol. 42, no. 1, pp. 1–12, 2020.

- [166] R. B. Ofstein, V. Efe, A. B. Kurs, A. P. McCauley, A. M. Roy, E. Rollano, A. S. Rhoufiry, B. K. Sampson, M. P. Kesler, M. J. MacDonald *et al.*, “Wireless power transfer,” Apr. 3 2014, uS Patent App. 14/044,437.
- [167] A. A. Ofori and H. Guo, “Magbb: Wireless charging for batteryless sensors using magnetic blind beamforming,” in *2021 IEEE 18th Annual Consumer Communications & Networking Conference (CCNC)*. IEEE, 2021, pp. 1–8.
- [168] M. G. Roes, J. L. Duarte, M. A. Hendrix, and E. A. Lomonova, “Acoustic energy transfer: A review,” *IEEE Transactions on Industrial Electronics*, vol. 60, no. 1, pp. 242–248, 2012.
- [169] A. A. Eteng, S. K. A. Rahim, C. Y. Leow, S. Jayaprakasam, and B. W. Chew, “Low-power near-field magnetic wireless energy transfer links: A review of architectures and design approaches,” *Renewable and Sustainable Energy Reviews*, vol. 77, pp. 486–505, 2017.
- [170] E. I. Shirokova, A. A. Azarov, and I. B. Shirokov, “The system of wireless energy transfer,” in *2019 IEEE Conference of Russian Young Researchers in Electrical and Electronic Engineering (EIConRus)*. IEEE, 2019, pp. 1060–1064.
- [171] I. Shirokov, A. Azarov, and I. Serdyuk, “The radiating structure of a short-range wireless energy transmission system,” in *2018 International Multi-Conference on Industrial Engineering and Modern Technologies (FarEastCon)*. IEEE, 2018, pp. 1–4.
- [172] M. Frivaldsky, M. Piri, P. Spanik, V. Jaros, and A. Kondelova, “Peak efficiency and peak power point operation of wireless energy transfer (wet) system—analysis and verification,” *Electrical Engineering*, vol. 99, no. 4, pp. 1439–1451, 2017.
- [173] J. Kim, B. Clerckx, and P. D. Mitcheson, “Signal and system design for wireless power transfer: Prototype, experiment and validation,” *IEEE Transactions on Wireless Communications*, vol. 19, no. 11, pp. 7453–7469, 2020.
- [174] L. Xie, Y. Shi, Y. T. Hou, W. Lou, H. D. Sherali, and S. F. Midkiff, “Multi-node wireless energy charging in sensor networks,” *IEEE/ACM Transactions on Networking*, vol. 23, no. 2, pp. 437–450, 2014.
- [175] W. Xu, W. Liang, J. Peng, Y. Liu, and Y. Wang, “Maximizing charging satisfaction of smartphone users via wireless energy transfer,” *IEEE Transactions on Mobile Computing*, vol. 16, no. 4, pp. 990–1004, 2016.
- [176] S. Nikolettseas, T. P. Raptis, and C. Raptopoulos, “Interactive wireless charging for energy balance,” in *2016 IEEE 36th International Conference on Distributed Computing Systems (ICDCS)*. IEEE, 2016, pp. 262–270.

-
- [177] M. Simic, C. Bil, and V. Vojisavljevic, "Investigation in wireless power transmission for uav charging," *Procedia Computer Science*, vol. 60, pp. 1846–1855, 2015.
- [178] A. Madhja, S. Nikolettseas, and T. P. Raptis, "Hierarchical, collaborative wireless energy transfer in sensor networks with multiple mobile chargers," *Computer Networks*, vol. 97, pp. 98–112, 2016.
- [179] A. Marincic, "Nikola tesla and the wireless transmission of energy," *IEEE Transactions on Power Apparatus and Systems*, no. 10, pp. 4064–4068, 1982.
- [180] G. Marconi, "Radio telegraphy," *Journal of the American Institute of Electrical Engineers*, vol. 41, no. 8, pp. 561–570, 1922.
- [181] —, "Wireless telegraphy," *Journal of the Institution of Electrical Engineers*, vol. 28, no. 139, pp. 273–290, 1899.
- [182] —, "Wireless telegraphic communication," *Resonance*, vol. 7, no. 1, pp. 95–101, 2002.
- [183] D. Ahire and V. J. Gond, "Wireless power transfer system for biomedical application: A review," in *2017 International Conference on Trends in Electronics and Informatics (ICEI)*. IEEE, 2017, pp. 135–140.
- [184] R. Shadid and S. Noghianian, "A literature survey on wireless power transfer for biomedical devices," *International Journal of Antennas and Propagation*, vol. 2018, 2018.
- [185] Q. Xu, H. Wang, Z. Gao, Z.-H. Mao, J. He, and M. Sun, "A novel mat-based system for position-varying wireless power transfer to biomedical implants," *IEEE Transactions on Magnetics*, vol. 49, no. 8, pp. 4774–4779, 2013.
- [186] Y. Liu, H.-N. Dai, H. Wang, M. Imran, X. Wang, and M. Shoaib, "Uav-enabled data acquisition scheme with directional wireless energy transfer for internet of things," *Computer Communications*, vol. 155, pp. 184–196, 2020.
- [187] O. L. López, H. Alves, R. D. Souza, S. Montejo-Sánchez, E. M. Fernandez, and M. Latva-aho, "Massive wireless energy transfer: Enabling sustainable iot towards 6g era," *IEEE Internet of Things Journal*, 2021.
- [188] W. Wang, Q. Zhang, H. Lin, M. Liu, X. Liang, and Q. Liu, "Wireless energy transmission channel modeling in resonant beam charging for iot devices," *IEEE Internet of Things Journal*, vol. 6, no. 2, pp. 3976–3986, 2019.

-
- [189] M. Y. Naderi, K. R. Chowdhury, S. Basagni, W. Heinzelman, S. De, and S. Jana, "Experimental study of concurrent data and wireless energy transfer for sensor networks," in *2014 IEEE Global Communications Conference*. IEEE, 2014, pp. 2543–2549.
- [190] Y. Shi, L. Xie, Y. T. Hou, and H. D. Sherali, "On renewable sensor networks with wireless energy transfer," in *2011 Proceedings IEEE INFOCOM*. IEEE, 2011, pp. 1350–1358.
- [191] J. C. Lin, "Wireless power transfer for mobile applications, and health effects [telecommunications health and safety]," *IEEE Antennas and Propagation Magazine*, vol. 55, no. 2, pp. 250–253, 2013.
- [192] A. Madhja, S. Nikolettseas, T. P. Raptis, C. Raptopoulos, and D. Tsolovos, "Peer-to-peer wireless energy transfer in populations of very weak mobile nodes," in *2017 IEEE Wireless Communications and Networking Conference Workshops (WCNCW)*. IEEE, 2017, pp. 1–6.
- [193] M. V. Tholl, H. G. Akarçay, H. Tanner, T. Niederhauser, A. Zurbuchen, M. Frenz, and A. Haerberlin, "Subdermal solar energy harvesting—a new way to power autonomous electric implants," *Applied energy*, vol. 269, p. 114948, 2020.
- [194] W. Sun, Z. Ding, Z. Qin, F. Chu, and Q. Han, "Wind energy harvesting based on fluttering double-flag type triboelectric nanogenerators," *Nano Energy*, vol. 70, p. 104526, 2020.
- [195] Y. Jia, "Review of nonlinear vibration energy harvesting: Duffing, bistability, parametric, stochastic and others," *Journal of Intelligent Material Systems and Structures*, vol. 31, no. 7, pp. 921–944, 2020.
- [196] X. Zhang, J. Grajal, M. López-Vallejo, E. McVay, and T. Palacios, "Opportunities and challenges of ambient radio-frequency energy harvesting," *Joule*, vol. 4, no. 6, pp. 1148–1152, 2020.
- [197] U. Aswathanarayana, T. Harikrishnan, and T. S. Kadher-Mohien, *Green energy: technology, economics and policy*. Crc Press, 2010.
- [198] O. Okoyeigbo, A. Olajube, O. Shobayo, A. Aligbe, and A. Ibhaze, "Wireless power transfer: a review," in *IOP Conference Series: Earth and Environmental Science*, vol. 655, no. 1. IOP Publishing, 2021, p. 012032.
- [199] D. V. Gretskih, A. Gomozov, N. Tsikalovskiy, and E. Sharapova, "Wireless radio power supply system for pilotless aircrafts," in *2015 International Conference on Antenna Theory and Techniques (ICATT)*. IEEE, 2015, pp. 1–3.

-
- [200] Y. Zeng, B. Clerckx, and R. Zhang, "Communications and signals design for wireless power transmission," *IEEE Transactions on Communications*, vol. 65, no. 5, pp. 2264–2290, 2017.
- [201] J. Sampe, N. H. M. Yunus, J. Yunas, and A. Pawi, "Architecture of an efficient dual band 1.8/2.5 ghz rectenna for rf energy harvesting," *Telkomnika*, vol. 17, no. 6, pp. 3137–3144, 2019.
- [202] K. L. Johnson, "One hundred years of hertz contact," *Proceedings of the Institution of Mechanical Engineers*, vol. 196, no. 1, pp. 363–378, 1982.
- [203] J. Santana Abril, G. Santana Sosa, J. Sosa, T. Bautista, and J. A. Montiel-Nelson, "A novel charging method for underwater batteryless sensor node networks," *Sensors*, vol. 21, no. 2, p. 557, 2021.
- [204] Y. Jin, J. Xu, S. Wu, L. Xu, D. Yang, and K. Xia, "Bus network assisted drone scheduling for sustainable charging of wireless rechargeable sensor network," *Journal of Systems Architecture*, p. 102059, 2021.
- [205] X. Ding, J. Guo, D. Li, and W. Wu, "Optimal wireless charger placement with individual energy requirement," *Theoretical Computer Science*, vol. 857, pp. 16–28, 2021.
- [206] N. Shinohara and T. Ichihara, "Coexistence of wireless power transfer via microwaves and wireless communication for battery-less zigbee sensors," in *2014 International Symposium on Electromagnetic Compatibility, Tokyo*. IEEE, 2014, pp. 445–448.
- [207] K. Li, W. Ni, L. Duan, M. Abolhasan, and J. Niu, "Wireless power transfer and data collection in wireless sensor networks," *IEEE Transactions on Vehicular Technology*, vol. 67, no. 3, pp. 2686–2697, 2017.
- [208] M. Molefi, E. D. Markus, and A. Abu-Mahfouz, "Wireless power transfer for iot devices—a review," in *2019 International Multidisciplinary Information Technology and Engineering Conference (IMITEC)*. IEEE, 2019, pp. 1–8.
- [209] M. Piñuela, P. D. Mitcheson, and S. Lucyszyn, "Ambient rf energy harvesting in urban and semi-urban environments," *IEEE Transactions on microwave theory and techniques*, vol. 61, no. 7, pp. 2715–2726, 2013.
- [210] D. Bouchouicha, F. Dupont, M. Latrach, and L. Ventura, "Ambient rf energy harvesting," in *International Conference on Renewable Energies and Power Quality*, vol. 13, 2010, pp. 2–6.

- [211] H. Jabbar, Y. S. Song, and T. T. Jeong, "Rf energy harvesting system and circuits for charging of mobile devices," *IEEE Transactions on Consumer Electronics*, vol. 56, no. 1, pp. 247–253, 2010.
- [212] T. S. Almomneef, F. Erkmen, and O. M. Ramahi, "Harvesting the energy of multi-polarized electromagnetic waves," *Scientific reports*, vol. 7, no. 1, pp. 1–14, 2017.
- [213] T. J. Cui, D. R. Smith, and R. Liu, *Metamaterials*. Springer, 2010.
- [214] N. Engheta and R. W. Ziolkowski, *Metamaterials: physics and engineering explorations*. John Wiley & Sons, 2006.
- [215] H.-H. Hsiao, C. H. Chu, and D. P. Tsai, "Fundamentals and applications of metasurfaces," *Small Methods*, vol. 1, no. 4, p. 1600064, 2017.
- [216] A. Li, S. Singh, and D. Sievenpiper, "Metasurfaces and their applications," *Nanophotonics*, vol. 7, no. 6, pp. 989–1011, 2018.
- [217] L. Zhang, S. Mei, K. Huang, and C.-W. Qiu, "Advances in full control of electromagnetic waves with metasurfaces," *Advanced Optical Materials*, vol. 4, no. 6, pp. 818–833, 2016. [Online]. Available: <http://dx.doi.org/10.1002/adom.201500690>
- [218] A. Pors and S. I. Bozhevolnyi, "Plasmonic metasurfaces for efficient phase control in reflection," *Optics express*, vol. 21, no. 22, pp. 27 438–27 451, 2013.
- [219] Y. Huang, M. Pu, F. Zhang, J. Luo, X. Li, X. Ma, and X. Luo, "Broadband functional metasurfaces: Achieving nonlinear phase generation toward achromatic surface cloaking and lensing," *Advanced Optical Materials*, p. 1801480, 2019.
- [220] K. Achouri and C. Caloz, "Design, concepts, and applications of electromagnetic metasurfaces," *Nanophotonics*, vol. 7, no. 6, pp. 1095–1116, 2018.
- [221] P. R. West, J. L. Stewart, A. V. Kildishev, V. M. Shalaev, V. V. Shkunov, F. Strohkendl, Y. A. Zakharenkov, R. K. Dodds, and R. Byren, "All-dielectric subwavelength metasurface focusing lens," *Optics express*, vol. 22, no. 21, pp. 26 212–26 221, 2014.
- [222] S. A. Kuznetsov, M. A. Astafev, M. Beruete, and M. Navarro-Cía, "Planar holographic metasurfaces for terahertz focusing," *Scientific reports*, vol. 5, no. 1, pp. 1–8, 2015.

- [223] L. Ouyang, D. Rosenmann, D. A. Czaplewski, J. Gao, and X. Yang, "Broadband infrared circular dichroism in chiral metasurface absorbers," *Nanotechnology*, vol. 31, no. 29, p. 295203, 2020.
- [224] D. Katrodiya, C. Jani, V. Sorathiya, and S. K. Patel, "Metasurface based broadband solar absorber," *Optical Materials*, vol. 89, pp. 34–41, 2019.
- [225] L. Chen, W. Hu, K. Jamieson, X. Chen, D. Fang, and J. Gummesson, "Pushing the physical limits of iot devices with programmable metasurfaces," *arXiv preprint arXiv:2007.11503*, 2020.
- [226] J. A. Hodge, K. V. Mishra, and A. I. Zaghoul, "Reconfigurable metasurfaces for index modulation in 5g wireless communications," in *2019 International Applied Computational Electromagnetics Society Symposium (ACES)*. IEEE, 2019, pp. 1–2.
- [227] F. Liu, J. Guo, L. Zhao, X. Shen, and Y. Yin, "A meta-surface decoupling method for two linear polarized antenna array in sub-6 ghz base station applications," *IEEE Access*, vol. 7, pp. 2759–2768, 2018.
- [228] T. Li and Z. N. Chen, "Metasurface-based shared-aperture band antenna using characteristic mode analysis," *IEEE Transactions on Antennas and Propagation*, vol. 66, no. 12, pp. 6742–6750, 2018.
- [229] A. Nemati, Q. Wang, M. Hong, and J. Teng, "Tunable and reconfigurable metasurfaces and metadevices," *Opto-Electronic Advances*, vol. 1, no. 5, p. 180009, 2018.
- [230] H. Jeong, D. H. Le, D. Lim, R. Phon, and S. Lim, "Reconfigurable metasurfaces for frequency selective absorption," *Advanced Optical Materials*, vol. 8, no. 13, p. 1902182, 2020.
- [231] B. Vasić, G. Isić, R. Beccherelli, and D. C. Zografopoulos, "Tunable beam steering at terahertz frequencies using reconfigurable metasurfaces coupled with liquid crystals," *IEEE Journal of Selected Topics in Quantum Electronics*, vol. 26, no. 5, pp. 1–9, 2019.
- [232] K. V. Mishra, J. A. Hodge, and A. I. Zaghoul, "Reconfigurable metasurfaces for radar and communications systems," in *2019 URSI Asia-Pacific Radio Science Conference (AP-RASC)*. IEEE, 2019, pp. 1–4.
- [233] N. Yu, P. Genevet, M. A. Kats, F. Aieta, J.-P. Tetienne, F. Capasso, and Z. Gaburro, "Light propagation with phase discontinuities: generalized laws of reflection and refraction," *science*, vol. 334, no. 6054, pp. 333–337, 2011.

- [234] E. G. Loewen, "Diffraction gratings, ruled and holographic," *Applied optics and optical engineering.*, vol. 9, pp. 33–71, 1983.
- [235] X. Ni, N. K. Emani, A. V. Kildishev, A. Boltasseva, and V. M. Shalaev, "Broadband light bending with plasmonic nanoantennas," *Science*, vol. 335, no. 6067, pp. 427–427, 2012.
- [236] M. Lawrence, D. R. Barton, J. Dixon, J.-H. Song, J. van de Groep, M. L. Brongersma, and J. A. Dionne, "High quality factor phase gradient metasurfaces," *Nature Nanotechnology*, vol. 15, no. 11, pp. 956–961, 2020.
- [237] D. Barton III, M. Lawrence, and J. Dionne, "Wavefront shaping and modulation with resonant electro-optic phase gradient metasurfaces," *Applied Physics Letters*, vol. 118, no. 7, p. 071104, 2021.
- [238] S. V. Hum and J. Perruisseau-Carrier, "Reconfigurable reflectarrays and array lenses for dynamic antenna beam control: A review," *IEEE Transactions on Antennas and Propagation*, vol. 62, no. 1, pp. 183–198, 2013.
- [239] Y. Li and B. M. Assouar, "Acoustic metasurface-based perfect absorber with deep subwavelength thickness," *Applied Physics Letters*, vol. 108, no. 6, p. 063502, 2016.
- [240] G. M. Akselrod, J. Huang, T. B. Hoang, P. T. Bowen, L. Su, D. R. Smith, and M. H. Mikkelsen, "Large-area metasurface perfect absorbers from visible to near-infrared," *Advanced Materials*, vol. 27, no. 48, pp. 8028–8034, 2015.
- [241] S. T. Bui, V. K. Bui, Y. Yoo, K. W. Kim, D. L. Vu, Y. Lee *et al.*, "Small-size metamaterial perfect absorber operating at low frequency," *Advances in Natural Sciences: Nanoscience and Nanotechnology*, vol. 5, no. 4, p. 045008, 2014.
- [242] H. Tao, N. I. Landy, C. M. Bingham, X. Zhang, R. D. Averitt, and W. J. Padilla, "A metamaterial absorber for the terahertz regime: design, fabrication and characterization," *Optics express*, vol. 16, no. 10, pp. 7181–7188, 2008.
- [243] J. W. Park, P. Van Tuong, J. Y. Rhee, K. W. Kim, W. H. Jang, E. H. Choi, L. Y. Chen, and Y. Lee, "Multi-band metamaterial absorber based on the arrangement of donut-type resonators," *Optics express*, vol. 21, no. 8, pp. 9691–9702, 2013.
- [244] H. Xiong, J.-S. Hong, C.-M. Luo, and L.-L. Zhong, "An ultrathin and broadband metamaterial absorber using multi-layer structures," *Journal of Applied Physics*, vol. 114, no. 6, p. 064109, 2013.

- [245] W. Zuo, Y. Yang, X. He, C. Mao, and T. Liu, "An ultrawideband miniaturized metamaterial absorber in the ultrahigh-frequency range," *IEEE Antennas and Wireless Propagation Letters*, vol. 16, pp. 928–931, 2016.
- [246] O. M. Ramahi, T. S. Almoneef, M. AlShareef, and M. S. Boybay, "Metamaterial particles for electromagnetic energy harvesting," *Applied Physics Letters*, vol. 101, no. 17, p. 173903, 2012.
- [247] T. Almoneef and O. M. Ramahi, "A 3-dimensional stacked metamaterial arrays for electromagnetic energy harvesting," *Progress In Electromagnetics Research*, vol. 146, pp. 109–115, 2014.
- [248] B. Ghaderi, V. Nayyeri, M. Soleimani, and O. M. Ramahi, "Pixelated metasurface for dual-band and multi-polarization electromagnetic energy harvesting," *Scientific reports*, vol. 8, no. 1, pp. 1–12, 2018.
- [249] —, "Multi-polarisation electromagnetic energy harvesting with high efficiency," *IET Microwaves, Antennas & Propagation*, vol. 12, no. 15, pp. 2271–2275, 2018.
- [250] S. Lee, K.-H. Shin, J.-S. Lee, T.-J. Lee, D.-M. Sim, D. Jung, H. Jung, and J.-H. Kim, "Heat energy harvesting by utilizing waste heat with small temperature differences between heat source and sink," *Journal of Mechanical Science and Technology*, vol. 34, no. 1, pp. 443–455, 2020.
- [251] C. Zhang, Z. Lai, M. Li, and D. Yurchenko, "Wind energy harvesting from a conventional turbine structure with an embedded vibro-impact dielectric elastomer generator," *Journal of Sound and Vibration*, vol. 487, p. 115616, 2020.
- [252] F. J. Arias and S. D. L. Heras, "Hydro energy harvesting by using compliant surfaces: Preliminary experimental assessment," *Journal of Energy Resources Technology*, vol. 142, no. 8, 2020.
- [253] B. AmbroŹkiewicz, G. Litak, and P. Wolszczak, "Modelling of electromagnetic energy harvester with rotational pendulum using mechanical vibrations to scavenge electrical energy," *Applied Sciences*, vol. 10, no. 2, p. 671, 2020.
- [254] P. Carneiro, M. P. S. dos Santos, A. Rodrigues, J. A. Ferreira, J. A. Simões, A. T. Marques, and A. L. Kholkin, "Electromagnetic energy harvesting using magnetic levitation architectures: A review," *Applied Energy*, vol. 260, p. 114191, 2020.
- [255] J. Kim, "A study on the optimal design and the performance evaluation of electromagnetic energy harvesting device for the rolling stock application," *Journal of Intelligent Material Systems and Structures*, vol. 31, no. 20, pp. 2362–2377, 2020.

- [256] S. Liu, D. Yang, Y. Chen, S. Huang, and Y. Xiang, "Broadband dual circularly polarized dielectric resonator antenna for ambient electromagnetic energy harvesting," *IEEE Transactions on Antennas and Propagation*, vol. 68, no. 6, pp. 4961–4966, 2020.
- [257] R. Ahmed, M. U. Mehmood, Y. Kim, J. Lee, and W. Chun, "Harnessing low-grade waste heat by operating a hybrid piezoelectric-electromagnetic energy harvester combined with a thermomagnetic engine," *International Journal of Energy Research*, vol. 44, no. 13, pp. 10 710–10 723, 2020.
- [258] M. Yao, P. Liu, and H. Wang, "Nonlinear dynamics and power generation on a new bistable piezoelectric-electromagnetic energy harvester," *Complexity*, vol. 2020, 2020.
- [259] M. Gholikhani, M. Sharzehee, S. A. Tahami, F. Martinez, S. Dessouky, and L. F. Walubita, "Effect of electromagnetic energy harvesting technology on safety and low power generation in sustainable transportation: a feasibility study," *International Journal of Sustainable Engineering*, vol. 13, no. 5, pp. 373–386, 2020.
- [260] K. T. Chandrasekaran, K. Agarwal, A. Alphones, R. Mittra, M. F. Karim *et al.*, "Compact dual-band metamaterial-based high-efficiency rectenna: An application for ambient electromagnetic energy harvesting," *IEEE Antennas and Propagation Magazine*, vol. 62, no. 3, pp. 18–29, 2020.
- [261] E. Vandelle, S. Hemour, T.-P. Vuong, G. Ardila, and K. Wu, "Rectenna optimization guidelines for ambient electromagnetic energy harvesting," *Wireless Power Transmission for Sustainable Electronics*, pp. 347–373, 2020.
- [262] A. Contreras, B. Rodríguez, L. Steinfeld, J. Schandy, and M. Siniscalchi, "Design of a rectenna for energy harvesting on wi-fi at 2.45 ghz," in *2020 Argentine Conference on Electronics (CAE)*. IEEE, 2020, pp. 63–68.
- [263] M. Wagih, A. S. Weddell, and S. Beeby, "Rectennas for radio-frequency energy harvesting and wireless power transfer: A review of antenna design [antenna applications corner]," *IEEE Antennas and Propagation Magazine*, vol. 62, no. 5, pp. 95–107, 2020.
- [264] A. Trikolikar and S. Lahudkar, "A review on different parameters considered for improvement in power conversion efficiency of rectenna," *ICCCE 2019*, pp. 79–85, 2020.
- [265] Z. Xiao, F. Lv, W. Li, H. Zou, and C. Li, "A three-dimensional ultra-broadband and polarization insensitive metamaterial absorber and application for electromagnetic energy harvesting," *Waves in Random and Complex Media*, pp. 1–9, 2020.

- [266] A. Hoque and M. T. Islam, "Numerical analysis of single negative broadband metamaterial absorber based on tri thin layer material in visible spectrum for solar cell energy harvesting," *Plasmonics*, vol. 15, no. 4, pp. 1061–1069, 2020.
- [267] K. S. L. Al-badri, "Electromagnetic broad band absorber based on metamaterial and lumped resistance," *Journal of King Saud University-Science*, vol. 32, no. 1, pp. 501–506, 2020.
- [268] A. Ghadimi, V. Nayyeri, M. Khanjarian, M. Soleimani, and O. M. Ramahi, "Design and simulation of a wideband, wide-angle and polarization-insensitive microwave absorber based on pattern optimization of resistive films," *Journal of Physics D: Applied Physics*, vol. 54, no. 5, p. 055102, 2020.
- [269] V. Benischek, M. Currie, R. Basantkumar, and G. Lyasko, "Electromagnetic based system and method for enhancing subsurface recovery of fluid within a permeable formation," Jul. 16 2013, uS Patent 8,485,251.
- [270] G. S. Lipworth, D. R. Smith, Y. Urzhumov, and O. Yurduseven, "Wireless power transfer in the fresnel zone with a dynamic metasurface antenna," Dec. 5 2019, uS Patent App. 16/381,901.
- [271] E. Salman, M. Stanacevic, W. Tutu, and Y. Karimi, "Radio frequency energy harvesting apparatus and method for utilizing the same," Nov. 24 2020, uS Patent 10,846,581.
- [272] E. K. Stefanakos, D. Y. Goswami, and S. Bhansali, "Rectenna solar energy harvester," Feb. 14 2012, uS Patent 8,115,683.
- [273] F. Xie, G.-M. Yang, and W. Geyi, "Optimal design of an antenna array for energy harvesting," *IEEE Antennas and Wireless Propagation Letters*, vol. 12, pp. 155–158, 2013.
- [274] S. M. Kamali, E. Arbabi, A. Arbabi, and A. Faraon, "A review of dielectric optical metasurfaces for wavefront control," *Nanophotonics*, vol. 7, no. 6, pp. 1041–1068, 2018.
- [275] B.-X. Wang, Y. He, P. Lou, and W. Xing, "Design of a dual-band terahertz metamaterial absorber using two identical square patches for sensing application," *Nanoscale Advances*, vol. 2, no. 2, pp. 763–769, 2020.
- [276] C. Cen, Y. Zhang, X. Chen, H. Yang, Z. Yi, W. Yao, Y. Tang, Y. Yi, J. Wang, and P. Wu, "A dual-band metamaterial absorber for graphene surface plasmon resonance at terahertz frequency," *Physica E: Low-dimensional Systems and Nanostructures*, vol. 117, p. 113840, 2020.

-
- [277] Q. Fan, P. Huo, D. Wang, Y. Liang, F. Yan, and T. Xu, “Visible light focusing flat lenses based on hybrid dielectric-metal metasurface reflector-arrays,” *Scientific reports*, vol. 7, p. 45044, 2017.
- [278] A. Pors, M. G. Nielsen, R. L. Eriksen, and S. I. Bozhevolnyi, “Broadband focusing flat mirrors based on plasmonic gradient metasurfaces,” *Nano letters*, vol. 13, no. 2, pp. 829–834, 2013.
- [279] F. Aieta, P. Genevet, M. A. Kats, N. Yu, R. Blanchard, Z. Gaburro, and F. Capasso, “Aberration-free ultrathin flat lenses and axicons at telecom wavelengths based on plasmonic metasurfaces,” *Nano letters*, vol. 12, no. 9, pp. 4932–4936, 2012.
- [280] H.-P. Li, G.-M. Wang, X.-J. Gao, J.-G. Liang, and H.-S. Hou, “An x/ku-band focusing anisotropic metasurface for low cross-polarization lens antenna application,” *Progress In Electromagnetics Research*, vol. 159, pp. 79–91, 2017.
- [281] T. Cai, G.-M. Wang, X.-F. Zhang, J.-G. Liang, Y.-Q. Zhuang, D. Liu, and H.-X. Xu, “Ultra-thin polarization beam splitter using 2-d transmissive phase gradient metasurface,” *IEEE Transactions on Antennas and Propagation*, vol. 63, no. 12, pp. 5629–5636, 2015.
- [282] I. Liberal, I. Ederra, J. Teniente, and R. Gonzalo, “Multifrequency radiator with spatial diversity based on metasurfaces,” *IEEE Antennas and Wireless Propagation Letters*, vol. 11, pp. 519–522, 2012.
- [283] —, “Multi-functional antennas based on meta-surfaces,” *IEEE transactions on antennas and propagation*, vol. 60, no. 6, pp. 3020–3024, 2012.
- [284] B. Alavikia, T. Almoneef, and O. M. Ramahi, “Electromagnetic energy harvesting using complementary split-ring resonators,” Oct. 20 2016, uS Patent App. 14/690,784.
- [285] O. Ramahi, T. Almoneef, and M. AlShareef, “Metamaterial particles for electromagnetic energy harvesting,” Sep. 18 2014, uS Patent App. 13/841,652.
- [286] R. Kashimura, T. Seki, and K. Sakaguchi, “A study of rectenna receiving area division for microwave wireless power transfer system,” in *2017 IEEE Asia Pacific Microwave Conference (APMC)*. IEEE, 2017, pp. 229–232.
- [287] N. Shinohara, “Trends in wireless power transfer: Wpt technology for energy harvesting, millimeter-wave/thz rectennas, mimo-wpt, and advances in near-field wpt applications,” *IEEE Microwave Magazine*, vol. 22, no. 1, pp. 46–59, 2020.

- [288] S. Hemour, X. Gu, K. Wu, and N. Shinohara, "Efficiency of rectenna," *Recent Wireless Power Transfer Technologies via Radio Waves*, pp. 95–132, 2018.
- [289] W. Geyi, W. Feng, and S. Long, "Design method of micro-strip array focusing antenna and micro-strip array focusing antenna," 2013.
- [290] B. D. Casse, G. Daniel, A. R. Volkel, and V. Liu, "Multiband radio frequency (rf) energy harvesting with scalable antenna," Apr. 3 2018, uS Patent 9,935,370.
- [291] J. I. Moon, S.-m. Kim, and I. K. Cho, "Antenna for harvesting rf energy," Jan. 17 2017, uS Patent 9,548,631.
- [292] A. A. Narayanan and A. R. Keith, "Radio frequency energy harvesting system," Mar. 27 2018, uS Patent 9,929,587.
- [293] L. Li, X. Zhang, C. Song, and Y. Huang, "Progress, challenges, and perspective on metasurfaces for ambient radio frequency energy harvesting," *Applied Physics Letters*, vol. 116, no. 6, p. 060501, 2020.
- [294] X. Li, S. Xiao, B. Cai, Q. He, T. J. Cui, and L. Zhou, "Flat metasurfaces to focus electromagnetic waves in reflection geometry," *Optics letters*, vol. 37, no. 23, pp. 4940–4942, 2012.
- [295] H. Yang, X. Cao, F. Yang, J. Gao, S. Xu, M. Li, X. Chen, Y. Zhao, Y. Zheng, and S. Li, "A programmable metasurface with dynamic polarization, scattering and focusing control," *Scientific reports*, vol. 6, no. 1, pp. 1–11, 2016.
- [296] B.-C. Lin, G.-M. Wang, and T. Cai, "Transmissive focusing meta-surface with nearly 100% efficiency," *Applied Physics A*, vol. 123, no. 10, pp. 1–6, 2017.
- [297] Y.-J. Tsai, S. Larouche, T. Tyler, G. Lipworth, N. M. Jokerst, and D. R. Smith, "Design and fabrication of a metamaterial gradient index diffraction grating at infrared wavelengths," *Optics express*, vol. 19, no. 24, pp. 24 411–24 423, 2011.
- [298] T. Hammi, N. B. Slimen, V. Deniau, J. Rioult, and S. Dudoyer, "Comparison between gsm-r coverage level and em noise level in railway environment," in *2009 9th International Conference on Intelligent Transport Systems Telecommunications (ITST)*. IEEE, 2009, pp. 123–128.
- [299] S. Dudoyer, V. Deniau, R. Adriano, M. N. B. Slimen, J. Rioult, B. Meyniel, and M. Berbineau, "Study of the susceptibility of the gsm-r communications face to the electromagnetic interferences of the rail environment," *IEEE Transactions on electromagnetic compatibility*, vol. 54, no. 3, pp. 667–676, 2011.

-
- [300] S. Dudoyer, V. Deniau, S. Ambellouis, M. Heddebaut, and A. Mariscotti, "Classification of transient em noises depending on their effect on the quality of gsm-r reception," *IEEE Transactions on Electromagnetic Compatibility*, vol. 55, no. 5, pp. 867–874, 2013.
- [301] M. Kod, J. Zhou, Y. Huang, M. Hussein, A. P. Sohrab, and C. Song, "An approach to improve the misalignment and wireless power transfer into biomedical implants using meandered wearable loop antenna," *Wireless Power Transfer*, vol. 2021, 2021.
- [302] B. J. DeLong, A. Kiourti, and J. L. Volakis, "A radiating near-field patch rectenna for wireless power transfer to medical implants at 2.4 ghz," *IEEE Journal of Electromagnetics, RF and Microwaves in Medicine and Biology*, vol. 2, no. 1, pp. 64–69, 2018.
- [303] S. Hui, "Planar wireless charging technology for portable electronic products and qi," *Proceedings of the IEEE*, vol. 101, no. 6, pp. 1290–1301, 2013.
- [304] R. George, M. Sreekala, and K. Deepa, "Single-stage boost rectifier for wireless charging of portable devices through magnetic resonant coupling," in *Artificial Intelligence and Evolutionary Computations in Engineering Systems*. Springer, 2016, pp. 443–452.
- [305] J. Feng, Q. Li, and F. C. Lee, "Omnidirectional wireless power transfer for portable devices," in *2017 IEEE Applied Power Electronics Conference and Exposition (APEC)*. IEEE, 2017, pp. 1675–1681.
- [306] A. Ahmad, M. S. Alam, and R. Chabaan, "A comprehensive review of wireless charging technologies for electric vehicles," *IEEE Transactions on Transportation Electrification*, vol. 4, no. 1, pp. 38–63, 2017.
- [307] P. Machura and Q. Li, "A critical review on wireless charging for electric vehicles," *Renewable and Sustainable Energy Reviews*, vol. 104, pp. 209–234, 2019.
- [308] V. Z. Barsari, D. J. Thrimawithana, and G. A. Covic, "An inductive coupler array for in-motion wireless charging of electric vehicles," *IEEE Transactions on Power Electronics*, 2021.
- [309] S. A. Q. Mohammed and J.-W. Jung, "A comprehensive state-of-the-art review of wired/wireless charging technologies for battery electric vehicles: Classification/common topologies/future research issues," *IEEE Access*, 2021.
- [310] R. La Rosa, P. Livreri, C. Trigona, L. Di Donato, and G. Sorbello, "Strategies and techniques for powering wireless sensor nodes through energy harvesting and wireless power transfer," *Sensors*, vol. 19, no. 12, p. 2660, 2019.

-
- [311] W. Ejaz, M. Naeem, M. Basharat, A. Anpalagan, and S. Kandeepan, "Efficient wireless power transfer in software-defined wireless sensor networks," *IEEE Sensors Journal*, vol. 16, no. 20, pp. 7409–7420, 2016.
- [312] J. Chen, C. W. Yu, and W. Ouyang, "Efficient wireless charging pad deployment in wireless rechargeable sensor networks," *IEEE Access*, vol. 8, pp. 39 056–39 077, 2020.
- [313] M. Poveda-García, J. Oliva-Sanchez, R. Sanchez-Iborra, D. Cañete-Rebenaque, and J. L. Gomez-Tornero, "Dynamic wireless power transfer for cost-effective wireless sensor networks using frequency-scanned beaming," *IEEE Access*, vol. 7, pp. 8081–8094, 2019.
- [314] H. Alawad and S. Kaewunruen, "Wireless sensor networks: Toward smarter railway stations," *Infrastructures*, vol. 3, no. 3, p. 24, 2018.
- [315] A. Takacs, A. Okba, H. Aubert, S. Charlot, and P.-F. Calmon, "Recent advances in electromagnetic energy harvesting and wireless power transfer for iot and shm applications," in *2017 IEEE International Workshop of Electronics, Control, Measurement, Signals and their Application to Mechatronics (ECMSM)*. IEEE, 2017, pp. 1–4.
- [316] P. S. Yedavalli, T. Riihonen, X. Wang, and J. M. Rabaey, "Far-field rf wireless power transfer with blind adaptive beamforming for internet of things devices," *IEEE Access*, vol. 5, pp. 1743–1752, 2017.
- [317] K. W. Choi, A. A. Aziz, D. Setiawan, N. M. Tran, L. Ginting, and D. I. Kim, "Distributed wireless power transfer system for internet of things devices," *IEEE Internet of Things Journal*, vol. 5, no. 4, pp. 2657–2671, 2018.
- [318] D. S. Gurjar, H. H. Nguyen, and H. D. Tuan, "Wireless information and power transfer for iot applications in overlay cognitive radio networks," *IEEE Internet of Things Journal*, vol. 6, no. 2, pp. 3257–3270, 2018.
- [319] A. A. Aziz, L. Ginting, D. Setiawan, J. H. Park, N. M. Tran, G. Y. Yeon, D. I. Kim, and K. W. Choi, "Battery-less location tracking for internet of things: simultaneous wireless power transfer and positioning," *IEEE Internet of Things Journal*, vol. 6, no. 5, pp. 9147–9164, 2019.
- [320] M. O. Ojo, S. Giordano, G. Procissi, and I. N. Seitanidis, "A review of low-end, middle-end, and high-end iot devices," *IEEE Access*, vol. 6, pp. 70 528–70 554, 2018.
- [321] M. A. Khan and K. Salah, "Iot security: Review, blockchain solutions, and open challenges," *Future Generation Computer Systems*, vol. 82, pp. 395–411, 2018.

- [322] S. Marchal, M. Miettinen, T. D. Nguyen, A.-R. Sadeghi, and N. Asokan, "Audi: Toward autonomous iot device-type identification using periodic communication," *IEEE Journal on Selected Areas in Communications*, vol. 37, no. 6, pp. 1402–1412, 2019.
- [323] M. Song, K. Zhong, J. Zhang, Y. Hu, D. Liu, W. Zhang, J. Wang, and T. Li, "In-situ ai: Towards autonomous and incremental deep learning for iot systems," in *2018 IEEE International Symposium on High Performance Computer Architecture (HPCA)*. IEEE, 2018, pp. 92–103.
- [324] R. J. Vullers, R. Van Schaijk, H. J. Visser, J. Penders, and C. Van Hoof, "Energy harvesting for autonomous wireless sensor networks," *IEEE Solid-State Circuits Magazine*, vol. 2, no. 2, pp. 29–38, 2010.
- [325] K. S. Adu-Manu, N. Adam, C. Tapparello, H. Ayatollahi, and W. Heinzelman, "Energy-harvesting wireless sensor networks (eh-wsns) a review," *ACM Transactions on Sensor Networks (TOSN)*, vol. 14, no. 2, pp. 1–50, 2018.
- [326] F. A. Kraemer, D. Palma, A. E. Braten, and D. Ammar, "Operationalizing solar energy predictions for sustainable, autonomous iot device management," *IEEE Internet of Things Journal*, vol. 7, no. 12, pp. 11 803–11 814, 2020.
- [327] J. Iannacci, G. Sordo, E. Serra, and U. Schmid, "A novel mems-based piezoelectric multi-modal vibration energy harvester concept to power autonomous remote sensing nodes for internet of things (iot) applications," in *2015 IEEE SENSORS*. IEEE, 2015, pp. 1–4.
- [328] A. Jushi, A. Pegatoquet, and T. N. Le, "Wind energy harvesting for autonomous wireless sensor networks," in *2016 Euromicro Conference on Digital System Design (DSD)*. IEEE, 2016, pp. 301–308.
- [329] H. Zhang, Y.-x. Guo, Z. Zhong, and W. Wu, "Cooperative integration of rf energy harvesting and dedicated wpt for wireless sensor networks," *IEEE Microwave and Wireless Components Letters*, vol. 29, no. 4, pp. 291–293, 2019.
- [330] L. Roselli, C. Mariotti, M. Virili, F. Alimenti, G. Orecchini, V. Palazzi, P. Mezzanotte, and N. Carvalho, "Wpt related applications enabling internet of things evolution," in *2016 10th European Conference on Antennas and Propagation (EuCAP)*. IEEE, 2016, pp. 1–2.
- [331] M. A. S. Abdelhameed, "On-chip adaptive power management for wpt-enabled iot," 2018.
- [332] I. Partin-Vaisband, "Efficient wireless power transfer for heterogeneous adaptive iot systems," in *Proceedings of the 2018 on Great Lakes Symposium on VLSI*, 2018, pp. 299–304.

- [333] Y. Li, C. Zhang, Q. Yang, J. Li, Y. Zhang, X. Zhang, and M. Xue, "Improved ant colony algorithm for adaptive frequency-tracking control in wpt system," *IET Microwaves, Antennas & Propagation*, vol. 12, no. 1, pp. 23–28, 2017.
- [334] Y. Liu and H. Feng, "Maximum efficiency tracking control method for wpt system based on dynamic coupling coefficient identification and impedance matching network," *IEEE Journal of Emerging and Selected Topics in Power Electronics*, vol. 8, no. 4, pp. 3633–3643, 2019.
- [335] H. Li, J. Li, K. Wang, W. Chen, and X. Yang, "A maximum efficiency point tracking control scheme for wireless power transfer systems using magnetic resonant coupling," *IEEE Transactions on Power Electronics*, vol. 30, no. 7, pp. 3998–4008, 2014.
- [336] G. Feng and J.-J. Sit, "An injection-locked wpt transmitter with automatic maximum efficiency tracking," *IEEE Transactions on Industrial Electronics*, 2020.
- [337] Y. Li, J. Zhang, S. Qu, J. Wang, H. Chen, Z. Xu, and A. Zhang, "Wideband radar cross section reduction using two-dimensional phase gradient metasurfaces," *Applied Physics Letters*, vol. 104, no. 22, p. 221110, 2014.
- [338] W. T. Chen, K.-Y. Yang, C.-M. Wang, Y.-W. Huang, G. Sun, I.-D. Chiang, C. Y. Liao, W.-L. Hsu, H. T. Lin, S. Sun *et al.*, "High-efficiency broadband meta-hologram with polarization-controlled dual images," *Nano letters*, vol. 14, no. 1, pp. 225–230, 2013.
- [339] L.-H. Gao, Q. Cheng, J. Yang, S.-J. Ma, J. Zhao, S. Liu, H.-B. Chen, Q. He, W.-X. Jiang, H.-F. Ma *et al.*, "Broadband diffusion of terahertz waves by multi-bit coding metasurfaces," *Light: Science & Applications*, vol. 4, no. e324, pp. 1–9, 2015.
- [340] G. Zheng, H. Mühlenbernd, M. Kenney, G. Li, T. Zentgraf, and S. Zhang, "Metasurface holograms reaching 80% efficiency," *Nature nanotechnology*, vol. 10, no. 4, pp. 308–312, 2015.
- [341] A. Ranjbar and A. Grbic, "Analysis and synthesis of cascaded metasurfaces using wave matrices," *Physical Review B*, vol. 95, no. 20, p. 205114, 2017.
- [342] S. Sun, Q. He, S. Xiao, Q. Xu, X. Li, and L. Zhou, "Gradient-index meta-surfaces as a bridge linking propagating waves and surface waves," *Nature materials*, vol. 11, no. 5, pp. 426–431, 2012.
- [343] A. Pors, O. Albrektsen, I. P. Radko, and S. I. Bozhevolnyi, "Gap plasmon-based metasurfaces for total control of reflected light," *Scientific reports*, vol. 3, no. 2155, pp. 1–6, 2013.

- [344] S. B. Glybovski, S. A. Tretyakov, P. A. Belov, Y. S. Kivshar, and C. R. Simovski, “Metasurfaces: From microwaves to visible,” *Physics Reports*, vol. 634, pp. 1–72, 2016.
- [345] V. Fusco and N. Buchanan, “Developments in retrodirective array technology,” *IET Microwaves, Antennas & Propagation*, vol. 7, no. 2, pp. 131–140, 2013.
- [346] A. Bunkowski, O. Burmeister, T. Clausnitzer, E.-B. Kley, A. Tünnermann, K. Danzmann, and R. Schnabel, “Optical characterization of ultrahigh diffraction efficiency gratings,” *Applied optics*, vol. 45, no. 23, pp. 5795–5799, 2006.
- [347] N. Destouches, A. Tishchenko, J. Pommier, S. Reynaud, O. Parriaux, S. Tonchev, and M. A. Ahmed, “99% efficiency measured in the-1 st order of a resonant grating,” *Optics Express*, vol. 13, no. 9, pp. 3230–3235, 2005.
- [348] Z.-L. Deng, S. Zhang, and G. P. Wang, “A facile grating approach towards broadband, wide-angle and high-efficiency holographic metasurfaces,” *Nanoscale*, vol. 8, no. 3, pp. 1588–1594, 2016.
- [349] E. Doumanis, G. Goussetis, G. Papageorgiou, V. Fusco, R. Cahill, and D. Linton, “Design of engineered reflectors for radar cross section modification,” *IEEE Transactions on Antennas and Propagation*, vol. 61, no. 1, pp. 232–239, 2013.
- [350] I. Lee and K. Lee, “The internet of things (iot): Applications, investments, and challenges for enterprises,” *Business Horizons*, vol. 58, no. 4, pp. 431–440, 2015.
- [351] J. M. Talavera, L. E. Tobón, J. A. Gómez, M. A. Culman, J. M. Aranda, D. T. Parra, L. A. Quiroz, A. Hoyos, and L. E. Garreta, “Review of iot applications in agro-industrial and environmental fields,” *Computers and Electronics in Agriculture*, vol. 142, pp. 283–297, 2017.
- [352] P. Schulz, M. Matthe, H. Klessig, M. Simsek, G. Fettweis, J. Ansari, S. A. Ashraf, B. Almeroth, J. Voigt, I. Riedel *et al.*, “Latency critical iot applications in 5g: Perspective on the design of radio interface and network architecture,” *IEEE Communications Magazine*, vol. 55, no. 2, pp. 70–78, 2017.
- [353] P. Fraga-Lamas, T. M. Fernández-Caramés, and L. Castedo, “Towards the internet of smart trains: A review on industrial iot-connected railways,” *Sensors*, vol. 17, no. 6, p. 1457, 2017.
- [354] A. Anusha and S. M. Ahmed, “Vehicle tracking and monitoring system to enhance the safety and security driving using iot,” in *2017 International Conference on Recent Trends in Electrical, Electronics and Computing Technologies (ICRTEECT)*. IEEE, 2017, pp. 49–53.

-
- [355] C. Zhang, G. Wang, H.-X. Xu, X. Zhang, and H.-P. Li, "Helicity-dependent multifunctional metasurfaces for full-space wave control," *Advanced Optical Materials*, vol. 8, no. 8, p. 1901719, 2020.
- [356] Y. Ra'di, D. L. Sounas, and A. Alù, "Metagratings: Beyond the limits of graded metasurfaces for wave front control," *Physical review letters*, vol. 119, no. 6, p. 067404, 2017.
- [357] V. Asadchy, M. Albooyeh, S. Tsvetkova, A. Díaz-Rubio, Y. Ra'di, and S. Tretyakov, "Perfect control of reflection and refraction using spatially dispersive metasurfaces," *Physical Review B*, vol. 94, no. 7, p. 075142, 2016.
- [358] A. Epstein and G. V. Eleftheriades, "Floquet-bloch analysis of refracting huygens metasurfaces," *Physical Review B*, vol. 90, no. 23, p. 235127, 2014.
- [359] M. Kalaagi and D. Seetharamdoo, "Design of dual polarized retrodirective metasurfaces," in *2018 IEEE Radio and Antenna Days of the Indian Ocean (RADIO)*. IEEE, 2018, pp. 1–2.
- [360] H. Srour, R. Gillard, S. Méric, and D. Seetharamdoo, "Analysis of the retrodirective mechanism of a flattened dihedral," *IET Microwaves, Antennas & Propagation*, vol. 12, no. 5, pp. 699–705, 2018.
- [361] Z. Chen, H. Deng, Q. Xiong, and C. Liu, "Phase gradient metasurface with broadband anomalous reflection based on cross-shaped units," *Applied Physics A*, vol. 124, no. 3, p. 281, 2018.
- [362] C. Shen, A. Díaz-Rubio, J. Li, and S. A. Cummer, "A surface impedance-based three-channel acoustic metasurface retroreflector," *Applied Physics Letters*, vol. 112, no. 18, p. 183503, 2018.
- [363] C. Yan, K.-Y. Yang, and O. J. Martin, "Fano-resonance-assisted metasurface for color routing," *Light: Science & Applications*, vol. 6, no. 7, p. e17017, 2017.
- [364] N. Verellen, Y. Sonnefraud, H. Sobhani, F. Hao, V. V. Moshchalkov, P. V. Dorpe, P. Nordlander, and S. A. Maier, "Fano resonances in individual coherent plasmonic nanocavities," *Nano letters*, vol. 9, no. 4, pp. 1663–1667, 2009.
- [365] S. P. Beeby, R. Torah, M. Tudor, P. Glynne-Jones, T. O'donnell, C. Saha, and S. Roy, "A micro electromagnetic generator for vibration energy harvesting," *Journal of Micromechanics and microengineering*, vol. 17, no. 7, p. 1257, 2007.
- [366] L. Zuo and X. Tang, "Large-scale vibration energy harvesting," *Journal of intelligent material systems and structures*, vol. 24, no. 11, pp. 1405–1430, 2013.

-
- [367] G. De Pasquale, A. Soma, and N. Zampieri, "Design, simulation, and testing of energy harvesters with magnetic suspensions for the generation of electricity from freight train vibrations," *Journal of Computational and Nonlinear Dynamics*, vol. 7, no. 4, p. 041011, 2012.
- [368] J. P. Lynch and K. J. Loh, "A summary review of wireless sensors and sensor networks for structural health monitoring," *Shock and Vibration Digest*, vol. 38, no. 2, pp. 91–130, 2006.
- [369] M. Mallouli and M. Chouchane, "Analytical modeling and analysis of a bimorph piezoelectric energy harvester," in *International Conference Design and Modeling of Mechanical Systems*. Springer, 2017, pp. 1179–1189.
- [370] D. R. Smith, J. B. Pendry, and M. C. Wiltshire, "Metamaterials and negative refractive index," *Science*, vol. 305, no. 5685, pp. 788–792, 2004.
- [371] S. Jahani and Z. Jacob, "All-dielectric metamaterials," *Nature nanotechnology*, vol. 11, no. 1, p. 23, 2016.
- [372] R. Feng, J. Yi, S. N. Burokur, L. Kang, H. Zhang, and D. H. Werner, "Orbital angular momentum generation method based on transformation electromagnetics," *Optics express*, vol. 26, no. 9, pp. 11 708–11 717, 2018.
- [373] J. Hao, W. Yan, and M. Qiu, "Super-reflection and cloaking based on zero index metamaterial," *Applied Physics Letters*, vol. 96, no. 10, p. 101109, 2010.
- [374] M. H. Rabah, D. Seetharamdoo, and M. Berbineau, "Analysis of miniature metamaterial and magnetodielectric arbitrary-shaped patch antennas using characteristic modes: Evaluation of the q factor," *IEEE Transactions on Antennas and Propagation*, vol. 64, no. 7, pp. 2719–2731, 2016.
- [375] J. Yi, M. Guo, R. Feng, B. Ratni, L. Zhu, D. H. Werner, and S. N. Burokur, "Design and validation of an all-dielectric metamaterial medium for collimating orbital-angular-momentum vortex waves at microwave frequencies," *Physical Review Applied*, vol. 12, no. 3, p. 034060, 2019.
- [376] P. T. Bowen, A. Baron, and D. R. Smith, "Theory of patch-antenna metamaterial perfect absorbers," *Physical Review A*, vol. 93, no. 6, p. 063849, 2016.
- [377] C. Wu and G. Shvets, "Design of metamaterial surfaces with broadband absorbance," *Optics letters*, vol. 37, no. 3, pp. 308–310, 2012.

- [378] M. Kalaagi and D. Seetharamdoo, "Electromagnetic energy harvesting systems in the railway environment: State of the art and proposal of a novel metamaterial energy harvester," in *2019 13th European Conference on Antennas and Propagation (EuCAP)*. IEEE, 2019, pp. 1–5.
- [379] —, "Multi-band metamaterial absorbers to efficient energy harvesters for railway applications," in *2020 International Workshop on Antenna Technology (iWAT)*. IEEE, 2020, pp. 1–3.
- [380] S. Lee, S. Baek, T.-T. Kim, H. Cho, S. Lee, J.-H. Kang, and B. Min, "Metamaterials for enhanced optical responses and their application to active control of terahertz waves," *Advanced Materials*, vol. 32, no. 35, p. 2000250, 2020.
- [381] W. Cai, U. K. Chettiar, A. V. Kildishev, and V. M. Shalaev, "Optical cloaking with metamaterials," *Nature photonics*, vol. 1, no. 4, p. 224, 2007.
- [382] N. A. Salama, M. Desouky, S. Obayya, and M. A. Swillam, "Free space super focusing using all dielectric hyperbolic metamaterial," *Scientific Reports*, vol. 10, no. 1, pp. 1–9, 2020.
- [383] X. Jiang, B. Liang, R.-q. Li, X.-y. Zou, L.-l. Yin, and J.-c. Cheng, "Ultra-broadband absorption by acoustic metamaterials," *Applied Physics Letters*, vol. 105, no. 24, p. 243505, 2014.
- [384] Y. P. Lee, J. Y. Rhee, Y. J. Yoo, and K. W. Kim, *Metamaterials for perfect absorption*. Springer, 2016, vol. 236.
- [385] M. Amiri, F. Tofigh, N. Shariati, J. Lipman, and M. Abolhasan, "Wide-angle metamaterial absorber with highly insensitive absorption for te and tm modes," *Scientific Reports*, vol. 10, no. 1, pp. 1–13, 2020.
- [386] F. Erkmen, T. S. Almoneef, and O. M. Ramahi, "Electromagnetic energy harvesting using full-wave rectification," *IEEE Transactions on Microwave Theory and Techniques*, vol. 65, no. 5, pp. 1843–1851, 2017.
- [387] S. Roundy, D. Steingart, L. Frechette, P. Wright, and J. Rabaey, "Power sources for wireless sensor networks," in *European workshop on wireless sensor networks*. Springer, 2004, pp. 1–17.
- [388] N. I. Zheludev and Y. S. Kivshar, "From metamaterials to metadevices," *Nature materials*, vol. 11, no. 11, pp. 917–924, 2012.
- [389] K. Fan and W. J. Padilla, "Dynamic electromagnetic metamaterials," *Materials Today*, vol. 18, no. 1, pp. 39–50, 2015.
- [390] A. M. Shaltout, V. M. Shalaev, and M. L. Brongersma, "Spatiotemporal light control with active metasurfaces," *Science*, vol. 364, no. 6441, 2019.
- [391] H. Gacanin and M. Di Renzo, "Wireless 2.0: Towards an intelligent radio environment empowered by reconfigurable meta-surfaces and artificial intelligence," *arXiv preprint arXiv:2002.11040*, 2020.
- [392] Y. Ruan, Q. F. Nie, L. Chen, and H. Y. Cui, "Optical transparent and reconfigurable metasurface with autonomous energy supply," *Journal of Physics D: Applied Physics*, vol. 53, no. 6, p. 065301, 2019.
- [393] E. Basar, M. Di Renzo, J. De Rosny, M. Debbah, M.-S. Alouini, and R. Zhang, "Wireless communications through reconfigurable intelligent surfaces," *IEEE access*, vol. 7, pp. 116 753–116 773, 2019.
- [394] M. A. ElMossallamy, H. Zhang, L. Song, K. G. Seddik, Z. Han, and G. Y. Li, "Reconfigurable intelligent surfaces for wireless communications: Principles, challenges, and opportunities," *IEEE Transactions on Cognitive Communications and Networking*, vol. 6, no. 3, pp. 990–1002, 2020.
- [395] P. Mursia, V. Sciancalepore, A. Garcia-Saavedra, L. Cottatellucci, X. Costa-Pérez, and D. Gesbert, "Risma: Reconfigurable intelligent surfaces enabling beamforming for iot massive access," *IEEE Journal on Selected Areas in Communications*, 2020.
- [396] M. Z. Chowdhury, M. Shahjalal, S. Ahmed, and Y. M. Jang, "6g wireless communication systems: Applications, requirements, technologies, challenges, and research directions," *IEEE Open Journal of the Communications Society*, vol. 1, pp. 957–975, 2020.